POLYETHER BASED BLOCK COPOLYMER MEMBRANES FOR CO$_2$ SEPARATION

POLYETHER BASED BLOCK COPOLYMER MEMBRANES FOR CO₂ SEPARATION

PROEFSCHRIFT

ter verkrijging van
de graad van doctor aan de Universiteit Twente,
op gezag van de rector magnificus,
prof. dr. H. Brinksma,
volgens besluit van het College voor Promoties
in het openbaar te verdedigen
op vrijdag 19 maart 2010 om 16:45 uur

door

Sander Rogier Reijerkerk

geboren op 28 mei 1982
te Deventer

Dit proefschrift is goedgekeurd door:

Promotor
Prof. Dr.-Ing. M. (Matthias) Wessling

Assistent-promotor
Dr. Ir. D.C. (Kitty) Nijmeijer

The end happens once. Everything else is just progress.

CONTENTS

CHAPTER 1

Introduction

1.1 World's energy dependence and climate change

The awareness of the occurrence of a global climate change, usually referred to as global warming, has increased due to, for instance, the media attention surrounding the Kyoto protocol in 1997 [1] and more recently by the documentary movie 'An inconvenient truth: A global warning' made by former vice-president of the United States of America (USA) Al Gore [2]. These climate changes mainly manifest themselves as a worldwide increase in the average temperature as shown by the famous hockey-stick figure (Figure 1.1) published in the third assessment report on climate change (2001) by the Intergovernmental Panel on Climate Change (IPCC) [3].
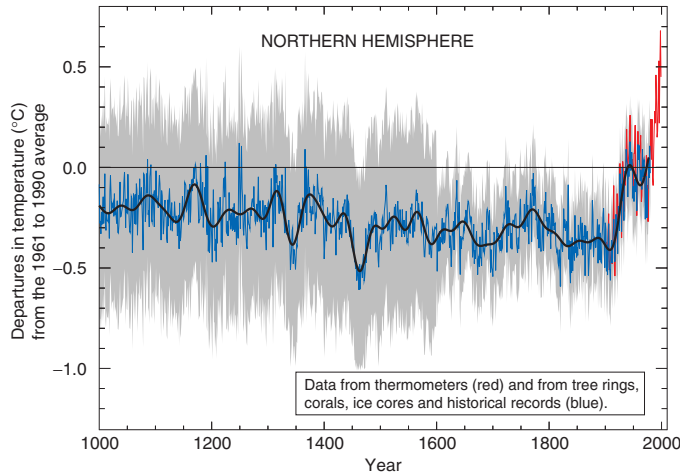
Figure 1.1: Millennial Northern Hemisphere (NH) temperature reconstruction (blue – tree rings, corals, ice cores, and historical records) and instrumental data (red) from AD 1000 to 1999. Smoother version of NH series (black), and two standard error limits (gray shaded) are shown [3].

These climate changes are not limited to an increase in global temperature, but also other phenomena are believed to be related to global warming, such as the rise in sea level and temperature, the retreat of glaciers, and the increased frequency of more extreme weather conditions. Overall, the reason for the current climate change is thought to be caused by an increase in the atmospheric concentration of greenhouse gases, such as carbon dioxide (CO_2), methane (CH_4), nitrous oxide (N_2O), hydrofluorocarbons (HFCs), perfluorocarbons (PFCs) and sulfur hexafluoride (SF6). Figure 1.2 shows the concentration of CO_2 and two other major greenhouse gases (CH_4 and N_2O) over the past 1000 years.
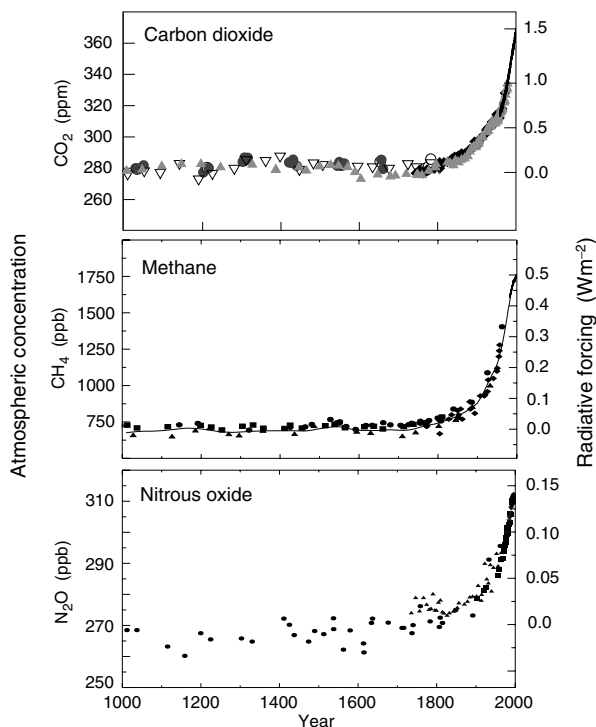
Figure 1.2: Records of changes in atmospheric composition of the atmospheric concentrations of CO_2, CH_4 and N_2O over the past 1,000 years. Ice core and firn data for several sites in Antarctica and Greenland (shown by different symbols) are supplemented with the data from direct atmospheric samples over the past few decades (shown by the line for CO_2 and incorporated in the curve representing the global average of CH_4). The estimated radiative forcing from these gases is indicated on the right-hand scale [3].

An exponential increase in the atmospheric concentration of all three gases is observed and the start of this increase ($\sim$1900) coincides with the start of the increase in temperature as shown in Figure 1.1. The worldwide consensus is that this sudden increase is not a natural phenomenon, but is related to the recent human activity on the planet. Since the Industrial Revolution, humans started to use large quantities of carbon containing fossil fuels (Figure 1.3).

From the early 1900's, which coincides with the trends observed in Figure 1.1 and Figure 1.2, the use of fossil fuels has increased tremendously. These fossil fuels are mainly burned to generate electricity or facilitate transportation, thereby emitting large amounts of CO_2 to the atmosphere, contributing to global warming. To mitigate
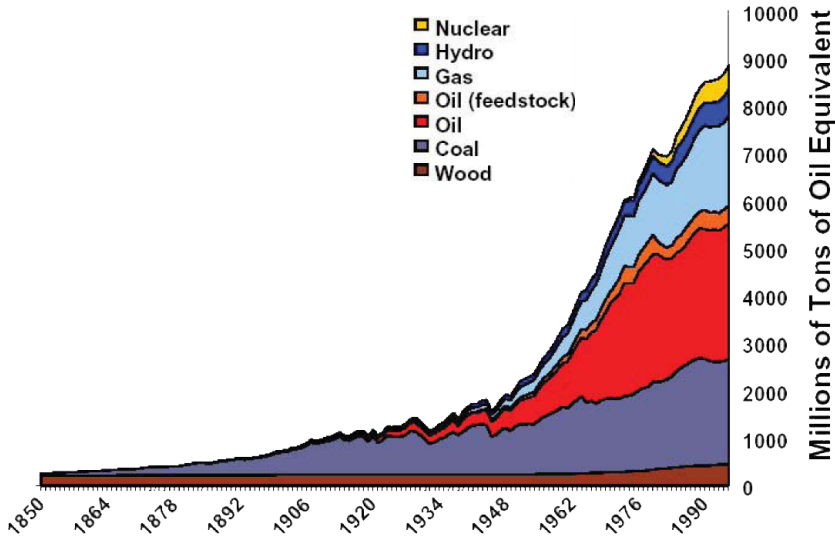
Figure 1.3: Worldwide use of energy in millions of tons of oil equivalent (MTOE) from 1850 till present [4].

the climate changes it is important to stabilize or even decrease the atmospheric concentration of greenhouse gases and in particular the concentration of CO_2 as it has the highest Global Warming Potential (GWP), indicated by a high value of the radiative forcing [1] (Figure 1.2). This is a challenging task as the worldwide CO_2 emissions reached a value of 23.5 $GtCO_2/yr$ in the year 2000 [5]. Approximately 60% of these emissions come from large stationary sources (> 0.1 $MtCO_2/yr$). The majority (80%) of these large stationary sources are fossil fuel based power plants, while the remaining 20% are mainly emitting sources related to the petrochemical and steel industry. The energy sector is thus by far ($\sim$50%) the largest contributor to the worldwide emissions of CO_2 and poses a significant potential for the worldwide reduction of CO_2 emissions.

---

[1]Radiative forcing is a measure of the influence a factor has (in this case the GHG concentration) in altering the balance of incoming and outgoing energy in the Earth-atmosphere system and is an index of the importance of the factor as a potential climate change mechanism.

1.2 Carbon dioxide capture and storage (CCS)

1.2.1 Carbon dioxide capture

A strategy that has been devised to reduce the worldwide emissions of CO_2, especially during the production of electricity in the energy sector, has become known as 'Carbon dioxide Capture and Storage', in short CCS. There are three pathways that can be pursued for CO_2 capture from a fossil fuel based power plant, known as post-combustion capture, pre-combustion capture, and oxy-combustion capture (Figure 1.4).
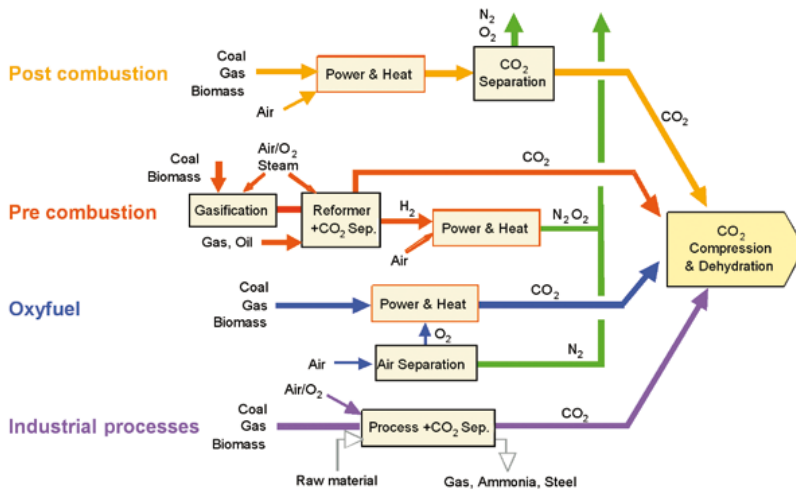
Figure 1.4: Overview of CO_2 capture processes and systems [5].

In post-combustion capture, CO_2 capture occurs after the combustion process. The CO_2 is separated from other flue gas constituents either originally present in the air or produced by combustion and it mainly involves the separation of CO_2 from N_2. In pre-combustion capture, the CO_2 is removed from the fuel before the actual combustion process takes place. The principle of this process is first to convert the fossil fuel into CO_2 and hydrogen gas (H_2) via gasification. Then, the CO_2 and H_2 are separated and this results in a hydrogen-rich gas, which can be combusted to yield electricity. In oxy-combustion capture, the fossil fuel is burned with an oxygen enriched stream that contains little or no nitrogen (N_2). The exhaust gas from this system is therefore highly concentrated in CO_2 and after the removal of water vapor, the CO_2 is ready for subsequent transport and storage.

All three pathways have their advantages and disadvantages. These are summarized in Table 1.1 [6].

Table 1.1: Advantages and disadvantages of different CO_2 capture pathways [6].

	Advantages	Barriers to implementation

Post-combustion	• Applicable to the majority of existing coal-fired power plants
	• Retrofit technology option
		Flue gas is …
		  • Dilute in CO_2
		  • At ambient pressure
		
		… resulting in …
		  • Low CO_2 partial pressure
		    • Significantly higher performance or circulation volume required for high capture levels
		    • CO_2 produced at low pressure compared to sequestration requirements

Pre-combustion	Synthesis gas is …
	  • Concentrated in CO_2
	  • High pressure
	
	… resulting in …
	  • High CO_2 partial pressure
	    • Increased driving force for separation
	    • More technologies available for separation
	  • Potential for reduction in compression costs/loads
		• Applicable mainly to new plants, as few gasification plants are currently in operation
		• Barriers to commercial application of gasification are common to pre-combustion capture
		  • Availability
		  • Cost of equipment
		  • Extensive supporting systems requirements

Oxy-combustion	• Very high CO_2 concentration in flue gas
	• Retrofit and repowering technology option
		• Large cryogenic O_2 production requirement may be cost prohibitive
		• Cooled CO_2 recycle required to maintain temperatures within limits of combustor materials
		  • Decreased process efficiency
		  • Added auxiliary load

Different technologies are currently considered or under investigation to effectively capture the CO_2 following either one of these three pathways (or a combination of them). Although this thesis focuses on the CO_2 capture (and not on the processes further downstream) the storage options of carbon dioxide are briefly discussed before going into more detail regarding these pathways and associated technologies.

1.2.2 Carbon dioxide storage

Two key options exist for the storage of CO_2, which are: geological storage and ocean storage [5]. Other options that are considered are (1) mineral carbonation, which involves the conversion of CO_2 into solid inorganic carbonates via chemical reactions and (2) the industrial usage of CO_2, for instance for the production of various carbon containing chemicals [5]. However, the capacity of these two last options is limited and would not match with the vast amounts of CO_2 that need to be captured from power plants. The research and industrial focus is therefore on the first two options and these will be shortly discussed hereafter.

⌐ *Geological storage*

In geological storage, CO_2 is injected into underground reservoirs. The CO_2 is expected to be isolated from the atmosphere for several hundreds of years [7]. An overview of geological storage options is presented in Figure 1.5.
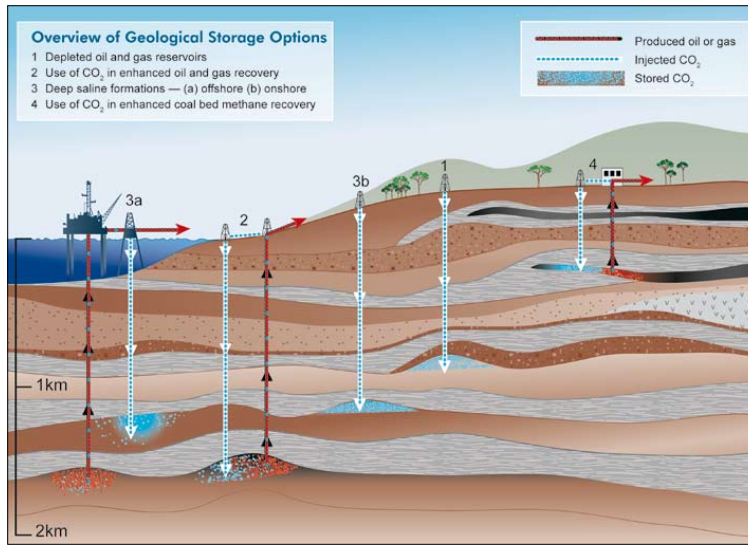
Figure 1.5: Methods for storing CO_2 in deep underground geological formations. Three methods may be combined with the recovery of hydrocarbons: EOR (2), EGR (2) and ECBM (4) [5].

Geological storage of CO_2 can performed in a variety of geological formations. CO_2 can be stored in empty oil and gas reservoirs (1) or deep saline formations (3). It is also possible to take advantage of the CO_2 and use it for enhanced oil recovery (EOR) (2), enhanced gas recovery (EGR) (2) or enhanced coal bed methane recovery (ECBM) (4). Currently, already some commercial scale projects operate based on these principles. The 'Sleipner' project, operated by Statoil in the North Sea, is the first project dedicated to geological CO_2 storage in a saline formation. The CO_2 (about 9%) from the Sleipner West Gas Field is separated, and then injected into a large, deep, saline formation 800 meter below the seabed of the North Sea. Another project, the 'In Salah' gas project, a joint venture among Sonatrach, BP and Statoil located in the central Saharan region of Algeria, is the world's first large-scale CO_2 storage project in a gas reservoir. The Krechba Field at In Salah produces natural gas containing up to 10% CO_2. After the natural gas has been processed to meet commercial specifications, the CO_2 is re-injected into a sandstone reservoir at a depth of 1800 meter and this stores up to 1.2 $MtCO_2$/yr [5].

⌐ *Ocean storage*

The Earth's oceans cover almost 70% of the Earth's surface with an average depth of 3,800 meters and these are the world's largest buffer to store CO_2. There have been small-scale field experiments and 25 years of theoretical, laboratory, and modeling studies of intentional ocean storage of CO_2, but ocean storage has not yet been deployed or thoroughly tested [5]. Various technologies have been envisioned to enable and increase ocean CO_2 storage (Figure 1.6) [5]. One class of options involves storing a relatively pure stream of carbon dioxide that has been captured and compressed. This CO_2 can be placed on a ship, injected directly into the ocean, or deposited on the bottom of the sea. CO_2 loaded on ships could either be dispersed from a towed pipe or transported to fixed platforms feeding a CO_2 lake on the sea floor. Such CO_2 lakes must be deeper than 3 km where CO_2 is denser than sea water. Any of these approaches could in principle be used in conjunction with neutralization of CO_2 with carbonate minerals.
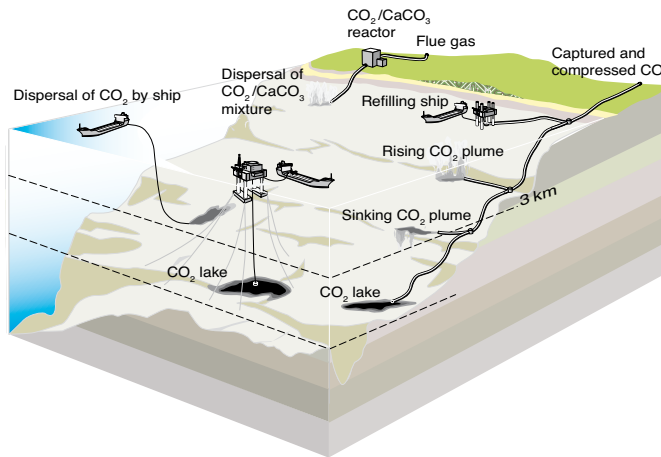
Figure 1.6: Methods of ocean storage [5].

1.3 CO$_2$ capture technologies and challenges

1.3.1 Absorption vs. membranes

Two promising technologies for CO$_2$ capture from these large point sources are solvent-based absorption processes and membrane-based separation processes [5]. An absorption based process can either rely on chemical solvents (envisioned for post-combustion), such as monoethanolamine (MEA) and methyldiethylamine (MDEA) or physical solvents (envisioned for pre-combustion), such as dimethylethers of poly(ethylene glycol) and methanol (trade names are respectively Selexol and Rectisol). However, such solvent-based absorption processes have several disadvantages that limit their applicability. The inherent disadvantage of absorption based processes is the very energy intensive solvent regeneration step [5, 8]. This regeneration step needs either a change in pressure or a change in temperature requiring a large amount of energy. Furthermore, in its design, a system that captures CO$_2$ from power plants should be very simple. Not only would lead an absorption based process to large installations and operating costs, also the presence of vast amounts of fluids that needs to be pumped around is likely to result in permanent maintenance issues.

In contrast, polymer-based membranes, in comparison to absorption, are less energy intensive, require no phase change in the process, and due to their inherent simplicity membranes have typically low-maintenance. This gives a membrane-based system considerable advantage with respect to engineering and economics and thus has the potential to compete with an absorption based process [9]. However, although membranes play a significant role in the removal of CO$_2$ from methane, commercial membrane systems for the removal of CO$_2$ from flue gas in either pre- or post-combustion are not yet available. As of today, numerous design and scale-up challenges remain, but membrane-based systems are moving forward [10]. These challenges will be further discussed in the next paragraph.

1.3.2   Pre- or post-combustion membrane technology?

The difference between pre- and post-combustion CO_2 capture is significant. Besides the fundamental difference of the separation (CO_2/H_2 vs. CO_2/N_2) as mentioned before, also the feed pressure, CO_2 partial pressure, total volume and temperature are considerably different. Post-combustion flue gas streams typically have a temperature around 50–60℃ and are generally high in volume due to the 79% nitrogen in air. Furthermore, they have a low pressure (atmospheric) and the concentration of CO_2 is usually low 10–15 vol.% [10]. On the contrary, pre-combustion flue gas streams, as found in integrated gasification combined cycle (IGCC) power plants, are available at high temperature 300℃, are typically smaller in volume (as they use nearly pure oxygen for the coal gasification) and the concentration of CO_2 is 40–50% corresponding to a CO_2 partial pressure of 26–38 bar [10]. Especially the large difference in the partial pressure of CO_2 between pre- and post-combustion has a profound influence on the membrane (process) design as the pressure difference across the membrane provides the driving force in any membrane-based gas separation. In this respect pre-combustion capture seems the most promising technique as it has a high partial pressure CO_2 stream providing such a system with inherent design advantages over a post-combustion capture system. Though, up till now worldwide only 4 IGCC facilities exist, which equals only ∼0.1% of the total fossil fuel fired power plants [11]. This signifies that there is an even more urgent need for post-combustion CO_2 capture systems as a retrofit option for the large fleet of current coal-fired power plants. However, the problem of a large volume, low pressure and very dilute stream makes post-combustion CO_2 capture a huge engineering challenge. As a result of the low driving force a prerequisite for any membrane material to be considered for this separation is the necessity of an extremely high permeability for CO_2 [4, 10]. Although some commercially available materials exists that have sufficiently high CO_2/N_2 selectivity (40–50) for this separation, like PEBAX® [12, 13] and Polyactive® [14], their relative low permeability remains an issue. As a result, worldwide CO_2 selective membranes with intrinsically higher permeability are being developed and these membranes are mainly based on soft, rubbery polymeric materials or concepts similar to PEBAX® or Polyactive®. As such, the necessity of a membrane material that combines a sufficiently high selectivity with the high permeability needed has been the motivation for the current research.

1.4   Project description

The research presented in this thesis has been carried out in the Membrane Technology Group of the University of Twente, which participates in the Institute for Mechanics, Processes and Control Twente (IMPACT). In particular this research has been carried out as part of the European Integrated Project (IP) 'Nanomembranes against global warming', acronym NanoGLOWA, which is a project with a consortium of 26 partners ranging from universities, research institutes, SME's, large membrane producers and power plants and involves 14 countries. The overall objective of this Integrated Project is the development of optimal nanostructured membranes and installations for CO_2 capture from power plants. At the start of the project (December 2006) 5 research universities contributed to the development of promising membrane materials for the separation of mixtures of CO_2 and non-polar gases and in particular the separation of CO_2 from N_2 as required for post-combustion CO_2 capture. The objective of the University of Twente has been to develop cheap, high flux, polymeric membranes and membrane modules that selectively remove CO_2 or simultaneously remove CO_2 and H_2O from power plants by nano functionalization of cheap base materials. Furthermore, polymer modification on a molecular level were subject of investigation as well.

This thesis describes the work done within the NanoGLOWA project on the development of these promising membrane materials for CO_2 capture. It especially focuses on the improvement of CO_2 permeability by smart polymer modification and/or the addition of smart additives.

Before the outline of the thesis is described in more detail the ongoing and future steps within the project will be briefly highlighted. The successful development of new, highly permeable, membrane materials within the project, research that is partially described in this thesis, has resulted in the selection of promising membrane materials for further membrane development. To obtain high fluxes, especially the development of thin film hollow fiber composite membranes consisting of a porous support (for mechanical stability) and a dense top layer, which ensures the actual separation, is of major importance. These thin film composite membranes are currently developed from support fibers prepared from cheap base material (e.g. polysulfone, polyethersulfone or poly(phenylene oxide)) and the actual new, highly permeable membrane material by a procedure called dip coating. After successful development of these thin film composite membranes, pilot scale module design and construction, field testing and preliminary process design are also part of the project to cover the complete chain from membrane development to actual module implementation.

1.5 Outline of the thesis

This thesis describes several design strategies for the development of highly permeable, polyether based block copolymer membranes suitable for the removal of CO_2 from light gases. These membrane materials are mainly developed for the separation of CO_2 from flue gas as required in post-combustion CO_2 capture. However, the separation of CO_2 from other light gases, such as H_2 and CH_4, has been subject of investigation as well. These separations can be of interest for the removal of CO_2 from synthesis gas (as required in pre-combustion) or the removal of CO_2 from natural gas to meet pipeline specifications. Although several different CO_2/light gas separations are discussed, the work described in this thesis can be divided in three different sections. **Chapter 2 and 3** investigate the systematic tuning on a molecular level of two different types of block copolymer systems for use in CO_2 separation. The second block copolymer system (**Chapter 3**) proved to be very successful and its performance is further explored in **Chapter 4, 5 and 6**. A completely different strategy (polymer blending) as a route to highly permeable polymeric membranes is explored in **Chapter 7**.

Chapter 2 investigates the effect of the type and length of the soft segment on the mass transport properties in polyether based block copolymers with a short uniform di-amide hard segment. In particular poly(ethylene oxide) (PEO), poly(propylene oxide) (PPO) and mixtures of both soft segments are used to tune the mass transport properties. These macroscopic mass transport properties are discussed in relation to the thermal-mechanical properties and the microdomain block copolymer morphology.

Chapter 3 describes the synthesis, thermal-mechanical and several other properties of a novel polyether based block copolymer system using a soft segment based on a random distribution of poly(ethylene oxide) and poly(propylene oxide) and a uniform tetra-amide based hard segment. The use of the uniform hard segment ensures exceptionally efficient phase separation, while the incorporation of a low amount of PPO (25 wt.%) in the predominantly PEO based soft segment restricts the PEO crystallization generally observed (which is detrimental to the mass transport properties).

Chapter 4 presents the pure gas permeation properties of the block copolymer system developed in **Chapter 3** for CO_2, H_2, N_2, CH_4 as well as He and O_2. The transport properties are investigated over a wide temperature range (-10℃ to $+50$℃) to address the importance of the incorporation of PPO in the suppression of PEO crystallinity.

The membrane performance is compared to commercially available PEO based block copolymer membranes and to the block copolymer membranes investigated in **Chapter 2**.

Chapter 5 investigates the block copolymer membranes discussed in **Chapter 3 and 4** for use in high pressure CO_2/H_2 and CO_2/CH_4 feed streams as high pressures are generally encountered in these separations. Pure as well as mixed gas experiments are performed at temperatures varying between $-10℃$ and $+35℃$. The influence of temperature and the CO_2 partial pressure on the membrane performance and the differences between pure and mixed gas conditions are extensively discussed. These discussions are supported by pure and mixed gas sorption experiments to identify the origin of the observed differences.

Chapter 6 investigates once more the block copolymer membranes discussed in **Chapter 3 and 4**. In this chapter the CO_2/N_2 post-combustion capture performance under more realistic process conditions, in the presence of water vapor, is studied. Simultaneous water vapor and gas transport measurements through a selection of the block copolymers discussed in **Chapter 3** are performed. The gas used is either a pure gas (N_2 or CO_2) or a mixed gas (90/10 N_2/CO_2). In particular, the influence of the water vapor activity on water vapor and gas transport is investigated as well as the CO_2/N_2 selectivity under pure and mixed gas conditions. Water vapor sorption experiments are performed to support the results obtained in permeation measurements.

Chapter 7 describes a different, but extremely versatile strategy to obtain highly permeable membranes for CO_2 capture. It describes the blending of a commercially available polyether based block copolymer with a smart additive. The effect of blending ratio on the performance of these blends is measured for a wide range of pure gases. Besides pure gas measurements, the performance of these blend membranes for high pressure CO_2/H_2 and CO_2/CH_4 separation, analogous to the data obtained in **Chapter 5**, is also investigated.

Finally, **Chapter 8** summarizes the main conclusions of this work and provides an outlook on the future of carbon dioxide capture and storage (CCS), mainly focusing on post-combustion capture technology.

1.6 References

[1] UNITED NATIONS FRAMEWORK CONVENTION OF CLIMATE CHANGE; *Kyoto protocol* (1997)

[2] D. GUGGENHEIM; *An Inconvenient Truth: A Global Warning*; Documentary, ©Paramount Pictures (2006)

[3] IPCC; *Third Assessment Report: Climate Change 2001*; Technical report; Cambridge University Press; Cambridge (England) (2001)

[4] T. C. MERKEL, H. LIN, Z. HE, R. DANIELS, S. THOMPSON, A. SERBANESCU AND R. W. BAKER; *A membrane process to capture CO_2 from power plant flue gas*; in *International Congress on Membranes and Membrane Processes (ICOM)*; Honolulu (HI), United States of America (2008)

[5] IPCC; *Special Report on Carbon Dioxide Capture and Storage*; Technical report; Cambridge University Press; Cambridge (England) (2005)

[6] J. D. FIGUEROA, T. FOUT, S. PLASYNSKI, H. MCILVRIED AND R. D. SRIVASTAVA; *Advances in CO_2 capture technology–The U.S. Department of Energy's Carbon Sequestration Program*; International Journal of Greenhouse Gas Control **2** (1) (2008) 9–20; DOI:10.1016/s1750-5836(07)00094-1

[7] S. M. KLARA, R. D. SRIVASTAVA AND H. G. MCILVRIED; *Integrated collaborative technology development program for CO_2 sequestration in geologic formations - United States Department of Energy R&D*; Energy Conversion and Management **44** (17) (2003) 2699–2712; DOI:10.1016/s0196-8904(03)00042-6

[8] H. H. KHOO AND R. B. H. TAN; *Life cycle evaluation of CO_2 recovery and mineral sequestration alternatives*; Environmental Progress **25** (3) (2006) 208–217; DOI:10.1002/ep.10139

[9] E. FAVRE; *Carbon dioxide recovery from post-combustion processes: Can gas permeation membranes compete with absorption?*; Journal of Membrane Science **294** (1-2) (2007) 50–59; DOI:10.1016/j.memsci.2007.02.007

[10] S. SHELLEY; *Capturing CO_2: Membrane-based systems move forward*; Chemical Engineering Progress **105** (4) (2009)

[11] S. SHELLEY; *IGCC Power Generation — Down But Not Out*; Chemical Engineering Progress **104** (9) (2008)

[12] V. I. BONDAR, B. D. FREEMAN AND I. PINNAU; *Gas sorption and characterization of poly(ether-b-amide) segmented block copolymers*; Journal of Polymer Science, Part B: Polymer Physics **37** (17) (1999) 2463–2475; DOI:

10.1002/(SICI)1099-0488(19990901)37:17⟨2463::AID-POLB18⟩3.0.CO;2-H

[13] V. I. Bondar, B. D. Freeman and I. Pinnau; *Gas transport properties of poly(ether-b-amide) segmented block copolymers*; Journal of Polymer Science, Part B: Polymer Physics **38** (15) (2000) 2051–2062; DOI:10.1002/1099-0488(20000801) 38:15⟨2051::AID-POLB100⟩3.0.CO;2-D

[14] S. J. Metz, M. H. V. Mulder and M. Wessling; *Gas-permeation properties of poly(ethylene oxide) poly(butylene terephthalate) block copolymers*; Macromolecules **37** (12) (2004) 4590–4597; DOI:10.1021/ma049847w

CHAPTER 2

Tuning of mass transport properties in multi-block copolymers for CO$_2$ capture applications

Abstract

Polyether and especially poly(ethylene oxide) (PEO) based segmented block copolymers are very well known for their high CO_2 permeability combined with a high CO_2/light gas selectivity, but most (commercially) available block copolymers have incomplete phase separation between the soft and hard blocks in the polymer leading to reduced performance. Here we present a polyether based segmented block copolymer system with improved phase separation behavior and gas separation performance using poly(ethylene oxide) (PEO) and/or poly(propylene oxide) (PPO) as a soft segment and short monodisperse di-amide (TΦT) as a hard segment.

In this work we tune the mass transport properties of such multi-block copolymers for CO_2 capture by systematically investigating the effect of the type and length of soft segment in the block copolymer at constant short hard segment. The effect of (1) the length of the PEO soft segment, (2) the type of soft segment (PPO vs. PEO) and (3) the use of a mixture of these two different types of soft segment as a method to tune the gas separation performance and its relation with the thermal-mechanical properties is investigated. The use of such a polyether based segmented block copolymer system as presented here offers a very versatile tool to tailor mass transfer and separation properties of membranes for gas and vapor separation.

2.1 Introduction

Block copolymers have been widely investigated for the removal of CO_2 from light gases [1–11]. In general, block copolymers consist of an alternating series of flexible soft segments and crystallizable hard segments [12]. The crystallizable hard segments provide the material its mechanical stability, while the soft segments are the dominant phase for gas permeation. The type of soft and hard segment can be chosen independently, which makes them a versatile instrument to tune the properties of gas separation membranes.

To obtain excellent membrane properties, the microdomain phase separation of the block copolymers is crucial and needs to be controlled. A block copolymer with improved properties for gas permeation should exhibit the following properties:

1. Good phase separation of the hard and soft segments;
2. Complete crystallization of the hard segment;
3. High PEO content;
4. Low glass transition temperature of the soft segment (high chain flexibility); and
5. No soft phase crystallinity or low soft segment melting temperature.

These properties are not met by today's (commercially) available block copolymers as they often have incomplete phase separation due to non-uniformity of the hard segment, leading to large amounts of non-crystallized hard segments within the soft amorphous phase (properties 1–2). This restricts the amount of PEO that can be used (property 3), it reduces chain flexibility (property 4) and moreover the soft PEO phase often shows semi-crystalline behavior as well (property 5). A schematic representation of the morphology of a typical commercially available block copolymer is shown in Figure 2.1a.

To improve the performance of the block copolymers and to allow us to control the microdomain phase separation Husken *et al.* used monodisperse crystallizable T6T6T hard segments (a tetra-amide) with strongly improved crystallization behavior, resulting in almost complete phase separation and enabling high soft phase concentrations (properties 1–3) (Figure 2.1b) [11, 13]. Although crystallization of the PEO phase was still present, this could be partially suppressed by extending low molecular weight PEO (600 g/mol) with terephthalic units (property 5) [11, 14]. To further improve membrane gas separation properties we propose the use of a short monodisperse di-amide hard segment (length ∼2 nm) instead of the longer tetra-amide hard segment (length ∼4.2
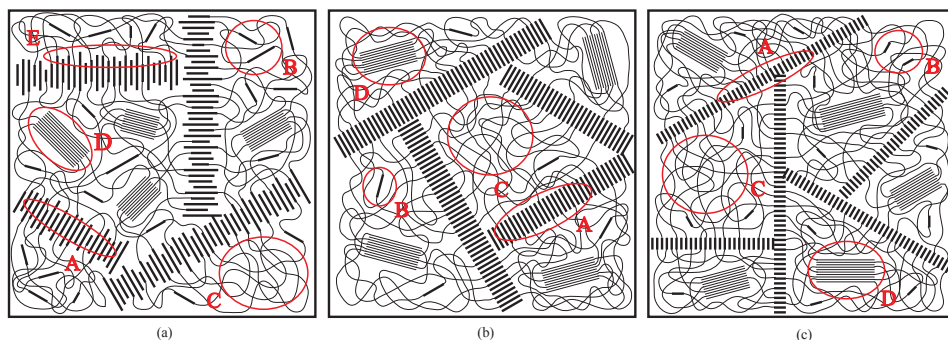
Figure 2.1: Schematic representation of the morphology of (a) commercially available block copolymers (e.g. the PEBAX® family), (b) PEO based block copolymers with monodisperse long T6T6T hard segments as used by Husken *et al.* [11] and (c) polyether based block copolymers with monodisperse short TΦT hard segments as used in this article. The circled areas are representative for (A) crystalline hard segments, (B) non-crystallized rigid hard segments, (C) continuous amorphous soft phase, (D) crystalline soft phase and (E) intermediate region with mixed crystalline hard segments and non-crystalline soft segments.

nm). The introduction of this type of hard segment will lead to the incorporation of higher amounts of soft segment (property 3). The resulting morphology is shown in Figure 2.1c.

Apart from the hard segment, also the type of soft segment can be used as a tool to tune the gas permeation properties of membranes made of such a block copolymer system. By changing the soft segment characteristics, we are able to control the crystallization behavior of the soft segment in the polymer, thus tailoring its gas permeation properties.

In this work we tune the mass transport properties of such multi-block copolymers for CO_2 capture by systematically investigating the effect of the type and length of soft segment in the block copolymer at constant short hard segment. The effect of (1) the length of the PEO soft segment, (2) the type of soft segment (PPO vs. PEO) and (3) a mixture of these two different types of soft segment as a method to tune the gas separation performance and its relation with the thermal-mechanical properties is investigated. The use of PPO soft segments avoids the regular chain packing that is observed in PEO [13]. As a result it suppresses the crystallization of the soft segment and a block copolymer with PPO soft segments is expected to be completely amorphous above its T_g. Furthermore, the use of PPO soft segments increases the free volume of the block copolymers, which should result in higher intrinsic gas permeabilities.

However, the extra methyl side group decreases the polarity and the CO_2 solubility of the soft segment compared to PEO, thus possibly reducing the CO_2/light gas selectivity.

To investigate the effect of the different aspects mentioned in the previous paragraph on membrane performance, monodisperse di-amide (TΦT) hard segments are used to prepare polyether based block copolymers with PEO, PPO and mixtures of both as soft segments. Their gas permeation properties are systematically studied and related to their thermal-mechanical properties as described in a separate article [15].

2.2 Theory

Gas diffusion in non-porous structures can be described using Fick's first law [16]. Under steady state conditions and expressing concentrations as partial pressures, using Henry's law, the following Equation (2.1) can be derived:

$$J_i = \frac{D_i S_i}{\ell} \triangle p_i \tag{2.1}$$

where J_i is the gas flux of component i through the membrane (cm^3 (STP)/(cm^2·s)), D_i is the diffusivity coefficient of component i (cm^2/s), S_i is the solubility coefficient of component i (cm^3 (STP)/(cm^3·cmHg)), l is the membrane thickness (cm), and $\triangle p_i$ is the partial pressure difference of component i over the membrane (cmHg). The product of the diffusivity and solubility is the permeability, which is generally expressed in units of Barrer, where 1 Barrer equals $1 \cdot 10^{-10}$ cm^3 (STP)·cm/(cm^2·s·cmHg). The ideal selectivity of a membrane for gas A over gas B is given by the ratio of the pure gas permeabilities

$$\alpha = \frac{P_A}{P_B} = \frac{D_A}{D_B} \cdot \frac{S_A}{S_B} \tag{2.2}$$

where D_A/D_B is the diffusivity selectivity and S_A/S_B is the solubility selectivity. Gas diffusivity is enhanced by decreasing penetrant size, increasing polymer chain flexibility, increasing polymer fractional free volume (FFV) and decreasing polymer-penetrant interactions [16]. Penetrant solubility is increased by increasing condensability of the penetrant (which increases with increasing critical temperature and boiling point) and increasing polymer-penetrant interactions [16]. In general, polyether based block copolymers exhibit a low T_g resulting in high CO_2 diffusivity but low diffusivity

selectivity. High CO_2/light gas selectivity is achieved by high CO_2/light gas solubility selectivity, as the quadrupolar CO_2 exhibit favorable interaction with the ether oxygen linkages, favoring the solubility of the polar CO_2 over the non-polar gases like H_2, N_2 and CH_4.

2.3 Experimental

2.3.1 Materials

1,1,1,3,3,3-Hexaflouroisopropanol (HFIP), *N*-methyl-2-pyrrolidone (NMP), *p*-phenylenediamine (PPA), phenol, 1,1,2,2-tetrachloroethane and difunctional poly(ethylene glycol)s (M_n of 1000, 1500 and 2000 g/mol) were obtained from Aldrich (The Netherlands). Poly(propylene oxide)s endcapped with 20 wt.% ethylene oxide (EO) and a molecular weight of 2200, 4200 and 6300 g/mol were kindly provided by Bayer AG (Germany). Tetra-isopropyl orthotitanate ($Ti(i\text{-}OC_3H_7)_4$) was obtained from Aldrich and diluted (0.05 M) in *m*-xylene (Fluka, The Netherlands). Irganox® 1330 (1,3,5-trimethyl-2,4,6-tris(3,5-di-*t*-butyl-4-hydroxybenzyl)benzene) was obtained from CIBA Specialty Chemicals (The Netherlands). Methyl-(4-chlorocarbonyl)benzoate (MCCB) was obtained from Dalian (China). All chemicals were used as received. Pure gases were obtained from Praxair (The Netherlands) and used without further purification.

2.3.2 Polymer synthesis

⌐ *Synthesis of TΦT-dimethyl hard segment*
TΦT-dimethyl was used as hard segment and synthesized from MCCB and PPA following the procedure described by Niesten *et al.* (Route II) [17]. The structure of the monodisperse TΦT-dimethyl is shown in Figure 2.2.
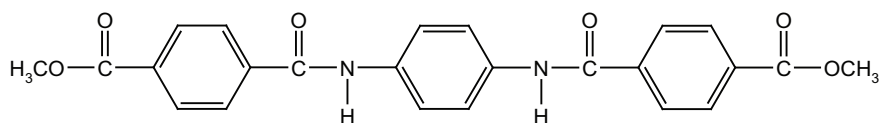
Figure 2.2: Chemical structure of TΦT-dimethyl di-amide hard segment.

⌐ *Synthesis of monodisperse segmented block copolymers*

Different monodisperse polyamide block copolymers were synthesized by a polycondensation reaction using PEO, PPO or a mixture of both soft segments and the prepared monodisperse TΦT-dimethyl di-amide hard segments as described elsewhere [15].

2.3.3 Analysis

⌐ *Viscometry*

Viscometry was used to examine the molecular weight of the synthesized polymers. The polymers were dissolved in a 1:1 (molar ratio) mixture of phenol/1,1,2,2-tetrachloroethane (0.1 g/dL) and the inherent viscosity (η_{inh}) of the solutions was determined at 25℃ using a capillary Ubbelohde type 0B [15].

⌐ *Differential Scanning Calorimetry (DSC)*

DSC was used to determine the melting and crystallization temperatures and enthalpies of the polyether block copolymers [15]. The melting enthalpies of the soft segment ($\Delta H_{m,s}$) and that of the hard segment ($\Delta H_{m,h}$) were determined from the endothermic peak areas of the second heating scan.

⌐ *Dynamic Mechanical Analysis (DMA)*

DMA was performed to determine the glass transition temperature (T_g), the flex temperature (T_{flex}) and the flow temperature (T_{flow}) as well as the storage modulus of the block polymers. A detailed description of the procedure can be found elsewhere [15].

⌐ *Fourier Transform Infrared (FT-IR)*

FT-IR was used to determine the crystallinity of the hard segment. Infrared spectra were obtained with a Biorad FTS-60 spectrometer with a resolution of 4 cm^{-1}. FT-IR spectroscopy was carried out at room temperature on samples prepared by adding a droplet of the block copolymer solution (1 g/L in 1,1,1,3,3,3-hexaflouroisopropanol (HFIP)) on a pressed KBr pellet. Further details relating to the exact determination of hard segment crystallinity can be found elsewhere [15].

2.3.4   Gas permeation

⌐ *Film formation*
Dense polymer films used for gas permeation experiments were prepared by hot pressing of dry polymer according to the procedure described earlier [11]. The films had a thickness of approximately 100 μm.

⌐ *Gas permeation*
Pure gas permeation properties of the prepared polyether based block copolymers were determined for N_2, O_2, He, H_2, CH_4 and CO_2 subsequently at different temperatures varying from -10℃ to 50℃. The experiments were performed following the constant volume, variable pressure method described in detail elsewhere [18].

2.4   Results & discussion

2.4.1   Thermal-mechanical properties

The thermal-mechanical properties (DSC, FT-IR and DMA) of the block copolymer systems studied in this article have been extensively described and discussed in a separate article [15]. For convenience and as a reference for discussions in this work Table A2.1 gives a summary of these data.

2.4.2   Effect of PEO soft segment length

⌐ *Influence of soft segment length on pure gas permeability & selectivity*
The synthesized PEO_x-TΦT block copolymers are considered to exhibit improved gas separation properties due to the increased crystallinity of the hard segment, improved phase separation and increased PEO contents, as proposed in Figure 2.1c. Gas permeation properties of these PEO based block copolymers are investigated in a temperature range from -10℃ to 50℃ and related to their thermal-mechanical properties. Due to the absence of a distinct crystalline hard phase in the block copolymer with a soft segment length of 2000 g/mol, this polymer has no mechanical stability and film formation and subsequent gas permeation analysis was not possible.

Table 2.1 summarizes the single gas permeabilities and the pure gas selectivities of CO_2 over H_2, N_2 and CH_4 at 35℃. At this temperature the soft PEO phase is fully amorphous in all block copolymers.

Table 2.1: Pure gas permeabilities and pure gas selectivities at 35℃ for PEO_x-TΦT block copolymers.

Polymer	TΦT	PEO	Gas permeability [Barrer]				Gas selectivity [–]		
	[wt.%]	[wt.%]	CO_2	H_2	N_2	CH_4	CO_2/H_2	CO_2/N_2	CO_2/CH_4
PEO_{1000}-TΦT	22.4	77.6	105	14.2	1.9	5.7	7.4	54.5	18.5
PEO_{1500}-TΦT	16.5	83.5	126	15.3	2.4	6.9	8.2	53.2	18.2

The CO_2 permeability (and of all other gases as well (not shown)) increases with increasing PEO soft segment length and its relative change increases with increasing kinetic diameter of the gas molecule (He, H_2, CO_2, O_2, N_2, CH_4). The increase in gas permeability is most likely caused by an increase in soft segment concentration, as the chain flexibility does not change with increasing soft segment chain length (as proven by DMA). Overall, there is no significant effect observed on the pure gas selectivities, and high CO_2/light gas selectivities are obtained due to the favorable interactions of CO_2 with the ether oxygen linkages in the polymer, resulting in high solubility selectivity.

⌐ *Influence of temperature on gas permeability*

The influence of the temperature on the CO_2 gas permeability of the PEO_x-TΦT block copolymers with a soft segment length of 1000 and 1500 g/mol is shown in Figure 2.3 (other gases show similar behavior).

The polymers show an increase in gas permeability with increasing temperature. In both cases two distinct regions can be distinguished due to the occurrence of crystallization of the soft PEO phase at a specific temperature, which results in a significant drop in permeability at temperatures below this crystallization temperature. The block copolymer containing PEO_{1500} as a soft segment shows a steep decrease in permeability below 20℃ due to the crystallization of PEO, forming a semi-crystalline PEO phase. This is in good agreement with the melting temperature of the PEO phase as found by DSC ($T_{m,PEO}$ = 27℃). This decrease in permeability is also observed for the PEO_{1000} containing block copolymer, but at a lower temperature (T ∼ −10℃, PEO_{1000} melting temperature is −8℃ as measured by DSC). The effect of PEO crystallization on gas permeability is more pronounced at higher soft segment lengths (stronger decrease) because PEO crystallinity increases with increasing soft segment length as shown by
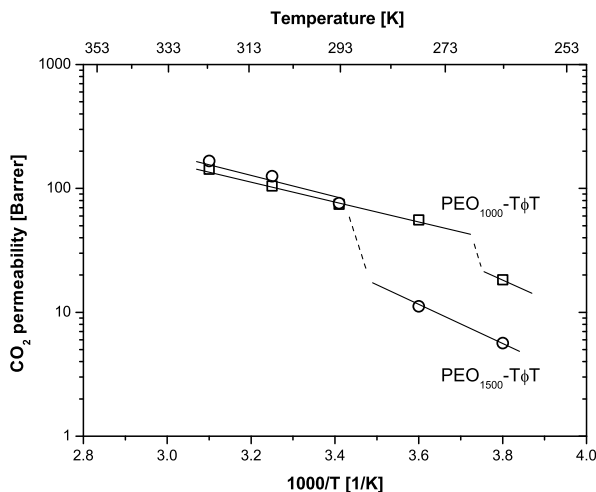
Figure 2.3: CO_2 permeability as a function of temperature for ($\square$) PEO_{1000}-TΦT and ($\bigcirc$) PEO_{1500}-TΦT.

an increase in melting enthalpy (as measured by DSC) of PEO from 14 J/g to 32 J/g for respectively the PEO_{1000} and PEO_{1500} block copolymer. In the fully amorphous state (higher temperature) the PEO_{1500}-TΦT block copolymer has a slightly higher CO_2 permeability than the PEO_{1000}-TΦT block copolymer as a result of the higher soft segment concentration. In the low temperature region (≤ 20℃) the opposite behavior is observed as the presence of a semi-crystalline PEO (as observed by DSC and DMA) severely restricts gas permeation especially for the PEO_{1500}-TΦT block copolymer.

⌐ *Influence of temperature on pure gas selectivity*
The effect of the temperature on the pure CO_2/light gas selectivity for H_2, N_2 and CH_4 is shown in Figure 2.4.

When the soft PEO phase is in a completely amorphous state (above 20℃, $1/T < 3.4$ K^{-1}), no differences are observed between the two different soft segment lengths, and the pure gas selectivities show a linear decrease with increasing temperature. The presence of a semi-crystalline phase at lower temperatures however reduces the gas permeability and influences the gas selectivity. Both polymers show a decrease in CO_2/H_2 selectivity below their PEO melting temperature ($T_m = 27$℃ and -8℃). This
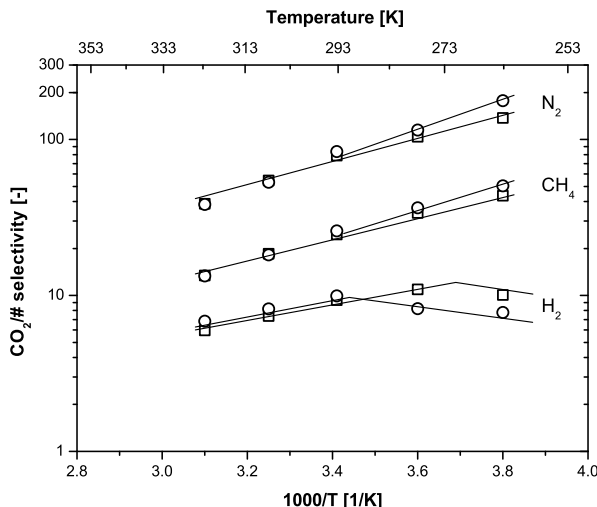
Figure 2.4: CO_2/light gas selectivity for H_2, N_2 and CH_4 as a function of temperature for (□) PEO_{1000}-TΦT and (○) PEO_{1500}-TΦT.

might be attributed to a more pronounced size-sieving ability of the block copolymer due to the formation of a semi-crystalline PEO phase decreasing diffusivity selectivity. Furthermore, at lower temperatures, also the contribution of the reverse-selective hard segment to the overall permeation behavior increases due to the increased crystallinity of the soft segment, further decreasing CO_2/H_2 selectivity. The selectivity of CO_2 over larger gases (e.g. N_2 and CH_4) shows the opposite behavior and the CO_2/N_2 and CO_2/CH_4 gas selectivity increases in the presence of a semi-crystalline PEO phase as a result of an increase in diffusivity selectivity. This effect can be clearly seen when the results of the PEO_{1000}-TΦT en PEO_{1500}-TΦT block copolymers below 20℃ are compared.

To evaluate the relation between the CO_2 permeability, CO_2/H_2 selectivity and the temperature, the CO_2/H_2 selectivity is presented as a function of the CO_2 permeability at different temperatures for PEO_x-TΦT block copolymers with a soft segment length of 1000 and 1500 g/mol in Figure 2.5.

The graphical representation of the relation between the CO_2 permeability and the CO_2 over H_2 selectivity shows the operating window of the PEO based block copolymer system presented in this work. In the presence of a fully amorphous PEO phase (at
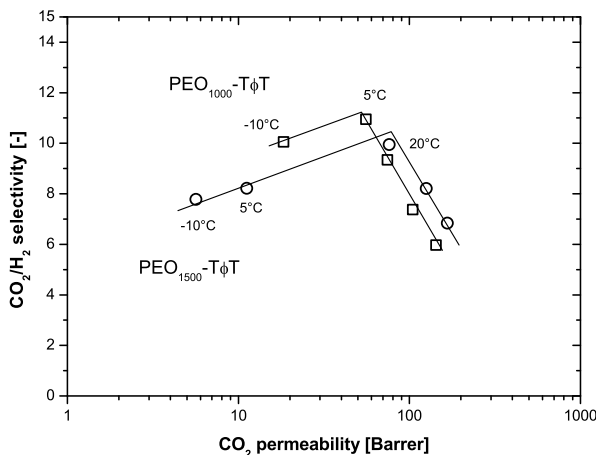
Figure 2.5: CO_2/H_2 selectivity as a function of CO_2 permeability and temperature for ($\square$) PEO_{1000}-TΦT and ($\bigcirc$) PEO_{1500}-TΦT.

higher temperatures) high permeabilities can be obtained and the PEO_{1500} block copolymer shows the highest CO_2 permeability, as discussed earlier. Upon the formation of a semi-crystalline PEO phase at lower temperatures, the CO_2/H_2 separation performance characteristics of the polymers decrease.

⌐ *Discussion*

As described earlier, block copolymers with improved gas permeation properties should exhibit

1. Good phase separation of the hard and soft segments;
2. Complete crystallization of the hard segment;
3. High PEO content;
4. Low glass transition temperature of the soft segment (high chain flexibility); and
5. No soft phase crystallinity or low soft segment melting temperature.

The use of the short monodisperse di-amide hard segments as presented in this work enabled us to prepare a block copolymer system with improved membrane gas separation performance characteristics due to the increased PEO content, while maintaining other properties. This resulted in a morphology schematically depicted in Figure 2.1c.

We compare the results of our study with the use of the longer tetra-amide hard segment as described by Husken *et al.* [11] and literature data on PEO based block copolymers [2, 6] (Figure 2.6). Although a direct quantitative comparison of the gas permeation properties proves to be difficult because many parameters, like soft segment concentration, soft/hard segment crystallinity and glass transition temperature change, a qualitative comparison can be made.

A comparison between PEO_{1000}-T6T6T with the longer hard segment ($\bullet$) and PEO_{1000}-TΦT with the short hard segment ($\blacksquare$) shows an increase in CO_2 permeability from 75 Barrer for the longer hard segment to 105 Barrer for the shorter hard segment. In this case the soft segment concentration changes from 62 wt.% (T6T6T, long segment) to 78 wt.% (TΦT, short segment) while maintaining reasonable high hard segment crystallinity. This proves that besides chain flexibility (property 4), which is mainly dependent on soft segment length, also the total soft segment concentration (property 3) is of importance. Furthermore, the necessity of good phase separation and complete crystallization of the hard segment (properties 1 and 2) becomes clear when the CO_2 permeability of PEO_{2000}-T6T6T (180 Barrer) and PEO_{1500}-TΦT (126 Barrer) are compared. Although PEO_{1500}-TΦT has a slightly
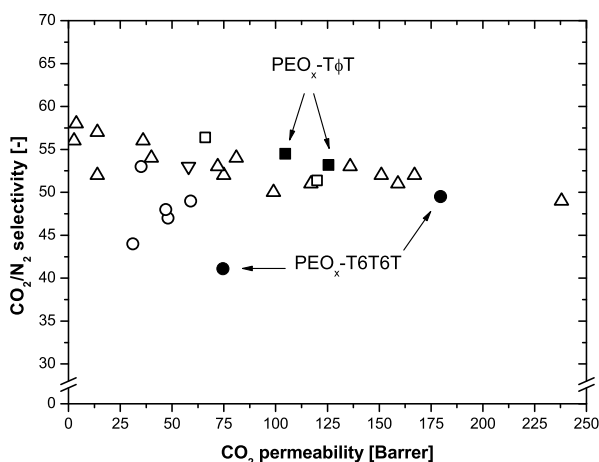
Figure 2.6: Comparison of CO_2 permeability vs. CO_2/N_2 selectivity of ($\blacksquare$) PEO_x-TΦT, ($\bullet$) PEO_x-T6T6T [11], ($\square$) PEBAX$^{\circledR}$ block copolymers [2], ($\bigcirc$) PEO-PU block copolymers [6], ($\triangle$) PEO-PI block copolymers [6] and a ($\bigtriangledown$) PEO-PA block copolymer [6].

shorter PEO soft segment length, its CO_2 gas permeability is remarkably lower than the value found for PEO_{2000}-T6T6T, despite a higher total soft segment concentration (84 wt.% instead of 76 wt.%). This can be explained from the lower hard segment crystallinity and less pronounced phase separation between the hard and soft segments, which results in a morphology where high amounts of non-crystallized hard segment are present in the soft amorphous phase restricting permeation of the gases (Figure 2.1a).

A comparison of our PEO_x-TΦT block copolymers with other PEO containing block copolymers is also shown in Figure 2.6 [2, 6]. Freeman *et al.* [2] and Okamoto *et al.* [6] state that the polarity of the hard segment influences the microdomain phase separation and thereby the gas separation performance. Okamoto *et al.* [6] investigated the thermal-mechanical properties and CO_2 gas separation performance of a series of PEO based block copolymers containing PU, PA and PI hard segments and found that the microdomain phase separation is strongly influenced by the type of hard segment. The degree of phase separation increased from PU<PA≪PI due to a decrease in intermolecular interaction (hydrogen bonding) between the hard and soft segments. Our polyamide based PEO_x-TΦT system (■) shows indeed higher CO_2 permeability compared to the PEO-PU based block copolymers (○) (better phase separation) and has a performance which coincides with an average PEO-PI based system (△). Freeman *et al.* investigated the commercially available PEBAX$^{®}$ block copolymers (□) (a PEO-PA) and found a reduction in gas permeability of almost 50% changing the hard segment from PA12 (120 Barrer) to the more polar PA6 (66 Barrer) at comparable soft segment concentration [2]. A PEO-PA block copolymer containing a similar type of hard segment compared to the TΦT di-amide has been reported by Okamoto *et al.* [6]. Their system (IPA-ODA/PEO3(80)) (▽) had a CO_2 permeability of 58 Barrer at a PEO concentration of 68 wt.%, which is approximately half of the maximum CO_2 permeability obtained for our system.

This indicates that although the phase separation behavior for our PEO-PA system is not fully optimal (especially at high soft segment length) due to the highly polar character of the short di-amide hard segment (compared to PA6 and PA12), a distinct improvement in gas separation performance has been achieved. The unique very short and monodisperse nature of the hard segment enabled us to incorporate high concentrations of soft segment resulting in increased CO_2 permeability at comparable selectivity (Figure 2.6) with much better defined block copolymer morphology.

2.4.3 Effect of soft segment type (PPO vs. PEO)

The gas permeation properties of the PPO based block copolymers are investigated in a temperature range from 5℃ to 50℃ and related to their thermal-mechanical properties as discussed and compared to the PEO_x-TΦT block copolymers. Films of the PPO_{6300} block copolymer could not be prepared due to the low storage modulus, causing too much shrinkage during film formation.

⌐ *Influence of soft segment length on pure gas permeability & selectivity*
Table 2.2 summarizes the single gas permeability and the pure gas selectivities of CO_2 over H_2, N_2 and CH_4 at 35℃.

Table 2.2: Pure gas permeabilities and pure gas selectivities at 35℃ for PPO_x-TΦT block copolymers.

Polymer	TΦT	PPO	Gas permeability [Barrer]				Gas selectivity [–]		
	[wt.%]	[wt.%]	CO_2	H_2	N_2	CH_4	CO_2/H_2	CO_2/N_2	CO_2/CH_4
PPO_{2200}-TΦT	12.1	70.3	418	68.3	15.8	52.4	6.1	26.5	8.0
PPO_{4200}-TΦT	6.8	74.6	520	84.3	20.5	69.5	6.2	25.4	7.5

The permeability of the PPO based block copolymers is a factor 4–5 higher than the permeability of the PEO based block copolymers. This can be attributed to the extra methyl side group in PPO compared to PEO, which prevents close chain packing (leading to soft phase crystallization), thus increasing the free volume and gas permeability [19]. The permeability of all gases increases with increasing soft segment length (and concentration) and its relative change increases with increasing kinetic diameter as already observed for PEO_x-TΦT block copolymers.

The CO_2/light gas selectivities are found to be independent of the soft segment length. Due to the introduction of PPO as a soft segment the CO_2/light gas selectivity for all investigated gas pairs is lowered compared to the PEO_x-TΦT block copolymers and the relative change in selectivity is different for each gas pair investigated. Due to a reduction in the polarity of the soft phase by replacing PEO with PPO the solubility of the quadrupolar CO_2 in the polymer matrix decreases, while the solubility of non-polar gases is much less influenced. Consequently, the CO_2/light gas solubility selectivity for the PPO based block copolymers is lower than that of the PEO based ones. Secondly, due to the increased free volume, diffusivity selectivity is altered as the diffusivity of larger molecules (like N_2 and CH_4) increases relatively more than the diffusivity of smaller gas molecules (like H_2) [20]. This change has a positive influence on the

CO_2/H_2 selectivity, as H_2 is smaller than CO_2, resulting in an increase in diffusivity selectivity partially counterbalancing the decrease in solubility selectivity. However, it has a negative influence on CO_2/N_2 and CO_2/CH_4 selectivity as N_2 and CH_4 are both larger than CO_2 thus decreasing diffusivity selectivity. As a consequence, the relative change in selectivity compared to the PEO_x-TΦT based block copolymers is the lowest for CO_2/H_2 (-21%) followed by CO_2/N_2 (-52%) and the highest for CO_2/CH_4 (-58%).

⌐ *Influence of temperature on gas permeability*

The influence of the temperature on the gas permeation properties of the PPO_x-TΦT block copolymers is shown in Figure 2.7. For comparison, the data for the PEO based block copolymers are also shown.

The PPO soft phase remains completely amorphous over the full temperature range investigated, independent of the segment length. Its lower polarity results in higher hard segment crystallinity and improved phase separation. Due to the absence of a semi-crystalline soft phase a linear relation between the CO_2 permeability and temperature is observed over the complete temperature range investigated (5–50℃). This results in extremely high permeable membranes with a much broader operating
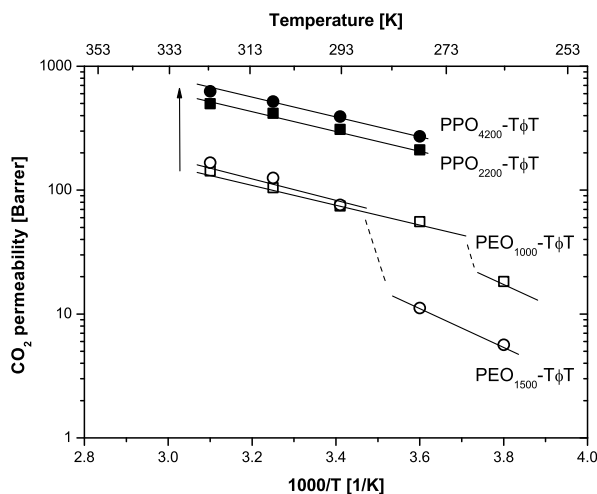
Figure 2.7: CO_2 permeability as a function of temperature for ($\blacksquare$) PPO$_{2200}$-TΦT, ($\bullet$) PPO$_{4200}$-TΦT, ($\square$) PEO$_{1000}$-TΦT and ($\bigcirc$) PEO$_{1500}$-TΦT.

window compared to the PEO_x-TΦT block copolymers, due to (1) higher soft segment concentration, (2) increased chain flexibility and (3) increased free volume originating from the methyl side group. The CO_2 permeability for the PPO_{4200}-TΦT block copolymer reaches values as high as 629 Barrer at 50℃ and maintains a high value of 272 Barrer at 5℃.

To conclude, two remarkable differences are observed between the PPO and PEO based membranes. A 4–5-fold increase in CO_2 permeability is observed when using PPO as a soft segment above a temperature of 20℃ in comparison to both PEO based membranes. This increase is mainly attributed to an enhancement of the diffusivity as discussed in the previous paragraph. Second, the drop in gas permeability of the PEO based block copolymers at its melting temperature is absent when PPO based block copolymers are considered. A 20–25-fold difference in CO_2 permeability is visible between the PPO based membranes and the PEO_{1500}-TΦT block copolymers at 5℃. Overall, the use of PPO as a soft segment avoids crystallization, thus improving membrane properties, in particular at lower temperatures.

⌐ *Influence of temperature on pure gas selectivity*
The effect of the temperature on the CO_2/light gas selectivity for H_2, N_2 and CH_4 is shown in Figure 2.8.

The present PPO based systems exhibit high CO_2 permeability with reasonable high CO_2/light gas selectivity. The CO_2/light gas selectivity is found to be independent of the soft segment length. More important, the pure gas selectivities show a linear decrease with temperature over the temperature range investigated, as the PPO phase remains completely amorphous.

⌐ *CO_2/H_2 separation*
The applicability of PPO_x-TΦT block copolymer membranes can be very promising at low temperatures, where the use of block copolymers with a semi-crystalline PEO soft phase results in reduced gas permeability. This is most evident for CO_2/H_2 separations. In this case the decrease in selectivity in the amorphous state is only 21%, while the increase in CO_2 permeability is around 400%. To demonstrate the applicability of PPO_x-TΦT block copolymer membranes for (especially low temperature) CO_2/H_2 separation, the CO_2/H_2 selectivity is presented as a function of the CO_2 permeability and temperature in Figure 2.9. For comparison, the results for PEO_x-TΦT are also shown.
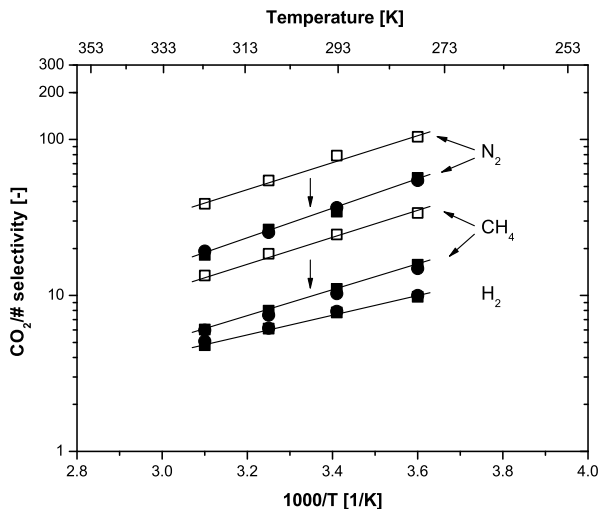
Figure 2.8: CO_2/light gas selectivity as a function of temperature for ($\blacksquare$) PPO_{2200}-TΦT, ($\bullet$) PPO_{4200}-TΦT and ($\square$) PEO_{1000}-TΦT (CO_2/H_2 selectivity of PEO_{1000}-TΦT is not shown for clarity as it almost overlaps with the PPO_x-TΦT block copolymers).
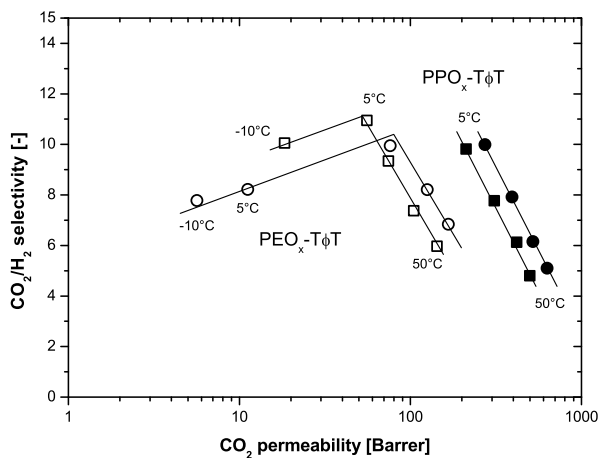
Figure 2.9: CO_2/H_2 selectivity as a function of CO_2 permeability for ($\blacksquare$) PPO_{2200}-TΦT, ($\bullet$) PPO_{4200}-TΦT, ($\square$) PEO_{1000}-TΦT and ($\bigcirc$) PEO_{1500}-TΦT.

When the performance of the PPO_x-TΦT block copolymers is compared to the PEO_x-TΦT block copolymers at temperatures where a fully amorphous PEO soft phase is present (50℃), the CO_2/H_2 selectivity is only slightly lowered, while a much higher CO_2 permeability is achieved (more than 300% increase). In the temperature region where a semi-crystalline PEO soft phase is present the PPO based block copolymers outperform the PEO based block copolymers on permeability as well as selectivity for CO_2/H_2 separation offering a high potential for future applications.

2.4.4 Effect of a mixture of PEO_{2000} and PPO_{2200} soft segments

The gas permeation properties of block copolymers based on a mixture of PEO_{2000} and PPO_{2200} soft segments are investigated in a temperature range from $-10℃$ to 50℃. The influence of the soft segment composition on the gas permeation properties is investigated and the information obtained by DSC, IR and DMA is used to explain the gas separation performance data. Due to the absence of a distinctive crystalline hard phase, the block copolymer containing 100 mol% PEO_{2000} as a soft phase has insufficient mechanical stability and film formation is not possible as discussed before. Therefore, data from PEO_{1500}-TΦT ($M_{w,PEO} = 1500$ g/mol) are taken as a reference for a 100 mol% PEO soft phase.

⌐ *Effect of soft segment composition*
The influence of the soft segment composition (mol% PEO) is evaluated at a temperature of 35℃. At that temperature (and at all temperatures above this value) the PEO phase is fully amorphous in all block copolymer systems. Figure 2.10 gives a graphical representation of the N_2, CH_4, H_2 and CO_2 permeability as a function of the PEO content in the mixed PEO/PPO soft phase.

The permeability of all gases in the PEO_{2000}/PPO_{2200}-TΦT block copolymers decreases linearly when the PEO content is increased (similar results are obtained at 50℃ but not shown). A similar trend has been observed by Patel *et al.* [21, 22] who investigated the CO_2 transport through crosslinked polyether membranes using a mixture of poly(ethyleneglycol diacrylate) (PEGDA) and poly(propyleneglycol diacrylate) (PPGDA). The decrease in gas permeability with increasing PEO content is most likely caused by a decrease is free volume with increasing PEO content. With increasing PEO content, the relative amount of PPO, which has bulky side groups that can contribute to an increased free volume in the polymer, decreases as well.
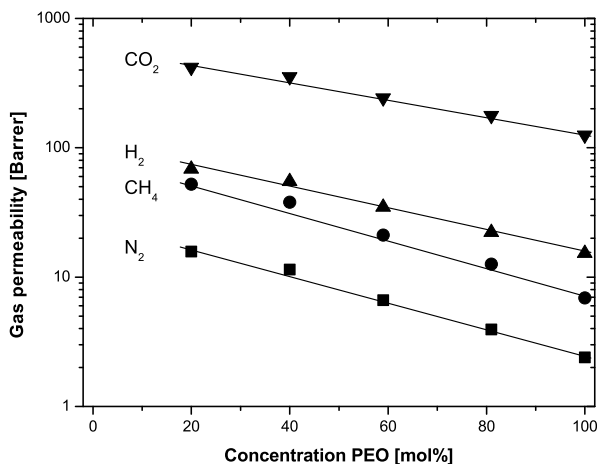
Figure 2.10: Gas permeability at 35℃ for ($\blacktriangledown$) CO_2, ($\blacktriangle$) H_2, ($\blacksquare$) N_2 and ($\bullet$) CH_4 as a function of PEO content in the polyether-TΦT block copolymers containing a mixture of PEO_{2000} and PPO_{2200} soft segments.

This hypothesis is supported by Freeman *et al.*, who investigated the relationship between the free volume and the gas permeability in crosslinked networks of PEGDA (polyethylene based) and PPGDA (polypropylene based). They found significantly higher free volume in the PPGDA based networks accompanied by corresponding higher permeability values [19, 23, 24].

The CO_2/light gas selectivity at 35℃ for H_2, N_2 and CH_4 as a function of the PEO content in the soft phase containing a mixture of PEO_{2000} and PPO_{2200} soft segments is presented in Figure 2.11.

The selectivity for all the three gas pairs increases linearly with increasing PEO content. The selectivity of these block copolymers is mainly based on solubility selectivity, due to favorable interactions of the polar ether oxygen linkages with the quadrupolar CO_2. Substitution of PPO for the more polar PEO increases the polarity of the soft phase. Consequently, especially the interaction of the polymer with CO_2 increases, resulting in an increase in solubility selectivity, while the diffusivity selectivity is only marginally influenced, because the diffusivity of both CO_2 and the light gases is influenced by an increase in free volume. The CO_2/light gas selectivity thus increases with increasing PEO content. The selectivity of CO_2 over N_2 has the highest value as solubility as well as diffusivity of N_2 is relatively low in comparison to H_2 and CH_4. H_2, which is
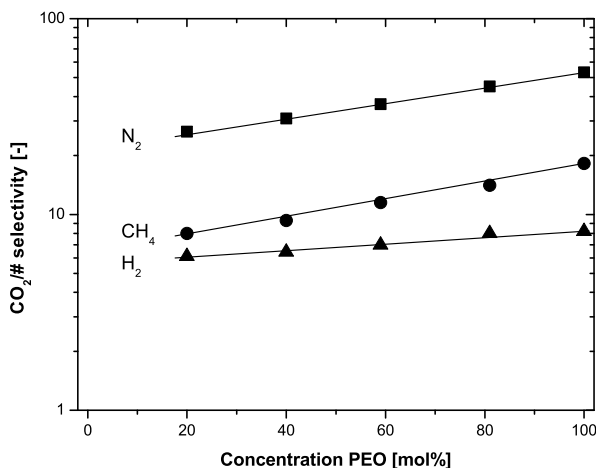
Figure 2.11: CO_2/light gas selectivity at 35℃ for (▲) H_2, (■) N_2 and (●) CH_4 as a function of PEO content in the polyether-TΦT block copolymers containing a mixture of PEO_{2000} and PPO_{2200} soft segments.

the smallest molecule of the three, has a much smaller kinetic diameter resulting in more favorable diffusion, while CH_4 has a higher condensability and thus solubility, which reduces the selectivity compared to N_2 [16].

⌐ *Membrane performance as a function of temperature*
The influence of the temperature on the CO_2 permeability of the block copolymers with a soft phase consisting of a mixture of PEO_{2000} and PPO_{2200} soft segments and TΦT as hard segment is shown in Figure 2.12.

The block copolymers with ≤ 40 mol% of PEO soft phase are fully amorphous over the temperature range investigated as shown by DSC and DMA, and show a linear relationship between the CO_2 permeability and the temperature over the full temperature range investigated (no discontinuity is observed). Different behavior is observed for the block copolymers containing 59 and 81 mol% PEO, which do show a discontinuity in CO_2 permeability with increasing PEO content. DSC and DMA indicate low (59 mol% PEO) and significant (81% mol% PEO) amounts of PEO crystallinity at lower temperatures, which is reflected in the temperature dependency of the CO_2 permeability of these polymers as well. As confirmed by DSC and DMA analysis, this discontinuity is in both cases observed at the melting temperature

37
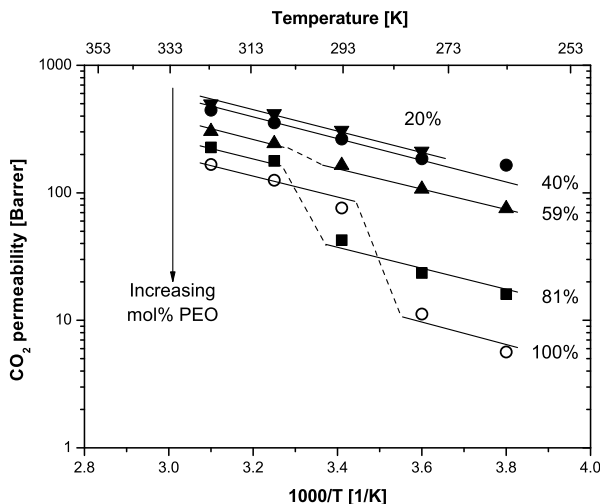
Figure 2.12: CO$_2$ permeability as a function of temperature for block copolymers with a soft phase consisting of a mixture of PEO$_{2000}$ and PPO$_{2200}$ soft segments and TΦT as a hard segment with ($\blacktriangledown$) 20 mol%, ($\bullet$) 40 mol%, ($\blacktriangle$) 59 mol% and ($\blacksquare$) 81 mol% PEO soft phase. The PEO$_{1500}$-TΦT ($\circ$) is given as a reference for a block copolymer containing 100 mol% PEO.

of the soft phase, i.e. at ~26℃ for the block copolymer containing 59 mol% PEO and at ~32℃ for the block copolymer containing 81 mol% PEO. This discontinuity significantly limits the operating window of these PEO/PPO based membranes for application in gas separation. Based on these results, a PPO content of at least 41 mol% of PPO is required to reduce PEO crystallinity in the soft phase sufficiently to maintain gas permeation properties.

The effect of the temperature on the pure gas selectivity of PEO$_{2000}$/PPO$_{2200}$-TΦT block copolymers containing a 100% pure PEO or PPO soft phase is discussed in the previous two sections. The use of a mixture of PEO and PPO results in intermediate pure gas selectivities. The linear relation between the gas selectivity and the composition of the soft phase (as shown for 35℃ in Figure 2.11) can be expanded to the complete temperature range investigated as long as the soft phase is fully amorphous. A semi-crystalline PEO phase leads to deviation from this linear behavior as demonstrated for PEO$_x$-TΦT block copolymers; a decrease in CO$_2$/H$_2$ selectivity and an increase in CO$_2$/N$_2$ and CO$_2$/CH$_4$ selectivity is observed in that case.

To demonstrate the effectiveness of PPO to suppress PEO crystallization and to identify the operating window of the block copolymers based on a mixture of PEO_{2000} and PPO_{2200} soft segments used in this study, the CO_2/light gas selectivity as a function of the CO_2 permeability for the different PEO_{2000}/PPO_{2200}-TΦT block copolymers investigated (40, 59 and 81 mol% PEO) is summarized in Figure 2.13. Higher CO_2 permeabilities represent higher temperatures (increasing from -10℃ to 50℃ in 15℃ steps).

The block copolymer containing 40 mol% PEO does not show crystallization in the temperature range investigated and a linear relationship between the CO_2/light gas selectivity and the CO_2 permeability is observed. It combines high CO_2 permeability with high CO_2/light gas selectivity, especially at low temperatures. At a PEO content $\geq$ 59 mol% PEO, PEO crystallization does play a role. A steep decrease in CO_2 permeability below the PEO melting temperature is observed, which becomes more pronounced at higher PEO/PPO ratios (81 mol% PEO) due to higher PEO crystallinity. The transition between a fully amorphous and a semi-crystalline soft phase is observed
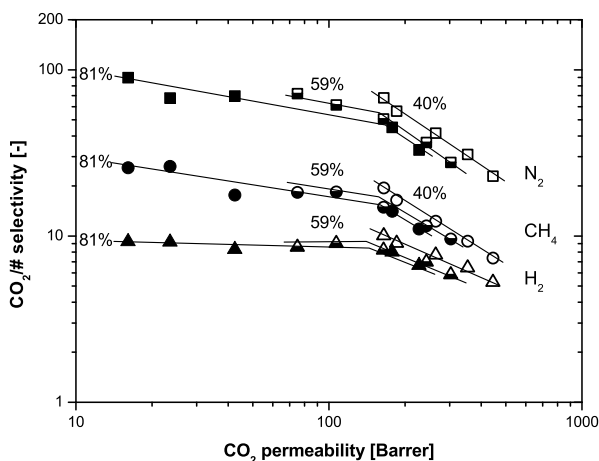
Figure 2.13: CO_2/light gas selectivity as a function of CO_2 permeability for H_2 (triangles), CH_4 (circles), and N_2 (squares) for block copolymers with a soft phase consisting of a mixture of PEO_{2000} and PPO_{2200} soft segments and TΦT as a hard segment as a function of the PEO content for 40 mol% PEO (open symbols), 59 mol% (partially filled symbols) and 81 mol% PEO (closed symbols). Higher CO_2 permeability represents higher temperature (increasing from -10℃ to 50℃ in 15℃ steps).

as a bend in the graph and occurs at ∼20℃ and ∼35℃ for the block copolymer containing respectively 59 and 81 mol% PEO.

The results show the existence of a delicate balance between membrane permeability, selectivity and polymer structure at the microdomain scale. Proper selection and tuning of the polymer on the micro scale, improves the performance of the membrane at the macro scale. Thus, the composition of the block copolymer needs to be carefully chosen, depending on the operating temperature of the process, to obtain optimal CO_2/light gas separation characteristics. Higher amounts of PPO in the block copolymer are especially beneficial at temperatures below the PEO melting temperature. This not only prevents PEO crystallization but also increases the CO_2 permeability at an only modest decrease in selectivity.

⌐ *Membrane performance compared to other polyether based systems*
In the last section of this article we have combined the benefits of PEO (high selectivity) with those of PPO (high permeability, amorphous) by using a mixture of PEO_{2000} and PPO_{2200} soft segments in a block copolymer system to tailor the mass transport properties of macromolecular structures. Figure 2.14 shows a Robeson trade-off curve of all the polyether based block copolymers described in this article and compares them with similar polyether based (block copolymer) systems described in literature.

The comparison of the PEO_x-TΦT block copolymers with literature data on PEO based block copolymer systems has been discussed in the corresponding section. Most remarkable is the fact that higher gas permeability has been observed compared to the commercially available PEBAX® family at comparable selectivity. Furthermore, if the comparison is expanded and crosslinked, pure networks of poly(ethylene oxide) diacrylates are included as well, the PEO block copolymer systems presented in our work have very similar gas permeability values at comparable selectivity [23–25].

Literature data on PPO or mixed polyether based (block copolymer) systems are scarce. Gas permeation data on block copolymers containing pure PPO as a soft segment have, to the best of our knowledge, not been reported previously. Patel *et al.* [21, 22] studied crosslinked mixed polyether networks based on PEG-diacrylate and PPG-diacrylate, but only reported gas transport properties for CO_2 and H_2. The CO_2 permeability at 35℃ ranged from 100 Barrer (100% PEGDA) to 180 Barrer (100% PPGDA), while CO_2/H_2 selectivity ranged from 9 (100% PEGDA) to 4 (100% PPGDA). Freeman *et al.* studied crosslinked networks of PPGDA and PPG-methyl ether acrylate (PPGMEA) and their system exhibit a CO_2 permeability of 160 Barrer

at 100% PPGDA content [19]. In general, the PPO based systems show higher CO_2 permeability at the cost of lower selectivity following the permeability/selectivity trade-off relationship described by Robeson [26]. The maximum CO_2 permeability obtained for pure PPO based systems based on difunctional monomers is less than 200 Barrer as described above. The polyether block copolymer system presented in our work, which is based on monodisperse di-amide hard segments, exceeds this value and CO_2 permeabilities up to 520 Barrer (PPO_{4200}-TΦT) can be obtained (a 3-fold increase) at comparable selectivity. Moreover, the permeability/selectivity balance can be tuned towards specific applications by clever design of the soft phase using a mixture of PEO and PPO soft segments maintaining the advantage on the previously reported systems due to the very well-defined block copolymer morphology.
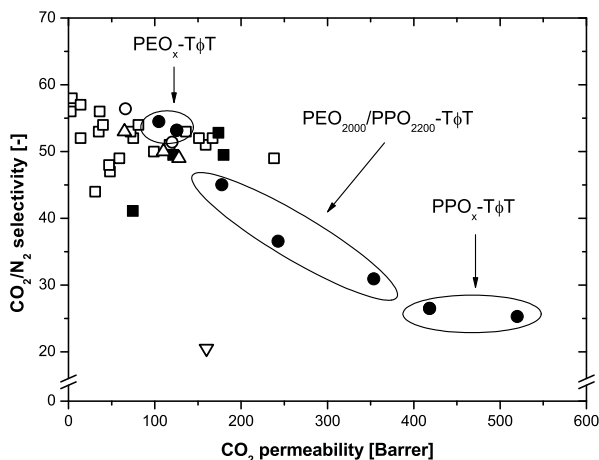
Figure 2.14: CO_2/N_2 selectivity as a function of CO_2 permeability at 35℃ for (■) PEO based block copolymers with monodisperse long T6T6T hard segments as described by Husken *et al.* [11] and (●) PEO_x, PPO_x or mixtures of PEO_{2000} and PPO_{2200} based block copolymers with monodisperse short hard segment (TΦT), as used in this article compared with (□) PEO based block copolymers [6], (○) commercially available PEBAX® [2], (△) pure PEO di(meth)acrylate crosslinked networks [23–25] and (▽) pure PPO diacrylate networks [19], as described in literature.

2.5   Conclusions

Polyether based segmented block copolymers with improved gas separation properties were synthesized using poly(ethylene oxide) (PEO) and/or poly(propylene oxide) (PPO) as soft segment and monodisperse di-amide (TΦT) as hard segment. It allowed us to incorporate higher concentrations of soft segment compared to a system using longer tetra-amide (T6T6T) hard segments, while maintaining sufficient mechanical stability. The influence of the soft segment type and length on the CO_2 permeability and CO_2/light gas selectivity was investigated in relation to their thermal-mechanical properties.

For a PEO based system improved permeation properties were observed at short soft segment lengths (1000 g/mol) due to an increase in total soft segment concentration. Higher soft segment lengths (1500 g/mol) resulted in lower hard segment crystallinity and less efficient phase separation with subsequent lower gas permeability. In addition, the permeability and selectivity of the gases was strongly affected by the presence of a semi-crystalline PEO phase at temperatures below the PEO melting temperature. Below this temperature gas permeability decreased significantly along with the CO_2/H_2 selectivity, while CO_2/N_2 and CO_2/CH_4 selectivity increased. The PPO based system showed higher gas permeability mainly due to an increase in free volume at slightly lower selectivity as a result of the reduced polarity of the soft phase. As the PPO soft phase remains completely amorphous over the entire temperature range investigated a linear correlation between temperature and permeability/selectivity was observed. Gas permeation properties of this block copolymer system could be further tuned by using a mixture of PEO and PPO soft segments. Intermediate gas permeabilities and selectivities could be obtained and the PPO has been proven successful in the suppression of PEO crystallization.

Comparison of the gas separation performance with similar systems described in literature showed the advantage of the well-defined block copolymer morphology. The present work clearly shows that the use of polyether based segmented block copolymers using monodisperse hard segments offers a very versatile tool to tailor mass transfer and separation properties of membranes for gas and vapor separations.

2.6   Acknowledgements

Chapter 2

2.7 References

[1] V. I. BONDAR, B. D. FREEMAN AND I. PINNAU; *Gas sorption and characterization of poly(ether-b-amide) segmented block copolymers*; Journal of Polymer Science, Part B: Polymer Physics **37** (17) (1999) 2463–2475; DOI: 10.1002/(SICI)1099-0488(19990901)37:17⟨2463::AID-POLB18⟩3.0.CO;2-H

[2] V. I. BONDAR, B. D. FREEMAN AND I. PINNAU; *Gas transport properties of poly(ether-b-amide) segmented block copolymers*; Journal of Polymer Science, Part B: Polymer Physics **38** (15) (2000) 2051–2062; DOI:10.1002/1099-0488(20000801) 38:15⟨2051::AID-POLB100⟩3.0.CO;2-D

[3] J. H. KIM, S. Y. HA AND Y. M. LEE; *Gas permeation of poly(amide-6-b-ethylene oxide) copolymer*; Journal of Membrane Science **190** (2) (2001) 179–193; DOI:10.1016/S0376-7388(01)00444-6

[4] V. BARBI, S. S. FUNARI, R. GEHRKE, N. SCHARNAGL AND N. STRIBECK; *SAXS and the gas transport in polyether-block-polyamide copolymer membranes*; Macromolecules **36** (3) (2003) 749–758; DOI:10.1021/ma0213403

[5] K.-I. OKAMOTO, M. FUJII, S. OKAMYO, H. SUZUKI, K. TANAKA AND H. KITA; *Gas permeation properties of poly(ether imide) segmented copolymers*; Macromolecules **28** (20) (1995) 6950–6956; DOI:10.1021/ma00124a035

[6] M. YOSHINO, K. ITO, H. KITA AND K.-I. OKAMOTO; *Effects of hard-segment polymers on CO_2/N_2 gas-separation properties of poly(ethylene oxide)-segmented copolymers*; Journal of Polymer Science, Part B: Polymer Physics **38** (13) (2000) 1707–1715; DOI:10.1002/1099-0488(20000701)38:13⟨1707::AID-POLB40⟩3.0.CO; 2-W

[7] S. J. METZ, M. H. V. MULDER AND M. WESSLING; *Gas-permeation properties of poly(ethylene oxide) poly(butylene terephthalate) block copolymers*; Macromolecules **37** (12) (2004) 4590–4597; DOI:10.1021/ma049847w

[8] A. CAR, C. STROPNIK, W. YAVE AND K. V. PEINEMANN; *PEG modified poly(amide-b-ethylene oxide) membranes for CO_2 separation*; Journal of Membrane Science **307** (1) (2008) 88–95; DOI:10.1016/j.memsci.2007.09.023

[9] A. CAR, C. STROPNIK, W. YAVE AND K. V. PEINEMANN; *Pebax®/polyethylene glycol blend thin film composite membranes for CO_2 separation: Performance with mixed gases*; Separation and Purification Technology **62** (1) (2008) 110–117; DOI:10.1016/j.seppur.2008.01.001

[10] A. CAR, C. STROPNIK, W. YAVE AND K. V. PEINEMANN; *Tailor-made polymeric*

Chapter 2

membranes based on segmented block copolymers for CO_2 separation; Advanced Functional Materials **18** (18) (2008) 2815–2823; DOI:10.1002/adfm.200800436

[11] D. Husken, T. Visser, M. Wessling and R. J. Gaymans; *CO_2 permeation properties of poly(ethylene oxide)-based segmented block copolymers*; Journal of Membrane Science **346** (1) (2010) 194–201; DOI:10.1016/j.memsci.2009.09.034

[12] G. Holden, H. R. Kricheldorf and R. P. Quirk; *Thermoplastic Elastomers*; 3rd edition (2004); Munich (Germany): Hanser Gardner Publications; ISBN 978-1569903643

[13] D. Husken, J. Feijen and R. J. Gaymans; *Hydrophilic segmented block copolymers based on poly(ethylene oxide) and monodisperse amide segments*; Journal of Polymer Science, Part A: Polymer Chemistry **45** (19) (2007) 4522–4535; DOI:10.1002/pola.22186

[14] D. Husken, J. Feijen and R. J. Gaymans; *Segmented block copolymers with terephthalic-extended poly(ethylene oxide) segments*; Macromolecular Chemistry and Physics **209** (5) (2008) 525–534; DOI:10.1002/macp.200700288

[15] A. Arun and R. J. Gaymans; *Hydrophilic poly(ethylene oxide)-aramide segmented block copolymers*; European Polymer Journal **45** (10) (2009) 2858–2866; DOI:10.1016/j.eurpolymj.2009.07.002

[16] M. Mulder; *Basic Principles of Membrane Technology*; 2nd edition (1996); Dordrecht (The Netherlands): Kluwer Academic Publishers; ISBN 978-0792342489

[17] M. C. E. J. Niesten, J. Feijen and R. J. Gaymans; *Synthesis and properties of segmented copolymers having aramid units of uniform length*; Polymer **41** (24) (2000) 8487–8500; DOI:10.1016/S0032-3861(00)00252-4

[18] A. Bos, I. G. M. Punt, M. Wessling and H. Strathmann; *Suppression of CO_2-plasticization by semiinterpenetrating polymer network formation*; Journal of Polymer Science, Part B: Polymer Physics **36** (9) (1998) 1547–1556; DOI: 10.1002/(SICI)1099-0488(19980715)36:9⟨1547::AID-POLB12⟩3.0.CO;2-5

[19] R. D. Raharjo, H. Lin, D. F. Sanders, B. D. Freeman, S. Kalakkunnath and D. S. Kalika; *Relation between network structure and gas transport in crosslinked poly(propylene glycol diacrylate)*; Journal of Membrane Science **283** (1-2) (2006) 253–265; DOI:10.1016/j.memsci.2006.06.038

[20] Y. Yampolskii, I. Pinnau and B. D. Freeman; *Materials Science of Membranes for Gas and Vapor Separation*; 1st edition (2006); West Sussex (England): John Wiley & Sons Ltd.; ISBN 978-0470853450

[21] N. P. Patel, M. A. Hunt, S. Lin-Gibson, S. Bencherif and R. J. Spontak; *Tunable CO_2 transport through mixed polyether membranes*; Journal of Membrane

Science **251** (1-2) (2005) 51–57; DOI:10.1016/j.memsci.2004.11.003

[22] N. P. Patel, C. M. Aberg, A. M. Sanchez, M. D. Capracotta, J. D. Martin and R. J. Spontak; *Morphological, mechanical and gas-transport characteristics of crosslinked poly(propylene glycol): Homopolymers, nanocomposites and blends*; Polymer **45** (17) (2004) 5941–5950; DOI:10.1016/j.polymer.2004.06.024

[23] H. Lin, T. Kai, B. D. Freeman, S. Kalakkunnath and D. S. Kalika; *The effect of crosslinking on gas permeability in crosslinked poly(ethylene glycol diacrylate)*; Macromolecules **38** (20) (2005) 8381–8393; DOI:10.1021/ma0510136

[24] H. Lin, E. van Wagner, J. S. Swinnea, B. D. Freeman, S. J. Pas, A. J. Hill, S. Kalakkunnath and D. S. Kalika; *Transport and structural characteristics of crosslinked poly(ethylene oxide) rubbers*; Journal of Membrane Science **276** (1-2) (2006) 145–161; DOI:10.1016/j.memsci.2005.09.040

[25] Y. Hirayama, Y. Kase, N. Tanihara, Y. Sumiyama, Y. Kusuki and K. Haraya; *Permeation properties to CO_2 and N_2 of poly(ethylene oxide)-containing and crosslinked polymer films*; Journal of Membrane Science **160** (1) (1999) 87–99; DOI:10.1016/S0376-7388(99)00080-0

[26] L. M. Robeson; *Correlation of separation factor versus permeability for polymeric membranes*; Journal of Membrane Science **62** (2) (1991) 165–185; DOI:10.1016/0376-7388(91)80060-J

Appendix

Table A2.1: Thermal-mechanical properties of polyether-TΦT block copolymers [15].

Polymer	PEO/PPO	TΦT	Soft segment		η_{inh}	DSC						DMA			FT-IR
			PEO	PEO		$T_{m,s}$	$\Delta H_{m,s}$	$T_{m,h}$	$\Delta H_{m,h}$	T_g	T_{flex}	$T_{m,TΦT}$	$G'(20°C)$	$G'(50°C)$	
	[mol ratio]	[wt.%]	[wt.%]	[mol%]	[dL/g]	[°C]	[J/g]	[°C]	[J/g]	[°C]	[°C]	[°C]	[MPa]	[MPa]	[%]
PEO$_{1000}$	100/0	22.4	77.6	100	1.4	−8	14	120	33	−42	−19	145	29	28	67
PEO$_{1500}$	100/0	16.5	83.5	100	1.5	27	32	na	na	−38	25	100	14	5	41
PEO$_{2000}$	100/0	13.1	86.9	100	2.0	35	64	na	na	−41	35	70	79	1	21
PEO$_{2000}$/PPO$_{2200}$	75/25	12.8	69.8	81	1.6	32	64	96	4	−45	35	105	46	6	25
	50/50	12.6	52.4	59	1.7	26	26	111	13	−52	35	115	10	5	33
	25/75	12.4	34.9	40	1.6	-	-	123	28	−60	10	135	9	8	57
PPO$_{2200}$	0/100	12.1	17.6	20	1.0	-	-	135	49	−59	−47	140	9	10	81
PPO$_{4200}$	0/100	6.8	18.6	20	1.12	-	-	na	na	−59	−48	100	3	3	59
PPO$_{6300}$	0/100	4.7	20.9	20	na	-	-	na	na	−48	−45	75	1	1	40

Chapter 2

CHAPTER 3

Poly(ethylene oxide) based block copolymers with exceptionally low soft phase melting temperature and crystallinity

Abstract

Segmented block copolymers based on novel PEO based flexible, soft segments and monodisperse crystallizable tetra-amide (T6T6T) hard segments have been synthesized. The soft segment was a random copolymer of PEO and PPO containing 75 wt.% PEO and 25 wt.% PPO, where the random distribution of PPO was expected to suppress the PEO crystallization observed in neat PEO based block copolymers. We hypothesize this approach to be particularly beneficial for mass transport applications. The total soft segment length was varied between 1000 and 10000 g/mol. The use of monodisperse hard segments resulted in fast and almost complete ($> 80\%$) crystallization of these segments and this led to a well-defined microdomain morphology. The thermal-mechanical properties of the synthesized polymers have been extensively investigated using DMA and DSC. The PEO melting temperature and crystallinity could be tremendously decreased and a PEO melting temperature below 0℃ has been obtained at all soft segment lengths. The low PEO melting temperature and crystallinity give the block copolymers good low temperature flexibility, especially at high soft segment lengths.

3.1 Introduction

Thermoplastic elastomers (TPE) are polymers that are elastic at their service temperature and can be melt processed at elevated temperatures. The difference with conventional, chemically crosslinked, elastomers is that they are physically crosslinked, the crosslinking is reversible and the materials are soluble in selected organic solvents. These materials are commonly produced by chemically combining a hard and a soft segment, obtaining a segmented block copolymer [1]. The different segments used usually differ in their chemical nature and material properties and the ultimate properties of the TPE are determined by the combination of the two. Usually polyethers are used as a soft segment to provide the material a low glass transition temperature, while the hard segment exists of a urethane, ester or amide which is able to crystallize, acting as physical crosslinks reinforcing the amorphous matrix. The used hard and soft segments are thermodynamically immiscible, which induces phase separation through liquid-liquid demixing or crystallization.

In literature several segmented block copolymers based on flexible poly(ethylene oxide) (PEO) soft segments and amide [2–11], urethane [6], ester [12, 13] and imide [14] types of hard segments are reported. These hydrophilic PEO based block copolymers, in particular the commercially available PEBAX® series, are used for breathable film applications (for instance in sport clothing and food packaging) [15], medical applications [15] and gas separation membranes [2–5, 7, 8]. These PEO based materials are especially interesting for CO_2/light gas separation applications [16], since the polar ether oxygens interact favorably with the quadrupolar CO_2, resulting in high solubility selectivity. Furthermore, the flexible PEO soft segment permits high diffusivity and together they combine a high permeability with a reasonable high selectivity.

It has been demonstrated that the mass transport through these block copolymer systems is mainly determined by the soft phase as the pure CO_2/N_2 selectivity (the most frequently studied gas pair) is fairly similar for all these materials [16]. The overall mass transport rate however, changes significantly with the type of hard segment and the molecular weight of the hard and soft segments used. This shows that the microdomain morphology of the specific block copolymer system has a significant effect on the mass transport of these block copolymer systems.

In most block copolymer systems reported to date, the phase separation between the hard and soft segments is incomplete (non-ideal) and the hard phase is (partially)

miscible with the soft phase. The dissolution of the hard segments in the soft phase has a large effect on the physical properties of the soft phase (for instance the T_g) leading to very diverse mass transport properties, as reviewed by Freeman *et al.* [16]. Effective mass transport through these block copolymer systems requires the control over the microdomain morphology. The relationship between microdomain morphology and mass transport properties has been recently discussed by Husken *et al.* [17] and in our previous work [11]. Block copolymers with improved mass transport properties should have the following characteristics:

1. Good phase separation of the hard and soft segments;
2. Complete crystallization of the hard segment;
3. High PEO content;
4. Low glass transition temperature of the soft segment (high chain flexibility); and
5. No soft phase crystallinity or low soft segment melting temperature.

In general, (commercially available) block copolymers suffer from incomplete phase separation (non-ideal) as the crystallinity of the hard segments is usually low ($\sim$30%) (Figure 3.1a). The crystallization of the hard segments can be improved by using monodisperse hard segments [18, 19]. Block copolymers with these monodisperse hard segments crystallize fast and almost complete (85%) (Figure 3.1b, c) and therefore virtually no amorphous hard segments are present in the amorphous soft phase (ideal morphology). Low concentrations of hard segment can consequently be used to maintain sufficient mechanical properties. The synthesis and mass transport properties of PEO based block copolymers containing such monodisperse tetra-amide (T6T6T) [9, 17] and di-amide (TΦT) [11, 20] hard segments has been previously studied.

To obtain high mass transport rates, high PEO concentrations and segment lengths are beneficial [12] as the mass transport preferentially takes place through the amorphous PEO soft phase. However, PEO is known for its very regular structure and its ease to crystallize, creating a semi-crystalline soft phase severely reducing mass transport [11, 12, 17, 21]. In general, as the length of the PEO soft segments is sufficiently long, crystallization easily occurs, creating an extra crystalline phase with a low melting temperature in the in the soft segment phase of the block copolymer. This PEO melting temperature and enthalpy were found to increase with PEO soft segment length [9, 11, 12].

To obtain high mass transport rates at relevant working temperatures in PEO based block copolymer systems, the absence of a semi-crystalline PEO soft phase at room
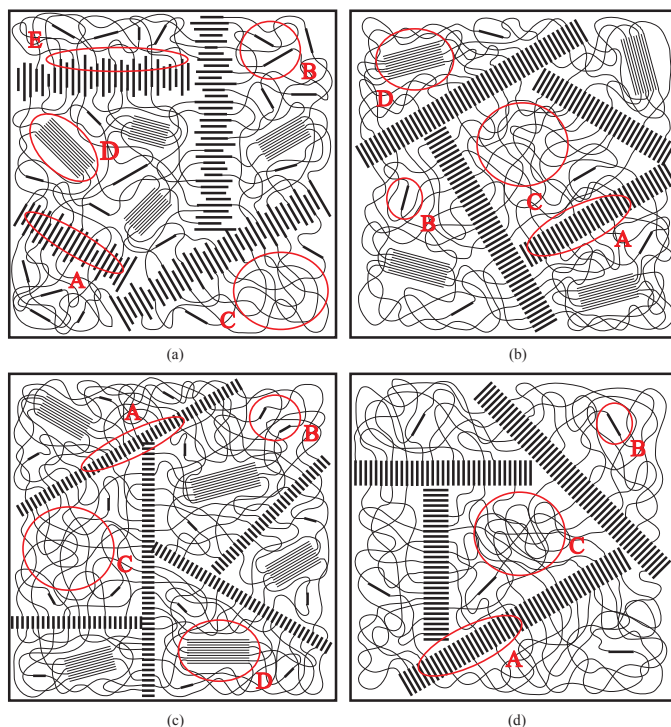
Figure 3.1: Schematic representation of the morphology of (a) commercially available block copolymers (e.g. the PEBAX® family), (b) PEO based block copolymers with the monodisperse long T6T6T hard segment as used by Husken *et al.* [17] and (c) PEO/PPO based block copolymers with the monodisperse short TΦT hard segment, as used in our previous work [11] and (d) PEO-*ran*-PPO based block copolymers as described in the current work. The indicated areas are representative for (A) crystalline hard segments, (B) non-crystallized rigid hard segments, (C) continuous amorphous soft phase, (D) crystalline soft phase and (E) intermediate region with mixed crystalline hard segments and non-crystalline soft segments.

temperature and even lower is crucial. Husken *et al.* [10] prepared block copolymers of short PEO soft segments (M_w 300–2000 g/mol) and monodisperse tetra-amide (T6T6T) hard segments and extended these short PEO soft segments with terephthalic units to obtain PEO lengths from 1250 up to 10000 g/mol. A short PEO soft segment with a molecular weight of 600 g/mol was found to be optimal and could be extended up to 10000 g/mol without significant crystallization of this soft segment to occur. Low temperature mass transport properties were improved compared to the PEO$_x$-T6T6T [17] as the PEO melting temperature and crystallinity could be reduced. In our previous work we attempted to suppress PEO crystallization by mixing two different

types of soft segments: PEO and poly(propylene oxide) (PPO) soft segments [11] as PPO is known to be fully amorphous due to the bulky side groups. High concentrations of PPO ($\geq$ 59 mol%) were nonetheless necessary to achieve reasonable suppression of PEO crystallization [11].

In this paper we present the synthesis and characterization of a PEO based segmented block copolymer system with exceptionally low soft phase melting temperature and crystallinity containing a total soft segment length up to 10000 g/mol and a soft segment concentration up to 89 wt.%. This system is based on the monodisperse tetra-amide (T6T6T, Figure 3.2a) hard segment and a soft segment containing PEO with a low amount of PPO randomly distributed in this PEO (PEO-*ran*-PPO) (Figure 3.2b). To obtain comparable block copolymers with longer soft segment lengths, the polymers with shorter PEO-*ran*-PPO soft segments were extended with terephthalic units (Figure 3.2c).

The weight ratio PEO:PPO of this soft segment building block is 3:1 (molar ratio 4:1). Due to the bulky structure of PPO, the regular structure of common PEO is expected to be disturbed and its tendency to crystallize minimized, resulting in a very well-defined microdomain morphology (Figure 3.1d). A polymer series based on this novel soft segment, in which the total soft segment length is varied between 1000 and 10000 g/mol, has been prepared. The synthesis, surface morphology, thermal-mechanical, hydrophilic and elastic properties are investigated and compared to the previously reported PEO based systems PEO_x-T6T6T [9] and $(PEO_x/T)_y$-T6T6T [10] to study the influence of the random distribution of PPO in the soft segment. The results presented in this paper are especially important for the next papers in this thesis as they will be used to discuss the results that are obtained using the block copolymers described here for gas separation applications.
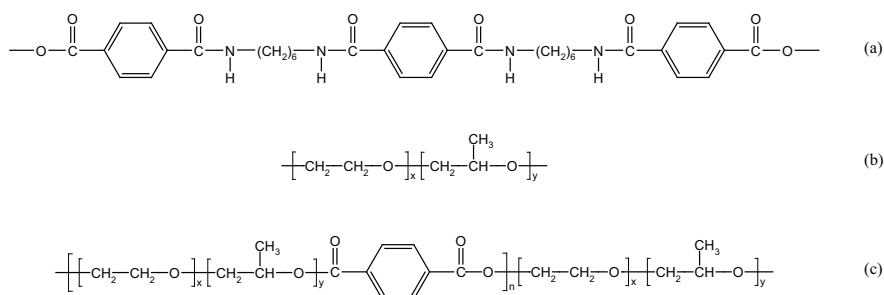
Figure 3.2: Chemical structure of (a) the T6T6T hard segment, (b) the PEO-*ran*-PPO soft segment and (c) the terephthalic extended PEO-*ran*-PPO soft segment.

3.2 Experimental

3.2.1 Materials

Terephthaloyl chloride (TCl), phenol, 1,6-hexamethylenediamine (HMDA), tetra-isopropyl orthotitanate ($\mathrm{Ti}(i\text{-}OC_3H_7)_4$), 1,1,1,3,3,3-hexafluoroisopropanol (HFIP) and 1,1,2,2,-tetrachloroethane were purchased from Aldrich (The Netherlands). Dimethyl terephthalate (DMT), N-methyl-2-pyrrolydone (NMP) and m-xylene were purchased from Merck. The soft segment, a random copolymer of poly(ethylene oxide) (PEO) and poly(propylene oxide) (PPO), denoted PEO-ran-PPO, with a molecular weight of 1000 g/mol and 2500 g/mol was obtained from DOW (The Netherlands) respectively Aldrich (The Netherlands). The copolymer has a PEO:PPO weight ratio of 3:1 (molar ratio 4:1). N-butyl acetate was purchased from Fluka and Irganox® 1330 (1,3,5-trimethyl-2,4,6-tris(3,5-di-t-butyl-4-hydroxybenzyl)benzene) from CIBA Specialty Chemicals (The Netherlands).

3.2.2 Polymer synthesis

The required monodisperse tetra-amide (T6T6T) hard segments were synthesized according to the procedure described by Krijgsman $et\ al.$ [22]. The segmented block copolymers were synthesized by a polycondensation reaction using the random copolymer of PEO and PPO (PEO-ran-PPO) as soft segment and the prepared monodisperse tetra-amide (T6T6T) as hard segment. The total soft segment length was varied and block copolymers with a soft segment length of 1000, 2500, 3750, 5000, 7500 and 10000 g/mol were prepared.

The block copolymers with a soft segment length of 1000 and 2500 g/mol were synthesized by the method described by Husken $et\ al.$ [9] and are denoted as PEO-ran-PPO$_x$-T6T6T, where x represents the molecular weight of the soft segment. The block copolymers with a soft segment length of 3750, 5000, 7500 and 10000 g/mol were prepared by extending the PEO-ran-PPO copolymer ($M_w = 2500$ g/mol) with terephthalic units (T) as described by Husken $et\ al.$ [10]. These extended polymers are denoted as (PEO-ran-PPO$_{2500}$/T)$_y$-T6T6T, where y represents the molecular weight of the total soft segment.

The melting temperature of the monodisperse T6T6T-diphenyl hard segment (316℃)

[22] is too high to allow direct melt polymerization as the polyether soft segment is prone to degradation at these high temperatures [23–26]. To prevent degradation of the soft phase during synthesis, the polymerization is carried out as a two-stage process. The first stage is performed as a solution polymerization in NMP. The reaction (and coupling) of T6T6T-diphenyl with the PEO-*ran*-PPO soft segment reduces the melting temperature of the T6T6T hard segment. In the second stage the pressure is reduced (P < 21 mbar) to distill off the NMP and allow polymerization in the melt. When all the solvent is removed, the block copolymers with high T6T6T content (PEO-*ran*-PPO length 5000 g/mol) are heated to 280℃ for 5 minutes to form a homogeneous melt. Low vacuum (< 1 mbar) is applied during the last hour to strip the phenol and shift the reaction to the product side.

The polymerization of (PEO-*ran*-PPO$_{2500}$/T)$_{10000}$-T6T6T is given as an example. The PEO-*ran*-PPO copolymer with a molecular weight of 2500 g/mol is extended with terephthalic units to give a total soft segment length of 10000 g/mol.

The reaction is carried out in a 250 mL stainless steel reactor equipped with mechanical stirrer and nitrogen inlet. The vessel contained T6T6T-diphenyl (1.62 g, 2.0 mmol), PEO-*ran*-PPO$_{2500}$ (20.0 g, 8.0 mmol), DPT (1.896 g, 6.0 mmol), Irganox$^{®}$ 1330 (0.20 g), catalyst solution (0.8 mL of 0.05 M Ti-(i-(OC$_3$H$_7$)$_4$) in m-xylene) and 50 mL NMP. The reaction mixture was heated in an oil bath to 180℃ under a nitrogen flow. After 30 minutes the temperature was increased to 250℃ in 1.5 hours. After 2 hours at 250℃ the pressure was slowly reduced (P < 21 mbar) to remove all NMP. Then the pressure was further reduced (P < 1 mbar) to allow melt polycondensation for 1 hour. The polymer was cooled to room temperature while maintaining the vacuum. Before use, the polymer was dried overnight in a vacuum oven at 80℃.

3.2.3   Sample preparation

Samples (70x9x2 mm) for dynamic mechanical analysis (DMA) and tensile testing were made by compression molding on a Lauffer OPS 40 press. The mould and polymer were heated to ∼30℃ above the hard segment melting temperature of the block copolymer as determined by DSC. Air was removed by quickly pressurizing/depressurizing the samples three times. Finally, the samples were pressed for 5 minutes at ∼8.5 MPa after which they were cooled while maintaining the pressure. To prevent the material from sticking to the metal plates of the press, glass-fiber reinforced Teflon films were used as a layer between the polymer film and the metal plates (Benetech type B105).

3.2.4 Analysis

⌐ *Atomic Force Microscopy*

Atomic force microscopy (AFM) was used to visualize the morphology of the prepared block copolymers. AFM samples were prepared by solution casting of a thin polymer layer on a silicon wafer using a 10 wt.% solution of the block copolymer in HFIP to obtain films with a thickness of 20 μm. Phase images were obtained with a Nanoscope IV controller operated in tapping mode using TESP cantilevers and a scan area of 1 x 1 μm^2.

⌐ *FTIR-ATR*

FTIR-ATR was used to determine the crystallinity of the hard segment. FTIR-ATR transmission spectra were recorded on a Nicolet 20SXB ATR (Nicolet, Cambridge, MA) spectrometer with a resolution of 4 cm^{-1}. The polymer films ($\sim$100 μm) were prepared by solution casting of a polymer solution (10 wt.% in HFIP) on a silicon wafer. The data were collected at room temperature between 700 cm^{-1} and 4000 cm^{-1}. The degree of crystallinity (X_c) of the hard segment was calculated from the height of the absorbance peak using Equation (3.1a) with a according to Equation (3.1b) [27].

$$
\begin{aligned}
X_{c,\text{ FT-IR}} &= \frac{\text{Crystalline amide peak}}{\text{Amorphous + crystalline amide peak}} \\
&= \frac{\lambda_{25\text{°C (1647 cm}^{-1})}}{a * \lambda_{25\text{°C (1674 cm}^{-1})} + \lambda_{25\text{°C (1647 cm}^{-1})}}
\end{aligned}
\tag{3.1a}
$$

$$
a = \frac{\lambda_{25\text{°C (1630 cm}^{-1})} - \lambda_{\text{melt (1630 cm}^{-1})}}{\lambda_{\text{melt (1670 cm}^{-1})} - \lambda_{25\text{°C (1670 cm}^{-1})}}
\tag{3.1b}
$$

⌐ *Differential Scanning Calorimetry*

Differential scanning calorimetry (DSC) spectra were recorded on a Perkin Elmer DSC7 apparatus equipped with a PE7700 computer and TAS-7 software. Polymer samples (5–10 mg) were heated from −90°C to 200°C at a rate of 20°C/min followed by a cooling scan at 5°C/min. This cycle was repeated with a cooling rate of 10°C/min and 20°C/min while maintaining the constant heating rate of 20°C/min.

Data from the last heating scan (at 20°C/min) and cooling scan (at 20°C/min) were used for further analysis. The glass transition temperature (T_g) was defined as the

midpoint of the heat capacity transition of the heating scan. The maxima of the endothermic peaks of the heating scan were defined as the melting temperature of the soft segment ($T_{m,PEO}$) and the hard segment ($T_{m,T6T6T}$). The surface area is used to calculate the melting enthalpy of the PEO-*ran*-PPO soft segment ($\Delta H_{m,PEO}$) and the T6T6T hard segment ($\Delta H_{m,T6T6T}$).

⌐ *Dynamic Mechanical Analysis*
The torsional behavior (storage modulus and loss modulus) as a function of temperature was measured using a Myrenne ATM3 torsion pendulum at a frequency of 1 Hz and 0.1% strain. Samples were cooled to −100℃ and then heated at 1℃/min. The glass transition temperature (T_g), the flex temperature (T_{flex}), the storage modulus at 20℃ and 55℃ (G'(20℃ / 55℃)), as well as the flow temperature (T_{flow}) were determined. The T_g is defined as the maximum of the loss modulus. The position where the rubbery plateau starts is defined as the flex temperature (T_{flex}). The flow temperature (T_{flow}) is defined as the temperature where the storage modulus reaches 0.5 MPa.

⌐ *Viscosity*
The inherent viscosity of the polymers was determined at 25℃ with a capillary Ubbelohde type 1A. The polymer solutions had a concentration of 0.1 g/dL in a 1:1 molar ratio of phenol/1,1,2,2-tetrachloroethane.

⌐ *Water absorption*
Equilibrium water vapor sorption was measured on vacuum dried samples. Samples of approximately 1 x 1 cm were cut from a compression molded polymer bar. The weight of the samples was determined and the samples were placed in a desiccator filled with demineralized water. The weight increase in time was monitored and the equilibrium water vapor sorption was finally calculated with Equation (3.2).

$$\text{Water absorption} = \frac{m - m_0}{m} \times 100\% \tag{3.2}$$

⌐ *Tensile tests*
Tensile tests were carried out on a Zwick Z020 universal tensile machine equipped with a 10 N load cell. The strain was measured by clamp displacement. Standard stress-strain curves were obtained at a strain rate of 250 mm/min with a starting clamp distance of 25 mm. The tests were performed in 5-fold.

3.3 Results & discussion

3.3.1 Polymer synthesis

A series of six PEO-*ran*-PPO-T6T6T based block copolymers with a soft segment length varying from 1000 to 10000 g/mol is made according to two different methods:

1. Block copolymers with a soft segment length of 1000 and 2500 g/mol are prepared by the reaction of T6T6T-diphenyl with PEO-*ran*-PPO of 1000 g/mol respectively 2500 g/mol and denoted PEO-*ran*-PPO$_x$-T6T6T, where x represents the soft segment length;

2. Block copolymers with higher soft segment lengths are prepared by extension of PEO-*ran*-PPO of 2500 g/mol with terephthalic units (T) to obtain a total soft segment length of 3750, 5000, 7500 and 10000 g/mol. These polymers are denoted as (PEO-*ran*-PPO$_{2500}$/T)$_y$-T6T6T, where y represents the total soft segment length.

All obtained block copolymers are transparent, though slight coloration is visible. This has been observed before and is ascribed to the simultaneous use of NMP and the titanium based catalyst, which together act as a color source at high temperatures [27]. This has no (negative) effect on the other properties of the block copolymer.

3.3.2 AFM

The surface morphology of the PEO-*ran*-PPO block copolymers is studied by AFM. A phase angle image (1 μm^2) of a 20 μm thick film of several PEO-*ran*-PPO-T6T6T block copolymers is presented in Figure 3.3.

The morphology of segmented block copolymers as proposed by Cella [28], with crystallized lamellae that form long ribbons, is visible in the AFM images and the crystalline T6T6T hard phase (lighter color) can be distinguished from the amorphous PEO-*ran*-PPO soft phase (darker color). The optical difference between the AFM pictures is caused by the difference in hard segment concentration. The hard segment concentration decreases from 20.0 wt.% (Figure 3.3a) to only 5.6 wt.% (Figure 3.3c), which enables the visualization of the individual nano-ribbons at very low hard segment concentration. Determination of the thickness of the nano-ribbons from the AFM images is nonetheless difficult due to the dimensions of the AFM tip, but it is expected
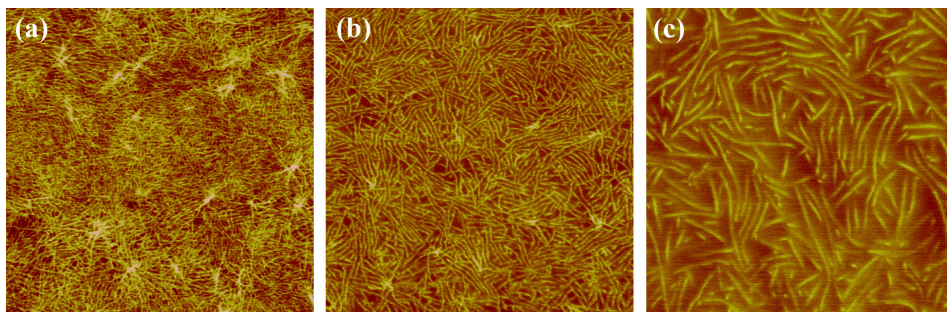
Figure 3.3: Surface morphology (1x1μm) as determined by AFM of (a) PEO-*ran*-PPO$_{2500}$-T6T6T, (b) (PEO-*ran*-PPO$_{2500}$/T)$_{5000}$-T6T6T and (c) (PEO-*ran*-PPO$_{2500}$/T)$_{10000}$-T6T6T block copolymer films with a thickness of 20 μm.

that the ribbon thickness corresponds to the length of a fully extended T6T6T hard segment, which is approximately 3.7 nm [9, 27, 29]. The total length of a ribbon cannot be determined by AFM as only the surface morphology is visualized and these ribbons can bend into the bulk of the material. However, transmission electron microscopy (TEM) images of poly(propylene oxide) (PPO) based T6T6T block copolymers have revealed ribbon lengths of 1000–5000 nm [29]. The aspect ratio of the crystalline ribbons, which is an important parameter to describe the relation between the storage modulus and the fiber reinforcing effect of the crystalline hard segments (as will be discussed later), in the present study were, therefore, expected to be between 250 and 1250.

3.3.3 FTIR-ATR

The FTIR-ATR spectra of the PEO-*ran*-PPO$_x$-T6T6T and the extended (PEO-*ran*-PPO$_{2500}$/T)$_y$-T6T6T block copolymers recorded at room temperature are given in Figure 3.4.

FTIR is a very powerful technique to study the crystallinity of the T6T6T hard segment in this type of block copolymers due to the presence of the amide carbonyl bands. The spectra from 1500–1800 cm^{-1} provide information on the state of the T6T6T hard segment and the terephthalic extender in the block copolymer, as the absorption bands of the carbonyl groups are present in this region. The spectra show peaks at 1718 cm^{-1}, 1657 cm^{-1}, 1625 cm^{-1} and 1540 cm^{-1}.

The peak at 1718 cm^{-1} is ascribed to the C=O stretching of the carbonyl group (COO)
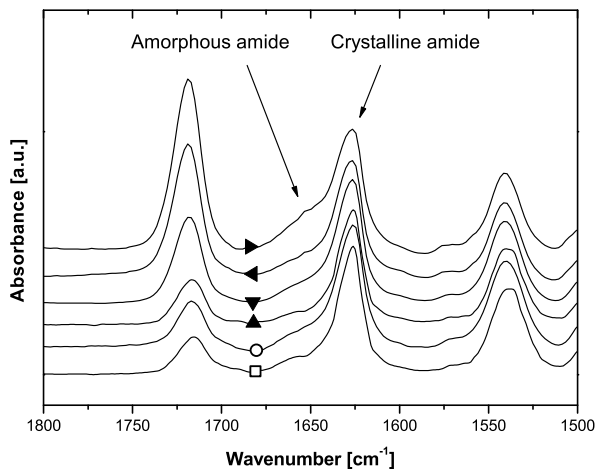
Figure 3.4: FTIR-ATR spectra of PEO-*ran*-PPO-T6T6T block copolymers recorded at room temperature with a total soft segment length of ($\square$) 1000 ($\bigcirc$) 2500 ($\blacktriangle$) 3750 ($\blacktriangledown$) 5000 ($\blacktriangleleft$) 7500 and ($\blacktriangleright$) 10000 g/mol.

[30]. The peaks at 1657 cm^{-1} (small) and 1625 cm^{-1} (large) are ascribed to the carbonyl vibration (C=O) of the amide group (CONH). The frequency of this amide band is very susceptible to the state of the hard segment as these amide carbonyl absorbance bands are sensitive to the hydrogen-bonding distance between the segments. In the amorphous state this distance is larger and has a broader distance distribution compared to the crystalline state. Therefore, the amorphous amide carbonyl group is located at a high wave number and the absorbance peak is broader. The peak at 1540 cm^{-1} is ascribed to the CNH vibration, with NH bending and CN stretching.

The peak at 1718 cm^{-1} increases for a soft segment length above 2500 g/mol. This is caused by the extension of the soft segment with terephthalic units, thereby increasing the number of carbonyl groups in the polymer. The peaks at 1657 cm^{-1} and 1625 cm^{-1} are on approximation constant for all copolymers except for (PEO-*ran*-PPO$_{2500}$/T)$_{10000}$-T6T6T. The absorbance at 1657 cm^{-1} is higher, while it is lower at 1625 cm^{-1}, indicating reduced hard segment crystallinity. The peak at 1540 cm^{-1} remained constant for all copolymers.

Table 3.1 summarizes the data obtained from FTIR-ATR and DSC measurements. The degree of hard segment crystallinity (X_c) is calculated using Equation (3.1a) and (3.1b), and a value of 2.35 for the factor a (Table 3.1). The factor a is not

determined specifically for the current system, but Husken *et al.* [9] determined that this factor, as calculated from temperature dependant FTIR, is 2.35 for the very similar PEO$_x$-T6T6T block copolymer system and is independent of the soft segment type used [27].

Table 3.1: FTIR-ATR and DSC (scan rate 20℃/min) results of PEO-*ran*-PPO-T6T6T block copolymers.

x or y	PEO-*ran*-PPO	T6T6T	T	X_c	T_g	$T_{m,PEO}$	$\Delta H_{m,PEO}$[†]	$T_{m,T6T6T}$	$\Delta H_{m,T6T6T}$
[g/mol]	[wt.%]	[wt.%]	[wt.%]	[%]	[℃]	[℃]	[J/g]	[℃]	[J/g]
(PEO-*ran*-PPO$_x$-T6T6T									
1000	61.6	38.4	-	81	−52	-	-	183	49
2500	80.0	20.0	-	80	−60	−13	16	163	57
(PEO-*ran*-PPO$_{2500}$/T)$_y$-T6T6T									
3750	85.1	14.2	0.7	85	−59	−5	30	151	63
5000	85.8	11.0	3.2	81	−60	−6	29	147	46
7500	88.2	7.3	4.5	76	−60	−5	33	149	35
10000	89.3	5.6	5.1	65	−60	−6	33	144	32

[†] The melting enthalpy per gram of PEO-*ran*-PPO soft segment.

The calculated degree of crystallinity of the hard segment in the polymers is very high and has a value of approximately 80% for all polymers except for the polymer with a soft segment length of 10000 g/mol ((PEO-*ran*-PPO$_{2500}$/T)$_{10000}$), which has a crystallinity of ∼65%. The reason for this deviation is not known and this lower crystallinity is not confirmed by the storage modulus (as determined by DMA). The hard segment crystallinity of this polymer as calculated from the storage modulus equals 80%, which is similar to the block copolymers with the shorter soft segment lengths.

3.3.4 Thermal-mechanical properties

⌐ *DSC*

The thermal properties of the PEO-*ran*-PPO based block copolymers are investigated with DSC (Table 3.1) and compared to the block copolymers with only PEO as soft phase (PEO$_x$-T6T6T [9] and (PEO$_{2000}$/T)$_y$-T6T6T [10]) to study the effect of the presence of PPO in the soft segment on the soft phase behavior of the polymer. The heating scan at 20℃/min of a selection of the prepared block copolymers is given in Figure 3.5.

Typically, on heating from −100℃ to 225℃, the block copolymers pass through an endothermic second order transition (1), the T_g. This transition is followed by an
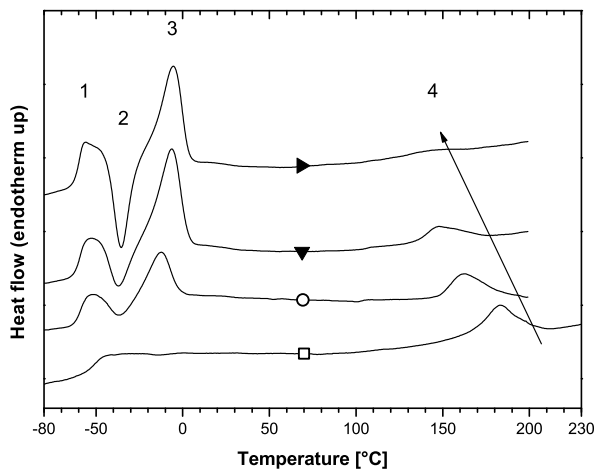
Figure 3.5: Heating scan at a scan rate of 20℃/min (obtained after a run at a cooling rate of 20℃/min) of PEO-*ran*-PPO-T6T6T block copolymers with a total soft segment length of (□) 1000 (○) 2500 (▼) 5000 and (►) 10000 g/mol.

exothermic peak (2) which is ascribed to the dynamic state of the block copolymer. This peak will not be discussed further as it is not relevant for the thermal properties of interest (the glass transition temperature, PEO melting temperature and crystallinity) for the application. The third peak (3), which characterizes an endothermic transition is not visible for the copolymer with a soft segment length of 1000 g/mol, but is present for all other polymers and is ascribed to the melting of the semi-crystalline PEO soft phase. The last endothermic peak (4) is the melting transition of the hard segment. This melting peak is only clearly visible for the block copolymers with a maximum soft segment length of 5000 g/mol. At longer soft segment lengths (7500 g/mol and 10000 g/mol) it becomes broader.

The glass transition temperature (T_g, peak 1) of the block copolymers is independent of the soft segment length except for PEO-*ran*-PPO$_{1000}$-T6T6T (Table 3.1). This is caused by the short soft segment length of this block copolymer and will be further addressed when the DMA results are discussed. The melting enthalpy of the soft phase shows that crystallization of the soft phase is still present when the soft segment length is higher than 1000 g/mol, although a random distribution of PEO and PPO exists in the soft phase. The determined melting enthalpy of the PEO phase, denoted as enthalpy per gram of soft segment [J/g soft segment], as a function of the soft
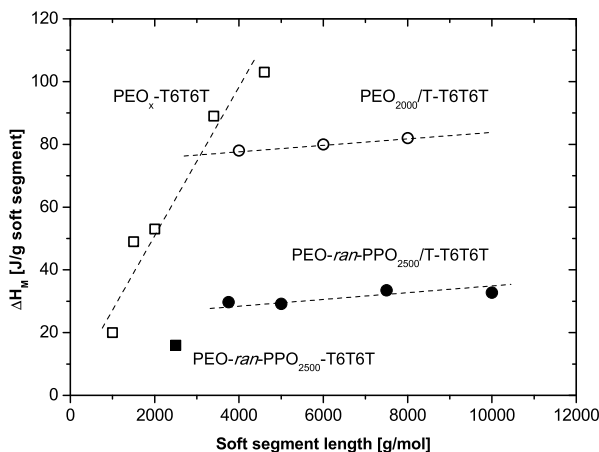
Figure 3.6: Melting enthalpy of PEO per gram of soft segment as a function of the total soft segment length for (■) PEO-*ran*-PPO$_{2500}$-T6T6T, (●) (PEO-*ran*-PPO$_{2500}$/T)$_y$-T6T6T, (□) PEO$_x$-T6T6T [9] and (○) (PEO$_{2000}$/T)$_y$-T6T6T [10].

segment length for PEO-*ran*-PPO-T6T6T block copolymers is shown in Figure 3.6. The values are compared to the values obtained for the block polymers only containing PEO as soft segment and no PPO (PEO$_x$-T6T6T [9] and (PEO$_{2000}$/T)$_y$-T6T6T [10]) to investigate the effect of the randomly distributed PPO in the soft segment on the crystallization behavior of the soft segment.

The use of PEO-*ran*-PPO as the soft segment reduces the degree of PEO crystallinity in the soft phase tremendously compared to the use of pure PEO as a soft phase, as presented in Figure 3.6. The melting enthalpy at a soft segment length of 2500 g/mol is reduced by approximately a factor four compared to the PEO$_x$-T6T6T block copolymer at similar soft segment length. The reduction in melting enthalpy between the terephthalic extended PEO-*ran*-PPO and PEO block copolymers is somewhat lower but still very significant. The incorporation of a bulky group (PPO) in the soft segment prevents the organized packing (i.e. crystallization) of the PEO blocks thus preventing crystallization. When the two PEO based polymers are compared (PEO$_x$-T6T6T and (PEO$_{2000}$/T)$_y$-T6T6T, it is clear that extension of the soft segment also suppresses crystallization of the soft segment [10]. The reduced soft segment flexibility (due to the terephthalic units) hinders the free rotation of the soft segment and restricts crystallization. This hypothesis cannot be directly confirmed by the PEO-

ran-PPO based block copolymers as no unextended and extended block copolymers of equal (total) soft segment length were synthesized. In contrast, simple mixing of PPO and PEO soft segments in an equal weight ratio does not prevent nor reduces crystallization [11], emphasizing the advantage of this new type of soft segment.

These DSC measurements reveal that the use of PEO-*ran*-PPO as soft segment is a very effective way to reduce soft phase crystallinity. The large reduction in soft phase crystallinity increases the total amount of soft amorphous phase available for mass transport in these block copolymers (compare Figure 3.1b and Figure 3.1d). Complete suppression of PEO crystallization was however not observed. Possible reasons for this could be (1) the distribution of PEO and PPO is not completely random and/or (2) 25 wt.% of PPO is not sufficient to entirely prevent PEO crystallization.

⌐ *DMA*

The storage and loss moduli of the prepared PEO-*ran*-PPO-T6T6T block copolymers are measured by DMA and especially the melting properties of the soft phase as obtained from the DMA measurements are compared to the corresponding properties of the polymers which contain only PEO as soft segment (the PEO_x-T6T6T [9] and $(PEO_{2000}/T)_y$-T6T6T [10] block copolymers). The storage modulus (G') of the different PEO-*ran*-PPO-T6T6T block copolymers as a function of the temperature is given in Figure 3.7.

At low temperatures the storage modulus is relatively high and comparable for all block copolymers investigated, but decreases rapidly above the T_g of the polymers. For all polymers (except PEO-*ran*-PPO_{1000}-T6T6T) a shoulder is observed after the T_g as a result of a semi-crystalline soft phase. After the melting temperature of the soft phase is reached, a broad and temperature independent rubbery plateau starts, which is characteristic for block copolymers containing monodisperse, crystallizable hard segments. A summary of the DMA results is given in Table 3.2.

Glass transition temperature

The T_g of the polymers decreases when the soft segment length is increased from 1000 g/mol to 2500 g/mol. Increase of the soft segment length to 3750 g/mol by terephthalic unit extension, sligthly increases the T_g again, after which further extension of the soft segment chain does not affect the T_g further (Table 3.2). According to Fox and Flory [31] the T_g depends on the molecular mass of the polymer. Nielsen *et al.* [31] used empirical data to adapt the theory of Fox and Flory to crosslinked polymers and
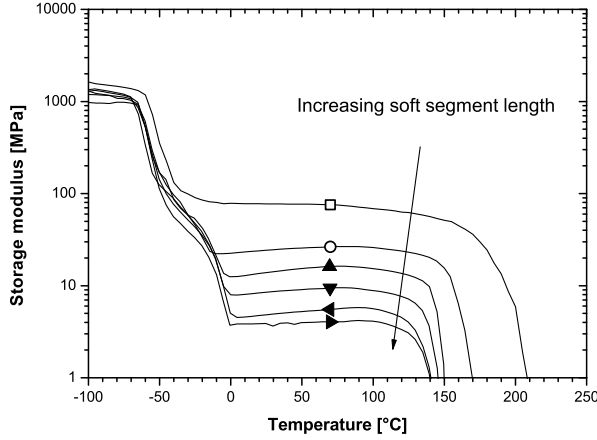
Figure 3.7: Storage modulus as a function of the temperature of PEO-*ran*-PPO-T6T6T block copolymers with a total soft segment length of (□) 1000 (○) 2500 (▲) 3750 (▼) 5000 (◄) 7500 and (►) 10000 g/mol.

Table 3.2: Dynamic mechanical properties of PEO-*ran*-PPO-T6T6T block copolymers.

x or y	PEO-*ran*-PPO	T6T6T	T	M_{CRL}†	T_g	T_{flex}	G'(20℃)	G'(55℃)	T_{flow}
[g/mol]	[wt.%]	[wt.%]	[wt.%]	[g/mol]	[℃]	[℃]	[MPa]	[MPa]	[℃]
(PEO-*ran*-PPO$_x$-T6T6T									
1000	61.6	38.4	-	935	−53	−35	77	77	212
2500	80.0	20.0	-	2337	−63	−15	24	28	170
(PEO-*ran*-PPO$_{2500}$/T)$_y$-T6T6T									
3750	85.1	14.2	0.7	3505	−59	−10	14	16	151
5000	85.8	11.0	3.2	4673	−60	−10	9	9	147
7500	88.2	7.3	4.5	7010	−60	−5	5	5	144
10000	89.3	5.6	5.1	9347	−60	−5	4	4	143

† M_{CRL} = Molecular weight of the soft segment between crosslinks.

determined that the T_g of crosslinked polymers is related to the distance between crosslinks in the polymer according to Equation (3.3)

$$T_g = T_g(\infty) + \frac{3.9 \times 10^4}{M_{CRL}} \tag{3.3}$$

with $T_g(\infty)$ the glass transition temperature of the polymer at infinite molecular weight and M_{CRL} the molecular weight of the soft segment between crosslinks [g/mol].

Figure 3.8 shows the T_g of the different types of polymers investigated (PEO-ran-PPO$_x$-T6T6T, (PEO-ran-PPO$_{2500}$/T)$_y$-T6T6T, PEO$_x$-T6T6T [9], (PEO$_{2000}$/T)$_y$-T6T6T [10] and PPO$_x$-T6T6T [29]) as a function of the reciprocal molecular weight of the soft segment between crosslinks M_{CRL}. It is assumed that M_{CRL} is equal to the length of the soft segment backbone, as the terephthalic units are not able to crystallize. A comparison of the block copolymers based on this assumption is allowed since all block copolymers investigate in this work phase separate by crystallization at comparable degree of hard segment crystallinity.

The T_g's of the PEO$_x$-T6T6T ($\square$) and PPO$_x$-T6T6T ($\triangle$) series decrease with increasing soft segment lengths. The two unextended PEO-ran-PPO based block copolymers (PEO-ran-PPO$_{1000}$-T6T6T and PEO-ran-PPO$_{2500}$-T6T6T) ($\blacksquare$) show similar behavior. This is as expected as chain flexibility increases with soft segment length and a reduction of the T_g indicates an increase in soft segment chain flexibility [32]. The terephthalic extended PEO-ran-PPO-T6T6T block copolymers do not show a decrease in T_g when the soft segment length is increased above 2500 g/mol by extending the soft segment length. This effect is also observed when PEO$_x$-T6T6T
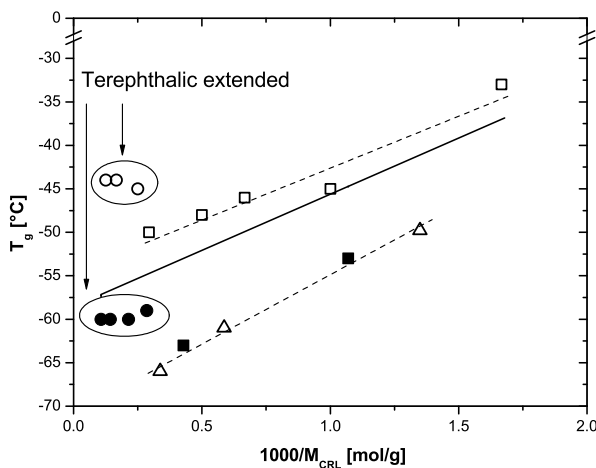
Figure 3.8: T_g as a function of the reciprocal molecular weight of the soft segment between crosslinks for ($\blacksquare$) PEO-ran-PPO$_x$-T6T6T, ($\bullet$) (PEO-ran-PPO$_{2500}$/T)$_y$-T6T6T, ($\square$) PEO$_x$-T6T6T, ($\circ$) (PEO$_{2000}$/T)$_y$-T6T6T and ($\triangle$) PPO$_x$-T6T6T. The solid line represents the calculated T_g's of PEO-ran-PPO$_x$-T6T6T according to Fox' theory on T_g of block copolymers [31].

block copolymers are extended with terephthalic units. This indicates that the soft segment chain flexibility is reduced by the introduction of the rigid terephthalic unit in the soft segment. It is suggested that the rotation energy of the soft segment chain in the proximity of the terephthalic units is high, increasing the T_g of the soft phase [10].

Based on calculations using the Equation given by Fox [31], it is expected that the T_g values of PEO-*ran*-PPO$_x$ based block copolymers have values in between the T_g values of the two block copolymers based on the two pure soft segments (either PEO (PEO$_x$-T6T6T) or PPO (PPO$_x$-T6T6T)):

$$\frac{1}{T_g} = \frac{w_1}{T_{g,1}} + \frac{w_2}{T_{g,2}} \tag{3.4}$$

with w_1, w_2 the weight concentration of polymer 1 and 2 respectively in the new polymer and $T_{g,1}$, $T_{g,2}$ the glass transition temperatures [°C] of polymer 1 and 2 respectively. The solid line in Figure 3.8 represents these theoretical T_g values of the PEO-*ran*-PPO based block copolymers as calculated using Equation (3.4). Figure 3.8 clearly shows that the experimentally determined T_g values of all the PEO-*ran*-PPO$_x$-T6T6T block copolymers however do not coincide with the values calculated using the Fox equation (as they do not coincide with the solid line). Surprisingly, the PEO-*ran*-PPO$_x$-T6T6T block copolymers show T_g values that are comparable to the T_g values determined for the block copolymers containing the pure PPO soft segment (PPO$_x$-T6T6T) [29] indicating similar chain flexibility. The reason for this behavior is not yet understood.

Flex temperature

The T_{flex}, defined as the temperature where the rubbery plateau starts, is related to the T_g (fully amorphous soft phase) or the melting temperature of PEO (semi-crystalline soft phase). The melting temperature of the semi-crystalline soft phase (and as such the flex temperature) is an important parameter as mass transport only occurs through the amorphous soft phase. The flex temperature of the synthesized PEO-*ran*-PPO based block copolymers as a function of the soft segment length is shown in Figure 3.9. To investigate the influence of the random distribution of PPO on the flex temperature, the data of the block copolymers containing only PEO as soft segment (PEO$_x$-T6T6T [9] and (PEO$_{2000}$/T)$_y$-T6T6T [10]) are presented as well.
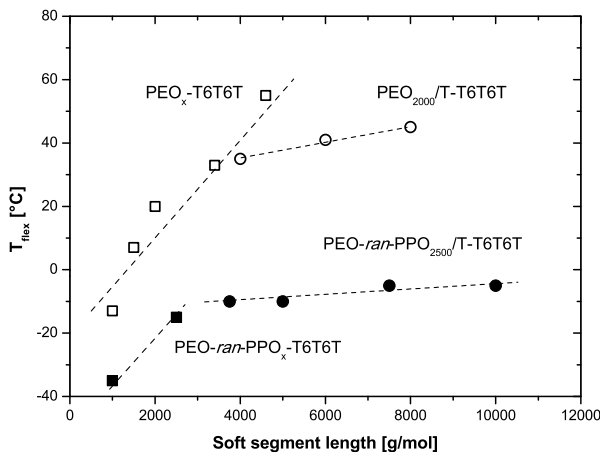
Figure 3.9: Flex temperature as a function of the soft segment length for (■) PEO-*ran*-PPO$_x$-T6T6T, (●) (PEO-*ran*-PPO$_{2500}$/T)$_y$-T6T6T, (□) PEO$_x$-T6T6T [9] and (○) (PEO$_{2000}$/T)$_y$-T6T6T [10].

The PEO-*ran*-PPO$_{1000}$-T6T6T block copolymer has a low flex temperature (-35°C) due to the absence of a semi-crystalline soft phase. The flex temperature increased to -15°C for the semi-crystalline PEO-*ran*-PPO$_{2500}$-T6T6T block copolymer. Extension of the PEO-*ran*-PPO$_{2500}$ segment up to 10000 g/mol slightly further increased the flex temperature to a maximum of -5°C. This trend is similar to the PEO melting temperature as observed by DSC.

As shown by DSC and DMA, the PEO-*ran*-PPO block copolymers still contain a semi-crystalline phase (except for PEO-*ran*-PPO$_{1000}$-T6T6T), however the PEO melting temperature is significantly reduced by approximately 40°C compared to the PEO melting temperature of the PEO$_x$-T6T6T [9] and the (PEO$_{2000}$/T)$_y$-T6T6T [10] block copolymers which contain only pure PEO as the soft phase. The use of a combination of PEO and PPO as building blocks for the soft segment instead of pure PEO results in clearly lower melting temperatures for the PEO-*ran*-PPO based polymers. We hypothesize that this stems from the fact that the random distribution of PPO in the soft segment limits the size of the PEO crystals that can be formed (disrupted chain packing) which results in a decrease in melting temperature according to the Gibbs-Thomson relation, which states that thicker lamellae in a crystalline phase show a higher melting temperature [33]. The increase of the PEO crystal size (increase of

PEO melting temperature) with increasing soft segment length is found to be less significant when the soft segments are extended with terephthalic units, as shown by Husken *et al.* [10] for PEO-T6T6T block copolymers. As already discussed in the DSC section this hypothesis cannot be directly confirmed by the PEO-*ran*-PPO based block copolymers as no unextended and extended block copolymers of equal total soft segment length were synthesized. It is however likely that this also occurs in the currently described system as the introduction of terephthalic units in the soft segment reduces the soft segment chain flexibility and hinders the rotation of the soft segment thus reducing crystallization as shown by an increase in the glass transition temperature.

In conclusion, the use of PPO randomly distributed in the PEO soft blocks significantly reduces the soft phase melting (flex) temperature and crystallinity compared to the block copolymers based on pure PEO as soft phase. This broadens the operating window of these materials towards lower temperature applications. Furthermore, high soft segment lengths and thus concentrations (up to 89 wt.%) can be incorporated increasing overall mass transport considerably.

Storage modulus

To investigate the mechanical strength, the storage modulus at 55℃ (G'55℃) as a function of the hard segment concentration of the PEO-*ran*-PPO based block copolymers is shown in Figure 3.10. For comparison also the storage modulus at 55℃ of the pure PEO based block copolymers PEO_x-T6T6T [9] is shown. The temperature of 55℃ is chosen as both block copolymer series have a fully amorphous soft phase over the full composition range at this temperature. To illustrate the effect of a semi-crystalline soft phase on the storage modulus [9] also the storage modulus at 20℃ of PEO_x-T6T6T and the extended PEO based polymer $((PEO_{2000}/T)_y$-T6T6T) with a soft segment melting temperature above 20℃ (PEO length > 2000 g/mol) are summarized in Figure 3.10.

The storage modulus at 55℃ increases with increasing hard segment concentration and this is related to the fiber reinforcing effect of the T6T6T hard segment crystallites. Similar values as for other block copolymer systems (PEO_x-T6T6T [9] and PPO_x-T6T6T [29]) are obtained. The increase in modulus with T6T6T concentration is in accordance with the model for random oriented fiber-reinforced systems as described by the Halpin-Tsai model [31, 34] employing an aspect ratio (l/d) of 1000 as determined by van der Schuur *et al.* [29]. The storage modulus of the PEO-*ran*-PPO based
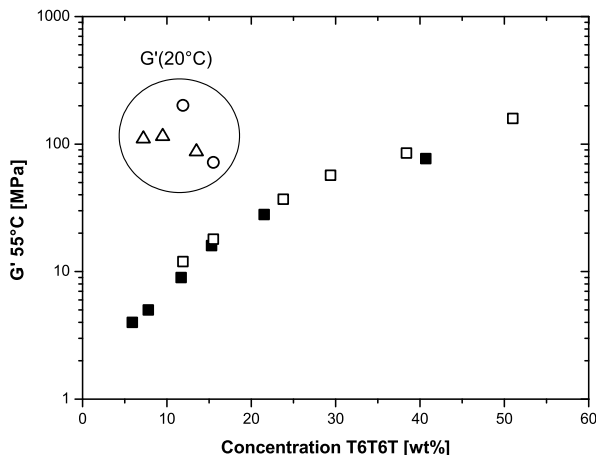
Figure 3.10: Storage modulus at 55℃ as a function of the concentration T6T6T for (■) PEO-*ran*-PPO-T6T6T and (□) PEO$_x$-T6T6T [9]. Values for the storage modulus at 20℃ are also shown for (○) PEO$_x$-T6T6T ($x > 2000$ g/mol) [9] and (△) (PEO$_{2000}$/T)$_y$-T6T6T ($y > 2000$ g/mol) [9].

block copolymers is temperature independent (similar values of the storage modulus are found at 20℃ and 55℃) as no semi-crystalline soft phase is present at room temperature.

The effect of a semi-crystalline soft phase on the storage modulus can be visualized when the data from PEO$_x$-T6T6T at 20℃ with a soft segment length > 2000 g/mol (○ and △) are compared to the PEO-*ran*-PPO based block copolymers (■). The presence of a semi-crystalline soft phase leads to a large increase in storage modulus. The use of this new PEO-*ran*-PPO soft segment thus allows us to synthesize PEO based block copolymers containing high PEO concentrations with a low modulus at room temperature ensuring excellent low temperature flexibility.

Flow temperature
Figure 3.11 shows the flow temperature as a function of the soft segment concentration for the different PEO-*ran*-PPO based block copolymers and this indicates the maximum temperature at which these block copolymers can still be used. The values obtained for the polymers based on pure PEO as soft phase (PEO$_x$-T6T6T) are also presented.

71
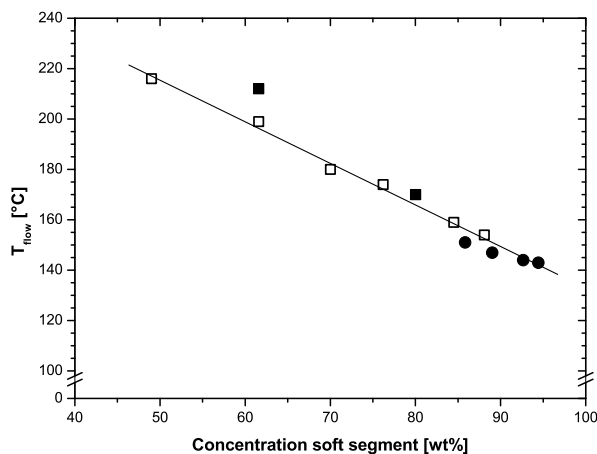
Figure 3.11: Flow temperature as a function of the soft phase concentration for (■) PEO-*ran*-PPO$_x$-T6T6T, (●) (PEO-*ran*-PPO$_{2500}$/T)$_y$-T6T6T and (□) PEO$_x$-T6T6T [9].

The flow temperature of the different polymers decreases with increasing soft segment concentration as shown in Figure 3.11. This can be explained by the solvent effect of Flory, which states that the amorphous soft phase acts as a solvent for the crystalline hard phase [31, 35] and this effect has also been observed for similar polyether-T6T6T block copolymer systems [9, 29, 36].

3.3.5 Water absorption

The hydrophilicity of the PEO-*ran*-PPO based block copolymers is of importance for applications where water (vapor) is present, such as breathable film applications and dehydration of gas streams. Because crystalline nylon, which is similar to the hard segment used in the current block copolymer system, does not absorb water [37] and the degree of hard segment crystallinity is high ($\sim$80%) it is assumed that water is only absorbed in the amorphous soft phase. It is expected that the amount of absorbed water in the polymer is affected by (1) the concentration of soft segment (and consequently that of the hard segment) as the crosslink density of the block copolymer influences its swelling behavior, (2) the type of soft segment and (3) the presence of the terephthalic extender.

The hydrophilicity of the synthesized polymers is studied performing water absorption measurements and the results are summarized in Table 3.3. The water absorption of the PEO-*ran*-PPO based block copolymers as well as the water absorption of pure PEO based block copolymers (PEO$_x$-T6T6T [38] and (PEO$_{2000}$/T)$_y$-T6T6T [38]) as a function of the reciprocal molecular weight of the soft segment between crosslinks (M_{CRL}) is presented in Figure 3.12.

The water absorption of the block copolymers is high and increases exponentially with increasing soft segment concentration (or length). A linear relation is observed between the logarithm of the weight percent of water absorbed and the reciprocal distance between crosslinks (Figure 3.12). This strong increase in water absorption with soft phase concentration can be explained by a decrease in the physical crosslink density, as the T6T6T concentration decreases simultaneously, thus allowing increased swelling of the amorphous regions, as already described by Husken *et al.* [38]. The increase in water absorption as a function of the reciprocal distance between the crosslinks for PEO-*ran*-PPO-T6T6T is similar to the PEO-T6T6T block copolymers (similar slope).
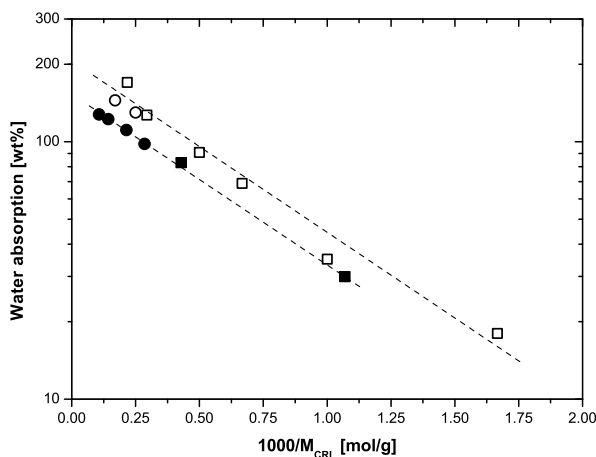
Figure 3.12: Water absorption by weight as a function of the reciprocal molecular weight of the soft segment between crosslinks for (■) PEO-*ran*-PPO$_x$-T6T6T, (●) (PEO-*ran*-PPO$_{2500}$/T)$_y$-T6T6T, (□) PEO$_x$-T6T6T [38] and (○) (PEO$_{2000}$/T)$_y$-T6T6T [38].

The $(PEO_{2000}/T)_y$-T6T6T block copolymers have a terephthalic unit concentration of approximately 3–4 wt.% and exhibit water absorption close to the PEO_x-T6T6T series. Similar behavior is observed for the extended PEO-*ran*-PPO block copolymers as similar low terephthalic concentrations are present. The effect of the terephthalic units is thus considered negligible at the low concentrations used in these series.

The difference in water absorption found between the PEO-*ran*-PPO and PEO_x series can therefore be mainly ascribed to the difference in soft segment composition. The PEO-*ran*-PPO soft segment contains 25 wt.% PPO, which has a more hydrophobic character in comparison with PEO, resulting in lower water absorption. Husken *et al.* found a linear relationship between the water absorption and the soft segment composition [38] for PEO and PTMO. It is therefore assumed that a combination of PEO and PPO will exhibit similar behavior and hence the water absorption decreases with increasing PPO concentration as observed. To illustrate this we determined that the water absorption of a PPO_{2200}-T6T6T block copolymer is only 10 wt.%. The expected water absorption based on the molar ratio of PEO:PPO can be calculated for the PEO-*ran*-PPO_{2500}-T6T6T block copolymer, which is approximately ∼80 wt.%. This relates well to the measured water absorption for this polymer, which is 83 wt.%.

3.3.6 Viscometry and tensile properties

Viscometry is used to obtain information on the polymer molecular weight. The tensile behavior of the block copolymers is characterized in terms of the E-modulus (or Young's-modulus), the fracture strain (ϵ_f) and the fracture stress (σ_f) and gives an indication of the mechanical strength. The viscometry and tensile properties of PEO-*ran*-PPO based block copolymers are summarized in Table 3.3 and the stress-strain curves are displayed in Figure 3.13.

Typical elastomeric behavior is observed for all samples. At small deformations elastic behavior occurs and the stress has a linear relationship with strain. Above the yield point, the stress continued to gradually increase with the strain and this strain hardening effect decreased with increasing soft segment length. Strain-induced crystallization of the soft segment has not been observed in any of the samples.

The modulus of the material depends on several factors, such as the soft phase modulus, the network density and the reinforcing effect of the crystallized hard segments [1].

Table 3.3: Water absorption, inherent viscosity and tensile properties of PEO-*ran*-PPO based block copolymers.

x or y	PEO-*ran*-PPO	T6T6T	T	WA	η_{inh}	E-modulus	G'	E/G'	ϵ_f	σ_f
[g/mol]	[wt.%]	[wt.%]	[wt.%]	[wt.%]	[dL/g]	[MPa]	[MPa]	[–]	[MPa]	[%]
PEO-*ran*-PPO$_x$-T6T6T										
1000	61.6	38.4	-	30	0.85	185	67 [†]	2.8	19	40
2500	80.0	20.0	-	85	0.92	60	24	2.5	8	57
(PEO-*ran*-PPO$_{2500}$/T)$_y$-T6T6T										
3750	85.1	14.2	0.7	98	0.77	35	14	2.5	4	26
5000	85.8	11.0	3.2	113	1.09	26	9	2.9	3	80
7500	88.2	7.3	4.5	123	1.22	13	5	2.6	3	136
10000	89.3	5.6	5.1	128	1.56	10	4	2.5	2	113

[†] The tensile tests were performed on PEO-*ran*-PPO$_{1000}$-T6T6T with less monodisperse crystallized T6T6T, hence G' is reduced compared to G' as determined with DMA.
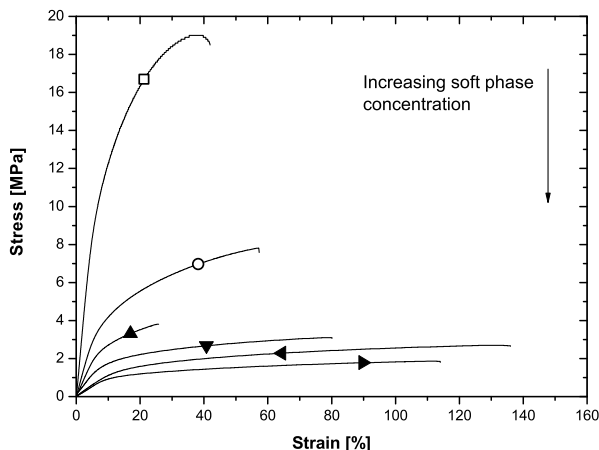
Figure 3.13: Stress-strain curves for PEO-*ran*-PPO-T6T6T block copolymers with a soft segment length of (□) 1000 (○) 2500 (▲) 3750 (▼) 5000 (◄) 7500 and (►) 10000 g/mol.

In this case the modulus is mainly determined by the hard segment concentration as the type of soft segment has little effect on the modulus [9, 10, 29, 36]. The storage modulus (G') has been discussed in section 3.4 and the E-modulus (or Young's modulus) shows similar behavior and decreases with increasing soft segment length as a result of decreasing T6T6T concentration. The E-modulus and the storage modulus are related according to Equation (3.5)

$$E = 2G'(1 + \nu) \tag{3.5}$$

where ν is the Poisson ratio, which gives information about the volume deformation. In the case of an ideal elastomer the Poisson ratio is 0.5 and Equation (3.5) reduces to E = 3G'. For all polymers investigated the E/G' ratio is ~2.5 indicating a constant volume deformation and near ideal elastomeric behavior [32].

The ultimate or fracture properties depend to a large extent on the polymer molecular weight and the possible strain hardening. In general, the fracture stress decreases and the fracture strain increases with increasing soft segment length (and decreasing T6T6T content and network density). The deviations from this general trend in our block copolymer series can be explained by the variation in molecular weight (indicated by variations in inherent viscosity). Overall, PEO-*ran*-PPO based block copolymers with sufficient mechanical strength for, for instance, flat sheet processing have been obtained. The ultimate properties might be further enhanced by optimization of the synthesis procedure to obtain block copolymers with a higher molecular weight.

3.4   Conclusions

Segmented block copolymers based on a PEO based flexible, soft segment and monodisperse, crystallizable tetra-amide (T6T6T) hard segments have been synthesized. The soft segment was a random copolymer of PEO and PPO containing 75 wt.% PEO and 25 wt.% PPO, where the random distribution of PPO suppresses the PEO crystallization observed in neat PEO based block copolymers. We hypothesize this approach to be particularly beneficial for mass transport processes. The total soft segment length was varied between 1000 and 10000 g/mol. The use of monodisperse hard segments (T6T6T) resulted in fast and almost complete ($> 80\%$) crystallization of these segments as demonstrated by FTIR and DMA. This led to very efficient phase separation between the hard and soft segments and only small amounts of non-crystallized hard segments were expected to be present in the soft phase.

Extensive DSC and DMA experiments showed that the PEO melting temperature and crystallinity, compared to the reference block copolymers (PEO_x-T6T6T and $(PEO_{2000}/T)_y$-T6T6T)), were lowered to a great extend by the presence of the PPO.

The PEO melting temperature could be lowered by approximately 40℃ at all soft segment lengths studied (up to 10000 g/mol) and a melting temperature below 0℃ could be obtained. Furthermore, the total PEO crystallinity was found to decrease by at least a factor three. In addition, other thermal-mechanical properties have been investigated. Due to the extremely low PEO melting temperature, block copolymers with a low modulus at room temperature could be obtained, which was not possible using neat PEO segments with a length > 2000 g/mol. The increase in modulus with increasing T6T6T concentration was found to be similar to earlier reported systems of PEO-T6T6T and PPO-T6T6T indicating equivalent reinforcing effects of the T6T6T crystallites.

Overall, PEO based block copolymers with greatly improved microdomain morphology and low PEO melting temperature were obtained. This resulted in block copolymers with a fully amorphous soft phase over a very broad temperature range, which is especially interesting for gas separation processes.

3.5   Acknowledgements

Chapter 3

3.6   References

[1] G. Holden, H. R. Kricheldorf and R. P. Quirk; *Thermoplastic Elastomers*; 3rd edition (2004); Munich (Germany): Hanser Gardner Publications; ISBN 978-1569903643

[2] V. I. Bondar, B. D. Freeman and I. Pinnau; *Gas sorption and characterization of poly(ether-b-amide) segmented block copolymers*; Journal of Polymer Science, Part B: Polymer Physics **37** (17) (1999) 2463–2475; DOI: 10.1002/(SICI)1099-0488(19990901)37:17⟨2463::AID-POLB18⟩3.0.CO;2-H

[3] V. I. Bondar, B. D. Freeman and I. Pinnau; *Gas transport properties of poly(ether-b-amide) segmented block copolymers*; Journal of Polymer Science, Part B: Polymer Physics **38** (15) (2000) 2051–2062; DOI:10.1002/1099-0488(20000801)38:15⟨2051::AID-POLB100⟩3.0.CO;2-D

[4] J. H. Kim, S. Y. Ha and Y. M. Lee; *Gas permeation of poly(amide-6-b-ethylene oxide) copolymer*; Journal of Membrane Science **190** (2) (2001) 179–193; DOI:10.1016/S0376-7388(01)00444-6

[5] V. Barbi, S. S. Funari, R. Gehrke, N. Scharnagl and N. Stribeck; *SAXS and the gas transport in polyether-block-polyamide copolymer membranes*; Macromolecules **36** (3) (2003) 749–758; DOI:10.1021/ma0213403

[6] M. Yoshino, K. Ito, H. Kita and K.-I. Okamoto; *Effects of hard-segment polymers on CO_2/N_2 gas-separation properties of poly(ethylene oxide)-segmented copolymers*; Journal of Polymer Science, Part B: Polymer Physics **38** (13) (2000) 1707–1715; DOI:10.1002/1099-0488(20000701)38:13⟨1707::AID-POLB40⟩3.0.CO;2-W

[7] A. Car, C. Stropnik, W. Yave and K. V. Peinemann; *PEG modified poly(amide-b-ethylene oxide) membranes for CO_2 separation*; Journal of Membrane Science **307** (1) (2008) 88–95; DOI:10.1016/j.memsci.2007.09.023

[8] A. Car, C. Stropnik, W. Yave and K. V. Peinemann; *Pebax®/polyethylene glycol blend thin film composite membranes for CO_2 separation: Performance with mixed gases*; Separation and Purification Technology **62** (1) (2008) 110–117; DOI:10.1016/j.seppur.2008.01.001

[9] D. Husken, J. Feijen and R. J. Gaymans; *Hydrophilic segmented block copolymers based on poly(ethylene oxide) and monodisperse amide segments*; Journal of Polymer Science, Part A: Polymer Chemistry **45** (19) (2007) 4522–4535; DOI:10.1002/pola.22186

[10] D. Husken, J. Feijen and R. J. Gaymans; *Segmented block copolymers with terephthalic-extended poly(ethylene oxide) segments*; Macromolecular Chemistry and Physics **209** (5) (2008) 525–534; DOI:10.1002/macp.200700288

[11] S. R. Reijerkerk, A. Arun, K. Nijmeijer, R. J. Gaymans and M. Wessling; *Tuning of mass transport in multi-block copolymers for CO_2 capture applications*; Journal of Membrane Science (2009); DOI:10.1016/j.memsci.2009.09.045

[12] S. J. Metz, M. H. V. Mulder and M. Wessling; *Gas-permeation properties of poly(ethylene oxide) poly(butylene terephthalate) block copolymers*; Macromolecules **37** (12) (2004) 4590–4597; DOI:10.1021/ma049847w

[13] A. Car, C. Stropnik, W. Yave and K. V. Peinemann; *Tailor-made polymeric membranes based on segmented block copolymers for CO_2 separation*; Advanced Functional Materials **18** (18) (2008) 2815–2823; DOI:10.1002/adfm.200800436

[14] K.-I. Okamoto, M. Fujii, S. Okamyo, H. Suzuki, K. Tanaka and H. Kita; *Gas permeation properties of poly(ether imide) segmented copolymers*; Macromolecules **28** (20) (1995) 6950–6956; DOI:10.1021/ma00124a035

[15] Arkema; *PEBAX: Polyether block amides* (2009); URL: http://www.pebax.com

[16] H. Lin and B. D. Freeman; *Materials selection guidelines for membranes that remove CO_2 from gas mixtures*; Journal of Molecular Structure **739** (1-3) (2005) 57–74; DOI:10.1016/j.molstruc.2004.07.045

[17] D. Husken, T. Visser, M. Wessling and R. J. Gaymans; *CO_2 permeation properties of poly(ethylene oxide)-based segmented block copolymers*; Journal of Membrane Science **346** (1) (2010) 194–201; DOI:10.1016/j.memsci.2009.09.034

[18] L. L. Harrell Jr; *Segmented polyurethans. Properties as a function of segment size and distribution*; Macromolecules **2** (6) (1969) 607–612; DOI: 10.1021/ma60012a008

[19] J. A. Miller, S. B. Lin, K. K. S. Hwang, K. S. Wu, P. E. Gibson and S. L. Cooper; *Properties of polyether-polyurethane block copolymers: Effects of hard segment length distribution*; Macromolecules **18** (1) (1985) 32–44; DOI: 10.1021/ma00143a005

[20] A. Arun and R. J. Gaymans; *Hydrophilic poly(ethylene oxide)-aramide segmented block copolymers*; European Polymer Journal **45** (10) (2009) 2585–2866; DOI:10.1016/j.eurpolymj.2009.07.002

[21] H. Lin and B. D. Freeman; *Gas solubility, diffusivity and permeability in poly(ethylene oxide)*; Journal of Membrane Science **239** (1) (2004) 105–117; DOI:10.1016/j.memsci.2003.08.031

Chapter 3

[22] J. Krijgsman, D. Husken and R. J. Gaymans; *Synthesis and characterisation of uniform bisester tetra-amide segments*; Polymer **44** (23) (2003) 7043–7053; DOI:10.1016/S0032-3861(03)00681-5

[23] G. Gordon Cameron, M. D. Ingram, M. Younus Qureshi, H. M. Gearing, L. Costa and G. Camino; *The thermal degradation of poly(ethylene oxide) and its complex with NaCNS*; European Polymer Journal **25** (7-8) (1989) 779–784; DOI:10.1016/0014-3057(89)90044-X

[24] L. Costa, A. M. Gad, G. Camino, G. G. Cameron and M. Y. Qureshi; *Thermal and thermooxidative degradation of poly(ethylene oxide)-metal salt complexes*; Macromolecules **25** (20) (1992) 5512–5518; DOI:10.1021/ma00046a059

[25] L. Costa, G. Camino, M. P. Luda, G. G. Cameron and M. Y. Qureshi; *The thermal degradation of poly(propylene oxide) and its complexes with LiBr and LiI*; Polymer Degradation and Stability **48** (3) (1995) 325–331; DOI:10.1016/0141-3910(95)00091-Y

[26] L. Costa, G. Camino, M. P. Luda, G. G. Cameron and M. Y. Qureshi; *The thermal oxidation of poly(propylene oxide) and its complexes with LiBr and LiI*; Polymer Degradation and Stability **53** (3) (1996) 301–310; DOI:10.1016/0141-3910(96)00094-8

[27] G. J. E. Biemond, J. Feijen and R. J. Gaymans; *Poly(ether amide) segmented block copolymers with adipic acid based tetraamide segments*; Journal of Applied Polymer Science **105** (2) (2007) 951–963; DOI:10.1002/app.26202

[28] R. J. Cella; *Morphology of segmented polyester thermoplastic elastomers*; Journal of Polymer Science: Polymer Symposia **42** (2) (1973) 727–740; DOI:10.1002/polc.5070420224

[29] M. van der Schuur and R. J. Gaymans; *Segmented block copolymers based on poly(propylene oxide) and monodisperse polyamide-6,T segments*; Journal of Polymer Science, Part A: Polymer Chemistry **44** (16) (2006) 4769–4781; DOI:10.1002/pola.21587

[30] N. B. Coltrup, L. H. Daly and S. E. Wiberly; *Introduction to Infrared and Raman Spectroscopy*; 3rd edition (1990); New York, NY (United States of America): Academic press; ISBN 978-0121825546

[31] D. W. van Krevelen and K. te Nijenhuis; *Properties of Polymers*; 4th edition (2009); Amsterdam (The Netherlands): Elsevier; ISBN 978-0080548197

[32] P. C. Hiemenz; *Polymer Chemistry: The Basic Concepts*; 1st edition (1984); New York, NY (United States of America): Marcel Dekker; ISBN 978-0824770822

[33] L. Mandelkern; *Crystallization of Polymers: Kinetics and Mechanisms*; 2nd

edition (2004); Cambridge (England): Cambridge University Press; ISBN 978-0521816823

[34] J. C. Halpin and J. L. Kardos; *Moduli of crystalline polymers employing composite theory*; Journal of Applied Physics **43** (5) (1972) 2235–2241; DOI: 10.1063/1.1661482

[35] P. J. Flory; *Theory of crystallization in copolymers*; Transactions of the Faraday Society **51** (1955) 848–857; DOI:10.1039/TF9555100848

[36] J. Krijgsman, D. Husken and R. J. Gaymans; *Synthesis and properties of thermoplastic elastomers based on PTMO and tetra-amide*; Polymer **44** (25) (2003) 7573–7588; DOI:10.1016/j.polymer.2003.09.043

[37] N. S. Murthy, M. Stamm, J. P. Sibilia and S. Krimm; *Structural changes accompanying hydration in nylon 6*; Macromolecules **22** (3) (1989) 1261–1267; DOI:10.1021/ma00193a043

[38] D. Husken and R. J. Gaymans; *The structure of water in PEO-based segmented block copolymers and its effect on transition temperatures*; Macromolecular Chemistry and Physics **209** (9) (2008) 967–979; DOI:10.1002/macp.200700584

Chapter 3

CHAPTER 4

Sub-ambient temperature CO$_2$ and light gas permeation through segmented block copolymers with tailored soft phase

Chapter 4

Abstract

The permeation properties of a series of block copolymers based on poly(ethylene oxide)-*ran*-poly(propylene oxide) (PEO-*ran*-PPO) soft segments and monodisperse tetra-amide (T6T6T) hard segments have been studied. The polyether soft segment used in the current study differs from the commonly used pure poly(ethylene oxide) (PEO) soft segment by the fact that it contains 25 wt.% randomly distributed poly(propylene oxide) (PPO). The presence of the methyl group of PPO suppresses crystallization of the soft segment and strongly improves the permeability of these materials, especially at sub-ambient temperatures. In addition, the unique monodisperse character of the hard segment ensures a very well phase separated morphology resulting in a very pure soft phase.

The soft segment length of these block copolymers was varied between 1000 and 10000 g/mol (62–89 wt.%). High soft segment concentrations and flexibility were obtained resulting in high CO_2 permeabilities (up to 570 Barrer at 50℃). Due to the random distribution of PPO in the predominantly PEO based soft segment crystallization of PEO was not observed at temperatures as low as -10℃. CO_2 permeabilities exceeding 200 Barrer could be obtained at this low temperature. The CO_2/light gas selectivity in these materials is governed by the solubility selectivity and consequently only slightly lowered due to the introduction of PPO in the soft segment.

Comparison with literature revealed that this block copolymer system has exceptionally high CO_2 permeabilities combined with reasonable CO_2/light gas selectivities. It is very interesting in CO_2 separation processes where sub-ambient conditions are present as at these low temperatures one can take maximum advantage of the increased separation ability of the polymer materials while maintaining excellent transport characteristics.

4.1 Introduction

The removal of carbon dioxide (CO_2) from mixtures with light gases such as hydrogen (H_2), nitrogen (N_2) and methane (CH_4) is an increasingly important application in industry. CO_2/H_2 and CO_2/CH_4 separation are relevant separation processes in the synthesis gas and natural gas production, while CO_2/N_2 separation (e.g. flue gases) has the potential to become a large scale application in order to reduce the antropogenic CO_2 emissions [1].

Currently, CO_2 is mainly removed by chemical or physical absorption or pressure swing adsorption (PSA), but also membrane technology (especially for CO_2/CH_4 separation) plays an important role. The use of membrane technology has inherent advantages, such as small footprint, mechanical simplicity (no rotating equipment) and a high energy efficiency [2]. The large scale of these separation processes requires large membrane areas and/or highly permeable membranes with sufficiently high CO_2/light gas selectivities to remove the CO_2.

Recently Freeman *et al.* [3] have reported extensive material selection guidelines that provide an overview of desirable membrane characteristics to achieve a combination of high CO_2 permeability and high CO_2/light gas selectivity. They identified polar groups, in particular ethylene oxide (EO) units, as a versatile building block to prepare highly permeable and sufficiently selective membranes. The polar ether oxygen linkages favor the solubility of the quadrupolar CO_2 over the non-polar light gases (high selectivity), whereas the flexible EO linkages permit high CO_2 diffusivity (high permeability). Specifically, they developed chemically crosslinked networks using acrylates based on poly(ethylene oxide). The use of 30 wt.% poly(ethyleneglycol diacrylate) (PEGDA) and 70 wt.% poly(ethyleneglycol monoethylacrylate) (PEGMEA) (PEGDA/PEGMEA 30/70) ensured a fully amorphous PEO phase (as low as the T_g) and subsequently a high CO_2 permeability (P_{CO_2} = 320 Barrer at 35℃) [4–6].

As an alternative route, segmented block copolymers containing poly(ethylene oxide) (PEO) are of specific interest as they can be easily processed (in the melt or by dissolving them in a suitable solvent) and their specific properties can be easily tuned by smart selection of the individual building blocks in the copolymer. In general, multi-block copolymers consist of an alternating series of flexible soft segments and crystallizable hard segments. The flexible soft segments usually have a low glass transition temperature and provide the material its flexibility and gas permeability,

while the rigid hard segments give the material its mechanical and heat stability [7].

The block copolymers studied in literature differ in amount of poly(ethylene oxide) (PEO) and type of hard segment used. Typical examples described in literature contain hard segments such as polyamides [8–16], polyimides [17], polyurethanes [12] and polyesters [18, 19]. Commercially available PEO based block copolymers are, for instance, produced by Arkema under the trade name PEBAX®. A typical example is PEBAX®1074, a block copolymer containing 55 wt.% PEO and 45 wt.% polyamide, which shows a reasonable CO_2 permeability of 120 Barrer at 10 atmosphere [9]. However, the low crystallinity of the PEBAX® amide phase leads to the dissolution of hard segment in the soft PEO phase deteriorating gas transport characteristics [9, 11]. Another commercially available PEO block copolymer family having poly(butylene terephthalate) (PBT) as a hard segment (Polyactive® produced by Isotis B.V.) was studied by Metz *et al.* [18]. They systematically studied the relationship between polymer composition and morphology on the gas separation performance of these block copolymers and demonstrated that dissolution of the PBT hard segment into the permeable soft phase reduced the CO_2 permeability.

Also studies on non-commercial block copolymers [12, 15–17] indicate that the degree of phase separation and soft segment flexibility highly influence the gas transport properties of the materials. These studies suggest that the incorporation of a second dispersed phase, e.g. the hard segment of a block copolymer, in the continuous soft domains reduces the chain flexibility of the PEO soft segments, thereby lowering the gas permeability of the material. A similar effect has been observed as a result of the formation of PEO crystalline domains [15, 16, 18]. These domains, which are formed below the PEO melting temperature, reduce the content of soft amorphous PEO phase available for gas permeation and at the same time decrease the flexible soft segment length between the crystallized hard segments. Consequently the gas permeability is reduced. To illustrate this effect, pure high molecular weight PEO (M_w = 1,000,000 g/mol, T_m = 68℃), which has a high crystallinity of 71 vol%, has a CO_2 permeability of only 12 Barrer at 35℃ [20].

Overall, the gas permeation properties of PEO based block copolymers are a complex function of amorphous phase content, dispersed impermeable phase content and soft segment flexibility. The ideal morphology of a block copolymer system desired for gas separation membranes would exhibit

1. Good phase separation of the hard and soft segments;

2. Complete crystallization of the hard segment;

3. High PEO content;

4. Low glass transition temperature of the soft segment (high chain flexibility); and

5. No soft phase crystallinity or low soft segment melting temperature.

Researchers attempt to obtain this ideal morphology and, for instance, Husken *et al.* [15] studied PEO based block copolymers with monodisperse tetra-amide (T6T6T) hard segments. These block copolymers, denoted as PEO-T6T6T, showed very high hard segment crystallinity ($\sim$85%) and this resulted in improved mass transport characteristics. The CO_2 permeability of a PEO_{2000}-T6T6T block copolymer ($M_{w,PEO}$ = 2000 g/mol) was 180 Barrer (an almost 50% increase compared to PEBAX®1074). Nonetheless, these block copolymers still contained large PEO crystalline domains below ambient temperature, thus restricting their applicability [15]. A method to suppress this crystallization is the use of poly(propylene oxide) (PPO) as a soft segment [21]. The presence of the methyl side group in PPO restricts regular chain packing of the soft phase and suppresses crystallization. This leads to highly permeable membranes due to an increase in soft segment flexibility and a larger fractional free volume as compared to PEO. Furthermore, as PPO is fully amorphous, the permeability remains high at temperatures as low as -10℃ [16]. Unfortunately the selectivity of PPO based block copolymers is lower compared to PEO based block copolymers due to the lower size sieving ability as well as the lower CO_2 solubility [16]. A combination of the beneficial properties of both types of soft segment (the high selectivity of PEO and the amorphous character of PPO) would be ideal.

Following this idea we synthesized a block copolymer system based on predominantly PEO based soft segments (75 wt.% PEO) containing a random distribution of 25 wt.% PPO (20 mol%) (PEO-*ran*-PPO) and monodisperse tetra-amide (T6T6T) hard segments. These block copolymers, denoted as PEO-*ran*-PPO-T6T6T, have a very low PEO melting temperature (< 0℃), as the methyl group present in PPO restricts crystallization of the PEO, combined with an extremely pure soft phase due to the very high hard segment crystallinity. Hence, these block copolymers approach the ideal morphology as described above and are therefore exceptionally interesting as a membrane material for CO_2 separation, especially at sub-ambient temperatures. We recently reported the synthesis and thermal-mechanical properties of this block copolymer system [22].

The present article investigates the pure gas separation properties of these PEO-*ran*-PPO-T6T6T block copolymers in a temperature range from −10℃ to 50℃ and highlights the advantage of the new soft segment by comparing the results with other PEO based block copolymers reported and in particular with the PEO-T6T6T block copolymers reported by Husken *et al.* [15].

4.2   Theory

Mass transport in non-porous polymeric structures following the solution-diffusion model has been well documented in literature [23–25]. The steady state gas permeability coefficient of a dense polymeric membrane is given by Equation (4.1)

$$P_i = \frac{N_i \cdot l}{f_{2,i} - f_{1,i}} \tag{4.1}$$

where P_i is the gas permeability coefficient (cm^3 (STP)·cm/(cm^2·s·cmHg)), N_i is the steady state flux of the component through the membrane (cm^3(STP)/(cm^2·s)), l the membrane thickness (cm) and $f_{2,i}$ and $f_{1,i}$ respectively the upstream and downstream fugacity (cmHg). The permeability coefficient is usually expressed in units of Barrer, where 1 Barrer equals $1 \cdot 10^{-10}$ (cm^3(STP)·cm/(cm^2·s·cmHg)) or $7.5 \cdot 10^{-18}$ (m^3 (STP)·m/(m^2·s·Pa)). The fugacity can be replaced by (partial) pressure if gas phase non-ideality is neglected.

When diffusion can be described using Fick's first law and the upstream pressure is significantly higher than the downstream pressure, the permeability coefficient can be expressed by Equation (4.2)

$$P_i = D_i \cdot S_i \tag{4.2}$$

where D_i is the average effective diffusion coefficient (cm^2/s) and S_i is the solubility coefficient (cm^3 (STP)/(cm^3·cmHg)). The ideal selectivity of a membrane for gas A over gas B is given by the ratio of the pure gas permeability coefficients according to Equation (4.3)

$$\alpha = \frac{P_A}{P_B} = \frac{D_A}{D_B} \cdot \frac{S_A}{S_B} \tag{4.3}$$

where D_A/D_B is the diffusivity selectivity and S_A/S_B is the solubility selectivity.

Gas diffusivity is enhanced by decreasing penetrant size, increasing polymer chain flexibility (often characterized by a decrease in glass transition temperature), increasing polymer fractional free volume (FFV) and decreasing polymer-penetrant interactions [23]. Penetrant solubility is increased by increasing condensability of the penetrant (which increases with increasing critical temperature and boiling point) and increasing polymer-penetrant interactions [23]. In general, polyether based block copolymers exhibit a low T_g resulting in high CO_2 diffusivity but lower diffusivity selectivity. In this case CO_2/light gas selectivity is mainly achieved by high CO_2/light gas solubility selectivity, as the quadrupolar CO_2 exhibits favorable interaction with the ether oxygen linkages, favoring the solubility of the polar CO_2 over the non-polar gases like H_2, N_2 and CH_4 [3].

4.3 Experimental

4.3.1 Polymer synthesis

Two series of polyether based segmented block copolymers using a soft segment containing a random distribution of PEO and PPO (weight ratio 3:1), denoted PEO-ran-PPO$_x$-T6T6T and (PEO-ran-PPO$_{2500}$/T)$_y$-T6T6T, were used (Figure 4.1a,b). In the first series the polyether soft phase was varied by changing the polyether molecular weight (x) up to a maximum of 2500 g/mol (Figure 4.1a). Segmented block copolymers with longer soft segments (> 4600 g/mol for PEO$_x$-T6T6T [26]) often experience liquid-liquid demixing during synthesis resulting in a low molecular weight material, which should be avoided. This problem can be overcome by extending short polyether soft segments with terephthalic groups [27]. Hence, in the second series short PEO-ran-PPO$_{2500}$ soft segments were extended with terephthalate groups up to a total segment length (y) of 10000 g/mol (Figure 4.1b). No liquid-liquid demixing was observed in this series and block copolymers with sufficient molecular weight were obtained. As such, by changing x and/or y, the total length of the soft segment was varied from 1000 to 10000 g/mol. The crystallizable hard segment used is a monodisperse tetra-amide (T6T6T) (Figure 4.1c). The actual synthesis and the thermal-mechanical properties of these segmented block copolymers are described in a separate article [22].
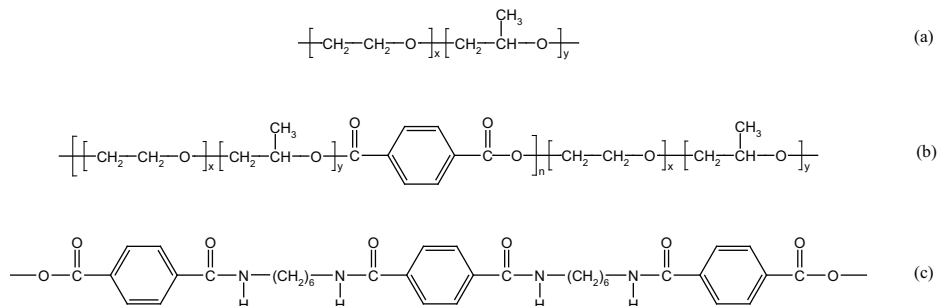
Figure 4.1: Chemical structure of (a) the PEO-*ran*-PPO soft segment, (b) the terephthalic extended PEO-*ran*-PPO soft segment and (c) the monodisperse tetra-amide (T6T6T) hard segment used.

⌐ *PEO-ran-PPO$_x$-T6T6T block copolymers*

The PEO-*ran*-PPO$_x$-T6T6T copolymers were synthesized by a polycondensation reaction using PEO-*ran*-PPO$_x$ soft segments with a molecular weight (x) of 1000 and 2500 g/mol and T6T6T hard segments [22].

⌐ *(PEO-ran-PPO$_{2500}$/T)$_y$-T6T6T block copolymers*

The (PEO-*ran*-PPO$_{2500}$/T)$_y$-T6T6T copolymers were synthesized by a polycondensation reaction using PEO-*ran*-PPO$_{2500}$ soft segments, which are extended with terephthalic units (T), and T6T6T hard segments [22]. The total molecular weight of the soft segment (y) was varied from 3750 to 10000 g/mol.

4.3.2 Membrane preparation

Films of approximately 100 μm in thickness were prepared from vacuum dried (50℃) block copolymers using a Lauffer OPS 40 press. The temperature of the mould was set at approximately 30℃ above the melting temperature (T_m) of the block copolymer as determined by DSC. Air was removed from the polymer in the mould by quickly pressurizing/depressurizing the samples. This pressurization/depressurization cycle was repeated three times before pressing the films at ∼8.5 MPa for 5 minutes. Subsequently, the samples were cooled to room temperature while maintaining the pressure. To prevent sticking of the polymer onto the metal plates of the press, glass-fiber reinforced PTFE sheets were used as an intermediate layer between the polymer film and the metal plates (Benetech type B105).

4.3.3 Gas permeation properties of the prepared films

The pure gas permeation properties of the prepared films were determined for sub-sequently N_2, O_2, He, H_2, CH_4 and CO_2 at different temperatures varying from -10℃ to 50℃. Pure gas permeability values were calculated from the steady-state pressure increase in time in a calibrated volume at the permeate side, following the constant volume/variable pressure method [28], at an upstream pressure of 4 bar. The feed pressure instead of fugacity has been used in Equation (4.1) to evaluate the gas permeability due to the low feed pressure used and consequential assumed nearly ideal behavior. Ideal gas selectivity values were calculated from the ratio of pure gas permeability values.

4.4 Results & discussion

4.4.1 Introduction

In this article the effect of the block copolymer composition and the soft segment flexibility on the mass transport characteristics of the synthesized PEO-*ran*-PPO based block copolymers are studied in a temperature range from -10℃ to 50℃. In particular, the effect of the random distribution of 25 wt.% PPO in the predominantly PEO (75 wt.%) based soft segment will be discussed. Hence, the gas separation performance of these new block copolymers will be primarily compared to the properties of a block copolymer system based on pure PEO (without PPO) with the same type of hard segment, denoted as PEO-T6T6T [15], and a block copolymer system with a slightly different hard segment (a di-amide denoted as TΦT) in which a mixture of PEO and PPO soft segments is used at an equal (3:1) weight ratio. This polymer is denoted as PEO_{2000}/PPO_{2200}-TΦT (75/25) [16]. The thermo-mechanical and gas transport properties of these reference block copolymers are reported elsewhere [15, 16, 21, 26, 27].

4.4.2 Effect of copolymer composition on gas permeability

The primary focus of this paper is the CO_2 separation performance of the developed materials. Figure 4.2 shows the CO_2 permeability at 35℃ as a function of the soft segment concentration in the PEO-*ran*-PPO block copolymers synthesized and compares its values with the results obtained for the two other block copolymer systems reported previously (PEO-T6T6T [15] and PEO_{2000}/PPO_{2200}-TΦT [16]). Yoshino *et al.* [12] and Freeman *et al.* [9] showed that the degree of phase separation between the flexible soft segments and the crystallizable hard segments of the block copolymer has a profound effect on the CO_2 permeability: A decrease in phase separation efficiency led to a significant decrease in CO_2 permeability. However, in our work the degree of phase separation of the block copolymer systems based on a monodisperse tetra-amide hard segment (T6T6T) is high (∼85%) and comparable for all block copolymers [22, 26, 27]. This allows direct comparison of their gas separation properties on the basis of soft segment concentration. Pure gas permeability values of the prepared PEO-*ran*-PPO-T6T6T block copolymers for all the six different gases studied are, for completeness, summarized in Table A4.1 (Appendix).
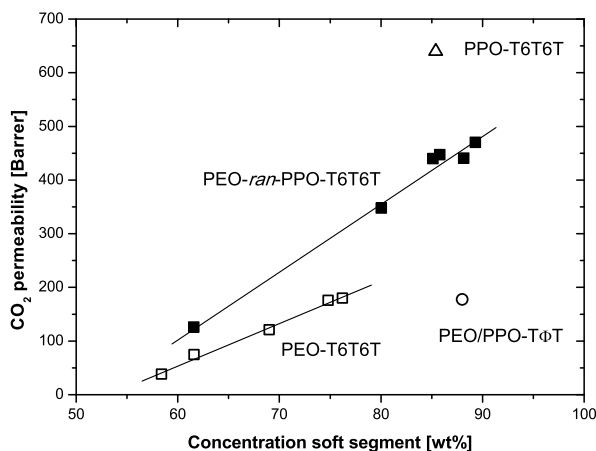
Figure 4.2: CO_2 permeability as a function of the soft segment concentration at 35℃ for (■) PEO-*ran*-PPO-T6T6T, (□) PEO-T6T6T [15], (○) PEO_{2000}/PPO_{2200}-TΦT (75/25) [16] and (△) PPO_{4200}-T6T6T block copolymers.

The CO_2 permeability of the PEO-*ran*-PPO based block copolymers increases strongly with increasing soft segment concentration in the block copolymer. The permeability of the other gases increases to a similar extent (see Table A4.1 (Appendix)). The same has been observed for other PEO based block copolymer systems [9, 12, 15–18]. As will be shown later, the CO_2/light gas selectivity is almost independent of the soft segment concentration, which suggests that gas permeation predominantly occurs through the soft polyether domains, whereas the crystallized hard domains act as impermeable filler, providing the material its mechanical and dimensional stability [9, 12, 15–18].

The CO_2 permeability of the PEO-*ran*-PPO based block copolymers increased by a factor of approximately two over the entire soft segment concentration range compared to their pure PEO based counterparts (PEO-T6T6T). This shows the strong benefit of the random replacement of 25 wt.% of PEO for PPO in the soft segment (compare ■ with ●) as it significantly enhances the gas permeability of the polyether based block copolymers. This increase can be attributed to a significant increase in soft segment flexibility (which is visible when the respective T_g's of both polymers are compared (Table A4.1 (Appendix)) enhancing gas diffusivity [3, 22], combined with, most likely, an increase in fractional free volume (FFV) as the FFV in PPO based materials is generally higher than in PEO based materials due to the presence of the methyl group in PPO [29]. The observed increase in permeability for PEO-*ran*-PPO is more than what would be expected based on simple mixing rules, which is most probably due to the random distribution of PPO which also influences the packing of PPO chains.

The prerequisite of a random distribution of the PEO and PPO moieties in a single soft segment is evident when the results are compared with the PEO_{2000}/PPO_{2200}-TΦT (75/25) block copolymer where the two soft segments are only physically mixed. Although this block copolymer has a rather low hard segment crystallinity (25%) due to the highly polar nature of the short monodisperse TΦT di-amide hard segment, it shows that simple mixing of PEO and PPO soft segments does not enhance CO_2 permeability (nor does it reduce PEO crystallinity [21]).

4.4.3 Effect of soft segment flexibility on CO_2 permeability

Although the soft segment concentration is an important parameter to tune the gas permeation characteristics in block copolymers, it is not considered to be the only one.

Yoshino *et al.* [12], Okamoto *et al.* [17] and Metz *et al.* [18] state that also the soft segment flexibility (typically characterized by changes in glass transition temperature) influences the gas separation performance of these block copolymer systems.

This effect becomes evident when the CO_2 permeability is normalized for the soft segment concentration (denoted as n-PCO_2 (= P_{CO_2}/wt.% soft segment) in Table A4.1 (Appendix)) and plotted versus the molecular weight between physical crosslinks (M_{CRL}) (Figure 4.3). This molecular weight between physical crosslinks (the crystallized hard segments) is defined as the actual soft segment length (methyl side-groups of PPO are not taken into account).

The sharp increase of the normalized CO_2 permeability as a function of M_{CRL} for the PEO-*ran*-PPO$_x$-T6T6T (■) block copolymer series with a soft segment length up to 2500 g/mol (and the reference PEO$_x$-T6T6T (□) block copolymer series with a soft segment length up to 2000 g/mol) shows that the mass transport properties of these polymer systems not only depend on the soft segment concentration, but also strongly depend on the soft segment length and consequently the soft segment flexibility. An increase in the soft segment length and thus flexibility (as proven by a decrease in T_g, see Table A4.1 (Appendix)) significantly increases the CO_2 permeability, which is
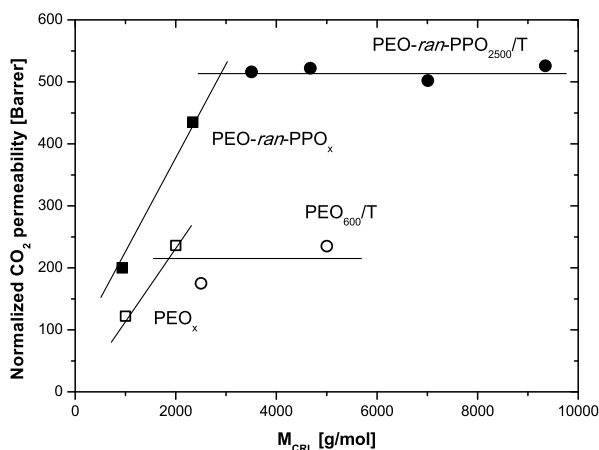
Figure 4.3: Normalized CO_2 permeability (n-PCO_2) as a function of the molecular weight between physical crosslinks (M_{CRL}) at 35°C for (■) PEO-*ran*-PPO$_x$-T6T6T, (●) (PEO-*ran*-PPO$_{2500}$/T)$_y$-T6T6T, (□) PEO$_x$-T6T6T [15] and (○) (PEO$_{600}$/T)$_y$-T6T6T [15].

also observed by other researchers [12, 17, 18]. This suggests that high soft segment lengths are beneficial for the mass transport properties.

In our work we prepared block copolymers containing higher soft segment lengths ($>$ 2500 g/mol) and thus higher anticipated soft segment flexibility by extending the PEO-*ran*-PPO soft segment (M_w = 2500 g/mol) with terephthalic units ($\bullet$, (PEO-*ran*-PPO$_{2500}$/T)$_y$-T6T6T) [22]. These terephthalic units do not crystallize and belong to the amorphous soft phase. As a consequence, the soft phase concentration is increased. However, the use of these terephthalic units limits the rotational freedom of the soft segment near this terephthalic unit [27]. This results in an increase in glass transition temperature (Table A4.1 (Appendix), compare PEO-*ran*-PPO$_{2500}$-T6T6T and (PEO-*ran*-PPO$_{2500}$/T)$_y$-T6T6T), which indicates that the soft segment flexibility of the (PEO-*ran*-PPO$_{2500}$/T)$_y$-T6T6T block copolymers is reduced compared to the PEO-*ran*-PPO$_{2500}$-T6T6T block copolymer, although a higher total soft segment length is obtained. This is clearly visualized in Figure 4.3, where the soft segment concentration normalized CO_2 permeability (n-PCO$_2$) of the terephthalic extended PEO-*ran*-PPO block copolymers ($\bullet$) reaches a plateau value, as the soft segment flexibility within this series is constant ($T_g \approx -60$℃) due to the presence of these terephthalic extender which limits the flexibility. This effect is also observed for the PEO based block copolymer systems studied by Husken *et al.* [15], in which terephthalic units where used to extend low molecular PEO of 600 g/mol ($\circ$).

These results indicate that besides the soft segment concentration also the soft segment flexibility (represented by the T_g of the soft segment of the polymer) is a crucial parameter that determines the mass transport properties as shown in Figure 4.4.

Lin *et al.* [3] showed this relation to be generally applicable to all PEO based materials (pure PEO, PEO based block copolymers and crosslinked PEO structures). For block copolymer systems this implies that the microdomain morphology is of great influence on the macroscopic gas permeation properties. One desires a very pure soft amorphous phase (to obtain an as low as possible T_g) and this is achieved in the current work by the use of the monodisperse tetra-amide hard segments.

The CO_2 permeability of the PEO-*ran*-PPO based block copolymer system could probably be even higher if a soft segment length above 2500 g/mol can be achieved without the use of terephthalic units. Unfortunately, the only other PEO-*ran*-PPO soft segment commercially available has a molecular weight of 12,000 g/mol, which proved to be unsuitable for block copolymer synthesis due to liquid-liquid demixing
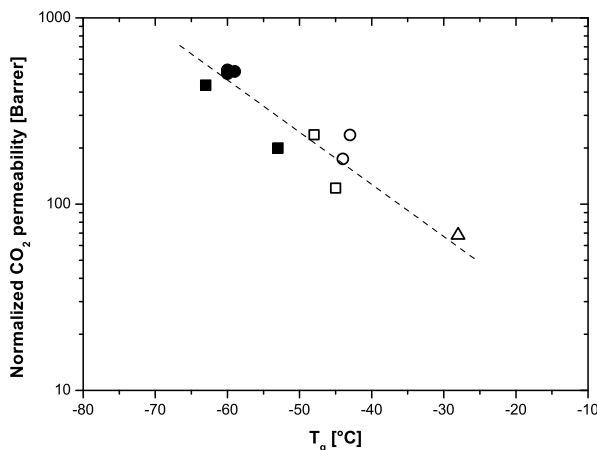
Figure 4.4: Normalized CO$_2$ permeability at 35℃ as a function of the glass transition temperature for (■) PEO-*ran*-PPO$_x$-T6T6T, (●) (PEO-*ran*-PPO$_{2500}$/T)$_y$-T6T6T, (□) PEO$_x$-T6T6T [15], (○) (PEO$_{600}$/T)$_y$-T6T6T [15] and (△) (PEO$_{300}$/T)$_{2500}$-T6T6T [15].

[22]. Husken *et al.* [26], who prepared PEO$_x$-T6T6T based block copolymers, could successfully prepare block copolymers with a soft segment length of up to 4600 g/mol. Due to the reduced polarity of the soft segment, PPO$_x$-T6T6T based block copolymers could successfully be prepared up to a soft segment length of 6200 g/mol. Therefore we think that PEO-*ran*-PPO based block copolymers with a maximum soft segment length of approximately 5000–6000 g/mol (a total soft segment concentration between 89–91 wt.%), which would exhibit even better performance, could be prepared.

4.4.4   Effect of block copolymer composition on CO$_2$/light gas selectivity

Table 4.1 summarizes the CO$_2$/light gas selectivity at 35℃ for a selection of the investigated PEO-*ran*-PPO based block copolymers and compares them with polyether based block copolymers reported in literature [15, 16]. The CO$_2$/light gas selectivity is practically independent of the soft segment length and only the CO$_2$/H$_2$ selectivity seems to decrease at short soft segment length ($x = 1000$ g/mol). This behavior is also observed by Husken *et al.* [15] and Metz *et al.* [18].

Table 4.1: CO_2/light gas selectivity for H_2, N_2 and CH_4 for a selection of PEO-*ran*-PPO-T6T6T block copolymers and several other block copolymers used as a reference at 35℃.

Sample	CO_2 permeability	Gas selectivity [–]		
	[Barrer]	CO_2/H_2	CO_2/N_2	CO_2/CH_4
PEO-*ran*-PPO$_{1000}$-T6T6T	123	7	46	13
PEO-*ran*-PPO$_{2500}$-T6T6T	348	10	45	13
(PEO-*ran*-PPO$_{2500}$/T)$_{10000}$-T6T6T	470	10	43	13
PEO$_{1000}$-T6T6T [15]	75	7	41	14
PEO$_{2000}$-T6T6T [15]	180	10	49	16
(PEO$_{600}$/T)$_{2500}$-T6T6T [15]	121	8	50	17
(PEO$_{600}$/T)$_{5000}$-T6T6T [15]	174	9	53	17
PPO$_{4200}$-T6T6T	640	6	24	7

In rubbery materials, like the polyether block copolymer systems studied in this work, the diffusion coefficient is not a strong function of penetrant size and the overall selectivity is primarily the result of a high solubility selectivity, due to the favorable interactions between CO_2 and the polar ether oxygen linkages [3]. Because the composition of the soft segment, and in particular the concentration of ether oxygen linkages in the soft segment, is not changed significantly by the random substitution of 25 wt.% PEO for PPO, it is expected that the solubility selectivity and thus the overall CO_2/light gas selectivity is not significantly affected. This is indeed visible in Table 4.1.

To illustrate this, we compare the gas separation performance of the different polymers at relative similar soft segment length ($\sim$2000–2500 g/mol). The PEO-*ran*-PPO$_{2500}$-T6T6T block copolymer ($M_{w,PEO-ran-PPO}$ = 2500 g/mol) has a CO_2 permeability of 348 Barrer, which is double the permeability of the PEO$_{2000}$-T6T6T block copolymer (180 Barrer), which has a soft segment length of 2000 g/mol. At this specific soft segment length the CO_2/H_2 selectivity is similar for both polymers ($\sim$10) as the small decrease in solubility selectivity (due to a decrease in polarity of the soft phase by the introduction of the less polar PPO) is offset by an small increase in diffusivity selectivity (as the diffusivity of the larger CO_2 is increased more as compared to the diffusivity of the smaller H_2). Furthermore, CO_2/N_2 ($\sim$45) and CO_2/CH_4 ($\sim$13) selectivity values have decreased only slightly compared to the PEO$_{2000}$-T6T6T based block copolymer, which has a CO_2/N_2 and CO_2/CH_4 selectivity of 49 respectively 16. This is due to a combination of a small decrease in solubility selectivity combined with a small decrease in diffusivity selectivity. A block copolymer containing a pure PPO

Chapter 4

soft segment (PPO$_{4200}$-T6T6T) has much lower CO_2/light gas selectivities (CO_2/H$_2$ = 6, CO_2/N$_2$ = 24 and CO_2/CH$_4$ = 7) essentially caused by a much more pronounced decrease in solubility selectivity. As such, the currently studied PEO-*ran*-PPO based block copolymers combine an increase in soft segment flexibility and corresponding large increase in gas permeability (compared to pure PEO based block copolymers) with a high selectivity attributable to the high fraction of PEO in the soft phase.

4.4.5   CO$_2$ permeability and CO$_2$/light gas selectivity as a function of temperature

The molecular organization of the block copolymer and especially the presence of crystalline polyether domains within the soft phase, which formation strongly depends on the temperature, has a major influence on the permeability [15, 16, 18]. In general polyether crystallization limits the amount of permeable amorphous soft phase and moreover it restricts the soft segment flexibility resulting in strongly reduced gas permeabilities. Therefore, crystallization of the polyether soft phase should be prevented at the temperatures of interest.

The influence of the temperature on the CO_2 permeability of the PEO-*ran*-PPO based block copolymers is shown in Figure 4.5 (filled symbols). The temperature dependence of the CO_2 permeability of a pure PEO based block copolymer (PEO$_{2000}$-T6T6T) [15] and a block copolymer containing a mixture of PEO$_{2000}$ and PPO$_{2200}$ soft segments in an equal weight ratio (PEO$_{2000}$/PPO$_{2200}$-TΦT (75/25)) [16] are both shown as well (open symbols, dashed line).

As a result of the remarkably low PEO melting temperature and low crystallinity in the PEO-*ran*-PPO based block copolymers [22], these materials show a linear increase in CO_2 permeability over the entire temperature range investigated (−10℃ – 50℃). The block copolymer with the highest soft segment length ((PEO-*ran*-PPO$_{2500}$/T)$_{10000}$-T6T6T) has a CO_2 permeability as high as 570 Barrer at 50℃. Furthermore, the CO_2 permeability at −10℃ remained also high at a value of 235 Barrer. This high permeability at lower temperatures is especially interesting as CO_2/light gas selectivity is significantly increased at these low temperatures, as will be described below. This gives the opportunity to apply these PEO based block copolymers in CO_2/light gas separations in a much broader temperature window as compared to currently available commercially materials like PEBAX$^{®}$ [8–11] or Polyactive$^{®}$ [18, 19], as these commercially available materials have a semi-crystalline PEO soft phase at
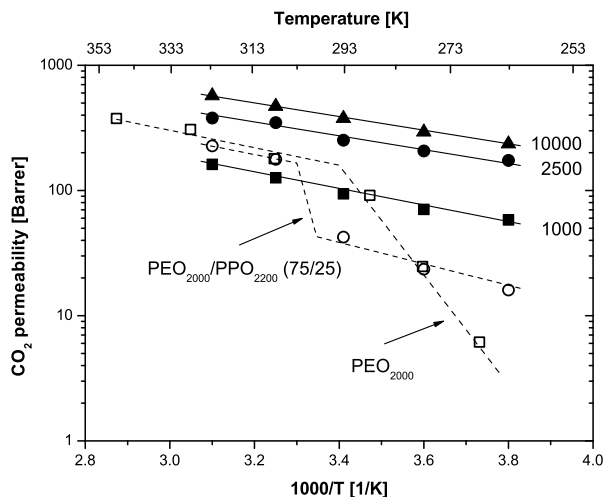
Figure 4.5: CO_2 permeability as a function of the temperature for the ($\blacksquare$) PEO-*ran*-PPO$_{1000}$-T6T6T, ($\bullet$) PEO-*ran*-PPO$_{2500}$-T6T6T, ($\blacktriangle$) (PEO-*ran*-PPO$_{2500}$/T)$_{10000}$-T6T6T, ($\square$) PEO$_{2000}$-T6T6T [15] and ($\bigcirc$) PEO$_{2000}$/PPO$_{2200}$-TΦT (75/25) [16] block copolymers.

these low temperatures which significantly reduces the gas permeability. The decrease in performance when crystallization occurs is also evident for the non-commercial reference block copolymers shown in Figure 4.5 (open symbols). The PEO$_{2000}$-T6T6T block copolymer [15] shows a linear increase in CO_2 permeability between 35°C and 75°Cas the PEO phase is completely amorphous at these temperatures. However, below 25°C a steep decrease in CO_2 permeability is observed due to the formation of crystalline PEO domains (T$_{m,PEO}$ = 21°C [26]), which decreases the amount of PEO accessible for gas transport and reduces the soft segment flexibility, thus decreasing diffusivity [15]. At −5°C this block copolymer has a CO_2 permeability of only 6 Barrer, which is almost two orders of magnitude lower than values obtained for the PEO-*ran*-PPO based block copolymers presented in this work. Moreover, the necessity of a random distribution of the PPO within the PEO soft segment is evident when the results of the PEO-*ran*-PPO block copolymers are compared with those of the PEO$_{2000}$/PPO$_{2200}$-TΦT (75/25) block copolymer in which the two types of soft segment (PEO and PPO) are simply mixed (Figure 4.5) (containing an equal PEO/PPO ratio compared to the PEO-*ran*-PPO based block copolymers) [16]. The use of a mixture of both soft segments did not successfully suppress PEO crystallinity (T$_{m,PEO}$ = 32°C [21]), and

99

consequently results in a significant decrease in gas permeability below this melting temperature. To illustrate this, the CO_2 permeability obtained with the PEO-*ran*-PPO soft segment (at a similar length of 2500 g/mol), in the temperature range where the PEO_{2000}/PPO_{2200}-TΦT (75/25) block copolymer has a semi-crystalline soft phase ($\leq$ 20℃), is approximately one order of magnitude higher.

These two comparative examples signify the importance of a random distribution of PPO within the PEO soft segment and demonstrate the benefits of this novel type of soft segment at temperatures where block copolymers containing pure PEO soft segments contain a semi-crystalline soft phase. Especially if a soft segment length above 2500 g/mol could be used (without the use of the terephthalic unit as an extender), as in general the PEO melting temperature increases with soft segment length [26]. For instance, a PEO_{4600}-T6T6T block copolymer ($M_{w,PEO}$ = 4600 g/mol) has a PEO melting temperature of 53℃ [26] severely limiting its applicability in gas separation applications below this temperature. The PEO-*ran*-PPO soft segment overcomes this disadvantage and combines a low PEO melting temperature with the ability to use high soft segment lengths. Hence, high soft segment flexibility and thus highly permeable membranes over a wide temperature range could be obtained.

The CO_2/light gas selectivity as a function of the temperature for the PEO-*ran*-PPO_{2500}-T6T6T block copolymer is shown in Figure 4.6 (filled symbols). The block copolymers with other soft segment lengths exhibit similar dependency of the CO_2/light gas selectivity on the temperature, but are for clarity not shown here. For comparison, the CO_2/light gas selectivity of a PEO_{2000}-T6T6T block copolymer (open symbols) (for T $\geq$ 35℃ as the PEO phase is completely amorphous at these temperatures and crystallizes at lower temperatures) has been added.

The ideal selectivity of the PEO-*ran*-PPO based block copolymers for CO_2/N_2, CO_2/CH_4 and CO_2/H_2 increases with decreasing temperature (Figure 4.6) and a linear behavior is observed over the complete temperature range investigated, as the soft phase is fully amorphous at all temperatures. Despite the addition of 25 wt.% PPO to the soft PEO phase, the selectivity of this polymer is only very slightly decreased compared to the PEO_{2000}-T6T6T block copolymer (open symbols). This is due to the only minor difference in chemical composition of the soft segment, as discussed before. The CO_2/light gas selectivity of a pure PPO based block copolymer (PPO_{4200}-T6T6T, Figure 4.6 and Table A4.1 (Appendix)) at 35℃ is shown for comparison as well (partially filled symbols). Although this block copolymer has a CO_2 permeability of 640 Barrer, which is likely to be achieved with a PEO-*ran*-PPO soft segment of
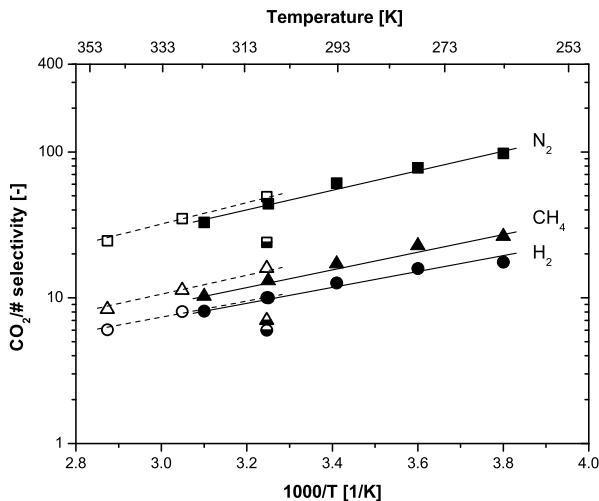
Figure 4.6: CO_2/light gas selectivity as a function of the temperature for CO_2/H_2 (circles), CO_2/CH_4 (triangles) and CO_2/N_2 (squares) for PEO-ran-PPO$_{2500}$-T6T6T (closed symbols), PEO$_{2000}$-T6T6T (open symbols) and PPO$_{4200}$-T6T6T (partially filled symbols).

similar length, its selectivity is only half the value found for the PEO-ran-PPO based block copolymers. The PEO-ran-PPO based block copolymers thus combine a high permeability with a high CO_2/light gas selectivity. This is especially important at temperatures below ambient, where other PEO based block copolymers exhibit inferior mass transport properties as a result of a semi-crystalline soft phase. This class of materials is as such very interesting in CO_2 separation processes where sub-ambient conditions are present as at these low temperatures one can take advantage of the increased separation ability of the polymer materials while maintaining excellent transport characteristics.

4.4.6 CO_2/N_2 upper bound relationship

Figure 4.7 presents a CO_2/N_2 permeability/selectivity trade-off curve in which the PEO-ran-PPO based block copolymers investigated in our work as well as relevant literature data are summarized. The existence of a relationship between the permeability and selectivity of polymer membranes, the so called upper bound or trade-off relationship, has been first described by Robeson [30] and later theoretically predicted by Freeman
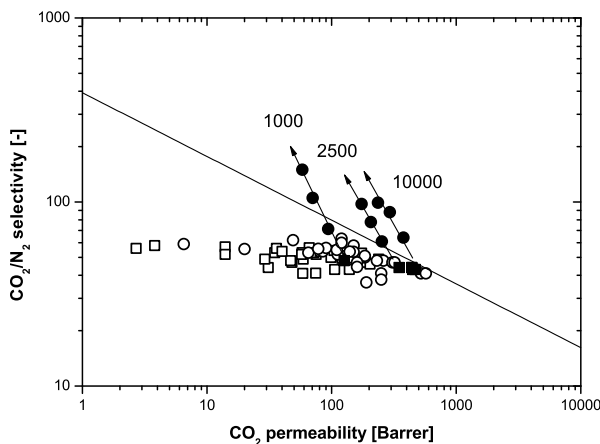
Figure 4.7: Robeson upper bound relationship between the CO_2/N_2 selectivity and the CO_2 permeability at 35℃. The PEO-*ran*-PPO block copolymers studied in this article are represented by the filled symbols (■). CO_2/N_2 permeability/selectivity data at reduced temperature (< 35℃) of the PEO-*ran*-PPO based block copolymers with a total soft segment length of 1000, 2500 and 10000 g/mol are also shown (●). Lower permeability represents lower temperature decreasing from 20℃ to -10℃ with steps of 15℃. Data obtained from literature on (□) pure PEO based block copolymers [9, 12, 15, 16, 18] and (○) PEO based crosslinked networks [4, 33, 34] have been added for comparison. The upper bound line has been drawn with data from [32].

[31]. Recently Robeson [32] revisited his original 1991 paper and included the latest literature data and several new gas pairs including CO_2/N_2. This CO_2/N_2 gas pair has been chosen here to assess our PEO-*ran*-PPO based block copolymer membranes, as it is the most widely documented gas pair regarding PEO based membranes.

The CO_2/N_2 selectivity at 35℃ for all studied polymers is rather constant at a level of $\sim$50 which reflects the fact that the soft PEO phase is the continuous domain for gas transport. The CO_2 permeability varies roughly from 1 to 500 Barrer due to differences in the microdomain morphology of the polymers [3]. The maximum CO_2 permeability at 35℃ reported in literature for PEO based block copolymers only (□) is around 200 Barrer using polyimide hard segments [12]. The very high permeability of the PEO-*ran*-PPO based block copolymers studied in our work (■) approaches the upper bound illustrated by Robeson. These PEO-*ran*-PPO block copolymers exhibit similar mass transport properties compared to the crosslinked PEO structures described by Freeman *et al.* [4–6], which reached a CO_2 permeability as high as 320

Barrer for a PEGDA/PEGMEA ratio of 30/70. Their PEGDA/PEGMEA networks containing more than 70% of PEGMEA reached higher permeability values (up to 570 Barrer), however these networks developed PEO crystalline domains below 0℃ due to the highly flexible nature of the monofunctional PEGMEA chains resulting in a distinct decrease in CO_2 permeability.

Since the block copolymers we studied keep high permeabilities at temperatures as low as -10℃, the temperature dependency of the CO_2/N_2 permeability/selectivity has been presented in Figure 4.7 as well (●). A decrease in temperature (below 35℃) moves the CO_2/N_2 separation performance significantly above the upper bound at all soft segment lengths. This highlights the advantage of these PEO-*ran*-PPO based block copolymers; a high CO_2 permeability combined with a good CO_2/N_2 selectivity even at temperatures as low as -10℃ could be reached. This is especially important at temperatures below ambient, where other PEO based block copolymers exhibit inferior mass transport properties as a result of a semi-crystalline soft phase (e.g. [12]). This class of materials is as such very interesting in CO_2 separation processes where sub-ambient conditions are present as at these low temperatures one can take maximum advantage of the increased separation ability of the polymer materials while maintaining excellent transport characteristics.

To summarize, Figure 4.8 presents the progress made in our work on polyether based block copolymer systems for CO_2 separation using monodisperse hard segments. First, Husken *et al.* (■) [15] prepared PEO based block copolymers using monodisperse tetra-amide hard (T6T6T) segments. PEO crystallization in these block copolymers, which is an issue, was partially suppressed by extending short PEO soft segments (M_w = 600 g/mol) with terephthalic units. Second, we prepared block copolymers based on a mixture of PEO_{2000} and PPO_{2200} soft segments and monodisperse di-amide (TΦT) hard segments (●) [16]. PEO crystallization could be successfully suppressed if at least 41 mol% of PPO was incorporated. Although the incorporation of PPO also resulted in an increase in permeability there has been made a significant sacrifice in selectivity (as shown by the downward slope of the data). In the current work (▲) we have shown that high CO_2 permeability and high CO_2/N_2 (and other light gas) selectivity can be achieved simultaneously by using long PEO based soft segments containing a random distribution of 25 wt.% PPO. As such, we overcome the usual trade-off dilemma (an increase in permeability gives a decrease in selectivity) by a smart design of the block copolymer system.

Chapter 4
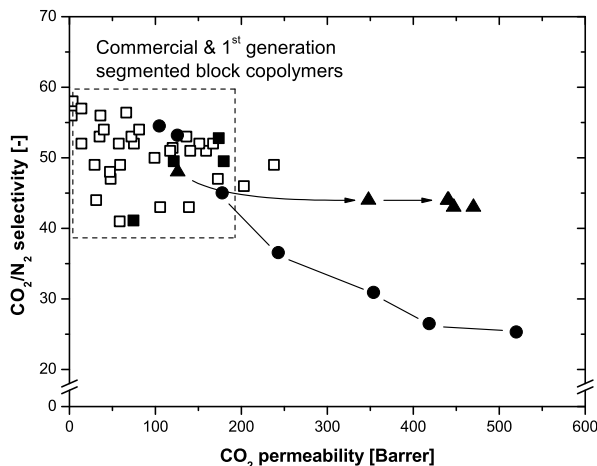
Figure 4.8: Robeson CO_2/N_2 upper bound relationship at 35℃. The filled symbols show the progress in our work on polyether based block copolymers systems for CO_2 separation using monodisperse hard segments, which are (■) PEO-T6T6T [15], (●) polyether-TΦT [16] and (▲) the current work on PEO-*ran*-PPO-T6T6T. Relevant literature data has been added (□) [9, 12, 18].

4.5   Conclusions

The mass transport properties of two block copolymer series based on poly(ethylene oxide)-ran-poly(propylene oxide) (PEO-*ran*-PPO) soft segments and monodisperse tetra-amide (T6T6T) hard segments have been studied. A commercially available polyether, which contains a random distribution of 75 wt.% PEO and 25 wt.% PPO, has been used as a soft segment and its length has been varied between 1000 and 10000 g/mol. The CO_2 permeability strongly increased as the soft segment length increased. High soft segment lengths (> 2500 g/mol) were obtained by extending the soft segment with a molecular weight of 2500 g/mol with terephthalic units. However, this terephthalic unit restricted the soft segment flexibility and thus influenced the mass transport properties. Overall, very high CO_2 permeabilities (up to 470 Barrer at 35℃) were obtained without any significant decrease in CO_2/light gas selectivity, when compared to commercially available and previously investigated PEO based polymers.

The temperature dependency of the mass transport properties between $-10℃$ and $50℃$ was investigated and a linear relationship between the logarithm of the gas permeability (and thus gas selectivity) as a function of the inverse temperature was observed. Due to the random presence of the methyl group of PPO, crystallization of the soft phase was restricted and the soft phase remained fully amorphous till temperatures as low as $-10℃$. This is a major advantage of these polymers when compared to PEO based block copolymer systems reported earlier, as these usually have a semi-crystalline PEO phase at or below ambient temperatures, which severely restricts gas permeation. In the current system the CO_2 permeability at $-10℃$ remained surprisingly high (> 200 Barrer) while CO_2/light gas selectivity increased to 19 and 99 for respectively CO_2/H_2 and CO_2/N_2. This class of materials is as such very interesting in CO_2 separation processes where sub-ambient conditions are present as at these low temperatures one can take advantage of the increased separation ability of the polymer materials while maintaining excellent transport characteristics.

4.6   Acknowledgements

Chapter 4

105

4.7   References

[1] IPCC; *Special Report on Carbon Dioxide Capture and Storage*; Technical report; Cambridge University Press; Cambridge (England) (2005)

[2] R. W. BAKER; *Membrane Technology and Applications*; 2nd edition (2000); West Sussex (England): John Wiley & Sons Ltd.; ISBN 978-0470854457

[3] H. LIN AND B. D. FREEMAN; *Materials selection guidelines for membranes that remove CO_2 from gas mixtures*; Journal of Molecular Structure **739** (1-3) (2005) 57–74; DOI:10.1016/j.molstruc.2004.07.045

[4] H. LIN, E. VAN WAGNER, J. S. SWINNEA, B. D. FREEMAN, S. J. PAS, A. J. HILL, S. KALAKKUNNATH AND D. S. KALIKA; *Transport and structural characteristics of crosslinked poly(ethylene oxide) rubbers*; Journal of Membrane Science **276** (1-2) (2006) 145–161; DOI:10.1016/j.memsci.2005.09.040

[5] H. LIN, E. VAN WAGNER, B. D. FREEMAN, L. G. TOY AND R. P. GUPTA; *Plasticization-enhanced hydrogen purification using polymeric membranes*; Science **311** (5761) (2006) 639–642; DOI:10.1126/science.1118079

[6] H. LIN, E. VAN WAGNER, R. RAHARJO, B. D. FREEMAN AND I. ROMAN; *High-performance polymer membranes for natural-gas sweetening*; Advanced Materials **18** (1) (2006) 39–44; DOI:10.1002/adma.200501409

[7] G. HOLDEN, H. R. KRICHELDORF AND R. P. QUIRK; *Thermoplastic Elastomers*; 3rd edition (2004); Munich (Germany): Hanser Gardner Publications; ISBN 978-1569903643

[8] V. I. BONDAR, B. D. FREEMAN AND I. PINNAU; *Gas sorption and characterization of poly(ether-b-amide) segmented block copolymers*; Journal of Polymer Science, Part B: Polymer Physics **37** (17) (1999) 2463–2475; DOI: 10.1002/(SICI)1099-0488(19990901)37:17⟨2463::AID-POLB18⟩3.0.CO;2-H

[9] V. I. BONDAR, B. D. FREEMAN AND I. PINNAU; *Gas transport properties of poly(ether-b-amide) segmented block copolymers*; Journal of Polymer Science, Part B: Polymer Physics **38** (15) (2000) 2051–2062; DOI:10.1002/1099-0488(20000801)38:15⟨2051::AID-POLB100⟩3.0.CO;2-D

[10] J. H. KIM, S. Y. HA AND Y. M. LEE; *Gas permeation of poly(amide-6-b-ethylene oxide) copolymer*; Journal of Membrane Science **190** (2) (2001) 179–193; DOI:10.1016/S0376-7388(01)00444-6

[11] V. BARBI, S. S. FUNARI, R. GEHRKE, N. SCHARNAGL AND N. STRIBECK; *SAXS and the gas transport in polyether-block-polyamide copolymer membranes*;

Macromolecules **36** (3) (2003) 749–758; DOI:10.1021/ma0213403

[12] M. Yoshino, K. Ito, H. Kita and K.-I. Okamoto; *Effects of hard-segment polymers on CO_2/N_2 gas-separation properties of poly(ethylene oxide)-segmented copolymers*; Journal of Polymer Science, Part B: Polymer Physics **38** (13) (2000) 1707–1715; DOI:10.1002/1099-0488(20000701)38:13⟨1707::AID-POLB40⟩3.0.CO; 2-W

[13] A. Car, C. Stropnik, W. Yave and K. V. Peinemann; *PEG modified poly(amide-b-ethylene oxide) membranes for CO_2 separation*; Journal of Membrane Science **307** (1) (2008) 88–95; DOI:10.1016/j.memsci.2007.09.023

[14] A. Car, C. Stropnik, W. Yave and K. V. Peinemann; *Pebax$^{®}$/polyethylene glycol blend thin film composite membranes for CO_2 separation: Performance with mixed gases*; Separation and Purification Technology **62** (1) (2008) 110–117; DOI:10.1016/j.seppur.2008.01.001

[15] D. Husken, T. Visser, M. Wessling and R. J. Gaymans; *CO_2 permeation properties of poly(ethylene oxide)-based segmented block copolymers*; Journal of Membrane Science **346** (1) (2010) 194–201; DOI:10.1016/j.memsci.2009.09.034

[16] S. R. Reijerkerk, A. Arun, K. Nijmeijer, R. J. Gaymans and M. Wessling; *Tuning of mass transport in multi-block copolymers for CO_2 capture applications*; Journal of Membrane Science (2009); DOI:10.1016/j.memsci. 2009.09.045

[17] K.-I. Okamoto, M. Fujii, S. Okamyo, H. Suzuki, K. Tanaka and H. Kita; *Gas permeation properties of poly(ether imide) segmented copolymers*; Macromolecules **28** (20) (1995) 6950–6956; DOI:10.1021/ma00124a035

[18] S. J. Metz, M. H. V. Mulder and M. Wessling; *Gas-permeation properties of poly(ethylene oxide) poly(butylene terephthalate) block copolymers*; Macromolecules **37** (12) (2004) 4590–4597; DOI:10.1021/ma049847w

[19] A. Car, C. Stropnik, W. Yave and K. V. Peinemann; *Tailor-made polymeric membranes based on segmented block copolymers for CO_2 separation*; Advanced Functional Materials **18** (18) (2008) 2815–2823; DOI:10.1002/adfm.200800436

[20] H. Lin and B. D. Freeman; *Gas solubility, diffusivity and permeability in poly(ethylene oxide)*; Journal of Membrane Science **239** (1) (2004) 105–117; DOI:10.1016/j.memsci.2003.08.031

[21] A. Arun and R. J. Gaymans; *Hydrophilic poly(ethylene oxide)-aramide segmented block copolymers*; European Polymer Journal **45** (10) (2009) 2858–2866; DOI:10.1016/j.eurpolymj.2009.07.002

[22] A. C. IJzer, A. Arun, S. R. Reijerkerk, K. Nijmeijer, M. Wessling

Chapter 4

AND R. J. GAYMANS; *Synthesis and properties of hydrophilic segmented block copolymers based on poly(ethylene oxide)-ran-poly(propylene oxide)*; Journal of Applied Polymer Science, accepted for publication

[23] J. G. WIJMANS AND R. W. BAKER; *The solution-diffusion model: A review*; Journal of Membrane Science **107** (1-2) (1995) 1–21; DOI:10.1016/0376-7388(95)00102-I

[24] M. MULDER; *Basic Principles of Membrane Technology*; 2nd edition (1996); Dordrecht (The Netherlands): Kluwer Academic Publishers; ISBN 978-0792342488

[25] Y. YAMPOLSKII, I. PINNAU AND B. D. FREEMAN; *Materials Science of Membranes for Gas and Vapor Separation*; 1st edition (2006); West Sussex (England): John Wiley & Sons Ltd.; ISBN 978-0470853450

[26] D. HUSKEN, J. FEIJEN AND R. J. GAYMANS; *Hydrophilic segmented block copolymers based on poly(ethylene oxide) and monodisperse amide segments*; Journal of Polymer Science, Part A: Polymer Chemistry **45** (19) (2007) 4522–4535; DOI:10.1002/pola.22186

[27] D. HUSKEN, J. FEIJEN AND R. J. GAYMANS; *Segmented block copolymers with terephthalic-extended poly(ethylene oxide) segments*; Macromolecular Chemistry and Physics **209** (5) (2008) 525–534; DOI:10.1002/macp.200700288

[28] A. BOS, I. G. M. PUNT, M. WESSLING AND H. STRATHMANN; *Suppression of CO_2-plasticization by semiinterpenetrating polymer network formation*; Journal of Polymer Science, Part B: Polymer Physics **36** (9) (1998) 1547–1556; DOI:10.1002/(SICI)1099-0488(19980715)36:9⟨1547::AID-POLB12⟩3.0.CO;2-5

[29] S. KALAKKUNNATH, D. S. KALIKA, H. LIN, R. RAHARJO AND B. D. FREEMAN; *Molecular dynamics of poly(ethylene glycol) and poly(propylene glycol) copolymer networks by broadband dielectric spectroscopy*; Macromolecules **40** (8) (2007) 2773–2781; DOI:10.1021/ma070016a

[30] L. M. ROBESON; *Correlation of separation factor versus permeability for polymeric membranes*; Journal of Membrane Science **62** (2) (1991) 165–185; DOI:10.1016/0376-7388(91)80060-J

[31] B. D. FREEMAN; *Basis of permeability/selectivity tradeoff relations in polymeric gas separation membranes*; Macromolecules **32** (2) (1999) 375–380; DOI:10.1021/ma9814548

[32] L. M. ROBESON; *The upper bound revisited*; Journal of Membrane Science **320** (1-2) (2008) 390–400; DOI:10.1016/j.memsci.2008.04.030

[33] V. A. KUSUMA, B. D. FREEMAN, M. A. BORNS AND D. S. KALIKA; *Influence of chemical structure of short chain pendant groups on gas transport properties*

   of cross-linked poly(ethylene oxide) copolymers; Journal of Membrane Science
   327 (1-2) (2009) 195–207; DOI:10.1016/j.memsci.2008.11.022

[34] Y. HIRAYAMA, Y. KASE, N. TANIHARA, Y. SUMIYAMA, Y. KUSUKI AND
   K. HARAYA; *Permeation properties to CO_2 and N_2 of poly(ethylene oxide)-
   containing and crosslinked polymer films*; Journal of Membrane Science **160** (1)
   (1999) 87–99; DOI:10.1016/S0376-7388(99)00080-0

Chapter 4

Appendix

Table A4.1: Pure gas permeation properties of PEO-*ran*-PPO-T6T6T block copolymers and several other block copolymers used as a reference at 35°C. SS: soft segment, T: terephthalic unit, M_{CRL}: the molecular weight between physical crosslinks in g/mol, T_g: glass transition temperature and n-P_{CO_2}: soft segment concentration normalized CO_2 permeability.

Sample	SS [wt.%]	T6T6T [wt.%]	T [wt.%]	M_{CRL} [g/mol]	T_g [°C]	Permeability [Barrer]						Selectivity [-]			n-P_{CO_2} [Barrer]
						CO_2	He	H_2	O_2	N_2	CH_4	CO_2/H_2	CO_2/N_2	CO_2/CH_4	
PEO-*ran*-PPO$_{1000}$-T6T6T	61.6	38.4	-	935	-53	123	11	17	8	3	9	7	46	13	200
PEO-*ran*-PPO$_{2500}$-T6T6T	80.0	20.0	-	2337	-63	348	19	35	19	8	26	10	45	13	435
(PEO-*ran*-PPO$_{2500}$/T)$_{3750}$-T6T6T	85.1	14.2	0.7	3505	-59	440	24	43	25	10	38	10	44	12	516
(PEO-*ran*-PPO$_{2500}$/T)$_{5000}$-T6T6T	85.8	11.0	3.2	4674	-60	448	25	44	25	11	35	10	43	13	522
(PEO-*ran*-PPO$_{2500}$/T)$_{7500}$-T6T6T	88.2	7.3	4.5	7010	-60	442	24	42	25	10	33	11	44	13	502
(PEO-*ran*-PPO$_{2500}$/T)$_{10000}$-T6T6T	89.3	5.6	5.1	9347	-60	470	26	45	27	11	37	10	43	13	526
PEO$_{1000}$-T6T6T [15]	61.6	38.4	-	1000	-45	75	6	10	5	2	6	7	41	14	122
PEO$_{2000}$-T6T6T [15]	76.2	23.8	-	2000	-48	180	11	18	8	4	11	10	49	16	236
(PEO$_{600}$/T)$_{2500}$-T6T6T [15]	69.0	20.0	11.0	2500	-44	121	9	15	6	2	7	8	50	17	175
(PEO$_{600}$/T)$_{5000}$-T6T6T [15]	74.8	11.1	14.1	5000	-43	174	12	19	9	3	10	9	53	17	235
PPO$_{4200}$-T6T6T	87.4	12.6	-			640	60	102	65	27	87	6	24	7	732
PEO$_{2000}$/PPO$_{2200}$-TΦT6T (75/25) [16]	87.2	12.8	-		-45	178	14	22	10	4	14	8	45	14	204

Chapter 4

CHAPTER 5

On the effects of plasticization in CO_2/light gas separation using polymeric solubility selective membranes

Chapter 5

Abstract

This paper reports the pure and mixed gas CO_2/H_2 and CO_2/CH_4 membrane separation performance of a highly permeable poly(ethylene oxide) based multi-block copolymer. The performance has been studied over a wide temperature (-10℃ to $+35$℃) and pressure range (up to 25 bar partial pressure of CO_2). In particular it addresses the effect of plasticization by CO_2. A strong dependency of the CO_2 permeability on the CO_2 concentration in the polymer matrix was observed in pure and mixed gas experiments. Plasticization effects increased the permeability of H_2 and CH_4 in mixed gas experiments compared to their pure gas values. The H_2 permeability was less influenced by plasticization than the CH_4 permeability due to their difference in kinetic diameter. As a result, mixed gas selectivities have been found to be systematically lower than pure gas selectivities. This difference between mixed and pure gas selectivity is exclusively dependent on the CO_2 concentration in the polymer matrix, which can be either the result of temperature or CO_2 fugacity. Consequently, mixed gas permeability and selectivity can be estimated at any temperature and CO_2 feed fugacity from pure gas data once a master curve of the correlation between the CO_2 concentration and the difference in selectivity is established.

5.1 Introduction

The availability of membrane materials with high separation performance that can operate under realistic process conditions is crucial for the large scale industrial application of membrane technology. Two separation challenges that are of major industrial relevance are the separation of carbon dioxide (CO_2) from hydrogen or from methane. Hydrogen is mainly produced by steam reforming of methane or other higher hydrocarbons and is generally combined with the water-gas shift reaction to maximize fuel efficiency [1]. This results in a hydrogen product stream containing CO_2 and other impurities, such as H_2S (depending on the feedstock), requiring efficient separation. On the other hand, the separation of CO_2 from methane is essential in natural gas processing and biogas upgrading to meet pipeline specifications [2].

Conventional membrane materials and those commercially used for CO_2/CH_4 separation (like cellulose acetate and several polyimides [3]) usually achieve their high selectivity due to high diffusivity selectivity. As a consequence, raw natural gas is usually pretreated to remove potential harmful components, such as H_2O, H_2S and higher hydrocarbons as these condensable penetrants show strong sorption behavior in the polymer. This sorption increases the polymer free volume and segmental mobility, which decreases the diffusivity selectivity and ultimately deteriorates the overall separation performance, a phenomenon usually referred to as plasticization [4].

In the case of CO_2/H_2 separation the use of diffusivity selective membrane materials would obtain a low pressure H_2 product as these membranes are more permeable to H_2 than to CO_2. Hence, a membrane that selectively permeates CO_2 over H_2 is especially interesting as it has the inherent advantage that the light gas remains at or near feed pressure avoiding expensive recompression.

Consequently, the development of membrane materials that preferentially permeate CO_2 over light gases and that remain their performance at high feed pressures is of major importance. In this respect, polymers containing ether oxygen linkages, especially ethylene oxide units, have attracted significant attention [5]. The polar ether oxygen linkages interact predominantly with the quadrupolar CO_2 as compared to the non-polar H_2 and CH_4, resulting in high CO_2/light gas solubility selectivities. Furthermore, the high flexibility of the ether oxygen linkages permits high CO_2 diffusivity and ultimately permeability, which is required as the scale of these operations is enormous. Additionally, it ensures a low size-sieving ability, being especially important for CO_2/H_2 separation, as H_2 is smaller than CO_2.

Chapter 5

Crosslinked polymers based on poly(ethylene oxide) PEO have been developed by Freeman *et al.* and have been extensively investigated for the separation of CO_2 from light gases over a wide temperature and pressure range [6–13]. They have shown excellent performance (a CO_2 permeability up to 570 Barrer at 35℃) and resistance against impurities such as H_2S, *n*-butane and toluene. The negative effects of plasticization by CO_2 (or the impurities) on the CO_2/CH_4 separation performance of these materials are minimal compared to their impact on traditional diffusivity selective materials [10]. In the case of CO_2/H_2 separation performance is even enhanced by plasticization as the diffusivity of CO_2 is increased more than the diffusivity of H_2, which increases diffusivity selectivity [11].

Another approach to design membranes that contain these polar ether oxygen linkages is the synthesis of multi-block copolymers [5]. In general, such block copolymers consist of an alternating series of flexible soft segments and crystallizable hard segments. The flexible soft segments hold the ether oxygen linkages and provide the material its flexibility and gas permeability, while the rigid hard segments give the material its mechanical and heat stability [14]. Bondar *et al.* [15, 16] and Metz *et al.* [17] have studied the commercially available PEBAX$^®$ and Polyactive$^®$ block copolymers. These materials exhibit high CO_2/light gas selectivity, but the permeability characteristics are poor due to inefficient phase separation and the presence of a semi-crystalline soft phase at relevant operating temperatures. Futhermore, they only performed pure gas experiments. Car *et al.* improved the permeability of these commercially available materials by the preparation of polymer blends using low molecular weight poly(ethylene glycol) [18–21]. In particular they studied the performance of PEBAX$^®$/PEG blends in high pressure, mixed gas conditions [19]. The molecular organization of these block copolymers (and their blends with PEG) is however very complex and up to five different phases can exist depending on the operating temperature. This complexity hinders the effective gas permeation through these block copolymers.

The permeability of these multi-block copolymers can be increased by the improvement of the molecular organization of the system. Complete phase separation between the hard and soft segments and/or the suppression of soft phase crystallization would largely increase the permeability. Recently, we have reported design strategies to enhance phase separation and suppress soft phase crystallization [22–26]. In particular, the development of block copolymers containing a soft segment with a random distribution of ethylene oxide and propylene oxide units has proven to be successful in the suppression of soft phase crystallization [25]. Pure gas permeation measurements

on these block copolymers revealed a combination of high CO_2 permeability (up to 470 Barrer at 35℃) and reasonable high CO_2/light gas selectivity [26]. The CO_2 permeability remained high at sub-ambient conditions (down to -10℃) as soft phase crystallization did not occur. In the present work we report the mixed gas, high pressure, separation performance for this type of block copolymer for CO_2/H_2 and CO_2/CH_4 separations and compare this to its pure gas behavior. The separation behavior is studied over a wide pressure range (4 to 25 bar CO_2 partial pressure) and temperature range (-10 to 35℃). Especially the influence of temperature and pressure on the plasticization behavior of CO_2 and its impact on membrane performance is investigated.

5.2   Theory

Mass transport in non-porous, dense, polymeric structures following the solution-diffusion model has been well documented in literature [4, 27]. The steady state gas permeability coefficient of a dense polymeric membrane is given by Equation (5.1):

$$P_i = \frac{N_i \cdot l}{f_{2,1} - f_{1,i}} \tag{5.1}$$

where P_i is the gas permeability coefficient (cm^3 (STP)$\cdot$cm/($cm^2 \cdot$s$\cdot$cmHg)), N_i is the steady state flux of component i through the membrane (cm^3 (STP)/($cm^2 \cdot$s)), l the membrane thickness (cm) and $f_{2,i}$ and $f_{1,i}$ respectively the upstream and downstream fugacity (cmHg). The permeability coefficient is usually expressed in units of Barrer, where 1 Barrer equals $1 \cdot 10^{-10}$ cm^3 (STP)$\cdot$cm/($cm^2 \cdot$s$\cdot$cmHg) or $7.5 \cdot 10^{-18}$ m^3 (STP)$\cdot$m/($m^2 \cdot$s$\cdot$Pa). The fugacity can be replaced by partial pressure if gas phase non-ideality is not significant.

When diffusion can be described using Fick's first law and the upstream pressure is significantly higher than the downstream pressure, the permeability coefficient can be expressed by Equation (5.2):

$$P_i = D_i \cdot S_i \tag{5.2}$$

where D_i is the average effective diffusion coefficient (cm^2/s) and S_i is the solubility coefficient (cm^3 (STP)/($cm^3 \cdot$cmHg)), where the solubility coefficient is defined as

the gas concentration in the polymer divided its fugacity according to Equation (5.3):

$$S_i = \frac{C_i}{f_i} \qquad (5.3)$$

The activity, a, of a gas is defined as the gas fugacity divided by the gas saturation fugacity at the temperature of interest ($f_i/f_{i,\text{sat}}$). The gas saturation fugacity can be derived from the gas saturation pressure by multiplication with the fugacity coefficient. The gas saturation pressure can be obtained using the modified Riedel equation [28]:

$$ln\, P_{\text{sat}} = A + \frac{B}{T} + C \cdot ln\, T + D \cdot T^E \qquad (5.4)$$

where P_{sat} is the gas saturation pressure, A, B, C, D and E are constants obtained from Perry's Handbook [28] and T is the temperature of interest (K). When the temperature of interest is above the critical temperature (this was the case for all temperatures for CH_4 and for CO_2 only for 35℃) the modified Riedel equation can be extrapolated to calculate a hypothetical gas saturation pressure.

The selectivity of a membrane for gas A over gas B is given by the ratio of the respective gas permeability coefficients according to Equation (5.5):

$$\alpha = \frac{P_A}{P_B} = \frac{D_A}{D_B} \cdot \frac{S_A}{S_B} \qquad (5.5)$$

where D_A/D_B is the diffusivity selectivity and S_A/S_B is the solubility selectivity. Gas diffusivity is enhanced by decreasing penetrant size, increasing polymer chain flexibility (often characterized by a decrease in glass transition temperature), increasing polymer fractional free volume and decreasing polymer-penetrant interactions [4]. Penetrant solubility is increased by increasing condensability of the penetrant (which increases with increasing critical temperature and boiling point) and increasing polymer-penetrant interactions [4].

5.3 Experimental

5.3.1 Polymer synthesis

The (PEO-*ran*-PPO$_{2500}$/T)$_{7500}$-T6T6T block copolymer was synthesized by a poly-condensation reaction using PEO-*ran*-PPO$_{2500}$ soft segments, which are extended with terephthalic units (T), and monodisperse tetra-amide (T6T6T) hard segments (Figure 5.1). The total molecular weight of the soft segment (y) was 7500 g/mol. The synthesis and thermal-mechanical properties of the block copolymer are described elsewhere [25].

5.3.2 Membrane fabrication

Films of approximately 100 μm thickness have been prepared from vacuum dried (50℃) block copolymer using a Lauffer OPS 40 press. The temperature of the mould was set approximately 30℃ above the melting temperature (T$_m$) of the block copolymer. First, air was removed from the polymer in the mould by quickly pressurizing/depressurizing the samples. This pressurization/depressurization cycle was repeated three times before actually pressing the samples at ∼8.5 MPa for 5 min. Subsequently, the samples were cooled to room temperature while maintaining the pressure. To prevent sticking of the polymer onto the metal plates of the press, glass-fiber reinforced PTFE sheets were used as an intermediate layer between the polymer film and the metal plates (Benetech type B105).

Figure 5.1: Chemical structure of (a) the PEO-*ran*-PPO$_{2500}$/T soft segment and (b) the monodisperse tetra-amide (T6T6T) hard segment.

5.3.3 Density

The density of the (PEO-*ran*-PPO$_{2500}$/T)$_{7500}$-T6T6T block copolymer required for use in gas sorption experiments was determined at room temperature. The samples were dried in a vacuum oven overnight (30℃) before use. Density measurements were performed using an AccuPyc 1330 Pycnometer (Micromeritics). The AccuPyc 1330 is a pycnometer of the gas expansion type and measures the amount of displaced gas (helium) at room temperature. Upon filling of the sample chamber and subsequent discharge into a second empty chamber with known volume the pressure is monitored. This allows calculation of the sample solid phase volume. The density is subsequently derived using the measured sample weight.

5.3.4 Gas sorption

Pure gas sorption isotherms of CO_2 and CH_4 at 35℃, 10℃ and −10℃ were determined gravimetrically by a magnetic suspension balance (MSB, Rubotherm) operated by MessPro software. Before each sorption experiment, the samples were degassed overnight by applying a vacuum. A sorption run consisted of several incremental pressure steps (from 4 to 25 bar) and the mass uptake as a function of time was measured. The measured equilibrium weight was corrected for buoyancy according to Archimedes' principle. The gas concentration in the polymer (cm^3 (STP)/cm^3 polymer) was calculated using the molar volume of the gas at standard temperature and pressure (STP, 1 bar and 273.15 K), the polymer volume (obtained from density measurements) and the molecular weight of the gas.

Mixed gas sorption isotherms using a 85/15 (vol.%) CO_2/CH_4 mixture were determined at 35℃, 10℃ and −10℃ using an apparatus based on the barometric, pressure-decay method [29] and described in detail by Raharjo *et al.* [10, 30]. The system consisted of three interconnected cells with known volume respectively the charge volume, the sample volume and the sampling volume. These cells were immersed in a temperature-controlled bath filled with an aqueous solution containing 50 wt.% methanol as cooling fluid. The sample with known weight was placed inside the sample volume and degassed overnight before starting an experiment. A sorption run consisted of several consecutive steps. First, a certain amount of gas was introduced in the charge volume and equilibrated. After the pressure stabilization, a known amount of gas was introduced into the sample chamber and the decrease in pressure was monitored.

After equilibrium was achieved ($\sim$ 1 day) a small amount of the gas mixture from the sample volume was expanded into the sampling volume and injected into the GC. Once the pressure in the sample volume was stable, additional gas from the charge volume was added. A sufficient pressure difference was maintained between the sample volume and the charge volume to avoid any gas flowing back from the sample volume into the charge volume. If needed additional gas was added to the charge volume afterwards. In this manner, the amount of each gas sorbed in the polymer sample as a function of its fugacity was determined. Calculations were performed using mass balances and the size of the gas sample withdrawn for GC analysis was taken into account as well. Fugacity coefficients for the pure as well as the mixed gas sorption isotherms were again calculated with the Soave-Redlich-Kwong equation of state and the simulation software package AspenPlus Properties (version 11).

5.3.5 Gas permeability

Gas permeation properties were determined at 35℃, 10℃ and -10℃ using a constant volume/variable pressure method with vacuum at the permeate side [31]. Gas permeance values were calculated from the pressure increase in time in a calibrated volume at the permeate side. The gas permeance values were normalized for the membrane thickness to obtain gas permeability. Pure gas permeability values were obtained at a pressure between 4 and 25 bar for CO_2, H_2 and CH_4. The ideal gas selectivity values were calculated from the ratio of pure gas permeability values. CO_2 mixed gas separation experiments were conducted using a 70/30 vol.% CO_2/H_2 or a 50/50 vol.% CO_2/CH_4 certified gas mixture. The feed pressure was varied between 4–25 bar partial pressure of CO_2. The feed and permeate compositions were analyzed using a Varian gas chromatograph (GC) equipped with a TCD and a HayeSep Q column. Helium was used as a carrier gas for the CO_2/CH_4 experiments, while nitrogen was used for the CO_2/H_2 experiments. The retentate flow was adjusted according to the applied pressure to provide stage-cuts $< 2\%$. The experiments were analyzed using fugacity instead of (partial) pressure, as especially CO_2 shows strong non-ideal behavior at high pressure and low temperature. Fugacity coefficients were calculated with the Soave-Redlich-Kwong equation of state and the simulation software package AspenPlus Properties (version 11).

Chapter 5

5.4 Results & discussion

5.4.1 Introduction

The results are divided in three different sections. In the first section, the membrane performance for the pure gases CO_2, H_2 and CH_4 will be discussed. Within this section we start the discussion on the pure gas sorption behavior followed by an analysis of the pure gas permeation behavior (permeability and selectivity). Subsequently, the pure gas sorption and permeability data are combined to discuss the pure gas diffusivity. In the second part, the membrane performance using CO_2/H_2 and CO_2/CH_4 gas mixtures is studied in detail and compared to its pure gas behavior. This section has the same organization as the pure gas section (sorption followed by permeation and diffusion). Third and last, a detailed analysis of the difference in membrane performance between pure and mixed gas transport is made. The role of the plasticizing effect of CO_2 is emphasized and the effect of pressure and temperature on the CO_2 concentration (and thus membrane separation performance) is discussed in detail.

5.4.2 Pure gas characteristics

⌐ *Pure gas sorption*
Figure 5.2 and Figure 5.3 present the pure gas CO_2 respectively the pure gas CH_4 sorption isotherms of the PEO-*ran*-PPO based block copolymer as a function of (a) fugacity and (b) activity. The gas activity is defined as the gas fugacity divided by the gas saturation fugacity ($f_i/f_{i,\text{sat}}$) at the corresponding temperature. The sorption of H_2 is very low (about one order of magnitude lower than that of CH_4 in this type of material [15]) and could not be determined accurately.

A non-linear increase in CO_2 concentration as a function of fugacity is observed (Figure 5.2a) This non-linearity is especially evident at a temperature of -10℃. At a fixed CO_2 fugacity the equilibrium CO_2 concentration is significantly higher when the experimental temperature is lowered as CO_2 is more condensable at lower temperatures. The solubility of CO_2 in the block copolymer is especially high due to the favorable interactions of the quadrupolar CO_2 with the polar ether oxygen linkages [5]. These polymer-penetrant interactions are even more favorable at lower temperatures, as shown in Figure 5.2b, as at any given activity the CO_2 concentration increases as the temperature decreases [6, 12].
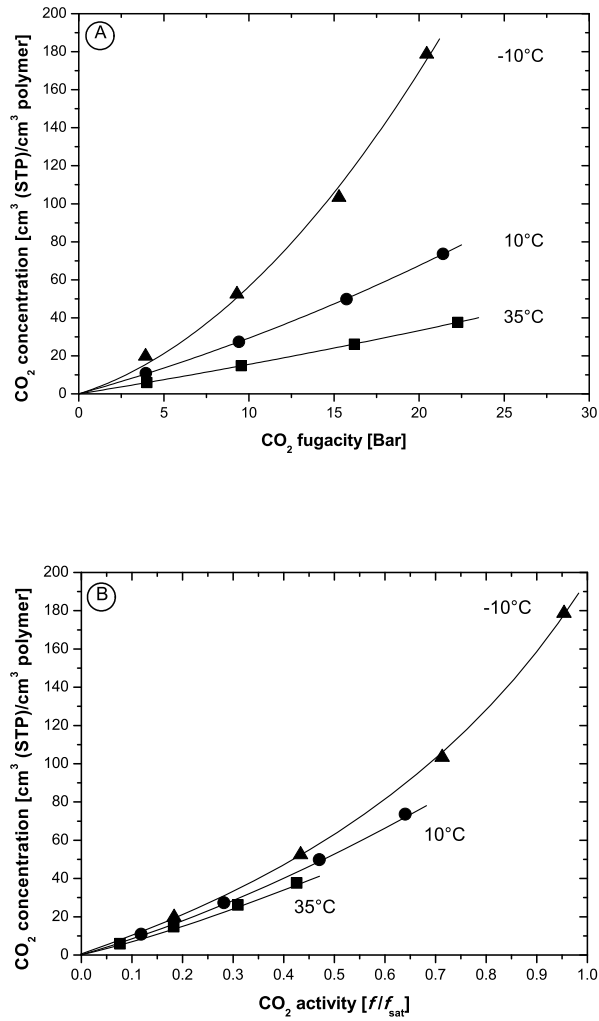
Figure 5.2: CO_2 concentration as a function of (a) fugacity and (b) activity for (PEO-*ran*-PPO$_{2500}$/T)$_{7500}$-T6T6T at a temperature of (■) 35℃, (●) 10℃ and (▲) −10℃.

Chapter 5

121
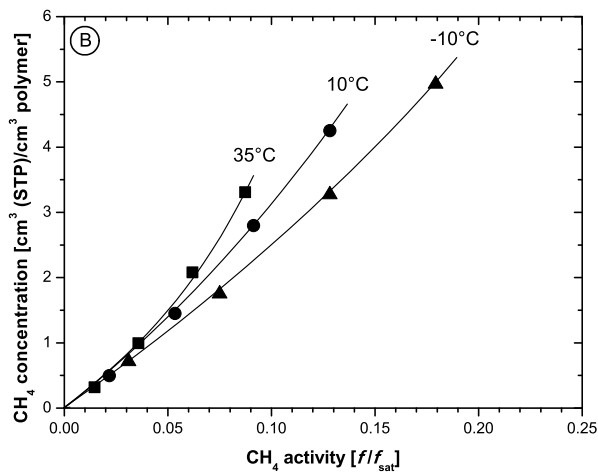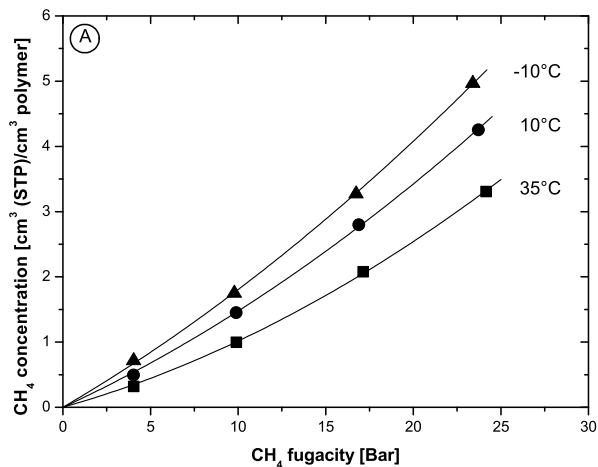
Figure 5.3: CH$_4$ concentration as a function of (a) fugacity and (b) activity for (PEO-*ran*-PPO$_{2500}$/T)$_{7500}$-T6T6T at a temperature of (■) 35℃, (●) 10℃ and (▲) −10℃.

Figure 5.3 shows the pure gas CH_4 sorption isotherms of the PEO-*ran*-PPO based block copolymer as a function of (a) fugacity and (b) activity.

The CH_4 sorption is significantly lower than the CO_2 sorption over the entire temperature and pressure range investigated (Figure 5.3a). This is a result of the lower critical temperature of CH_4 (191 K) compared to that of CO_2 (304 K), which makes CH_4 less condensable in the block copolymer compared to CO_2. Furthermore, CH_4 does not possess the favorable quadrupolar-polar interactions which contribute to the high solubility of CO_2. In addition, the sorption of the non-polar CH_4 becomes less favorable at lower temperatures as the CH_4 concentration at a fixed CH_4 activity decreases as temperature decreases (Figure 5.3b), which is opposite to the behavior of CO_2. This is in agreement with the polymer/penetrant interaction parameters (χ) calculated (not shown) and the result obtained by Freeman *et al.* [6, 12] for CO_2 and C_2H_6 in chemically similar crosslinked PEO structures.

⌐ *Pure gas permeation*

Figure 5.4 presents the pure gas CO_2 permeability as a function of the CO_2 fugacity in the PEO-*ran*-PPO block copolymer at a temperature of 35℃, 10℃ and −10℃.
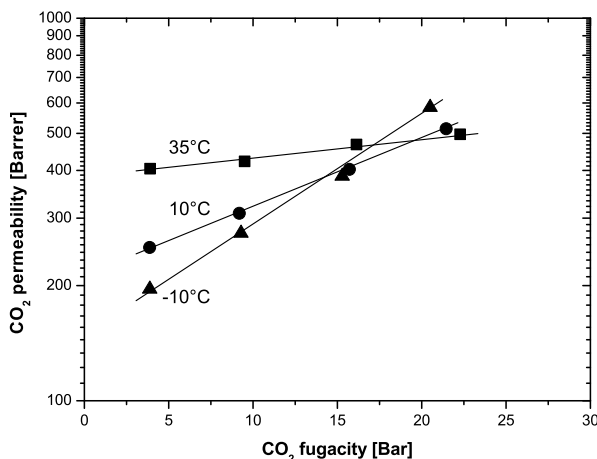
Figure 5.4: Pure gas CO_2 permeability as a function of the CO_2 fugacity for (PEO-*ran*-PPO$_{2500}$/T)$_{7500}$-T6T6T at a temperature of (■) 35℃, (●) 10℃ and (▲) −10℃.

The CO_2 permeability increases with increasing fugacity and this increase is much more pronounced at lower temperatures. Interestingly, above a certain fugacity, a lower temperature may even result in a higher CO_2 permeability at the same fugacity. For example, the CO_2 permeability at 10℃ is higher than that at 35℃ above a fugacity of approximately 20 bar. As the dependency of the CO_2 permeability on the fugacity is even stronger at -10℃ it surpasses the CO_2 permeability at 35℃ at an even lower fugacity of approximately 17 bar. This strong dependency of the CO_2 permeability as a function of fugacity is related to the amount of CO_2 sorbed in the polymer matrix (as discussed in the previous paragraph). The sorption of CO_2 plasticizes the polymer matrix, resulting in an increase in fractional free volume, mobility of the polymer chains and gas permeability. As temperature decreases, the effect of the fugacity on the CO_2 sorption becomes more pronounced (as shown before) and hence, plasticization effects and the resulting increase in gas permeability with increasing fugacity are more prominent at lower temperatures. A similar dependence of the CO_2 permeability on temperature and CO_2 fugacity has been observed by Freeman *et al.* [7, 10–12].

Figure 5.5 presents the pure gas permeability of the non-polar light gases H_2 and CH_4 as a function of their fugacity in the PEO-*ran*-PPO block copolymer at a temperature of 35℃, 10℃ and -10℃.

The permeability of these non-polar light gases is almost independent of its fugacity. At a temperature of 35℃ the H_2 permeability decreases from 38.9 to 34.9 Barrer as its fugacity increases from 4.0 to 25.3 bar, while the CH_4 permeability decreases from 31.8 to 29.7 Barrer as its fugacity increases from 4.1 to 24.1 bar. Although a more significant decrease is visible at -10℃, even at that temperature differences remain very small. This significantly different behavior for the non-polar gases H_2 and CH_4 compared to the quadrupolar gas CO_2 can be explained by the differences in sorption behavior. The solubility of CH_4 is more than one order of magnitude lower than the solubility of CO_2. As mentioned the solubility of H_2 could not be measured due to limitations in the experimental equipment, but its solubility in the PEO-*ran*-PPO based block copolymer will be even lower than that of CH_4 as the critical temperature of H_2, which gives a good estimation of penetrant solubility, is even lower than that of CH_4. Consequently, as the amount of light gas (H_2 or CH_4) sorbed in the block copolymer is much lower than the amount of CO_2, it cannot reach a sufficiently high level to induce considerable plasticization. Consequently its permeability is almost independent of the fugacity. In fact, as discussed, a slight decrease is observed and this can generally be attributed to a slight decrease in polymer fractional free volume as a function of the hydrostatic feed pressure due to compaction [16].
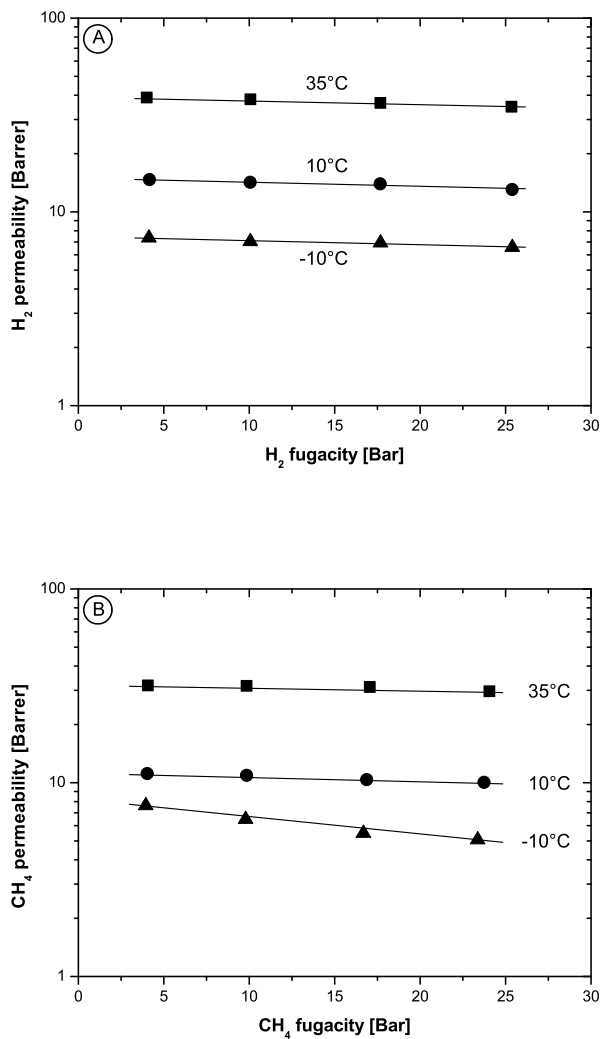
Figure 5.5: Pure gas H_2 permeability (a) and CH_4 permeability (b) as a function of their fugacity for (PEO-*ran*-PPO$_{2500}$/T)$_{7500}$-T6T6T at a temperature of (■) 35℃, (●) 10℃ and (▲) −10℃.

The pure gas permeability values are used to calculate the ideal, pure gas CO_2/light gas selectivities. Figure 5.6 presents these pure CO_2/light gas selectivities for CO_2 over (a) H_2 and (b) CH_4 as a function of the CO_2 fugacity in the PEO-*ran*-PPO block copolymer at a temperature of 35℃, 10℃ and −10℃.

The CO_2/light gas selectivity (H_2 as well as CH_4) increases as a function of CO_2 fugacity and this increase is more pronounced at lower temperatures. This increase is caused by an increase in CO_2 permeability, which is especially visible at lower temperatures.

⌐ *Pure gas diffusivity*

The pure gas diffusivity coefficients for CO_2 and CH_4 as a function of their respective fugacity at 35℃, 10℃ and −10℃ are presented in Figure 5.7. The diffusivities have been calculated from the measured pure gas permeabilities and solubilities according to Equation (5.2). The solubility coefficients are derived from the measured sorption isotherms according to Equation (5.3). As H_2 sorption could not be measured no H_2 diffusivity coefficients could be calculated.

The CO_2 diffusivity (Figure 5.7a) is nearly constant at a temperature of 35℃ and plasticization phenomena are not yet significant at this temperature. Different behavior is observed at 10℃ and −10℃ where the CO_2 diffusivity is a stronger function of its concentration in the polymer. It increases with increasing fugacity. Although the absolute increase in CO_2 diffusivity seems to be lower at −10℃ the relative increase at −10℃ is higher. This is because the amount of CO_2 sorbed and thus the associated plasticization effects are more significant at lower temperature. The CH_4 diffusivity (Figure 5.7b) shows completely different behavior. The sorption levels of CH_4 are significantly lower than those of CO_2 and plasticization effects do not occur. As a result a decrease in CH_4 diffusivity as a function of its fugacity is observed due to a slight reduction in polymer fractional free volume at higher fugacities. This reduction is the result of compaction imposed by the hydrostatic feed pressure acting on the membrane. The relative reduction is similar at all temperatures ($\sim$40%) as the feed pressure range is similar.
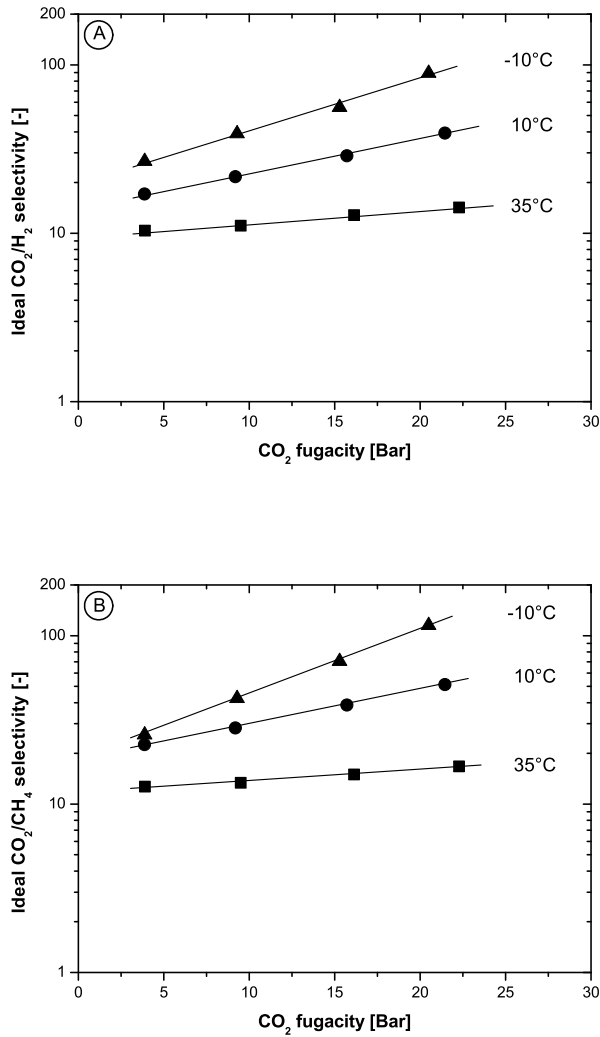
Figure 5.6: Ideal CO_2/H_2 selectivity (a) and CO_2/CH_4 selectivity (b) as a function of the CO_2 fugacity for (PEO-*ran*-PPO$_{2500}$/T)$_{7500}$-T6T6T at a temperature of (■) 35℃, (●) 10℃ and (▲) −10℃.
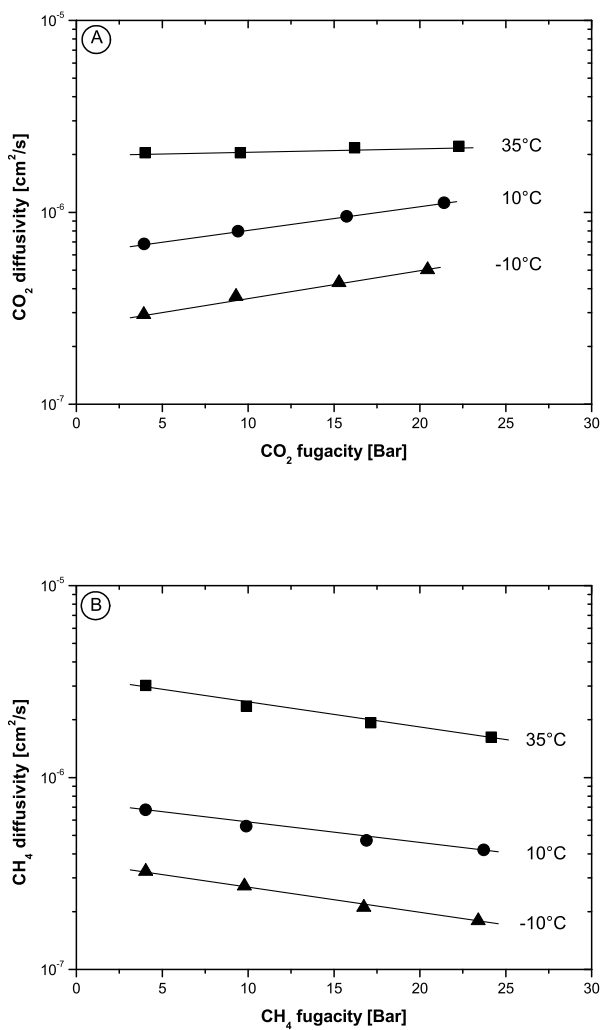
Figure 5.7: CO$_2$ diffusivity (a) and CH$_4$ diffusivity (b) as a function of their fugacity in the polymer for (PEO-*ran*-PPO$_{2500}$/T)$_{7500}$-T6T6T at a temperature of (■) 35℃, (●) 10℃ and (▲) −10℃.

5.4.3 Mixed gas characteristics

The presence of a strongly sorbing component (in the current work CO_2) might have a distinct effect on the mixed gas separation performance due to the occurrence of plasticization. Hence, in this section we investigate the CO_2/H_2 and CO_2/CH_4 mixed gas separation performance and compare its behavior to the pure gas data discussed before. Furthermore, we study the effect of plasticization on CO_2/CH_4 mixed gas separation in more detail. In particular, we performed CO_2/CH_4 mixed gas sorption measurements, which enable us to attribute changes in mixed gas permeability to a change in solubility and/or diffusivity.

⌐ *Mixed gas sorption*

Figure 5.8 presents the mixed gas CO_2 sorption isotherms from a mixed feed of 85/15 (vol.%) CO_2/CH_4 at the different temperatures investigated. The pure gas sorption isotherms previously discussed have been added as well for comparison. The CO_2/CH_4 ratio used for mixed gas sorption (85/15) is higher compared to mixed gas permeation (50/50) (as will be discussed hereafter). This has been done to be able to achieve reasonably high CO_2 fugacities as this would not be possible with a 50/50 ratio as a result of constrains in equipment design. Due to the low sorption of H_2 and the resulting difficulty in its experimental determination, mixed gas CO_2/H_2 sorption experiments have not been performed.

Figure 5.8 shows that there is no significant difference between the mixed and pure gas CO_2 concentration in the polymer. This indicates that the sorption of the plasticizing component (CO_2) is independent of the other component in the gas mixture (in this case CH_4). Although the CO_2/H_2 mixed sorption behavior has not been measured, it is expected that the same effect will be visible in that case and CO_2 sorption will be independent of the presence of H_2 as well. Therefore, plasticization effects, which are related to the concentration of CO_2 in the polymer, are expected to be similar in both pure and mixed gas conditions.

Figure 5.9 presents the mixed gas CH_4 sorption isotherms from the same 85/15 (vol.%) CO_2/CH_4 gas mixture. Once more, the pure gas sorption isotherms previously discussed have been added as well for comparison. Due to the low partial pressure and subsequently low sorption values of CH_4 in the block copolymer its exact determination is to some extent limited.
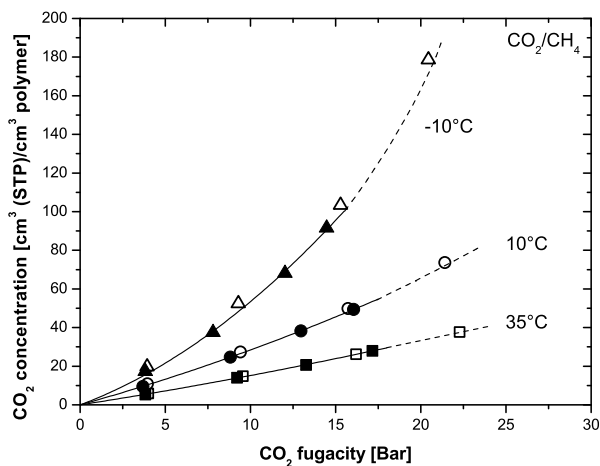
Figure 5.8: CO_2 concentration as a function of the CO_2 fugacity for a 85/15 (vol.%) CO_2/CH_4 gas mixture (closed symbols) and pure gas CO_2 (open symbols) for (PEO-*ran*-PPO$_{2500}$/T)$_{7500}$-T6T6T at a temperature of ($\blacksquare$,$\square$) 35℃, ($\bullet$,$\circ$) 10℃ and ($\blacktriangle$,$\triangle$) −10℃.
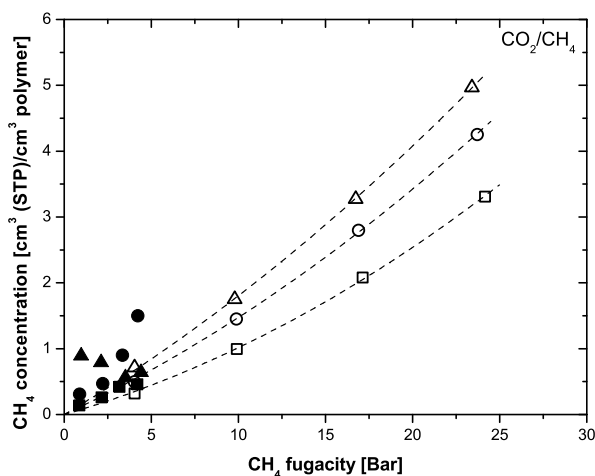
Figure 5.9: CH_4 concentration as a function of the CH_4 fugacity for a 85/15 (vol.%) CO_2/CH_4 gas mixture (closed symbols) and pure gas CH_4 (open symbols) for (PEO-*ran*-PPO$_{2500}$/T)$_{7500}$-T6T6T at a temperature of ($\blacksquare$,$\square$) 35℃, ($\bullet$,$\circ$) 10℃ and ($\blacktriangle$,$\triangle$) −10℃.

Although the sorption values of CH_4 are low, a distinctively different behavior compared to CO_2 can be observed. At 35℃ (■ ,□) and thus low levels of CO_2 sorption and anticipated plasticization the mixed gas sorption of CH_4 is almost similar to its pure gas values. At lower temperatures the stronger sorption of CO_2 results in deviation of the mixed sorption values form the pure gas analogs.

⌐ *Mixed gas permeation*

The mixed gas permeation properties of the PEO-*ran*-PPO based block copolymer have been tested using two different gas mixtures, a 70/30 (vol.%) CO_2/H_2 mixture and a 50/50 (vol.%) CO_2/CH_4 mixture. Figure 5.10 presents the mixed gas CO_2 and H_2 permeability coefficients for the CO_2/H_2 mixture, while Figure 5.11 presents the mixed gas CO_2 and CH_4 permeability coefficients for the CO_2/CH_4 mixture. Both figures also contain the corresponding pure gas permeabilities as discussed in the previous part for comparison.

For both cases, the mixed gas CO_2 permeabilities are similar to their pure gas values at all three temperatures investigated. This indicates that the presence of the second component (H_2 or CH_4) has negligible influence on the CO_2 permeability in mixed gas conditions. This can be expected as the previous paragraph showed that CO_2 sorption (and thus anticipated plasticization) is independent on the presence of the second component. The mixed gas H_2 and CH_4 permeabilities however, show very different behavior compared to their pure gas analogs. Their mixed gas permeabilities are higher than the pure gas values at all temperatures investigated. Furthermore, the difference between the mixed and pure gas values increases with increasing feed fugacity and decreasing temperature as expected because of the higher CO_2 concentration in the polymer at higher CO_2 fugacities and lower temperatures.

The mixed gas selectivity for the CO_2/H_2 as well as the CO_2/CH_4 gas mixture at the different temperatures investigated as determined from the mixed gas permeability values is presented in Figure 5.12. The pure gas selectivity for both gas mixtures is added as well for comparison.

The plasticizing effect of CO_2 increases the permeability of H_2 and CH_4 (compared to their pure gas values) while the CO_2 permeability is almost independent of the presence of a second component. Consequently, the mixed gas selectivities are lower than the corresponding pure gas selectivities. In the case of CO_2/H_2 the mixed gas selectivity slightly increases as a function CO_2 fugacity. This is identified as plasticization-enhanced gas separation [11]. The increase in free volume and gas
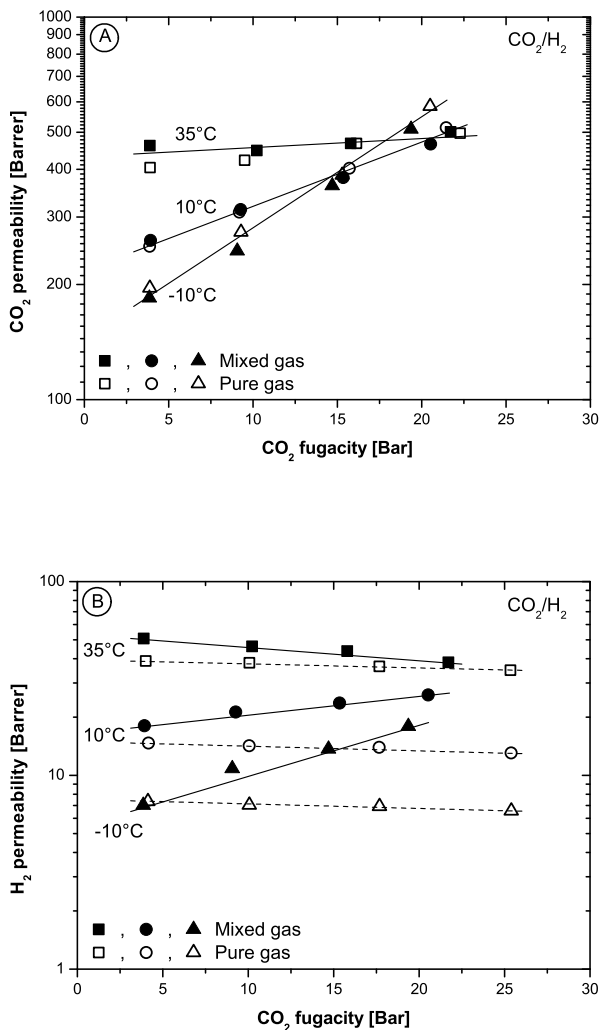
Figure 5.10: CO_2 permeability (a) and H_2 permeability (b) for a 70/30 (vol.%) CO_2/H_2 gas mixture (closed symbols) and pure gas (open symbols) as a function of the CO_2 fugacity for (PEO-*ran*-PPO$_{2500}$/T)$_{7500}$-T6T6T at a temperature of ($\blacksquare$,$\square$) 35℃, ($\bullet$,$\circ$) 10℃ and ($\blacktriangle$,$\triangle$) −10℃.
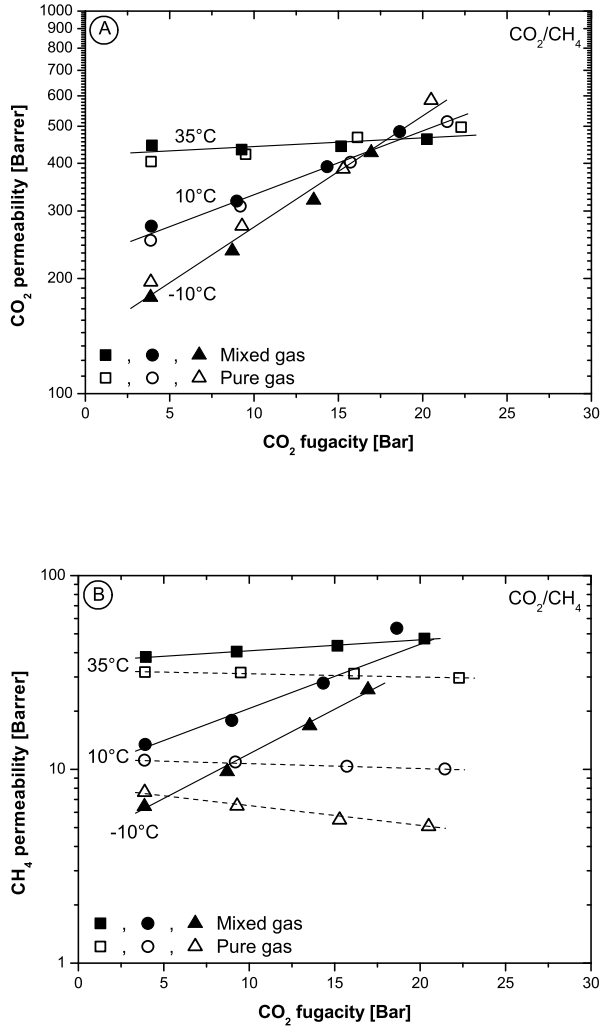
Figure 5.11: CO_2 permeability (a) and CH_4 permeability (b) for a 50/50 (vol.%) CO_2/CH_4 gas mixture (closed symbols) and pure gas (open symbols) as a function of the CO_2 fugacity for (PEO-*ran*-PPO$_{2500}$/T)$_{7500}$-T6T6T at a temperature of (■ , □) 35℃, (● , ○) 10℃ and (▲ , △) −10℃.
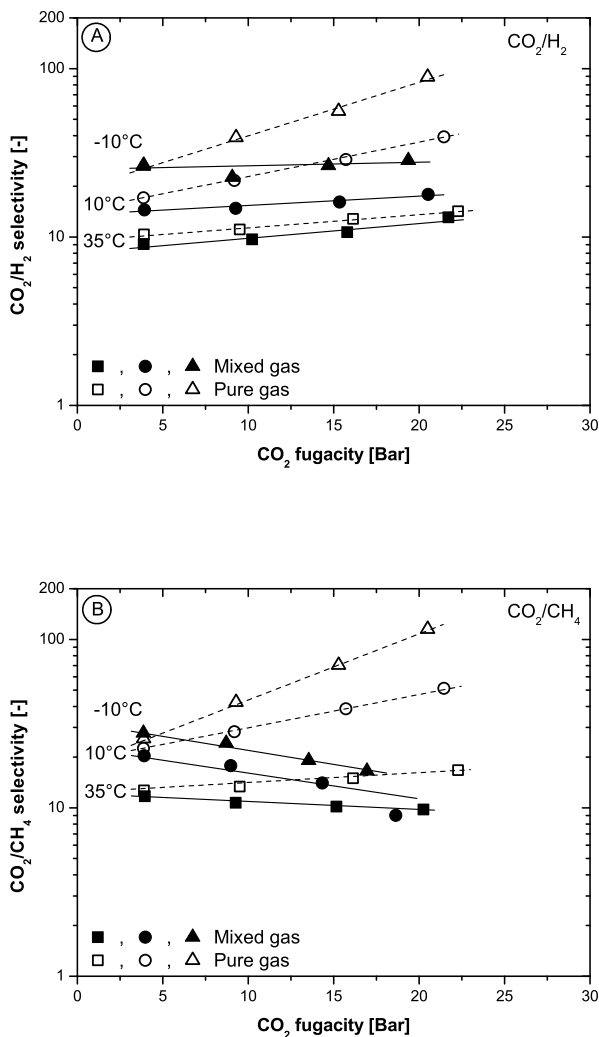
Figure 5.12: Mixed gas CO_2/H_2 selectivity (a) and mixed gas CO_2/CH_4 selectivity (b) for a 70/30 (vol.%) CO_2/H_2 respectively a 50/50 (vol.%) CO_2/CH_4 gas mixture (closed symbols) and their pure gas selectivity (open symbols) as a function of the CO_2 fugacity for (PEO-*ran*-PPO$_{2500}$/T)$_{7500}$-T6T6T at a temperature of ($\blacksquare$,$\square$) 35℃, ($\bullet$,$\circ$) 10℃ and ($\blacktriangle$,$\triangle$) −10℃.

diffusivity has a relatively larger effect on CO_2 than on H_2, because CO_2 has a larger kinetic diameter (3.30 Å) than H_2 (2.89 Å). Therefore, the CO_2 permeability shows a relatively larger increase with increasing fugacity than the H_2 permeability. Overall this results in an increase in CO_2/H_2 mixed gas selectivity as a function of CO_2 fugacity. The opposite behavior is observed for CO_2/CH_4 [10]. As the kinetic diameter of CH_4 (3.80 Å) is larger than that of CO_2 (3.30 Å), the enhancement of the gas diffusivity of CH_4 is stronger than that of CO_2, resulting in a decrease in CO_2/CH_4 mixed gas selectivity with increasing CO_2 fugacity.

⌐ *Mixed gas diffusivity*

The mixed gas sorption and permeability data for CO_2/CH_4 are used to calculate the diffusion coefficients for CO_2 and CH_4 according to Equation (5.2). These data are presented in Figure 5.13. The gas mixtures used for the mixed gas sorption contained a higher vol.% of CO_2 (85 vol.%) than those used for mixed gas permeation (50 vol.%) due to constrains in equipment design as discussed before. This has no influence on the membrane performance as its performance is dependent on the CO_2 fugacity and thus concentration and not on the gas mixture composition.

As expected based on the permeation and sorption data no noticeable difference of the CO_2 diffusivity is observed when either pure or mixed gases are used. However, the diffusivity of the non-polar CH_4, which decreased as a function of concentration (or pressure) under pure gas conditions (as discussed before), now shows a strong increase. The strong sorption of CO_2 plasticizes the polymer and enhances the diffusivity of CH_4. The increase is more pronounced at high CO_2 fugacity and low temperature as these conditions favor CO_2 sorption.

⌐ *Mixed gas CO_2/CH_4 solubility and diffusivity selectivity*

From the previous results the individual contributions of the solubility selectivity and the diffusivity selectivity for the mixed gas separation of CO_2/CH_4 can be calculated. These results are presented in Figure 5.14.

At a temperature of 35℃ and 10℃ the solubility selectivity is only modestly dependent on the CO_2 fugacity (Figure 5.14a). The small increase in solubility selectivity with increasing CO_2 fugacity at these temperatures is accompanied by a decrease in diffusivity selectivity (Figure 5.14b). The relative increase in solubility selectivity is however smaller than the relative decrease in diffusivity selectivity, resulting in an overall decrease in mixed gas permeability selectivity. At −10℃, the sorption of CO_2
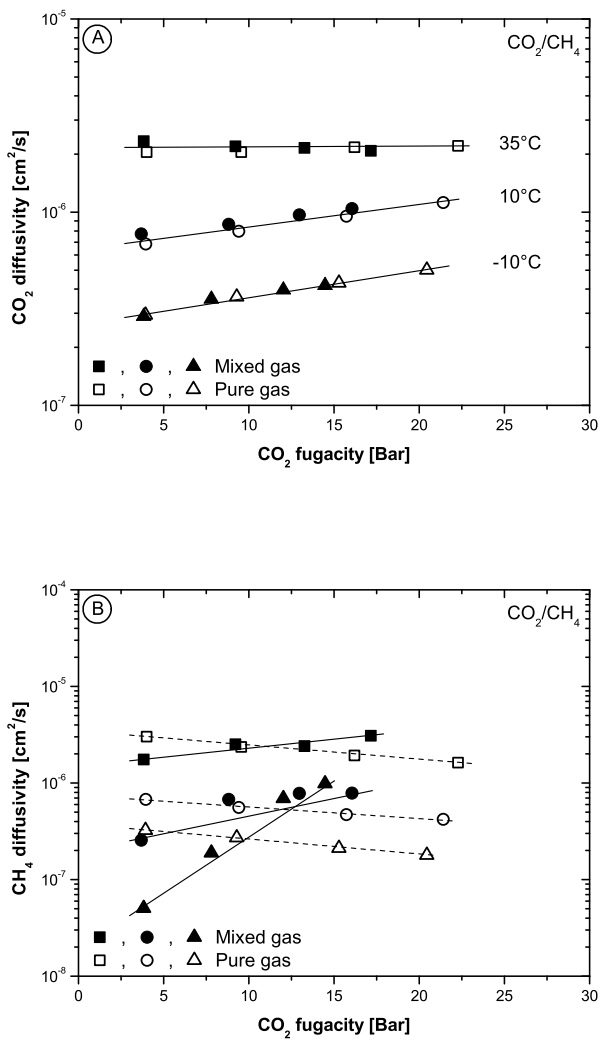
Figure 5.13: CO$_2$ diffusivity (a) and CH$_4$ diffusivity (b) under mixed gas (closed symbols) and pure gas (open symbols) conditions as a function of the CO$_2$ fugacity for (PEO-*ran*-PPO$_{2500}$/T)$_{7500}$-T6T6T at a temperature of (■ , □) 35℃, (● , ○) 10℃ and (▲ , △) −10℃.
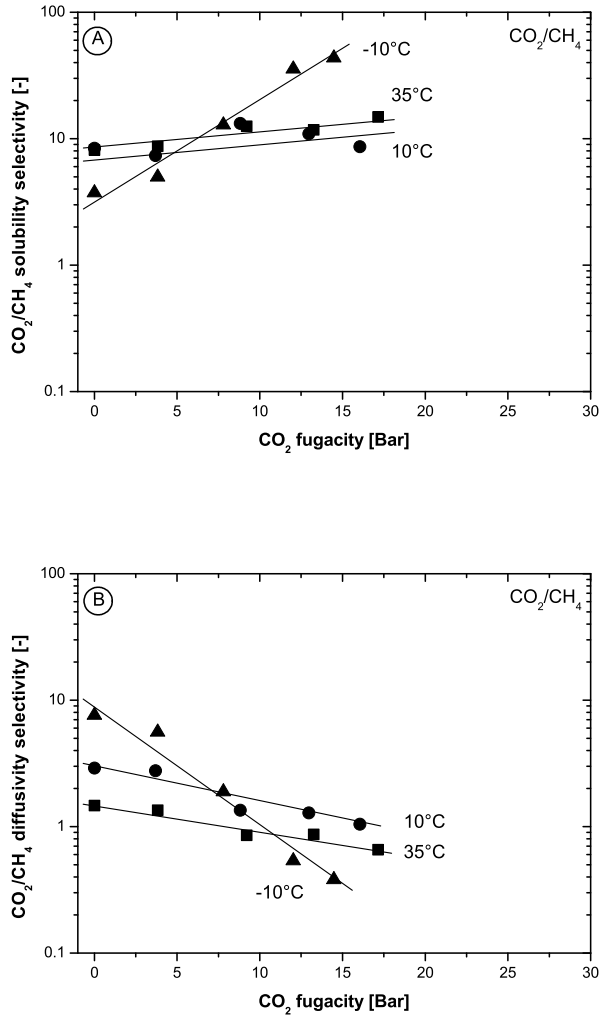
Figure 5.14: Mixed gas CO_2/CH_4 solubility selectivity (a) and CO_2/CH_4 diffusivity selectivity (b) as a function of the CO_2 fugacity for (PEO-*ran*-PPO$_{2500}$/T)$_{7500}$-T6T6T at a temperature of (■) 35℃, (●) 10℃ and (▲) −10℃.

is a strong function of its fugacity (Figure 5.8). Consequently, the CO_2/CH_4 solubility selectivity is also a strong function of the CO_2 fugacity and the solubility selectivity increases from 5 to 44 as the CO_2 fugacity increases from 3.8 to 14.5 bar.

The strong dependency of the CO_2 concentration on the CO_2 fugacity at $-10℃$ also affects the diffusivity selectivity to a large extent. At low CO_2 fugacity (~ 3.8 bar) and thus low CO_2 sorption (< 20 cm^3 (STP)/cm^3), the CO_2/CH_4 diffusivity selectivity at $-10℃$ is considerably higher than that at $35℃$. A decrease in temperature decreases the segmental mobility of the polymer chains increasing diffusivity selectivity. However, as CO_2 fugacity and thus CO_2 sorption levels increase rapidly, plasticization effects more than offset this decrease in segmental mobility and a steep decrease in diffusivity selectivity is observed. To illustrate this, the diffusivity selectivity at $-10℃$ decreases from 5.6 to 0.38 as the CO_2 fugacity increases from 3.8 to 14.5 bar.

Based on the data discussed above and the pure gas sorption and diffusion values (discussed in the previous section) the relative contribution of the diffusivity selectivity and solubility selectivity for the pure and mixed gas CO_2/CH_4 has been calculated. Figure 5.15 presents (a) the normalized (to infinite dilution) pure and mixed gas solubility selectivity and (b) the normalized (to infinite dilution) pure and mixed gas diffusivity selectivity as a function of the CO_2 fugacity for the different experimental temperatures used.

The difference in normalized solubility selectivity (Figure 5.15a) between pure and mixed gas conditions is not significant at a temperature of $35℃$ (squares) and $10℃$ (circles). More noteworthy differences are observed at a temperature of $-10℃$, where the normalized solubility selectivity in mixed gas conditions is reasonably higher compared to pure gas conditions. The plasticizing effects, which influence the diffusivity selectivity, associated with CO_2 are clearly visible in Figure 5.15b. The diffusivity selectivity increases as a function of CO_2 fugacity in pure gas conditions due to a combination of an increase in CO_2 diffusivity (plasticization) and a decrease in CH_4 diffusivity (compaction) (see Figure 5.7). However, in mixed gas conditions it decreases as a function of CO_2 fugacity at all temperatures and this decrease is stronger at lower temperatures (especially at $-10℃$) as a result of more pronounced plasticization. This indicates that the difference between the pure and mixed gas CO_2/CH_4 selectivity is predominantly caused by a decrease in diffusivity selectivity.
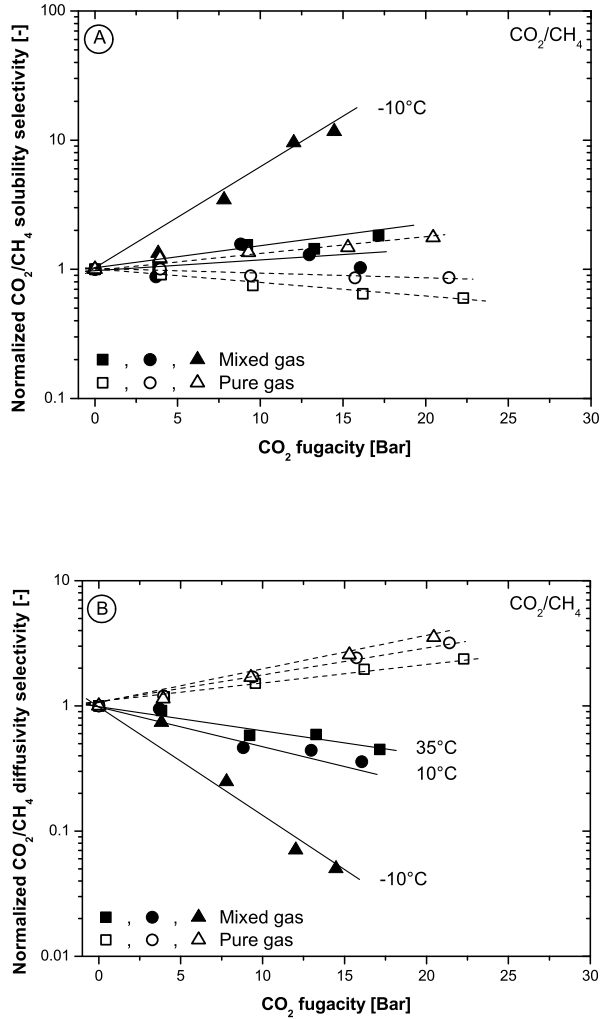
Figure 5.15: Normalized pure (open symbols) and mixed gas (closed symbols) CO_2/CH_4 solubility selectivity (a) and CO_2/CH_4 diffusivity selectivity (b) as a function of the CO_2 fugacity for (PEO-*ran*-PPO$_{2500}$/T)$_{7500}$-T6T6T at a temperature of (■ , □) 35°C, (● , ○) 10°C and (▲ , △) −10°C.

Chapter 5

5.4.4 Superposition principle

Based on the data from the pure and mixed gas permeability measurements the difference between the mixed and pure gas selectivity is calculated ($\Delta\alpha = \alpha_{\text{mixed gas}} - \alpha_{\text{pure gas}}$). Figure 5.16 presents this difference for the CO_2/H_2 as well as the CO_2/CH_4 gas pair as a function of the CO_2 fugacity.

The difference between the mixed and pure gas selectivity ($\Delta\alpha$) increases with increasing CO_2 fugacity and decreasing temperature (Figure 5.16). Due to the smaller kinetic diameter of H_2 compared to CH_4, the change in selectivity for CO_2/CH_4 is always more pronounced than the change in selectivity for CO_2/H_2.

As the differences discussed in this paper are all ascribed to the plasticizing effects due to the concentration of CO_2 in the polymer, we present the change in selectivity as a function of the CO_2 concentration in the polymer matrix in Figure 5.17. Here we use the pure gas CO_2 concentration values as we did not perform mixed gas CO_2/H_2 solubility measurements. However, we have shown that the CO_2 sorption is independent of the second component in CO_2/CH_4 sorption experiments and this is also likely to occur in CO_2/H_2 experiments as the critical temperature of H_2 is even lower than that of CH_4.
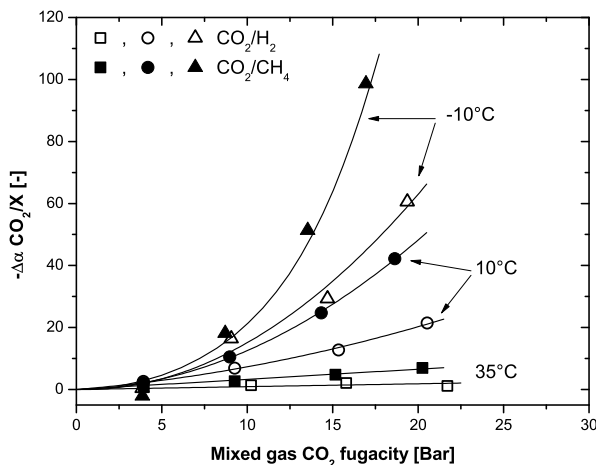
Figure 5.16: Difference between mixed and pure gas CO_2/H_2 (open symbols) and CO_2/CH_4 (closed symbols) selectivity as a function of the mixed gas CO_2 fugacity for (PEO-*ran*-PPO$_{2500}$/T)$_{7500}$-T6T6T at a temperature of (■,□) 35℃, (●,○) 10℃ and (▲,△) −10℃.

Figure 5.17: Difference between mixed and pure gas CO_2/H_2 (open symbols) and CO_2/CH_4 (closed symbols) selectivity as a function of the CO_2 concentration for (PEO-*ran*-PPO$_{2500}$/T)$_{7500}$-T6T6T at a temperature of (■, □) 35℃, (●,○) 10℃ and (▲, △) −10℃.

All data obtained coincide in one master curve for CO_2/H_2 and one for CO_2/CH_4. This demonstrates that the difference between mixed and pure gas selectivity is exclusively dependent on the CO_2 concentration. The means by which this concentration is established (by either a change in temperature or a change fugacity) is not of any influence on this difference in selectivity. As such, a certain concentration can either be achieved by an increase in CO_2 fugacity or a decrease in experimental temperature. For instance, at 10℃ a CO_2 fugacity of ∼15 bar results in a CO_2 concentration of approximately 50 cm^3 (STP)/cm^3 polymer. A similar CO_2 concentration can be reached at −10℃ at a CO_2 fugacity of only approximately 9 bar. The effect on the difference between the mixed and pure gas selectivity ($\Delta\alpha$) however is similar in both cases and the mixed gas CO_2/CH_4 selectivity drops by ∼21 points, while the mixed gas CO_2/H_2 selectivity drops by ∼15 points (compared to their pure gas values). The effect of the CO_2 concentration on the change in selectivity is smaller for the gas pair CO_2/H_2 (open symbols) compared to the gas pair CO_2/CH_4 (closed symbols). This can be ascribed to differences in kinetic diameter between H_2 and CH_4 as described earlier. The result shows that once a reliable master curve is obtained, the difference between the mixed and pure gas selectivity at any given temperature and CO_2 feed gas fugacity can be obtained from pure gas permeability data by only measuring the pure gas CO_2 concentration at these specific conditions.

5.5   Conclusions

The pure and mixed gas separation performance of a highly permeable PEO based block copolymer have been investigated over a wide temperature and pressure range for the separation of CO_2 from hydrogen or methane. As a result of the highly polar nature of the ether oxygen linkages in the block copolymer, CO_2 exhibits strong sorption in this material. Particularly at high feed fugacities and low temperatures, this induces significant plasticization effects which have a pronounced effect on the CO_2 permeability. Plasticization effects for H_2 and CH_4 are not observed. This results in high pure gas permeability selectivities for CO_2/H_2 as well as CO_2/CH_4. At a CO_2 feed fugacity of 20.5 bar and a temperature of -10℃ the CO_2/H_2 and CO_2/CH_4 selectivity reached values as high as 72 respectively 101. The CO_2 permeabilities in mixed gas experiments are similar to their pure gas values at any given CO_2 fugacity. However, the light gas permeabilities increase significantly as a function of the CO_2 fugacity in the mixture. Consequently, the mixed gas CO_2/H_2 and CO_2/CH_4 selectivities are reduced compared to their pure gas values. The CO_2/H_2 selectivity at -10℃ and a CO_2 fugacity of 19.4 bar is 29, combined with a remarkably high CO_2 permeability of 510 Barrer. CO_2/CH_4 selectivity at the same temperature reached a value of 17 combined with a CO_2 permeability of 426 Barrer at a CO_2 fugacity of 16.4 bar. CO_2/CH_4 mixed gas sorption experiments showed that the plasticization by CO_2 had a dominant effect on the CH_4 diffusivity. Finally, we demonstrated that the difference between mixed and pure gas selectivity is exclusively dependent on the CO_2 concentration. All measurement values for a single gas pair coincide to one master curve. The means by which this concentration is established (by either a change in temperature or a change fugacity) is not of any influence on this difference in selectivity. Consequently, mixed gas selectivity can be estimated at any temperature and CO_2 feed fugacity from pure gas data once a reliable data set has been obtained.

5.6   Acknowledgements

5.7   References

[1] R. B. GUPTA; *Hydrogen Fuel: Production, Transport, and Storage*; 1st edition (2008); Boca Raton, FL (United States of America): CRC Press; ISBN 978-1420045758

[2] R. W. BAKER; *Future directions of membrane gas separation technology*; Industrial and Engineering Chemistry Research **41** (6) (2002) 1393–1411; DOI: 10.1021/ie0108088

[3] R. W. BAKER; *Membrane Technology and Applications*; 2nd edition (2000); West Sussex (England): John Wiley & Sons Ltd.; ISBN 978-0470854457

[4] Y. YAMPOLSKII, I. PINNAU AND B. D. FREEMAN; *Materials Science of Membranes for Gas and Vapor Separation*; 1st edition (2006); West Sussex (England): John Wiley & Sons Ltd.; ISBN 978-0470853450

[5] H. LIN AND B. D. FREEMAN; *Materials selection guidelines for membranes that remove CO_2 from gas mixtures*; Journal of Molecular Structure **739** (1-3) (2005) 57–74; DOI:10.1016/j.molstruc.2004.07.045

[6] H. LIN AND B. D. FREEMAN; *Gas and vapor solubility in crosslinked polyethylene glycol diacrylate*; Macromolecules **38** (20) (2005) 8394–8407; DOI:10.1021/ma051218e

[7] H. LIN AND B. D. FREEMAN; *Gas permeation and diffusion in cross-linked poly(ethylene glycol diacrylate)*; Macromolecules **39** (10) (2006) 3568–3580; DOI: 10.1021/ma051686o

[8] H. LIN, T. KAI, B. D. FREEMAN, S. KALAKKUNNATH AND D. S. KALIKA; *The effect of crosslinking on gas permeability in crosslinked poly(ethylene glycol diacrylate)*; Macromolecules **38** (20) (2005) 8381–8393; DOI:10.1021/ma0510136

[9] H. LIN, E. VAN WAGNER, J. S. SWINNEA, B. D. FREEMAN, S. J. PAS, A. J. HILL, S. KALAKKUNNATH AND D. S. KALIKA; *Transport and structural characteristics of crosslinked poly(ethylene oxide) rubbers*; Journal of Membrane Science **276** (1-2) (2006) 145–161; DOI:10.1016/j.memsci.2005.09.040

[10] H. LIN, E. VAN WAGNER, R. RAHARJO, B. D. FREEMAN AND I. ROMAN; *High-performance polymer membranes for natural-gas sweetening*; Advanced Materials **18** (1) (2006) 39–44; DOI:10.1002/adma.200501409

[11] H. LIN, E. VAN WAGNER, B. D. FREEMAN, L. G. TOY AND R. P. GUPTA; *Plasticization-enhanced hydrogen purification using polymeric membranes*; Science **311** (5761) (2006) 639–642; DOI:10.1126/science.1118079

Chapter 5

[12] S. KELMAN, H. LIN, E. S. SANDERS AND B. D. FREEMAN; *CO₂/C₂H₆ separation using solubility selective membranes*; Journal of Membrane Science **305** (1-2) (2007) 57–68; DOI:10.1016/j.memsci.2007.07.035

[13] H. LIN, B. D. FREEMAN, S. KALAKKUNNATH AND D. S. KALIKA; *Effect of copolymer composition, temperature, and carbon dioxide fugacity on pure- and mixed-gas permeability in poly(ethylene glycol)-based materials: Free volume interpretation*; Journal of Membrane Science **291** (1-2) (2007) 131–139; DOI: 10.1016/j.memsci.2007.01.001

[14] G. HOLDEN, H. R. KRICHELDORF AND R. P. QUIRK; *Thermoplastic Elastomers*; 3rd edition (2004); Munich (Germany): Hanser Gardner Publications; ISBN 978-1569903643

[15] V. I. BONDAR, B. D. FREEMAN AND I. PINNAU; *Gas sorption and characterization of poly(ether-b-amide) segmented block copolymers*; Journal of Polymer Science, Part B: Polymer Physics **37** (17) (1999) 2463–2475; DOI: 10.1002/(SICI)1099-0488(19990901)37:17⟨2463::AID-POLB18⟩3.0.CO;2-H

[16] V. I. BONDAR, B. D. FREEMAN AND I. PINNAU; *Gas transport properties of poly(ether-b-amide) segmented block copolymers*; Journal of Polymer Science, Part B: Polymer Physics **38** (15) (2000) 2051–2062; DOI:10.1002/1099-0488(20000801) 38:15⟨2051::AID-POLB100⟩3.0.CO;2-D

[17] S. J. METZ, M. H. V. MULDER AND M. WESSLING; *Gas-permeation properties of poly(ethylene oxide) poly(butylene terephthalate) block copolymers*; Macromolecules **37** (12) (2004) 4590–4597; DOI:10.1021/ma049847w

[18] A. CAR, C. STROPNIK, W. YAVE AND K. V. PEINEMANN; *PEG modified poly(amide-b-ethylene oxide) membranes for CO₂ separation*; Journal of Membrane Science **307** (1) (2008) 88–95; DOI:10.1016/j.memsci.2007.09.023

[19] A. CAR, C. STROPNIK, W. YAVE AND K. V. PEINEMANN; *Pebax®/polyethylene glycol blend thin film composite membranes for CO₂ separation: Performance with mixed gases*; Separation and Purification Technology **62** (1) (2008) 110–117; DOI:10.1016/j.seppur.2008.01.001

[20] A. CAR, C. STROPNIK, W. YAVE AND K. V. PEINEMANN; *Tailor-made polymeric membranes based on segmented block copolymers for CO₂ separation*; Advanced Functional Materials **18** (18) (2008) 2815–2823; DOI:10.1002/adfm.200800436

[21] W. YAVE, A. CAR, K. V. PEINEMANN, M. Q. SHAIKH, K. RÄTZKE AND F. FAUPEL; *Gas permeability and free volume in poly(amide-b-ethylene oxide)/polyethylene glycol blend membranes*; Journal of Membrane Science **339** (1-2) (2009) 177–183; DOI:10.1016/j.memsci.2009.04.049

Chapter 5

[22] D. HUSKEN, T. VISSER, M. WESSLING AND R. J. GAYMANS; *CO_2 permeation properties of poly(ethylene oxide)-based segmented block copolymers*; Journal of Membrane Science **346** (1) (2010) 194–201; DOI:10.1016/j.memsci.2009.09.034

[23] A. ARUN AND R. J. GAYMANS; *Hydrophilic poly(ethylene oxide)-aramide segmented block copolymers*; European Polymer Journal **45** (10) (2009) 2858–2866; DOI:10.1016/j.eurpolymj.2009.07.002

[24] S. R. REIJERKERK, A. ARUN, K. NIJMEIJER, R. J. GAYMANS AND M. WESSLING; *Tuning of mass transport in multi-block copolymers for CO_2 capture applications*; Journal of Membrane Science (2009); DOI:10.1016/j.memsci. 2009.09.045

[25] A. C. IJZER, A. ARUN, S. R. REIJERKERK, K. NIJMEIJER, M. WESSLING AND R. J. GAYMANS; *Synthesis and properties of hydrophilic segmented block copolymers based on poly(ethylene oxide)-ran-poly(propylene oxide)*; Journal of Applied Polymer Science, accepted for publication

[26] S. R. REIJERKERK, A. C. IJZER, K. NIJMEIJER, A. ARUN, R. J. GAYMANS AND M. WESSLING; *Subambient temperature CO_2 and light gas permeation through segmented block copolymers with tailored soft phase*; ACS Applied Materials & Interfaces (2010); DOI:10.1021/am900754z

[27] J. G. WIJMANS AND R. W. BAKER; *The solution-diffusion model: A review*; Journal of Membrane Science **107** (1-2) (1995) 1–21; DOI:10.1016/0376-7388(95) 00102-I

[28] *Perry's Chemical Engineers's Handbook*; 7th edition (1997); New York, NY (United States of America): McGraw-Hill; ISBN 978-0070498415

[29] E. S. SANDERS, W. J. KOROS, H. B. HOPFENBERG AND V. T. STANNETT; *Mixed gas sorption in glassy polymers: Equipment design considerations and preliminary results*; Journal of Membrane Science **13** (2) (1983) 161–174; DOI: 10.1016/S0376-7388(00)80159-3

[30] R. D. RAHARJO, B. D. FREEMAN AND E. S. SANDERS; *Pure and mixed gas CH_4 and n-C_4H_{10} sorption and dilation in poly(dimethylsiloxane)*; Journal of Membrane Science **292** (1-2) (2007) 45–61; DOI:10.1016/j.memsci.2007.01.012

[31] A. BOS, I. G. M. PUNT, M. WESSLING AND H. STRATHMANN; *Suppression of CO_2-plasticization by semiinterpenetrating polymer network formation*; Journal of Polymer Science, Part B: Polymer Physics **36** (9) (1998) 1547–1556; DOI: 10.1002/(SICI)1099-0488(19980715)36:9⟨1547::AID-POLB12⟩3.0.CO;2-5

Chapter 5

CHAPTER 6

Highly hydrophilic, rubbery membranes for CO_2 capture and dehydration of flue gas

THIS CHAPTER HAS BEEN SUBMITTED FOR PUBLICATION:

S.R. Reijerkerk, R. Jordana, K. Nijmeijer, M. Wessling, *Highly hydrophilic, rubbery membranes for CO₂ capture and dehydration of flue gas*, International Journal of Greenhouse Gas Control

Abstract

This paper reports the potential of highly hydrophilic, poly(ethylene oxide) based block copolymers for the simultaneous removal of CO_2 and water vapor from flue gas in a post-combustion capture configuration. Water vapor sorption measurements show strong sorption of water vapor in these block copolymers especially above a water vapor activity of 0.6. Plasticization effects due to water vapor sorption were not observed. Mixed water vapor/gas permeability measurements as a function of water vapor activity were performed using binary (H_2O/CO_2 and H_2O/N_2) and ternary ($H_2O/CO_2/N_2$) feed mixtures. The water vapor permeability increased exponentially with the water vapor activity whereas the gas permeability in all cases slightly decreased. As the effect of the presence of water vapor was relatively stronger on the N_2 permeability, the CO_2/N_2 selectivity increased slightly with increasing water vapor activity. No noticeable differences between the pure gas (from binary mixtures) and the mixed gas (from ternary mixtures) membrane performance have been observed. This indicates that plasticization effects, due to the sorption of CO_2, are not significant at the low feed pressure (2.5 bar) used. Overall, the block copolymers studied in this work combine a high CO_2 permeability with a reasonable CO_2/N_2 gas selectivity. Due to their highly hydrophilic character, they also have the ability to simultaneously remove CO_2 and water vapor from flue gases, which makes these PEO-*ran*-PPO based block copolymers an attractive membrane material for post-combustion CO_2 capture applications.

6.1   Introduction

The awareness of the global climate change has increased significantly over the last decades. The average temperature is predicted to rise by several degrees over the coming decades if no efforts to mitigate these climate changes are taken [1]. Most probably and generally accepted, one of the main reasons for these changes is the increase in the atmospheric concentration of carbon dioxide (CO_2), mainly due to the dependence of the world's economy on fossil fuels [2]. Worldwide considerable efforts to reduce the emission of carbon dioxide to the atmosphere are put into practice. In particular, the capture of carbon dioxide from large point sources, such as power plants, is recognized as an important step, as their contribution to the total worldwide CO_2 emission is approximately 50% [2]. Typically, a flue gas from a coal-fired power plant contains mainly nitrogen ($\sim$72 vol.%), but also reasonable quantities of CO_2 ($\sim$14 vol.%) and water vapor ($\sim$11 vol.%) [3]. Currently two different approaches to effectively capture the CO_2 from these existing large point sources are mainly considered, which are (1) post-combustion capture and (2) oxy-combustion capture (or a combination of these two) [4]. In post-combustion capture the CO_2 is captured after the fossil fuel has been burned with normal air, while in oxy-combustion capture, the fossil fuel is burned using oxygen enriched air. As such oxy-combustion generates a higher concentration of CO_2 in the flue gas, which facilitates the efficient removal of CO_2.

Although the capture of carbon dioxide using amine-based solvents is the most mature technology, membrane-based CO_2 capture technologies are particularly interesting as they combine inherent simplicity (no rotating equipment), a small footprint and above all a low energy consumption [5]. Research efforts on the development of suitable polymeric membranes that can effectively separate CO_2 and N_2 for use in post-combustion capture have been reviewed by Powell *et al.* [6]. However, they only considered dry, pure gas membrane separation performance. In general, literature lacks data on the membrane CO_2 capture performance in the presence of minor components, such as SO_x, NO_x, CO, H_2S and water vapor, as recently reviewed by Scholes *et al.* [7]. From these minor components water vapor is particularly important as flue gas generally is close to saturation with water vapor (a $\sim$ 0.8–1.0) and this has to be considered when evaluating the performance of membranes for flue gas treatment.

Nowadays, the flue gas is reheated to prevent any condensation of water vapor in the stack as this would cause corrosion problems due to the presence of aggressive minor components, such as SO_2, HCl and HF, in the flue gas [3]. To prevent reheating of the flue gas stream to achieve significant savings in energy, the partial removal of water vapor is very beneficial. Another major benefit of such a process is the fact that the water removed from the flue gas stream is of a very high purity and can be almost directly reused in the steam cycle of the power plant [3]. Sijbesma *et al.* [3] and Potreck *et al.* [8] studied the selective removal of water vapor from flue gas using highly hydrophilic membrane materials. In particular next to the use of sulphonated poly(ether ether ketone) (SPEEK) as membrane material [3], they studied the performance of the commercially available poly(ethylene oxide) (PEO) based block copolymer PEBAX®1074. Potreck *et al.* [8] recognized that, next to very high water vapor permeabilities, this material also is an interesting candidate for carbon capture and subsequently the simultaneous removal of carbon dioxide and water vapor from flue gases. Besides a high water vapor permeability, it combines a reasonably high CO_2 permeability with a good CO_2/N_2 selectivity in dry, pure gas feed streams [9, 10]. However, to the best of our knowledge, no literature data exist that study the performance of this PEBAX®1074 block copolymer for the separation of CO_2 from flue gas in the presence of water vapor.

The development of a membrane process for the simultaneous removal of CO_2 and water vapor is a challenging task. The flue gas that exits the power plant is at atmospheric pressure and only contains 10–15 vol.% CO_2. This makes the driving force for CO_2 to permeate through any membrane very low as the separation in all membrane-based processes relies on the partial pressure difference of the component to be removed over the membrane. A membrane with extremely high permeabilities for CO_2 is therefore required for flue gas treatment to compensate for the low driving force [11, 12]. Although the PEBAX®1074 block copolymer has a reasonably high CO_2 permeability, the development of membranes with a considerably higher intrinsic permeability value is necessary for the successful implementation of membrane technology in post-combustion capture systems [11, 12]. In recent years several researchers reported block copolymer systems based on poly(ethylene oxide) with improved permeability compared to PEBAX®1074 [13–19]. In particular, we reported a block copolymer system based on soft segments containing a random distribution of 75 wt.% PEO and 25 wt.% PPO and uniform tetra-amide (T6T6T) hard segments, denoted as PEO-*ran*-PPO-T6T6T [20]. This block copolymer system reached a CO_2 permeability

up to four times the value of PEBAX®1074, while selectivity is maintained, making this material an interesting candidate for post-combustion CO_2 capture applications [19].

In the current work we investigate this block copolymer system (PEO-*ran*-PPO-T6T6T) for the simultaneous removal of CO_2 and water vapor from flue gas for use in post-combustion CO_2 capture. In particular the effect of the presence of water vapor on the CO_2 capture performance of the membranes will be investigated. The first part of the work evaluates the water vapor sorption and kinetic diffusion behavior. These data serve as a tool to analyze the CO_2 and H_2O permeation behavior of the membranes. Permeation experiments have been performed with binary (2 component) mixtures, containing water vapor and either CO_2 or N_2, as well as ternary (3 component) mixtures, containing water vapor and a CO_2/N_2 mixed gas, which almost resembles the composition of the real flue gas. These measurements allow the simultaneous determination of the permeability of the gas(es) as well as that of the water vapor, something which is very rarely found in literature, but highly relevant for realistic purposes. Such measurements are very scarce as the challenge in these experiments especially lays in the determination of the permeability of rapidly and strongly permeating components (i.e. water vapor) and the simultaneous determination of the permeability of relatively low permeating gases (i.e. N_2). Furthermore, by conducting these experiments with binary as well as ternary mixtures we are able to analyze the gas permeability and selectivity in pure gas (ideal) as well as mixed gas (real) conditions and detect any differences that might result. Especially the study on the influence of water vapor using a real CO_2/N_2 mixed gas (ternary mixture) is very special, as to the best of our knowledge literature does not report any values on the simultaneous permeation of all these three components.

6.2 Theory

6.2.1 Block copolymers

In general, block copolymers consist of an alternating series of flexible soft segments and crystallizable hard segments. The flexible soft segments usually have a low glass transition temperature and provide the material its flexibility and gas and vapor permeability, while the rigid hard segments give the material its mechanical and heat

stability [21]. The different segments used usually differ in their chemical nature and material properties and the ultimate properties of the block copolymer are determined by the combination of the two. Usually polyethers are used as a soft segment to provide the material a low glass transition temperature and a high specific transport for CO_2 [22], while the hard segment exists of a urethane, ester or amide which is able to crystallize, acting as physical crosslinks reinforcing the amorphous matrix. Overall, block copolymers are of specific interest as they can be easily processed (in the melt or by dissolving them in a suitable solvent) and their specific properties can be easily tuned by smart selection and combination of the individual building blocks in the copolymer. The block copolymers studied in the current work distinct themselves from commercially available block copolymer systems, like PEBAX® (Figure 6.1a), by the fact that the hard segment has a unique uniform length. This ensures very fast and foremost efficient crystallization of the hard segments leading to a very good phase separation between the hard and soft segments (Figure 6.1b). This result in a very well controlled microdomain morphology with enhanced mass transport properties.
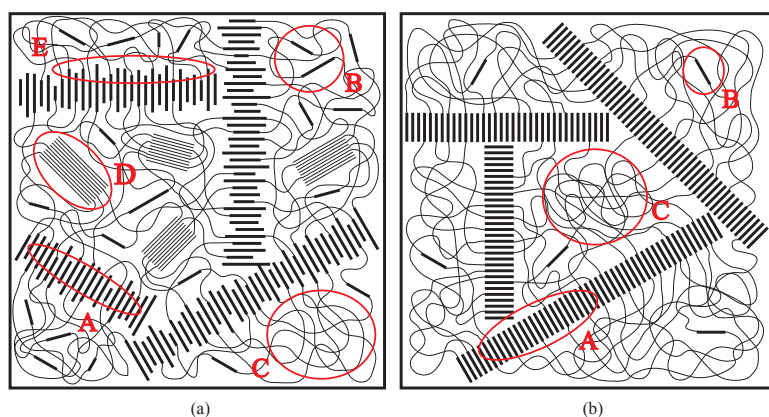
Figure 6.1: Schematic representation of the morphology of (a) commercially available block copolymers (e.g. the PEBAX® family) and (b) the PEO-*ran*-PPO based block copolymers using monodisperse tetra-amide (T6T6T hard segments as described in the current work. The indicated areas are representative for (A) crystalline hard segments, (B) non-crystallized rigid hard segments, (C) continuous amorphous soft phase, (D) crystalline soft phase and (E) intermediate region with mixed crystalline hard segments and non-crystalline soft segments.

6.2.2   Water vapor and gas permeability

The transport of gases and vapors through non-porous, dense polymer membranes is generally described with the solution-diffusion model [23, 24]. This model describes the transport as a three-step process. First, a component absorbs in the membrane at the upstream side. Next, it diffuses through the membrane and finally it desorbs at the downstream side. The result of this model is commonly known as the permeability coefficient of component i (P_i) and is defined according to Equation (6.1):

$$P_i = D_i \cdot S_i \qquad (6.1)$$

where D_i is the average effective diffusion coefficient (cm^2/s) and S_i is the solubility coefficient (cm^3 (STP)/(cm^3·cmHg)) of component i. The permeability coefficient is usually expressed in units of Barrer, where 1 Barrer equals $1 \cdot 10^{-10}$ cm^3 (STP)·cm/(cm^2·s·cmHg) or $7.5 \cdot 10^{-18}$ m^3 (STP)·m/(m^2·s·Pa). The separation of gases and/or vapors is obtained due to differences in diffusivity and/or solubility of the components and the selectivity of a membrane for component A over component B is given by the ratio of the their respective permeability coefficients P_A/P_B according to Equation (6.2):

$$\alpha = \frac{P_A}{P_B} = \frac{D_A}{D_B} \cdot \frac{S_A}{S_B} \qquad (6.2)$$

where D_A/D_B is the diffusivity selectivity and S_A/S_B is the solubility selectivity. The membrane selectivity can either be expressed as an ideal selectivity (based on the measured permeability of pure, single gases) or a real selectivity (based on the measured permeability using mixed, multi-component gases).

6.2.3   Water vapor sorption

In general, the solubility of a vapor in a polymer can be obtained from equilibrium sorption experiments. The concentration of water vapor inside a polymer film (cm3 (STP)/cm3 polymer) can be calculated from the equilibrium mass uptake of the polymer sample in equilibrium with a certain water vapor activity using Equation (6.3):

$$c_i = \frac{(m_\infty - m_{\text{polymer,dry}}) \cdot V_{\text{H}_2\text{O}}}{V_{\text{polymer,dry}} \cdot M_{\text{w,H}_2\text{O}}} \qquad (6.3)$$

153

where m_∞ (g) is the equilibrium mass of the polymer sample at the conditions of interest, $m_{polymer,dry}$ (g) is the dry weight of the polymer, V_{H_2O} (22,414 cm^3) is the volume of 1 mol of H_2O at standard temperature (273.15 K) and standard pressure (1.01325 bar), $V_{polymer,dry}$ (cm^3) is the volume of the dry polymer and M_{w,H_2O} (18 g/mol) is the molecular mass of water.

6.2.4 Fickian diffusion model

The diffusion coefficients of penetrants in polymers can be obtained from kinetic sorption data. In the current study only rubbery polymers are considered and these are able to adapt rapidly to changes in their conditions. The diffusion process in these rubbery materials is referred to as 'Fickian' and obeys Fick's first law [23]. If the thickness of the polymer film is sufficiently thin, any diffusion from the edges of the film can be neglected. In combination with Fick's second law, which predicts how diffusion causes the concentration field to change with time, Crank [25] deduced that for rubbery polymers the diffusion coefficient at short timescales can be described by Equation (6.4):

$$\frac{M_t}{M_\infty} = \frac{4}{l_p}\sqrt{\frac{D \cdot t}{\pi}} \tag{6.4}$$

where M_t (g) is the mass of sorbed water vapor at time t (s), M_∞ (g) is the mass sorbed at $t = \infty$ (at equilibrium), l_p (m) is the polymer film thickness and D (m^2/s) is the Fickian diffusion coefficient. The Fickian diffusion coefficient for water in the polymer matrix can thus be determined from the initial slope of a plot of M_t/M_∞ versus $\sqrt{t}$. At longer time scales, the Fickian diffusion coefficient can be described by Equation (6.5):

$$ln\left(1 - \frac{M_t}{M_\infty}\right) = ln\frac{8}{\pi^2} - \frac{\pi^2 \cdot D \cdot t}{l_p^2} \tag{6.5}$$

where M_t (g) is the mass of sorbed water at time t (s), M_∞ (g) is the mass sorbed at $t = \infty$ (at equilibrium), l_p (m) is the polymer film thickness and D (m^2/s) is the Fickian diffusion coefficient. Now, a plot of $ln(1 - M_t/M_\infty)$ versus t can be used to extract the Fickian diffusion coefficient. Both equations cross at $D \cdot t/l^2 = 0.05326$. This is when $M_t/M_\infty \approx 0.52$. A combination of these two Fickian diffusion coefficients gives an good approximation of the diffusion coefficient at any specific time during the sorption process [26].

When highly hydrophilic polymers are used, the polymer film thickness, which is assumed to be constant in Equation (6.4) and (6.5), cannot be considered as a constant anymore. As a result of the high water vapor uptake, especially at high water vapor concentrations, the polymer film will swell and the thickness thus increases. This would result in an underestimation of the diffusion coefficient and this increase in thickness should be taken into account [8, 27]. Consequently, the corrected Fickian diffusion coefficient can be calculated according to Equation (6.6):

$$D_c = \frac{D}{(1 - \phi_w)^{5/3} \cdot (\partial lna/\partial ln\phi_w)} \tag{6.6}$$

where D_c is the Fickian diffusion coefficient corrected for the increase in polymer film thickness due to water vapor sorption (m^2/s), ϕ_w is the water volume fraction (–) and a is the water vapor activity (–) at the conditions of interest.

6.2.5 Zimm and Lundberg clustering analysis

Vapor molecules, when absorbed in a polymer, may have the tendency to form clusters. In the case of water molecules, this effect has been attributed to hydrogen bonding between water molecules [28]. If present, such water clusters can affect the diffusion of other water molecules and/or the diffusion of gas(es) (for instance CO_2) that permeate simultaneously through the membrane. A cluster analysis can be performed if proper equilibrium vapor sorption isotherms are available. In general, the extent of clustering is analyzed using the clustering function as defined by Zimm and Lundberg [28] according to Equation (6.7):

$$\frac{G_{ww}}{V_w} = -(1 - \phi_w)\left[\frac{\partial(a/\phi_w)}{\partial a}\right] - 1 \tag{6.7}$$

where a is the water vapor activity (–) and ϕ_w is the water volume fraction (–) as obtained from equilibrium water vapor sorption experiments. G_{ww} is the so-called cluster integral and V_w is the partial molar volume (cm^3/mol) of the water vapor penetrant. If $G_{ww}/V_w = -1$, the system is ideal, and the water molecules exclude only their own volume to other water molecules, not affecting their distribution. When the value of the clustering function is lower than -1, the water molecules prefer to remain isolated. If $G_{ww}/V_w > 0$, there is a tendency to cluster and the concentration of water molecules in the neighborhood of a given water molecule is higher than would be in the case for random distribution. When $G_{ww}/V_w > 0$, a higher value of the clustering function corresponds to a stronger tendency of the water molecules to cluster.

6.3   Experimental

6.3.1   Materials

The block copolymer system studied consists of monodisperse tetra-amide hard segments (T6T6T, Figure 6.2a) and polyether based soft segments. The polyether based soft segments comprise a random distribution of 75 wt.% poly(ethylene oxide) and 25 wt.% poly(propylene oxide) (Figure 6.2b). The length of the soft segment can be tailored and in the current study polymer membranes with a soft segment length of 1000, 2500 and 10,000 g/mol (a soft segment concentration of respectively 62, 80 and 89 wt.%) have been used. A detailed description of the synthesis procedure, the thermal-mechanical properties [20] and the pure gas permeation characteristics [19] of this block copolymer system, denoted as PEO-*ran*-PPO-T6T6T, can be found elsewhere. For convenience and as a reference for discussions in this work a summary of the most relevant thermal-mechanical properties has been added as Table 6.1 [20].

Figure 6.2: Chemical structure of (a) the monodisperse tetra-amide (T6T6T) hard segment and (b) the PEO-*ran*-PPO soft segment.

Table 6.1: Selected properties of the PEO-*ran*-PPO-T6T6T block copolymers studied [20]. SS: soft segment, T: terephthalic unit, M_{CRL}: the molecular weight between physical crosslinks in g/mol, T_g: glass transition temperature and $T_{m,PEO}$ and $T_{m,T6T6T}$ respectively the melting temperature of the semi-crystalline soft phase and the crystalline hard phase.

Sample	SS	T6T6T	T	M_{CRL}	T_g	$T_{m,PEO}$	$T_{m,T6T6T}$
	[wt.%]	[wt.%]	[wt.%]	[g/mol]	[℃]	[℃]	[℃]
PEO-*ran*-PPO$_{1000}$-T6T6T	61.6	38.4	-	935	−53	-	183
PEO-*ran*-PPO$_{2500}$-T6T6T	80.0	20.0	-	2337	−63	−13	163
(PEO-*ran*-PPO$_{2500}$/T)$_{10000}$-T6T6T	89.3	5.6	5.1	9347	−60	−6	144

Calibrated gas mixtures of 10/90 (v/v) CO_2/N_2 to study the membrane performance using realistic mixed gas feed conditions as well as carbon dioxide in helium (1000, 1500 and 2500 ppm CO_2 in He) for the calibration of the gas chromatograph (GC) were obtained from Praxair (Belgium).

6.3.2 Membrane preparation

Films of the PEO-*ran*-PPO based block copolymers of approximately 100 μm thickness have been prepared from vacuum dried (50℃) block copolymer using a Lauffer OPS 40 press. The temperature of the mould was set approximately 30℃ above the melting temperature (T_m) of the block copolymer. First, air was removed from the polymer in the mould by quickly pressurizing/depressurizing the samples. This pressurization/depressurization cycle was repeated three times before actually pressing the samples at ∼8.5 MPa for 5 min. Subsequently, the samples were cooled to room temperature while maintaining the pressure. To prevent sticking of the polymer onto the metal plates of the press, glass-fiber reinforced PTFE sheets were used as an intermediate layer between the polymer film and the metal plates (Benetech type B105).

6.3.3 Density

The density of the block copolymer films required for use in water vapor sorption experiments was determined at room temperature. The samples were dried in a vacuum oven (30℃) before use. Density measurements were performed using an AccuPyc 1330 Pycnometer (Micromeritics). The AccuPyc 1330 is a pycnometer of the gas expansion type and measures the amount of displaced gas (helium) at room temperature. Upon filling of the sample chamber and subsequent discharge into a second empty chamber with known volume the pressure is monitored. This allows calculation of the sample solid phase volume. The density is subsequently derived using the measured sample weight.

6.3.4 Water vapor sorption

Water vapor sorption experiments were carried out using a gravimetric sorption balance (SGA-100 symmetrical gravimetric analyzer from VTI (USA) supplied by Ankersmid

Chapter 6

(The Netherlands)). A detailed description of the balance has been provided by Potreck *et al.* [8, 29]. A film of the block copolymer (with a film thickness of 50–100 μm and a weight of 30–50 mg) was placed in the sample chamber and the chamber was subsequently flushed with dry nitrogen for 24 hours to completely remove any absorbed moisture from the air. After 24 hours a sorption run immediately followed be a desorption run started automatically and the corresponding isotherms were obtained at 50℃ through a stepwise increase or decrease of the water vapor activity.

6.3.5 Mixed water vapor/gas permeability

Mixed water vapor/gas permeation experiments were performed on a setup described earlier by Sijbesma *et al.* [3] and Metz *et al.* [30] with the modifications described by Potreck *et al.* [8]. The GC column in the setup has been replaced by a Hayesep DB (Alltech) to allow the simultaneous detection of CO_2 and N_2. Consequently, the GC has been recalibrated for CO_2 and N_2. The setup allows the simultaneous permeation of water vapor and CO_2, N_2 or any CO_2/N_2 mixture at different water vapor activities and temperatures. The water vapor flux and the (total) gas flux were measured simultaneously in time and the respective permeabilities were calculated according to the method earlier described [3, 30]. When a gas mixture was used the feed pressure has been replaced by the corresponding partial feed pressures. In the current study binary mixtures of water vapor/CO_2 and water vapor/N_2 and a ternary mixture of water vapor/CO_2/N_2 (10/90 v/v CO_2/N_2) were used to study the membrane separation performance as a function of the water vapor activity at 50℃ and an upstream pressure of 2.5 bar.

6.4 Results & discussion

### 6.4.1 Water vapor sorption

This section describes the water vapor sorption behavior in the PEO-*ran*-PPO based block copolymers. The obtained data give insight in the amount of water vapor sorbed and the state of water in the polymer. These data serve as a tool for analysis of the CO_2 (and N_2) permeation behavior and the influence of the presence of water vapor as will be discussed later.

⌐ **Water vapor sorption**

Water vapor sorption experiments with the PEO-*ran*-PPO based block copolymers have been performed at 50°C. Figure 6.3 shows the water vapor concentration (cm³ (STP)/cm³ polymer) in the investigated block polymers as a function of the water vapor activity during sorption. Because of the rubbery state of the polymers, hysteresis phenomena in these materials are not observed and data for sorption and desorption perfectly coincide. Consequently we will only consider sorption isotherms (and not the desorption isotherms).

The water vapor concentration in the block polymers increases exponentially as a function of the water vapor activity. The sorption isotherms show typical Flory-Huggins type of behavior (convex to the activity axis) as can be expected from the sorption of a condensable penetrant in a rubbery polymer [24]. The water vapor concentration in the PEO-*ran*-PPO block copolymers increases when the soft segment length (and thus soft segment concentration, Table 6.1) increases from 1000 to 10,000 g/mol. This is especially prominent above a water vapor activity of 0.6. This increase in water vapor concentration with increasing soft segment length is generally related to two separate effects. In the first place an increase in concentration of the hydrophilic PEO-*ran*-PPO soft domains, which provides more hydrophilic area available for sorption, and in the second place a decrease in physical crosslink density due to the lower concentration of
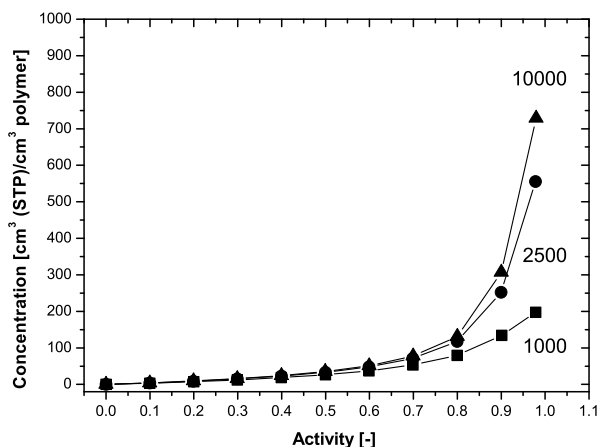
Figure 6.3: Concentration of water in the polymer membranes as a function of water vapor activity at 50°C for PEO-*ran*-PPO based block copolymers with a soft segment length of (■) 1000, (●) 2500 and (▲) 10,000 g/mol expressed per cm³ polymer.
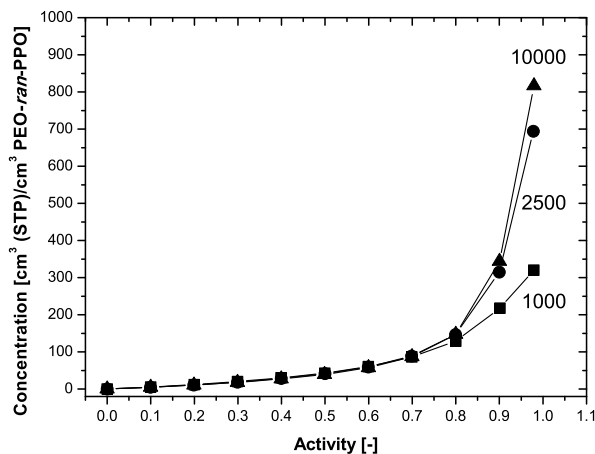
Figure 6.4: Concentration of water in the polymer membrane as a function of water vapor activity at 50℃ during sorption for PEO-*ran*-PPO based block copolymers with a soft segment length of (■) 1000, (●) 2500 and (▲) 10,000 g/mol expressed per cm^3 PEO-*ran*-PPO soft segment.

hard segments (Table 6.1), thus allowing a higher swelling degree. To separate these two effects, Figure 6.4 presents the water vapor concentration per cm^3 PEO-*ran*-PPO soft segment instead of cm^3 polymer. In this way the concentration is normalized for the total amount of hydrophilic domains available in the different polymers and any remaining difference observed is related to a change in physical crosslink density due to the lower amounts of hard segment available at higher block lengths (see Table 6.1).

If the effect of the physical crosslink density would not be significant, all three curves would coincide. However, Figure 6.4 almost equals Figure 6.3, indicating that the physical crosslink density is dominant in this case. The physical crosslink density (due to the crystallized hard segments) decreases rapidly as the soft segment length increases [20], Table 6.1). This allows a strong increase in swelling of the hydrophilic PEO-*ran*-PPO soft domains especially at high water vapor activity (a > 0.6). Similar results have been obtained by Metz *et al.*, who investigated the water vapor sorption in PEO-PBT block copolymers [31, 32].

⌐ **Fickian diffusion**

The obtained kinetic sorption data are used to calculate the Fickian diffusion coefficients of water vapor in the block copolymers at every individual water vapor activity (sorption step) according to Equation (6.4) and (6.5). However, due to the significant swelling of the polymer films, especially at higher water vapor activities, the assumed constant dimensional frame of reference as considered in Equation (6.4) and (6.5) is no longer valid. Therefore, the obtained diffusion coefficients are corrected for the swelling of the polymer film due to the large quantities of water absorbed using Equation (6.6) [27]. Figure 6.5 presents both the uncorrected (dashed lines), as well as these corrected (solid lines) Fickian diffusion coefficients of water vapor as a function of the water vapor activity at 50℃ for the PEO-*ran*-PPO based block copolymers.

The uncorrected Fickian diffusion coefficients of water vapor (indicated by the dashed lines) decrease as a function of the water vapor activity as soon as the activity is higher than 0.2 for all investigated block copolymers. Similar results have been obtained by Potreck *et al.* [8] for the hydrophilic PEBAX®1074 block copolymer. They hypothesized that at least part of this decrease is caused by the fact that the high degree of swelling influences the membrane thickness, and consequently the assumption of a constant dimensional frame of reference is no longer valid.
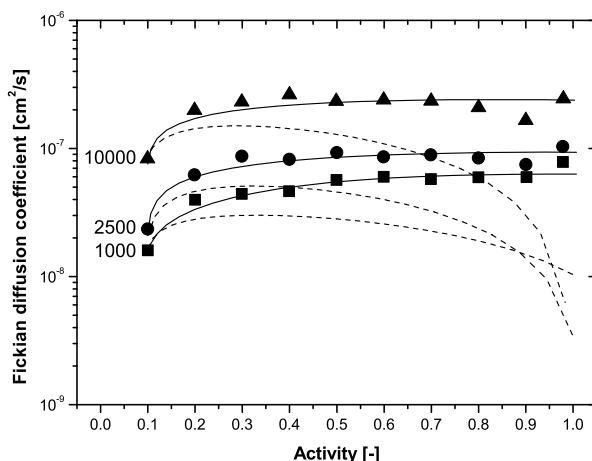
Figure 6.5: Fickian diffusion coefficient corrected for swelling as a function of water vapor activity at 50℃ for PEO-*ran*-PPO based block copolymers with a soft segment length of (■) 1000, (●) 2500 and (▲) 10,000 g/mol. The dashed lines represent the uncorrected Fickian diffusion coefficients calculated according to Equation (6.4) and (6.5).

The importance of the applied correction on the diffusion coefficient is evident when the corrected values (solid lines) are compared with the uncorrected values (dashed lines). Especially at high water vapor activities (a > 0.6), extensive sorption (as shown in the previous paragraph) and thus swelling occurs, and large differences between the corrected and uncorrected Fickian water vapor diffusion coefficient can be observed. The corrected Fickian diffusion coefficient increases as the soft segment length (and consequently soft segment concentration, see Table 6.1) increases. This is similar to the results obtained by Metz *et al.* [31] who studied PEO-PBT block copolymers with various concentrations of PEO and found progressively higher diffusion coefficients when the PEO concentration in the block copolymers was increased. At fixed soft segment length, the corrected Fickian water vapor diffusion coefficient seems to be almost independent of the water vapor activity with the exception of an activity of 0.1. The somewhat lower diffusion coefficient at a water vapor activity of 0.1 can be related to the difficulty in its determination due to instabilities at the start of a sorption run. As hysteresis is not observed Fickian diffusion coefficients determined from the desorption isotherms give similar results for a > 0.1. However, analysis of the diffusion coefficient at an activity of 0.1 during desorption shows a higher diffusion coefficient similar to its value at an activity of 0.2, suggesting that the value determined for an activity of 0.1 during sorption is somewhat too low.

The fact that the diffusion coefficient is nearly independent of the penetrant activity might be counter intuitively. Generally the diffusion coefficient of highly sorbing penetrants increases (either linearly or exponentially) as a result of plasticization, due to the high concentrations of such a penetrant in the polymer [24]. This plasticization increases the free volume and enhances polymer chain mobility, which result in an increase in penetrant diffusion coefficients. We hypothesize that in the current block copolymer system, which already has a very high polymer chain mobility (characterized by a low T_g of ~ -60–$65°C$ [20]), plasticization effects due to the sorption of water vapor are not significant and this results in a diffusion coefficient which is almost independent of water vapor activity. The absence of plasticization due to extensive water vapor sorption is supported by gas permeation measurements (performed under the influence of water vapor), as will be discussed later.

⌐ *Clustering analysis of sorption isotherms*

The state of the absorbed water molecules in the highly hydrophilic PEO-*ran*-PPO block copolymers can be evaluated using the cluster integral as described by Zimm and Lundberg [28]. Figure 6.6 presents the cluster integral as a function of the water vapor activity for the PEO-*ran*-PPO based block copolymers investigated.

The water molecules have a tendency to form clusters if the value of the cluster integral (G_{ww}/V_w) is higher than 0. It is obvious from Figure 6.6 that water molecules present in the PEO-*ran*-PPO based block copolymers have strong tendency to cluster over the full activity range. At high water vapor activities (a > 0.6) the cluster tendency slightly decreases as an additional water molecule that absorbs in the highly water swollen membrane will more and more experience a more water-like due to the exponential increase in water vapor concentration observed at these high activities (Figure 6.3) [8, 33]. This decreases the tendency to form clusters slightly. For the same reason, the tendency to form water clusters decreases slightly when the length of the PEO-*ran*-PPO soft segment is increased. This can be explained by the fact that the block copolymer has a more hydrophilic character at longer soft segment lengths (due to the higher concentration of hydrophilic domains) and at the same time a lower physical crosslink density (induced by the crystallized hard segments), allowing increased water uptake in the polymer.
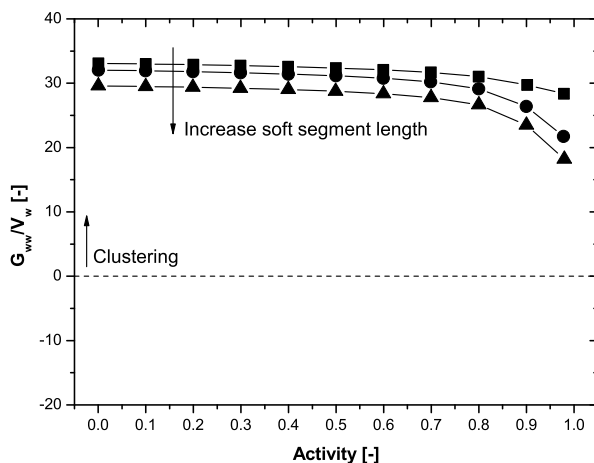
Figure 6.6: Cluster integral as a function of water vapor activity at 50℃ for PEO-*ran*-PPO based block copolymers with a soft segment length of (■) 1000, (●) 2500 and (▲) 10,000 g/mol.

6.4.2   Mixed water vapor/gas permeation

Pure, dry gas permeation experiments with only CO_2 or N_2 have shown that the PEO-*ran*-PPO based block copolymers have highly improved permeation characteristics (especially above a soft segment length of 1000 g/mol) when compared to 1st generation and commercially available PEO based block copolymers, such as PEBAX®1074 [19]. The current paper intends to provide a more realistic view on the CO_2 separation performance of these block copolymers for post-combustion CO_2 capture and this section describes the simultaneous permeation of water vapor and CO_2 and/or N_2 through these block copolymer membranes as flue gas is generally close to saturation and has a water vapor activity of $\sim$0.8–1.0. In this way the influence of the presence of water vapor in the feed gas stream on the CO_2 separation performance of the membranes as well as the membranes potential for the dehydration of the flue gas can be studied. The water vapor sorption data discussed in the previous section are used to support the data presented here. Next to binary (2 component) feed mixtures, containing water vapor and either pure gas CO_2 or pure gas N_2, which provide the ideal CO_2/N_2 selectivity in the presence of water vapor, the permeation behavior of a ternary (3 component) feed mixture, containing water vapor and both CO_2 and N_2 is discussed. These measurements allow us to study the mixed gas CO_2 and N_2 permeability of the membranes, as well as the real, mixed gas CO_2/N_2 selectivity in the presence of water vapor.

⌐ *Binary water vapor/pure gas permeation (H₂O/N₂ and H₂O/CO₂)*
Figure 6.7 presents the water vapor permeability as a function of the water vapor activity for the PEO-*ran*-PPO based block copolymers with a soft segment length of 1000, 2500 and 10,000 g/mol for the binary mixtures water vapor/CO_2 and water vapor/N_2.

The water vapor permeability of all block copolymers is high as water vapor has both a high solubility (due to its high critical temperature, T_c = 647 K) as well as a high diffusivity (due to its small kinetic diameter, d_k = 2.65 Å) in the membrane material. Furthermore, the water vapor permeability increases exponentially with increasing water vapor activity. The increase is dominated by an increase in the water vapor solubility as diffusion is nearly independent of the water vapor activity as shown before (Figure 6.5). The nature of the co-permeating species (CO_2 or N_2) does not seem to have an effect on the water vapor permeability, as no significant differences are observed between both binary mixtures (compare open and closed
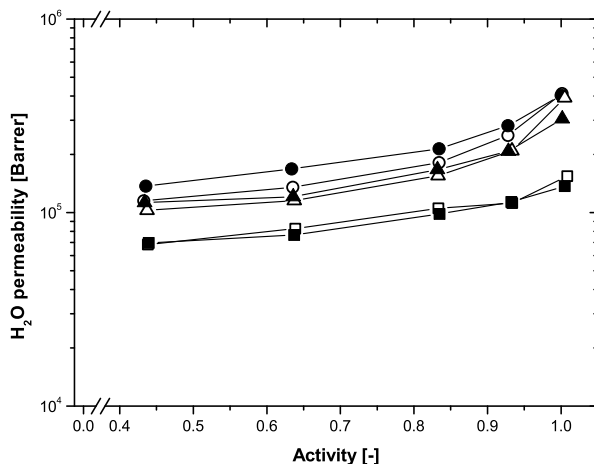
Figure 6.7: Water vapor permeability as a function of water vapor activity at 50℃ as determined from binary feed mixtures of water vapor/CO_2 (closed symbols) and water vapor/N_2 (open symbols) for PEO-*ran*-PPO based block copolymers with a soft segment length of 1000 (squares), 2500 (circles) and 10,000 g/mol (triangles).

symbols). The PEO-*ran*-PPO block copolymers with a soft segment length ≥ 2500 g/mol exhibit higher water vapor permeability than the block copolymer with a soft segment length of 1000 g/mol. This is expected as sorption as well as diffusion for the latter polymer (1000 g/mol) were found to be considerably lower in water vapor sorption measurements as discussed previously.

Figure 6.8 presents the CO_2 and N_2 permeability as a function of the water vapor activity in the feed gas as determined from binary H_2O/CO_2 and H_2O/N_2 measurements.

Over the full activity range the CO_2 and N_2 permeability increases as the soft segment length of the PEO-*ran*-PPO based block copolymers increases. The gas permeability increases due to a combination of a higher concentration of soft phase available for permeation and a simultaneous increase in the mobility of this soft phase [19, 20].

At lower activities, the gas permeability seems to be almost independent of the water vapor activity. Particularly at higher water vapor activities, a slight decrease in gas permeability is observed for all block copolymers investigated. Consequently, this decrease at higher water vapor activities is expected to be related to the water vapor

Chapter 6
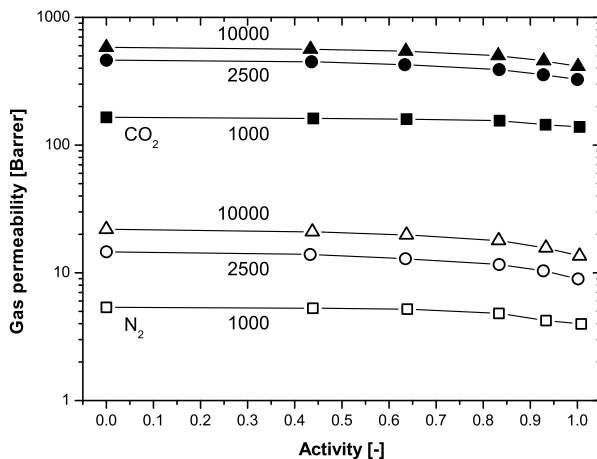
Figure 6.8: Gas permeability for CO_2 (closed symbols) and N_2 (open symbols) as a function of water vapor activity at 50℃ as determined from binary feed mixtures of water vapor/CO_2 and water vapor/N_2 for PEO-*ran*-PPO based block copolymers with a soft segment length of 1000 (squares), 2500 (circles) and 10,000 g/mol (triangles).
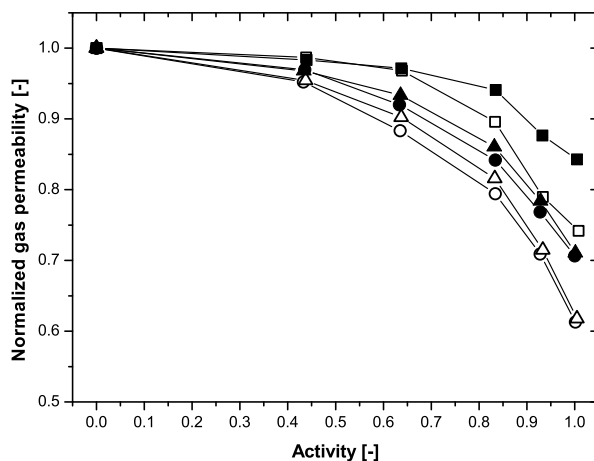
Figure 6.9: Normalized gas permeability for CO_2 (closed symbols) and N_2 (open symbols) as a function of water vapor activity at 50℃ as determined from binary feed mixtures of water vapor/CO_2 and water vapor/N_2 for PEO-*ran*-PPO based block copolymers with a soft segment length of 1000 (squares), 2500 (circles) and 10,000 g/mol (triangles).

sorption in the block copolymer membranes, as extensive sorption occurs at these high activities. To analyze the effect of the simultaneous water vapor permeation on the gas permeability in more detail Figure 6.9 presents the normalized gas permeability (normalized to its 'dry' permeability at a = 0) for the PEO-*ran*-PPO based block copolymers as a function of water vapor activity.

The extensive sorption of water vapor can result in complex changes in the permeability behavior of the gases as their diffusivity as well as solubility can be influenced simultaneously. The relative decrease in gas permeability is fairly similar over the full activity range for a soft segment length of 2500 and 10,000 g/mol. The decrease is less severe for a block copolymer with a soft segment length of 1000 g/mol. Furthermore, the relative decrease of N_2 is always more significant than the relative decrease of CO_2. We hypothesize that the strong sorption of water vapor (especially at a > 0.6) increases the tortuosity of the gas diffusion path and that this increase in length of the gas diffusion path ultimately decreases the gas permeability. The water vapor sorption of the block copolymers with a length of 2500 and 10,000 g/mol is much higher than the block copolymer with a soft segment length of 1000 g/mol (Figure 6.4). As a result the relative decrease in gas permeability would be more significant at these high soft segment lengths (as indeed observed). Furthermore, the increase in tortuosity would have a larger effect on N_2 compared to CO_2 as the kinetic diameter of N_2 (3.64 Å) is larger than the kinetic diameter of CO_2 (3.30 Å). This is also reflected in Figure 6.9 and explains the difference in relative decrease between N_2 and CO_2. On the other hand, the difference between N_2 and CO_2 can also be (partly) related to their respective solubilities in water. The solubility of CO_2 in water is higher than the solubility of N_2 in water [34] and this could contribute to the observed differences as well. However, in this work it is not possible to distinguish between nor quantify the contribution of either one of these possibilities (diffusivity or solubility).

Figure 6.10 presents the water vapor/gas selectivity for water vapor over CO_2 and water vapor over N_2 as a function of the water vapor activity as determined from the binary water vapor/gas permeation experiments presented in the previous graphs.

The water vapor/gas selectivity increases as a function of the water vapor activity. This increase is the result of an increase in water vapor permeability (Figure 6.7) combined with a decrease in gas permeability (Figure 6.8) at higher water vapor activities. The water vapor/N_2 selectivity is approximately 1–2 orders of magnitude higher than the water vapor/CO_2 selectivity. This is foremost the result of a significantly higher CO_2 permeability due to its specific interaction with the ether oxygen linkages in

Figure 6.10: Water vapor over gas selectivity for CO_2 (closed symbols) and N_2 (open symbols) as a function of water vapor activity at 50℃ as determined from binary feed mixtures of water vapor/CO_2 and water vapor/N_2 for PEO-*ran*-PPO based block copolymers with a soft segment length of 1000 (squares), 2500 (circles) and 10,000 g/mol (triangles).
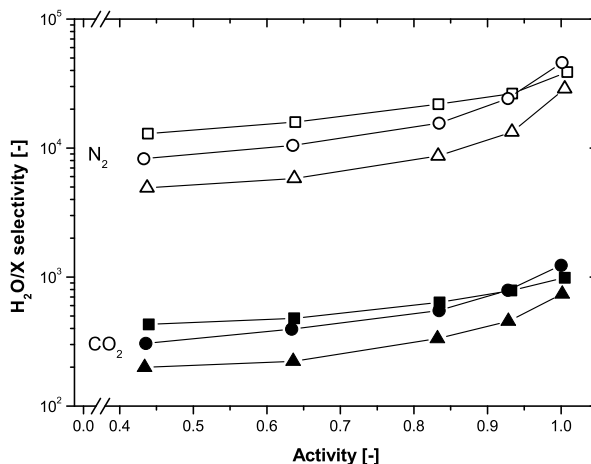
the block copolymers [22] Most likely and especially at higher water vapor activities, also the higher solubility of CO_2 in water vapor plays a role at higher activities as in that case also the gas will experience a more water-like environment. Furthermore, the different effect of the tortuosity on the CO_2 permeability compared to the N_2 permeability might be of influence as discussed before. An increase in soft segment length for the PEO-*ran*-PPO based block copolymers results in a decrease in the water vapor/gas selectivity as the relative increase in gas permeability is higher than the relative increase in water vapor permeability with increasing length of the soft block.

From the gas permeability data of the binary water vapor/CO_2 and water vapor/N_2 measurements the pure gas, ideal selectivity of CO_2 over N_2 as a function of the water vapor activity has been determined. This is analogous to the determination of an ideal selectivity using pure, dry gas measurements as usually performed. Figure 6.11 presents these results.

Due to the specific interactions of the ether oxygen linkages with CO_2 and the high flexibility of the polyether chain [22], a high CO_2 permeability combined with a
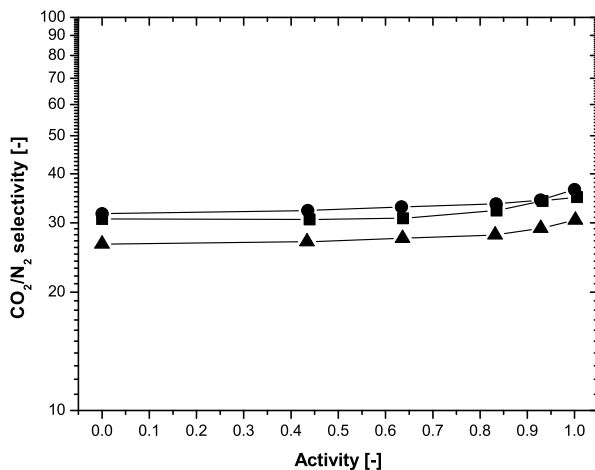
Figure 6.11: Calculated ideal CO_2/N_2 gas selectivity as a function of water vapor activity at 50℃ as determined from binary feed mixtures of water vapor/CO_2 and water vapor/N_2 for PEO-*ran*-PPO based block copolymers with a soft segment length of 1000 (squares), 2500 (circles) and 10,000 g/mol (triangles).

reasonable high selectivity of CO_2 over N_2 is obtained at 50℃ for all PEO-*ran*-PPO based block copolymers investigated. The CO_2/N_2 selectivity is fairly similar for all three block copolymers (as the chemical composition of the soft phase is the same) and suitable for the post-combustion capture of CO_2, as the required membrane selectivity for such a process would be between 20 and 50 [11, 12]. The selectivity increases slightly with an increase in water vapor activity in the feed stream. This originates from the fact that the permeability of N_2 is decreased relatively more as a function the of water vapor activity than the permeability of CO_2, resulting in a modest increase in selectivity.

Despite the valuable information seduced from single component permeation measurement (either a gas or a vapor), such experimental data for ideal performance parameters would overestimate the gas permeability and underestimate the water/vapor gas selectivity, especially at high water vapor activities (a > 0.6), which are characteristic for flue gases from fossil fuel fired power plants. Also, the CO_2/N_2 selectivity of the membrane from binary water vapor/CO_2 and water vapor/N_2 measurements still represent an ideal, pure gas selectivity as it relies on the separate determination of CO_2 and N_2 permeability. This addresses the importance of the simultaneous determination

Chapter 6

of water vapor and gas permeation. The separation performance can be different when CO_2 and N_2 permeate simultaneously in the presence of water vapor through the membrane as especially in glassy polymers, the presence of CO_2 is well-known to influence the permeation behavior of other gases in polymer membranes as well [35–38].

⌐ *Ternary water vapor/mixed gas permeation ($H_2O/CO_2/N_2$)*

To study the influence of water vapor on the CO_2 permeability and especially the CO_2/N_2 separation performance in more realistic process conditions and obtain real, mixed gas CO_2/N_2 selectivity values, the membrane performance using a ternary feed mixture containing water vapor and a CO_2/N_2 feed gas mixture (thus a three component system), has been studied. The gas mixture has a CO_2/N_2 volume ratio of 10/90, which is representative for the CO_2 concentration typically found in flue gases. Figure 6.12 presents the water vapor permeability of all investigated block copolymers as a function of water vapor activity for these ternary mixtures.

The water vapor permeability of all block copolymer membranes is similar to the water vapor permeability measured using binary feed mixtures (compare Figure 6.12 and Figure 6.7). This is expected as no noticeable difference was observed between
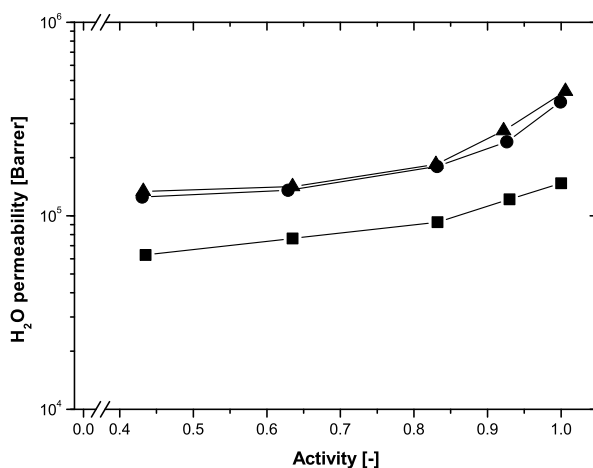
Figure 6.12: Water vapor permeability as a function of water vapor activity at 50℃ as determined from a ternary feed mixture of water vapor/CO_2/N_2 (10/90 v/v CO_2/N_2) for PEO-*ran*-PPO based block copolymers with a soft segment length of 1000 (squares), 2500 (circles) and 10,000 g/mol (triangles).

the two different binary water vapor/pure gas mixtures (containing either CO_2 or N_2) and as such any arbitrary combination of these is expected not to lead to significant changes in the behavior of the water vapor permeability.

The influence of the presence of CO_2 on the N_2 permeability (and vice versa) is shown in Figure 6.13, which presents the mixed gas CO_2 and N_2 permeability as a function of water vapor activity. The pure gas permeability values of both components as determined from binary feed mixtures are added as well (dashed lines) to visualize the difference between binary and ternary mixtures.

The gas permeability shows comparable behavior as the water vapor permeability (Figure 6.12) and no significant differences have been observed in the CO_2 and N_2 permeability as a function of water vapor activity using either binary (dashed lines) or ternary (solid lines) feed mixtures. This indicates that at the low feed pressures (and thus low partial pressures of CO_2) typically encountered in a post-combustion CO_2 capture process the simultaneous presence of CO_2 and N_2 is not expected to
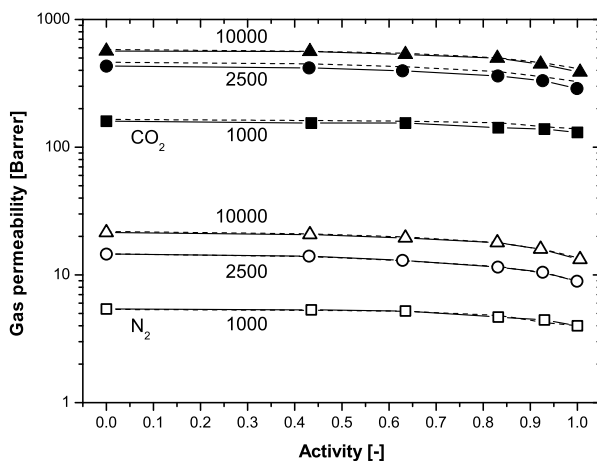
Figure 6.13: Mixed gas permeability for CO_2 (closed symbols) and N_2 (open symbols) as a function of water vapor activity at 50°C as determined from a ternary feed mixture of water vapor/CO_2/N_2 (10/90 vol.% CO_2/N_2) for PEO-*ran*-PPO based block copolymers with a soft segment length of 1000 (squares), 2500 (circles) and 10,000 g/mol (triangles). The 'pure' gas permeability using binary feed mixtures as shown in Figure 6.8 is added for comparison (dashed lines). No noticeable difference between the CO_2 and N_2 gas permeability using either binary or ternary feed mixtures is observed.

influence the membrane performance. This is oppositely to the behavior generally observed for rubbery polymers at high CO_2 partial pressures [38]. Consequently, also the real, mixed gas CO_2/N_2 selectivity is comparable to the ideal, pure gas selectivity (not shown). The implications of the previously described results for the applicability of these block copolymers in the post-combustion capture of CO_2 will be discussed in the next paragraph.

6.4.3 Applicability for post-combustion CO_2 capture

In summary, the PEO-*ran*-PPO based block copolymers exhibit a high water vapor permeability and most important they have a high CO_2 permeability, especially when compared to currently commercially available rubbery materials like PEBAX®1074 [19], combined with a reasonably high CO_2/N_2 selectivity under relevant (mixed gas) process conditions. Due to their highly hydrophilic character, these block copolymers have the ability to simultaneously remove CO_2 as well as water vapor from flue gases. This makes these PEO-*ran*-PPO based block copolymers an attractive membrane material for post-combustion CO_2 capture applications. In particular because post-combustion capture requires very high permeabilities and only reasonable selectivities to make the process economically viable [11, 12].

6.5 Conclusions

The potential of highly permeable, hydrophilic poly(ethylene oxide) based block copolymers for post-combustion CO_2 capture has been investigated. Emphasis has been placed on the effect of the presence of water vapor in the feed gas stream on the gas separation performance, as in general flue gases are close to water vapor saturation and have activities in the range of 0.8 to 1.0. The difference between pure (H_2O/CO_2 and H_2O/N_2) and mixed gas ($H_2O/CO_2/N_2$) feed conditions has been investigated. Water vapor sorption isotherms showed Flory-Huggins type behavior and the amount of water vapor sorbed was especially high above water vapor activities above 0.6. Hysteresis was not observed. Despite the strong water vapor sorption, plasticization effects were not observed and the water vapor diffusion coefficient was nearly independent on the water vapor activity. Binary (H_2O/CO_2 and H_2O/N_2) and ternary ($H_2O/CO_2/N_2$) permeation measurements showed that the gas permeability decreased as a function of the water vapor activity in the feed stream. This decrease

was especially evident at high concentrations of water vapor in the block copolymer. Because the dependency of the permeability on the water vapor activity was somewhat stronger for N_2 than for CO_2, the CO_2/N_2 permeability slightly increased ($\sim$10%) as a function of the water vapor activity. No noticeable differences between the pure and mixed gas permeabilities of all components have been observed. This indicates that plasticization effects, due to the sorption of CO_2, are not significant at the low feed pressure (2.5 bar) used. Overall, the block copolymers studied combine a high CO_2 permeability with a reasonable CO_2/N_2 gas selectivity. Due to their highly hydrophilic character, these block copolymers also have the ability to simultaneously remove CO_2 and water vapor from flue gases, which makes these PEO-*ran*-PPO based block copolymers an attractive membrane material for post-combustion CO_2 capture applications.

6.6   Acknowledgements

Chapter 6

6.7   References

[1] IPCC; *Third Assessment Report: Climate Change 2001*; Technical report; Cambridge University Press; Cambridge (England) (2001)

[2] IPCC; *Special Report on Carbon Dioxide Capture and Storage*; Technical report; Cambridge University Press; Cambridge (England) (2005)

[3] H. SIJBESMA, K. NYMEIJER, R. VAN MARWIJK, R. HEIJBOER, J. POTRECK AND M. WESSLING; *Flue gas dehydration using polymer membranes*; Journal of Membrane Science **313** (1-2) (2008) 263–276; DOI:10.1016/j.memsci.2008.01.024

[4] E. FAVRE, R. BOUNACEUR AND D. ROIZARD; *A hybrid process combining oxygen enriched air combustion and membrane separation for post-combustion carbon dioxide capture*; Separation and Purification Technology **68** (1) (2009) 30–36; DOI:10.1016/j.seppur.2009.04.003

[5] R. W. BAKER; *Membrane Technology and Applications*; 2$^{\text{nd}}$ edition (2000); West Sussex (England): John Wiley & Sons Ltd.; ISBN 978-0470854457

[6] C. E. POWELL AND G. G. QIAO; *Polymeric CO_2/N_2 gas separation membranes for the capture of carbon dioxide from power plant flue gases*; Journal of Membrane Science **279** (1-2) (2006) 1–49; DOI:10.1016/j.memsci.2005.12.062

[7] C. A. SCHOLES, S. E. KENTISH AND G. W. STEVENS; *Effects of minor components in carbon dioxide capture using polymeric gas separation membranes*; Separation and Purification Reviews **38** (1) (2009) 1–44; DOI:10.1080/15422110802411442

[8] J. POTRECK, K. NIJMEIJER, T. KOSINSKI AND M. WESSLING; *Mixed water vapor/gas transport through the rubbery polymer PEBAX$^{®}$ 1074*; Journal of Membrane Science **338** (1-2) (2009) 11–16; DOI:10.1016/j.memsci.2009.03.051

[9] V. I. BONDAR, B. D. FREEMAN AND I. PINNAU; *Gas sorption and characterization of poly(ether-b-amide) segmented block copolymers*; Journal of Polymer Science, Part B: Polymer Physics **37** (17) (1999) 2463–2475; DOI: 10.1002/(SICI)1099-0488(19990901)37:17⟨2463::AID-POLB18⟩3.0.CO;2-H

[10] V. I. BONDAR, B. D. FREEMAN AND I. PINNAU; *Gas transport properties of poly(ether-b-amide) segmented block copolymers*; Journal of Polymer Science, Part B: Polymer Physics **38** (15) (2000) 2051–2062; DOI:10.1002/1099-0488(20000801)38:15⟨2051::AID-POLB100⟩3.0.CO;2-D

[11] T. C. MERKEL, H. LIN, Z. HE, R. DANIELS, S. THOMPSON, A. SERBANESCU AND R. W. BAKER; *A membrane process to capture CO_2 from power plant flue*

gas from power plant flue gas; in *International Congress on Membranes and Membrane Processes (ICOM)*; Honolulu (HI), United States of America (2008)

[12] S. Shelley; *Capturing CO₂: Membrane-based systems move forward*; Chemical Engineering Progress **105** (4) (2009)

[13] A. Car, C. Stropnik, W. Yave and K. V. Peinemann; *PEG modified poly(amide-b-ethylene oxide) membranes for CO₂ separation*; Journal of Membrane Science **307** (1) (2008) 88–95; DOI:10.1016/j.memsci.2007.09.023

[14] A. Car, C. Stropnik, W. Yave and K. V. Peinemann; *Pebax®/polyethylene glycol blend thin film composite membranes for CO₂ separation: Performance with mixed gases*; Separation and Purification Technology **62** (1) (2008) 110–117; DOI:10.1016/j.seppur.2008.01.001

[15] A. Car, C. Stropnik, W. Yave and K. V. Peinemann; *Tailor-made polymeric membranes based on segmented block copolymers for CO₂ separation*; Advanced Functional Materials **18** (18) (2008) 2815–2823; DOI:10.1002/adfm.200800436

[16] S. J. Metz, M. H. V. Mulder and M. Wessling; *Gas-permeation properties of poly(ethylene oxide) poly(butylene terephthalate) block copolymers*; Macromolecules **37** (12) (2004) 4590–4597; DOI:10.1021/ma049847w

[17] D. Husken, T. Visser, M. Wessling and R. J. Gaymans; *CO₂ permeation properties of poly(ethylene oxide)-based segmented block copolymers*; Journal of Membrane Science **346** (1) (2010) 194–201; DOI:10.1016/j.memsci.2009.09.034

[18] S. R. Reijerkerk, A. Arun, K. Nijmeijer, R. J. Gaymans and M. Wessling; *Tuning of mass transport in multi-block copolymers for CO₂ capture applications*; Journal of Membrane Science (2009); DOI:10.1016/j.memsci.2009.09.045

[19] S. R. Reijerkerk, A. C. IJzer, K. Nijmeijer, A. Arun, R. J. Gaymans and M. Wessling; *Subambient temperature CO₂ and light gas permeation through segmented block copolymers with tailored soft phase*; ACS Applied Materials & Interfaces (2010); DOI:10.1021/am900754z

[20] A. C. IJzer, A. Arun, S. R. Reijerkerk, K. Nijmeijer, M. Wessling and R. J. Gaymans; *Synthesis and properties of hydrophilic segmented block copolymers based on poly(ethylene oxide)-ran-poly(propylene oxide)*; Journal of Applied Polymer Science, accepted for publication

[21] G. Holden, H. R. Kricheldorf and R. P. Quirk; *Thermoplastic Elastomers*; 3rd edition (2004); Munich (Germany): Hanser Gardner Publications; ISBN 978-1569903643

[22] H. Lin and B. D. Freeman; *Materials selection guidelines for membranes that*

Chapter 6

remove CO_2 from gas mixtures; Journal of Molecular Structure **739** (1-3) (2005) 57–74; DOI:10.1016/j.molstruc.2004.07.045

[23] J. G. WIJMANS AND R. W. BAKER; *The solution-diffusion model: A review*; Journal of Membrane Science **107** (1-2) (1995) 1–21; DOI:10.1016/0376-7388(95)00102-I

[24] Y. YAMPOLSKII, I. PINNAU AND B. D. FREEMAN; *Materials Science of Membranes for Gas and Vapor Separation*; 1$^{\text{st}}$ edition (2006); West Sussex (England): John Wiley & Sons Ltd.; ISBN 978-0470853450

[25] J. CRANK; *The Mathematics of Diffusion*; 2$^{\text{nd}}$ edition (1975); London (United Kingdom): Oxford University Press; ISBN 978-0198534112

[26] C. M. BALIK; *On the extraction of diffusion coefficients from gravimetric data for sorption of small molecules by polymer thin films*; Macromolecules **29** (8) (1996) 3025–3029; DOI:10.1021/ma9509467

[27] I. BLUME, P. J. F. SCHWERING, M. H. V. MULDER AND C. A. SMOLDERS; *Vapour sorption and permeation properties of poly (dimethylsiloxane) films*; Journal of Membrane Science **61** (1991) 85–97; DOI:10.1016/0376-7388(91)80008-T

[28] B. H. ZIMM AND J. L. LUNDBERG; *Sorption of vapors by high polymers*; Journal of Physical Chemistry **60** (4) (1956) 425–428; DOI:10.1021/j150538a010

[29] J. POTRECK, F. UYAR, H. SIJBESMA, K. NIJMEIJER, D. STAMATIALIS AND M. WESSLING; *Sorption induced relaxations during water diffusion in S-PEEK*; Physical Chemistry Chemical Physics **11** (2) (2009) 298–308; DOI:10.1039/b810638j

[30] S. J. METZ, W. J. C. VAN DE VEN, J. POTRECK, M. H. V. MULDER AND M. WESSLING; *Transport of water vapor and inert gas mixtures through highly selective and highly permeable polymer membranes*; Journal of Membrane Science **251** (1-2) (2005) 29–41; DOI:10.1016/j.memsci.2004.08.036

[31] S. J. METZ, W. J. C. VAN DE VEN, M. H. V. MULDER AND M. WESSLING; *Mixed gas water vapor/N_2 transport in poly(ethylene oxide) poly(butylene terephthalate) block copolymers*; Journal of Membrane Science **266** (1-2) (2005) 51–61; DOI:10.1016/j.memsci.2005.05.010

[32] S. J. METZ, N. F. A. VAN DER VEGT, M. H. V. MULDER AND M. WESSLING; *Thermodynamics of water vapor sorption in poly(ethylene oxide) poly(butylene terephthalate) block copolymers*; Journal of Physical Chemistry B **107** (49) (2003) 13629–13635; DOI:10.1021/jp035640d

[33] J. POTRECK, K. NIJMEIJER, N. F. A. VAN DER VEGT AND M. WESSLING; *Thermodynamics of water vapor sorption in hydrophilic polymers*; submitted for

Chapter 6

publication

[34] D. R. LIDE; *CRC Handbook of Chemistry and Physics*; 90th edition (2009); Boca Raton, FL (United States of America): CRC Press/Taylor and Francis; ISBN 978-1420090840

[35] L. S. WHITE, T. A. BLINKA, H. A. KLOCZEWSKI AND I. F. WANG; *Properties of a polyimide gas separation membrane in natural gas streams*; Journal of Membrane Science **103** (1-2) (1995) 73–82; DOI:10.1016/0376-7388(94)00313-n

[36] A. BOS, I. G. M. PÜNT, M. WESSLING AND H. STRATHMANN; *CO_2-induced plasticization phenomena in glassy polymers*; Journal of Membrane Science **155** (1) (1999) 67–78; DOI:10.1016/s0376-7388(98)00299-3

[37] C. STAUDT-BICKEL AND W. J. KOROS; *Improvement of CO_2/CH_4 separation characteristics of polyimides by chemical crosslinking*; Journal of Membrane Science **155** (1) (1999) 145–154; DOI:10.1016/S0376-7388(98)00306-8

[38] S. R. REIJERKERK, K. NIJMEIJER, C. P. RIBEIRO JR., B. D. FREEMAN AND M. WESSLING; *On the effects of plasticization in CO_2/light gas separation using polymeric solubility selective membranes*; in preparation

Chapter 6

CHAPTER 7

Poly(ethylene glycol) and poly(dimethyl siloxane): Combining their advantages into efficient CO$_2$ gas separation membranes

Abstract

Polymer blending is a versatile tool to combine the beneficial properties of two or more components in one single material. Here, we present the preparation, thermal- and mass transport properties of a series of blend membranes made from the commercially available PEBAX$^{®}$ MH 1657 and a poly(ethylene glycol) (PEG) based additive. The additive (PDMS-PEG) consists for 80 wt.% of PEG and the remaining 20 wt.% is poly(dimethyl siloxane) (PDMS), which is highly flexible and permeable. As such, we combine the high selectivity of PEG for CO_2 with the high permeability of PDMS. We extensively study the gas transport properties, and in particular the CO_2/light gas separation performance, using pure and mixed gases. The pure gas CO_2 permeability in the PEBAX$^{®}$1657/PDMS-PEG blend membranes increased by a factor 5 to approximately 530 Barrer at 50 wt.% PDMS-PEG loading. CO_2 sorption measurements revealed only a 50% increase in CO_2 solubility and the increase in permeability could be mainly attributed to an increase in diffusivity. Remarkably, the CO_2/H_2 selectivity is enhanced ($\sim$10%) at 50 wt.% loading, while the CO_2/N_2 and CO_2/CH_4 selectivity only slightly decreases. Mixed gas CO_2/H_2 and CO_2/CH_4 permeation measurements up to CO_2 partial pressures of 25 bar reveal that the CO_2 permeability is slightly reduced when gas mixtures are used. The CO_2/H_2 selectivity was found to be independent of the PDMS-PEG loading and feed pressure at a value of approximately 9 to 10. CO_2/CH_4 mixed gas selectivity decreased slightly with PDMS-PEG loading and pressure, but always remained above 10.

Chapter 7

7.1 Introduction

The atmospheric concentration of greenhouse gases (GHGs) has increased significantly over the last century. This large increase in concentration is believed to contribute to global warming and carbon dioxide (CO_2) has been identified as one of the main contributors [1]. CO_2 is predominantly emitted to the atmosphere by fossil fuel combustion processes [1]. To mitigate these climate changes, the Intergovernmental Panel on Climate Change (IPCC) states in its third assessment report that to achieve the stabilization of the atmospheric GHG concentration during the 21st century, the emissions of CO_2 need to be reduced by a substantial amount [2]. Hence, a considerable amount of research is dedicated to the development of suitable techniques to capture and subsequently store CO_2 (Carbon Capture & Storage (CCS)).

Current technologies employed for the separation of CO_2 from light gases are mainly absorption (amines) and cryogenic distillation [1]. Membrane technology can offer several advantages over these established techniques, such as lower energy consumption, mechanical simplicity, ease to scale up and smaller footprints [3]. Unfortunately, besides CO_2/CH_4 separation [3–5], the use of membranes for the separation of CO_2 from other light gases (such as H_2 and N_2) in large industrial scale applications is still limited.

The use of membrane technology for the separation of CO_2 from light gases gains increasing interest due to development of membranes with high polar/non-polar selectivity [6, 7]. These polar membranes separate CO_2 from light gases based on differences in solubility instead of size. Compared to the non-polar gases (H_2, N_2, CH_4), the quadrupolar CO_2 has a much higher solubility in these polar membranes. Recently, Freeman *et al.* [8] have published an overview of design strategies to obtain such high polar/non-polar selectivity. They have identified that ethylene oxide (EO) units are able to combine a high permeability with a reasonable high CO_2/light gas selectivity. PEO containing block copolymers in particular have been extensively described and investigated [9–13]. Especially the commercially available Pebax® block copolymers, which are synthesized from polyoxyalkylene glycols (such as PEG or PTMG) and dicarboxylic acid terminated aliphatic polyamides (such as nylon-6 or nylon-12) [14–17] have shown potential as CO_2 separation materials [6, 7, 18–21]. These block copolymers exhibit a microphase separated morphology and the gas permeates preferably through the soft amorphous polyether phase, while the hard polyamide phase provides the mechanical stability of the membrane material [7, 20].

Chapter 7

The performance of PEBAX® block copolymers can be enhanced by the physical blending of, for instance, PEBAX®1657 with low molecular weight PEG (M_w = 200 g/mol) [22–24]. The beneficial effect of PEG as a homogeneous blending component to enhance the CO_2 separation performance was shown by several researchers [25–30]. Furthermore, heterogeneous PEG blends such as those with poly(dimethyl siloxane) (PDMS) [31] or poly(1-trimethylsilyl-1-propyne) (PTMSP) [32] have been studied as well. They are especially interesting as PDMS and PTMSP are among the most permeable polymers known. PDMS has a CO_2 permeability of 3,800 Barrer [33], while PTMSP has a value as high as 28,000 Barrer [32]. In contrast, the CO_2 permeability in amorphous PEO is only 143 Barrer as estimated by Freeman *et al.* [34]. The CO_2/N_2 selectivity on the other hand, has a value of only 5.6 for PTMSP [32] and 9.5 for PDMS [33], while for amorphous PEO it is 48 [34]. It would therefore be interesting to combine the high permeability of PDMS or PTMSP with the high selectivity of PEO. This has been pursued with limited success. For example, the addition of 30 wt.% PEG (M_W = 300 g/mol) to PTMSP increased the CO_2/N_2 selectivity from 5.6 to 25, but the CO_2 permeability of such a blend is only 146 Barrer at 30℃ [32], which is only a fraction of the values obtainable for PTMSP.

The strategy to combine the beneficial properties of highly permeable polymers, such as PDMS, and polyethers (especially PEG) in one single membrane has also been obtained by copolymerization of these moieties in one (block) copolymer. Examples containing PDMS and PEG [35–37], PPG [37, 38] and PTMG [37, 39] polyethers have been reported in literature. Park *et al.* [37] showed that the copolymerization of small amounts of PDMS in polyurethane-polyether block copolymers could increase CO_2 permeability as well as selectivity. However, the CO_2 permeability was always below 100 Barrer. The opposite, the copolymerization of small amounts of polyether in polyurethane-PDMS block copolymers resulted in a significant decrease in CO_2 permeability, while gas selectivity was not affected and values normally obtained for PDMS block copolymers were obtained. De Pinho *et al.* [38] synthesized PDMS/PPO urethane/urea bi-soft segment membranes with a maximum CO_2 permeability of 800-900 Barrer (at 75% PDMS content) and a CO_2/N_2 selectivity of 18, however their experimental temperature is not given.

In this work we elaborate on the recent work by Car *et al.* [22–24] who successfully prepared PEBAX®1657/PEG$_{200}$ blend membranes with improved mass transport properties compared to the pristine PEBAX®1657 block copolymer. In contrast to the regular PEG used by Car *et al.*, the additive used in our work consists of two

different segments. The first part of the additive consists of 80 wt.% low molecular weight PEG analogous to the work of Car *et al.*. This ensures high selectivity and excellent compatibility in the blend. The remaining 20 wt.% of the additive consists of the highly permeable PDMS. We hypothesize that the combination of these two moieties in the additive combines of the beneficial properties of both moieties and as such will result in highly permeable and selective membranes. Below, we report the synthesis and gas transport properties of such PEBAX®1657/PDMS-PEG blend membranes. Pure gas characteristics are analyzed in detail and compared to the results obtained by Car *et al.* [22] to proof the permeability enhancing effect of the PDMS. Furthermore, CO_2/H_2 and CO_2/CH_4 mixed gas permeation up to 25 bar CO_2 partial pressure has been studied and the difference between pure and mixed gas conditions is discussed.

7.2   Theory

Mass transport in non-porous, dense, polymeric structures following the solution-diffusion mechanism has been well documented in literature [40–42]. The steady state gas permeability coefficient of a dense polymeric membrane is given by Equation (7.1):

$$P_i = \frac{N_i \cdot l_i}{f_{2,i} - f_{1,i}} \tag{7.1}$$

where P_i is the gas permeability coefficient (cm^3 (STP)·cm/(cm^2·s·cmHg)), N_i is the steady state flux of the component through the membrane (cm^3 (STP)/(cm^2·s)), l the membrane thickness (cm) and $f_{2,i}$ and $f_{1,i}$ respectively are the upstream and downstream fugacity (cmHg). The permeability coefficient is usually expressed in units of Barrer, where 1 Barrer equals $1 \cdot 10^{-10}$ (cm^3 (STP)·cm/(cm^2·s·cmHg) or $7.5 \cdot 10^{-18}$ (m^3 (STP)·m/(m^3·s·Pa)). If gas phase non-ideality is not significant, fugacities can be replaced by partial pressures.

The permeability may be described using Fick's first law, resulting in the permeability coefficient as expressed by Equation (7.2), representing the solution-diffusion mechanism.

$$P_i = D_i \cdot S_i \tag{7.2}$$

Chapter 7

In Equation (7.2) D_i is the average effective diffusion coefficient (cm^2/s) and S_i is the solubility coefficient (cm^3 (STP)/(cm^3·cmHg)), where the solubility coefficient is defined as the gas concentration in the polymer divided by the fugacity according to Equation (7.3):

$$S_i = \frac{C_i}{f_i} \tag{7.3}$$

In the most ideal case of mass transport P, D and S are independent of feed or permeate pressure. The selectivity of a polymer membrane for gas A over gas B is given by the ratio of the gas permeability coefficients according to Equation (7.4). The selectivity is also a product of diffusivity and solubility selectivity.

$$\alpha = \frac{P_A}{P_B} = \frac{D_A}{D_B} \cdot \frac{S_A}{S_B} \tag{7.4}$$

where D_A/D_B is the diffusivity selectivity and S_A/S_B is the solubility selectivity. Gas diffusivity is in general enhanced by decreasing penetrant size, increasing polymer chain flexibility (often characterized by a decrease in glass transition temperature), increasing polymer fractional free volume and decreasing polymer-penetrant interactions [42]. Penetrant solubility is increased by increasing condensability of the penetrant (which increases with increasing critical temperature and boiling point) and increasing polymer-penetrant interactions [42]. In general, polyether based block copolymers, like PEBAX®, exhibit a low T_g resulting in high CO_2 diffusivity. The size sieving ability (diffusivity selectivity) however is low and high overall CO_2/light gas selectivity is mainly achieved by high CO_2/light gas solubility selectivity [6–8].

7.3 Experimental

7.3.1 Materials

PEBAX® MH 1657, obtained from Arkema (The Netherlands), is a polyether-block-amide comprising 60 wt.% poly(ethylene glycol) (PEG) and 40 wt.% aliphatic polyamide (PA6, nylon-6) and will be further referred to as 'PEBAX®1657' (Figure 7.1). The block size of the PEG segment is around 1500 g/mol (given by Arkema), which means, based on the mass fractions, that one repeating unit (n) consists of a PE-block containing approximately 35 ethylene oxide units and a PA-block containing
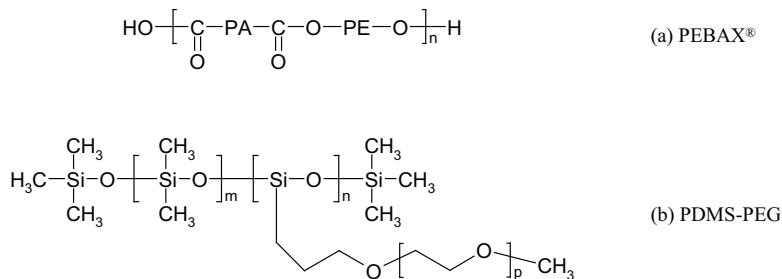
Figure 7.1: Chemical structures of PEBAX® and PDMS-PEG (20 wt.% PDMS, 80 wt.% PEG).

approximately 9 nylon-6 repeating units. The additives, PEG_{200} ($M_w = 200$ g/mol) and poly[dimethylsiloxane-co-methyl(3-hydroxypropyl)siloxane]-graft-poly(ethylene glycol) methyl ether (PDMS-PEG), were obtained from Aldrich (The Netherlands). The PDMS oligomer (Figure 7.1) is grafted with low molecular weight PEG (80 wt.%). According to the supplier, the PDMS-PEG has a molecular weight around 3800 g/mol, however the exact numbers of m, n and p are not provided. Ethanol (purity ≥ 99.9 %) is obtained from Merck (The Netherlands). All chemicals were used as received. Pure gases and calibrated gas mixtures of CO_2/H_2 (70/30 vol.%) and CO_2/CH_4 (50/50 vol.%) were obtained from Praxair (The Netherlands).

7.3.2 Membrane preparation

A mixture of ethanol and water (70/30 wt.%) was used as a solvent to prepare the polymer solution (3 wt.% PEBAX®1657). The PEBAX®1657 was dissolved under reflux and continuous stirring at 80℃ (∼2 hours). After complete dissolution of the polymer, the solution was cooled to room temperature and a homogeneous solution was obtained (no gelation). PEBAX®1657 blend membranes were prepared by the addition of different amounts of additive (either PEG_{200} or PDMS-PEG) to this solution ranging from 10 to 50 wt.% relative to the amount of PEBAX®1657. After the addition, the solution was stirred again for at least another hour. Membrane films were prepared by pouring the obtained solution in a Petri dish (∅ 7 cm). Subsequently, the membranes were placed under a nitrogen atmosphere at room temperature for at least 3 days to evaporate the solvent. After removal from the Petri dish, the films were dried in a vacuum oven overnight at 30℃ to remove any residual solvent. The thickness of the prepared membrane films was measured using a digital screw micrometer (Preisser digi-met) and varied from 50 to 100 μm.

Chapter 7

7.3.3   Density

The density of the PEBAX®1657/additive blends was determined at room temperature for use in gas sorption experiments and to obtain qualitative information about the polymer free volume. The samples were dried in a vacuum oven (30℃) before use. Density measurements were performed using an AccuPyc 1330 Pycnometer (Micromeritics). The AccuPyc 1330 is a pycnometer of the gas expansion type and measures the amount of displaced gas (helium) at room temperature. Upon filling of the sample chamber and subsequent discharge into a second empty chamber with known volume the pressure is monitored. This allows calculation of the sample solid phase volume. The density is subsequently derived using the measured sample weight.

7.3.4   Gas permeability

All gas permeation properties were determined with the constant volume/variable pressure method using vacuum at the permeate side, i.e. the gas permeance values were calculated from the pressure increase in time in a calibrated volume at the permeate side [43]. All measurements were performed at a constant temperature of 35℃. The gas permeance values were corrected for membrane thickness to obtain gas permeability. Pure gas permeability values were obtained at a feed pressure of 4 bar for He, H_2, O_2, N_2, CO_2 and CH_4 and at high pressure (up to 25 bar CO_2 partial pressure) for H_2, CO_2 and CH_4. The ideal gas selectivity values were calculated from the ratio of pure gas permeability values. CO_2 mixed gas separation experiments were conducted using a 70/30 vol.% CO_2/H_2 or a 50/50 vol.% CO_2/CH_4 gas mixture. The feed pressure was varied between 4–25 bar partial pressure of CO_2. The feed and permeate compositions were analyzed using a Varian gas chromatograph (GC) equipped with a TCD and a HayeSep Q column. Helium was used as a carrier gas for the CO_2/CH_4 experiments, while nitrogen was used for the CO_2/H_2 experiments. The retentate flowrate was kept constant at a value between 40 and 250 ml/min, depending on the additive fraction and pressure, to provide stage-cuts < 2%. The experiments were analyzed using fugacity instead of (partial) pressure, as especially CO_2 shows strong non-ideal behavior at high pressure (up to 20% difference compared to assuming ideal behavior). Fugacity coefficients were calculated with the Soave-Redlich-Kwong equation of state and the simulation software package AspenPlus Properties (version 11).

186

7.3.5 Pure gas sorption

Gas sorption isotherms of CO_2 at 35℃ for PEBAX®1657/PDMS-PEG blends were determined gravimetrically by a magnetic suspension balance (MSB, Rubotherm) operated by MessPro software. Before each sorption experiment, the samples were degassed overnight by applying a vacuum. A sorption run consisted of several incremental pressure steps (from 4 to 25 bar) and the mass uptake as a function of time was measured. Each pressure step took around 2 hours, since the sorption stabilizes quickly in these rubbery polymer blends. The measured equilibrium weight was corrected for buoyancy according to Archimedes' principle. The gas concentration in the polymer (cm^3 (STP) / cm^3 polymer) was calculated using the molar volume of CO_2 at standard temperature and pressure (STP, 1 bar and 273.15 K), the polymer volume (obtained from density measurements) and the CO_2 molecular weight.

7.4 Results & discussion

7.4.1 Introduction

PEBAX®1657/PDMS-PEG blend membranes were prepared as described. Membranes containing between 0–50 wt.% PDMS-PEG are transparent and have sufficient mechanical strength. Blend membranes prepared with 75 wt.% PDMS-PEG are mechanically not stable for gas permeation experiments. To be able to assess the effect of the PDMS-PEG additive and to compare its performance to the recent results obtained by Car *et al.* [22–24], also PEBAX®1657 membranes containing pure PEG (PEG_{200}) as an additive were prepared.

7.4.2 Pure gas permeation characteristics at 4 bar feed pressure

The gas transport preferentially occurs through the soft phase and crystallization of PEG is detrimental to the gas transport properties [11–13]. To exemplify, Freeman *et al.* [34] determined that the CO_2 permeability of pure semi-crystalline PEG (71 vol.% crystalline) is only 12 Barrer. The mass transport properties of the PEBAX®/PDMS-PEG additive blends are therefore only attractive at temperatures were the crystallization of the soft phase does not occur. To identify this temperature range, the thermal

properties of the material have been extensively studied. This is described in the supplementary material provided. The results of the thermal analysis reveal that the mass transport properties of the PEBAX®/PDMS-PEG additive blends are only attractive at or above room temperature, as at these temperatures the PEG from the PEBAX®1657 matrix as well as the PDMS-PEG additive are in the amorphous state.

Consequently, all gas permeation properties of the membranes as a function of the PDMS-PEG additive content (0–50 wt.%) have been determined at a temperature of 35℃ and a feed pressure of 4 bar. Table 7.1 summarizes the CO_2 permeability and CO_2/light gas selectivity for CO_2 over He, H_2, O_2, N_2 and CH_4 of these PEBAX®1657/PDMS-PEG blend membranes. For comparison, the results obtained for the PEBAX®1657/PEG_{200} blend membranes are also shown. The results for the membranes containing only PEG_{200} as additive show reasonable good agreement with the results of Car *et al.*, considering the somewhat higher experimental temperature (35℃ instead of 30℃ [22]).

Table 7.1: Pure gas CO_2 permeability and CO_2/light gas selectivity at 35℃ and 4 bar for PEBAX®1657, PEBAX®1657/PDMS-PEG and PEBAX®1657/PEG_{200} blend membranes.

Sample	CO_2 permeability	CO_2/light gas selectivity [–]				
	[Barrer]	CO_2/He	CO_2/H_2	CO_2/O_2	CO_2/N_2	CO_2/CH_4
PEBAX®	98	15.9	9.5	20.8	53.2	16.1
PEBAX®/PDMS-PEG blends						
10 wt.% PDMS-PEG	179	17.1	9.9	19.2	48.0	14.5
20 wt.% PDMS-PEG	245	18.1	10.3	18.0	42.6	13.0
30 wt.% PDMS-PEG	326	19.1	10.5	17.1	40.1	12.0
40 wt.% PDMS-PEG	457	19.4	10.5	16.4	37.4	11.2
50 wt.% PDMS-PEG	532	19.9	10.6	15.9	36.1	10.8
PEBAX®/PEG_{200} blends						
10 wt.% PEG_{200}	127	16.8	10.0	21.3	52.6	16.4
20 wt.% PEG_{200}	136	16.8	10.0	21.0	49.9	15.9
30 wt.% PEG_{200}	153	17.2	10.2	20.9	48.2	15.9
40 wt.% PEG_{200}	159	17.6	10.4	20.8	49.0	15.7
50 wt.% PEG_{200}	172	18.0	10.5	21.0	50.5	15.7

⌐ *CO_2 permeability*

Figure 7.2 shows the CO_2 pure gas permeability for the PEBAX®1657/PDMS-PEG blend membranes. For comparison, the CO_2 permeability of PEBAX®1657/PEG_{200} blend membranes up to 50 wt.% PEG_{200} has been added as well (Table 7.1).
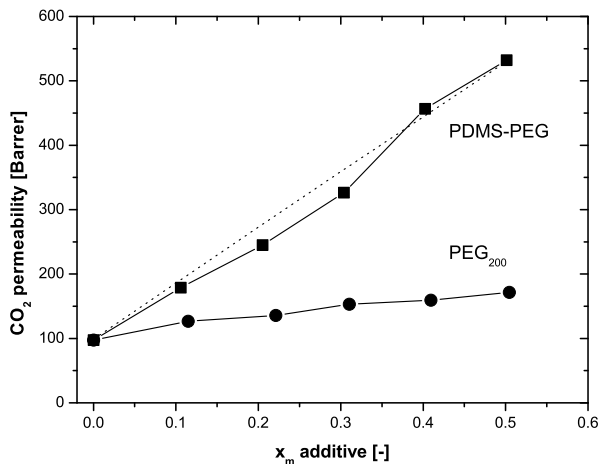
Figure 7.2: Pure gas CO_2 permeability at 35℃ and 4 bar as a function of additive mass fraction for PEBAX®1657 blend membranes, with (■) PDMS-PEG and (●) PEG$_{200}$. The dashed line represents the theoretical PDMS contribution to CO_2 permeability in the PEBAX®1657/PDMS-PEG blend membranes from a theoretical blend of PEBAX®1657 and pure PDMS calculated with data from Merkel *et al.* [33] and Singh *et al.* [44] according to the parallel model (Equation (7.5)) [45].

The CO_2 permeability (and the permeability of the other light gases as well) strongly increases with the PDMS-PEG mass fraction. CO_2 permeability values higher than 500 Barrer can be obtained. The increase in permeability with increasing additive fraction is much more pronounced compared to the addition of PEG$_{200}$. To illustrate this, the CO_2 permeability increases from ∼100 Barrer for PEBAX®1657 to 532 Barrer for PEBAX®1657 with 50 wt.% PDMS-PEG additive, while the addition of 50 wt.% PEG$_{200}$ results in an increase in CO_2 permeability to only 172 Barrer. We hypothesize that this significant increase can be attributed to two separate effects. In the first place to the increase in amorphous PEG concentration (from 60 wt.% for PEBAX®1657 to 70 wt.% for PEBAX®/50PDMS-PEG), which results in a higher overall concentration of amorphous EO units. This increases the CO_2 solubility (as will be discussed later) and the free volume available for permeation due to the plasticizing effect of the additive, analogous to the results obtained by Car *et al.* [22, 24]. Second, and more significant, the addition of the highly flexible and permeable PDMS, which creates a ”high diffusion” pathway for the penetrants within the amorphous soft phase.

Chapter 7

To identify the significance of the highly flexible and permeable PDMS to the observed increase in permeability, its theoretical contribution to the CO_2 permeability is calculated as well. For a homogeneous blend, the gas permeability is usually expressed empirically according to the logarithmic additive model [46] or the Maxwell model [47]. Although the PDMS-PEG additive consists for 80 wt.% of PEG, the prepared membrane blends cannot be considered as homogeneous blends and both models fail to predict the increase in CO_2 permeability. The prediction of gas permeability in heterogeneous polymer blends has been documented [45, 48] and is generally described using either the parallel or the series model (or a combination of these two). For the current system the theoretical contribution of PDMS to the overall CO_2 permeability can be best described by the parallel model according to Equation (7.5) [45]

$$P_b = \phi_1 P_1 + \phi_2 P_2 \tag{7.5}$$

in which P_b is the permeability of the blend, P_1 and P_2 are respectively the permeabilities of component 1 and 2, and ϕ_1 and ϕ_2 are respectively the volume fractions of component 1 and component 2. The dashed line in Figure 2 represents the calculated PDMS contribution to the CO_2 permeability in the PEBAX®1657/PDMS-PEG blend membranes from a blend of PEBAX®1657 and pure PDMS, calculated using the data from Merkel et $al.$ [33] ($P_{CO_2} = 3800$ Barrer) and Singh et $al.$ [44] ($\rho = 0.98$ g/cm^3). For instance, in a PEBAX®1657/PDMS-PEG blend containing 50 wt.% PDMS-PEG the pure PDMS mass fraction equals 10 wt.% (the PDMS-PEG consists for only 20 wt.% of PDMS), which gives a theoretical permeability value of approximately 528 Barrer. This line shows the good agreement between the measured CO_2 permeability and the predicted contribution of PDMS.

⌐ *Permeability of non-polar gases*

Figure 7.3 shows the normalized gas permeability of all investigated gases as a function of the PDMS-PEG additive mass fraction in the PEBAX®1657 matrix.

The normalized permeability of all gases investigated strongly increases with increasing additive weight fraction and the normalized increase in gas permeability is a function of the kinetic diameter of the gases. The relative increase is larger for bigger molecules and higher mass fractions of additive. This supports the assumption that the main contribution to the increase in gas permeability due to the addition of the additive is an increase in free volume and consequently gas diffusivity through the blend membranes.
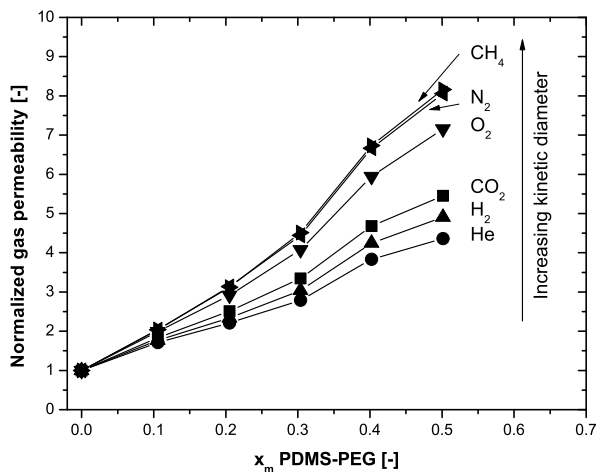
Figure 7.3: Normalized pure gas permeability at 35°C and 4 bar as a function of PDMS-PEG additive mass fraction in PEBAX$^{®}$1657/PDMS-PEG blend membranes for (●) He (2.6 Å), (▲) H$_2$ (2.89 Å), (■) CO$_2$ (3.3 Å), (▼) O$_2$ (3.46 Å), (◄) N$_2$ (3.64 Å) and (►) CH$_4$ (3.8 Å).

⌐ *CO$_2$/light gas selectivity*

Table 7.1 summarizes the pure CO$_2$/light gas selectivities for the PEBAX$^{®}$1657/PDMS-PEG blend membranes and Figure 7.4 shows the normalized CO$_2$/light gas selectivity as a function of PDMS-PEG additive mass fraction.

In all blend membranes the CO$_2$ permeability is significantly higher than the permeability of the other light gases, which is ascribed to the unique character of the polar ether oxygens in the polymer, which favors the solubility of quadrupolar CO$_2$ over the other non-polar light gases [6–8, 19]. This results in reasonably high CO$_2$/light gas selectivities. The CO$_2$/He and CO$_2$/H$_2$ selectivity increase and the CO$_2$/N$_2$, CO$_2$/O$_2$ and CO$_2$/CH$_4$ selectivity decrease as a function of PDMS-PEG additive mass fraction. This difference in selectivity behavior is directly related to the difference in kinetic diameter of the different gases as discussed in the previous paragraph.
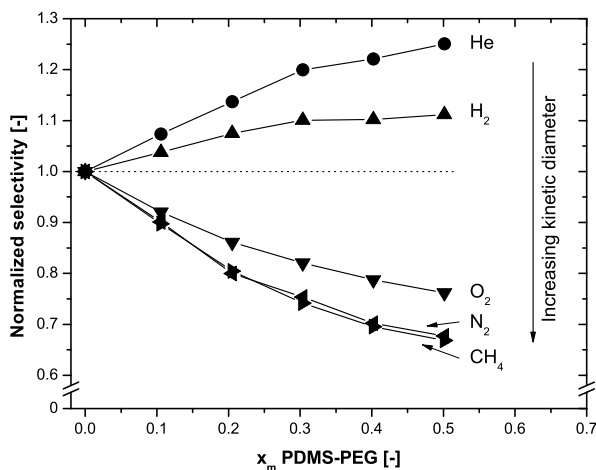
Chapter 7

191

Figure 7.4: Normalized pure CO_2/light gas selectivity at 35℃ and 4 bar as a function of PDMS-PEG additive mass fraction in PEBAX®1657/PDMS-PEG blend membranes for (●) CO_2/He, (▲) CO_2/H_2, (▼) CO_2/O_2, (◄) CO_2/N_2 and (►) CO_2/CH_4.

7.4.3 CO_2 sorption and diffusion

To examine the contribution of the CO_2 diffusivity to the overall increase in CO_2 permeability and its relation with the polymer specific volume, the pure gas CO_2 sorption behavior is studied. Figure 7.5 shows the pure gas CO_2 concentration (cm^3 (STP)/cm^3 polymer) at 35℃ as a function of the CO_2 fugacity for the PEBAX®1657/PDMS-PEG blend membranes.

The CO_2 concentration in the blend membranes is high and increases with increasing CO_2 fugacity. This high CO_2 sorption is ascribed to the favorable interaction of the quadrupolar CO_2 with the polar ether oxygen moieties in the polymer [6, 8]. The sorption isotherms are slightly convex to the pressure axis, which is characteristic for vapor dissolution in polymeric membranes and described by Florry-Huggins [42]. The CO_2 sorption measurements confirm the hypothesis that an increase in amorphous PEG concentration by an increase in PDMS-PEG additive mass fraction results in an increase in CO_2 solubility (as the CO_2 concentration at equal fugacity increases with increasing PDMS-PEG content).

Chapter 7
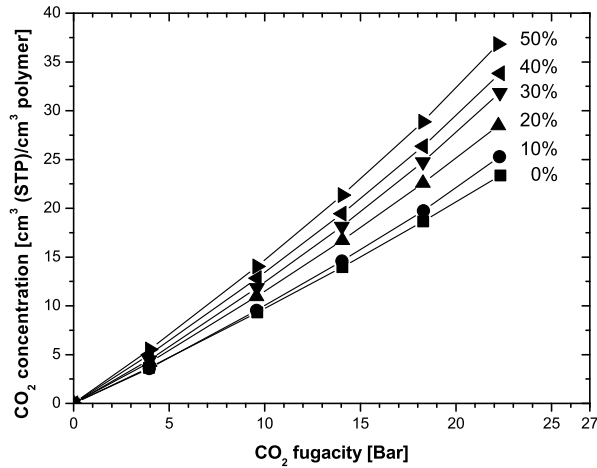
Figure 7.5: CO_2 concentration (cm^3 (STP)/cm^3 polymer) as a function of CO_2 fugacity at 35℃ for PEBAX®1657/PDMS-PEG blend membranes, with (■) PEBAX®1657 and PEBAX®1657 with (●) 10 wt.%, (▲) 20 wt.%, (▼) 30 wt.%, (◄) 40 wt.% and (►) 50 wt.% PDMS-PEG additive.

From the measured CO_2 permeability and solubility coefficients, the CO_2 diffusivity coefficients are calculated according to the solution-diffusion model (Equation (7.2)). Table 7.2 summarizes the measured CO_2 permeability and solubility coefficients and the calculated CO_2 diffusion coefficient for the PEBAX®1657/PDMS-PEG blend membranes at 35℃ and 4 bar.

Table 7.2: Absolute and normalized pure gas CO_2 permeability, solubility and diffusion coefficients at 35℃ and 4 bar for PEBAX®1657/PDMS-PEG blend membranes.

Sample	Absolute			Normalized		
	Permeability	Solubility	Diffusion	P	S	D
	[Barrer]	[cm^3 (STP)/(cm^3·cmHg)]	$\cdot 10^{-7}$ [cm^2/s]	[–]	[–]	[–]
PEBAX®	98	0.0123	7.9	1.00	1.00	1.00
PEBAX®/10PDMS-PEG	179	0.0124	14.4	1.83	1.01	1.81
PEBAX®/20PDMS-PEG	245	0.0143	17.1	2.51	1.17	2.15
PEBAX®/30PDMS-PEG	326	0.0152	21.4	3.35	1.25	2.67
PEBAX®/40PDMS-PEG	457	0.0165	27.7	4.68	1.36	3.45
PEBAX®/50PDMS-PEG	532	0.0181	29.4	5.46	1.48	3.67

The calculated CO_2 diffusion coefficient ($7.9 \cdot 10^{-7}$ cm^2/s) for PEBAX®1657 from the data presented here has the same order of magnitude as the values reported by others.

Chapter 7
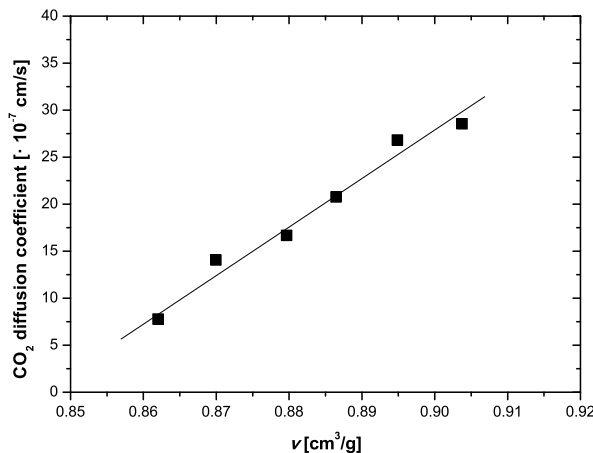
Figure 7.6: CO_2 diffusion coefficient at 35℃ as a function of the polymer specific volume for PEBAX®1657/PDMS-PEG blends. A higher specific volume represents higher PDMS-PEG concentration in the blend.

Car *et al.* [22] determined the CO_2 diffusivity for PEBAX®1657 with a pressure increase time-lag apparatus and obtained a CO_2 diffusion coefficient of $4.6 \cdot 10^{-7}$ cm²/s at 30℃ and 600 mbar feed pressure. Kim *et al.* [19] determined the CO_2 diffusivity for PEBAX®1657 using a continuous flow technique and obtained a CO_2 diffusion coefficient of $15.2 \cdot 10^{-7}$ cm²/s at 25℃ and 3 atmosphere feed pressure. Figure 7.6 shows the calculated CO_2 diffusion coefficient of the PEBAX®1657/PDMS-PEG blend membranes as a function of the polymer specific volume.

The results illustrate that the CO_2 diffusivity scales with the specific volume of the polymer and is correlated to the openness of the polymer. The increase in openness (free volume) is most likely caused by the incorporation of the PDMS, as the PEG glass transition temperature, which characterizes chain mobility and has been correlated with the fractional free volume in rubbery PEO materials, does not change [8].

Figure 7.7 presents the measured normalized CO_2 permeability and solubility coefficient and the calculated normalized CO_2 diffusion coefficient (according to Equation (7.2)) as a function of PDMS-PEG additive mass fraction.

The overall CO_2 permeability increases by a factor 5.5 upon the addition of 50 wt.% PDMS-PEG. This increase can now be analyzed in more detail and the normalized diffusivity increase (a factor 3.7 increase) is significantly higher than the normalized
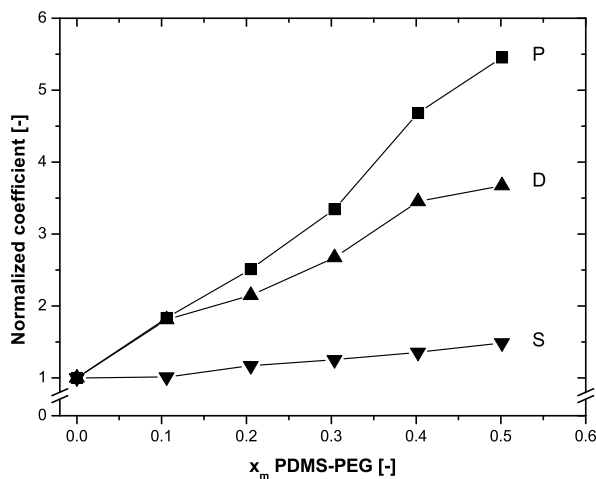
Figure 7.7: Normalized pure gas CO_2 (■) permeability, (▼) solubility and (▲) diffusion coefficient at 35℃ and 4 bar as a function of PDMS-PEG additive mass fraction in PEBAX®1657/PDMS-PEG blend membranes.

solubility increase (a factor 1.5 increase). At other additive fractions a similar trend is observed and the increase in diffusivity is always more significant than the increase in solubility. The strong increase in CO_2 permeability with an increase in mass fraction of additive can thus be mainly attributed to an increase in gas diffusivity and only to a smaller extent to an increase in corresponding solubility.

7.4.4   Pure gas permeation characteristics at high feed pressure

The influence of the feed pressure on the pure gas permeation characteristics of PEBAX®1657/PDMS-PEG blend membranes (0–10–30–50 wt.%) is determined for CO_2, H_2 and CH_4 at 35℃ in the range of 4 to 25 bar.

⌐ *Influence of feed pressure on pure gas permeability*
Figure 7.8 shows the CO_2 permeability as a function of the CO_2 fugacity of the PEBAX®1657/PDMS-PEG blend membranes (0–10–30–50 wt.%).

The CO_2 permeability of the PEBAX®1657/PDMS-PEG blend membranes increases with increasing feed fugacity. This increase is more pronounced at lower PDMS-PEG
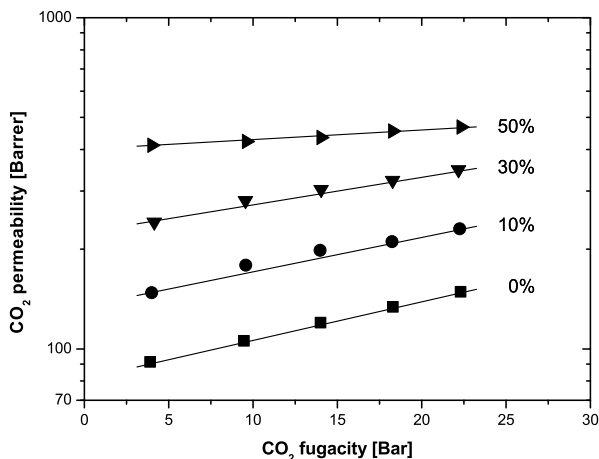
Figure 7.8: Pure gas CO_2 permeability at 35℃ as a function of CO_2 fugacity for ($\blacksquare$) PEBAX®1657 and PEBAX®1657/PDMS-PEG blend membranes with ($\bullet$) 10 wt.%, ($\blacktriangledown$) 30 wt.% and ($\blacktriangleright$) 50 wt.% PDMS-PEG additive.

fractions in the PEBAX®1657 matrix. We assume that this effect can be explained by the competition between plasticization effects (which increases chain flexibility and thus permeability) and the hydrostatic pressure (which slightly decreases polymer free volume and thus permeability [7]. For the blend membranes with low PDMS-PEG content (and presumably lower free volume) the plasticization effect dominates the hydrostatic pressure. This results in an increase in permeability with increasing pressure. For blend membranes with high PDMS-PEG content, which have a higher free volume (as indicated be an increase in specific volume), the reduction in free volume due to the increased pressure becomes more important and this leads to a relative lower increase in permeability as a function of pressure.

Figure 7.9 presents the H_2 and CH_4 permeability as a function of their fugacity for PEBAX®1657/PDMS-PEG blend membranes (0–10–30–50 wt.%).

The solubility of the non-polar H_2 and CH_4 in the individual constituents of the blend membranes (PEBAX®1657 [6], PDMS [33] and PEG [34]) is significantly lower than the solubility of CO_2 in these constituents. As such, the permeability of these gases is more governed by their diffusivity than their solubility. A change in free volume has a more pronounced effect on the larger molecules (i.e. CH_4) than on the smaller molecules (i.e. H_2). For pristine PEBAX®1657 and blend membranes with

Chapter 7
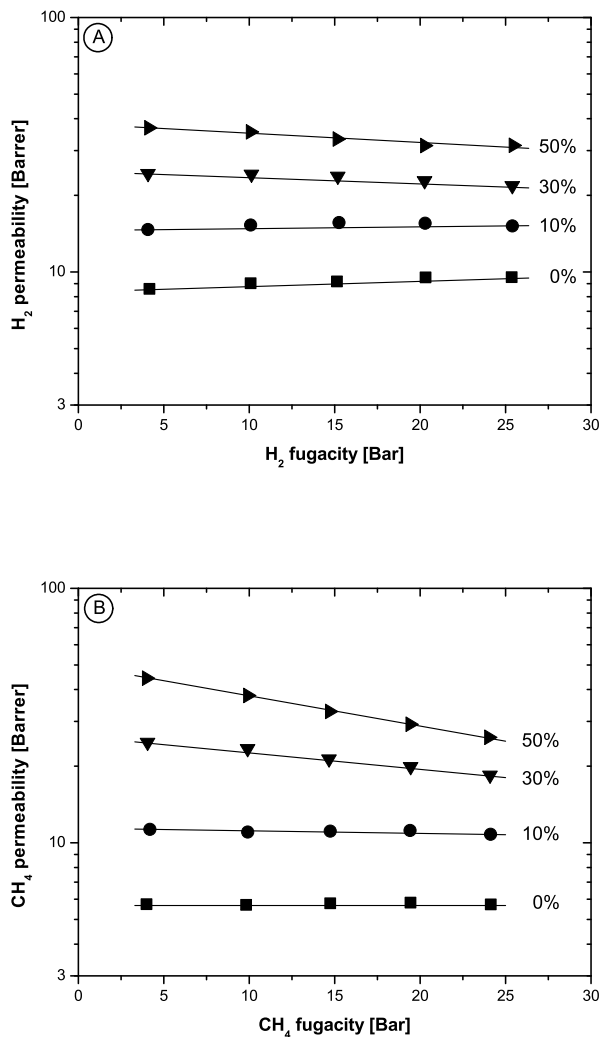
Figure 7.9: Pure gas H$_2$ permeability (a) and CH$_4$ permeability (b) at 35℃ as a function of feed gas fugacity for (■) PEBAX$^{®}$1657 and PEBAX$^{®}$1657/PDMS-PEG blend membranes with (●) 10 wt.%, (▼) 30 wt.% and (►) 50 wt.% PDMS-PEG additive.

Chapter 7
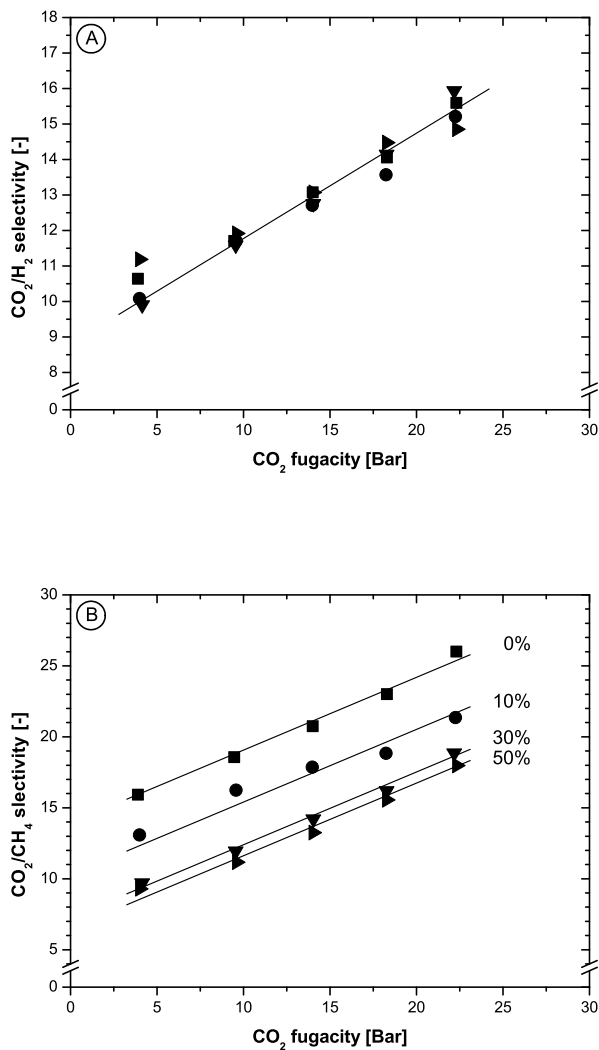
Figure 7.10: Pure gas CO_2/H_2 selectivity (a) and CO_2/CH_4 selectivity (b) at 35°C as a function of CO_2 fugacity for ($\blacksquare$) PEBAX$^{\textregistered}$1657 and PEBAX$^{\textregistered}$1657/PDMS-PEG blend membranes with ($\bullet$) 10 wt.%, ($\blacktriangledown$) 30 wt.% and ($\blacktriangleright$) 50 wt.% PDMS-PEG additive.

low (∼10 wt.%) PDMS-PEG concentration and thus lower anticipated amounts of free volume, an increase in pressure does not result in a significant change in free volume nor in H_2 or CH_4 permeability. At higher PDMS-PEG additive fractions, the effect of the increased free volume is visible in the response of the permeability to the increased pressure. An increase in feed pressure results in a decrease in free volume, which also decreases the gas permeability for both H_2 and CH_4. Because of its larger kinetic diameter, the diffusivity of CH_4 is more sensitive to changes in free volume, which is visible in the steeper decrease in CH_4 permeability with pressure at higher additive fractions. This in contrast to the results obtained for H_2, where a much smaller decrease in permeability with increasing feed pressure is observed. A similar trend for all three gases has as also been observed by Koros *et al.* in pure PDMS [49].

⌐ *Influence of feed pressure on pure CO_2/light gas selectivity*
The CO_2/H_2 and CO_2/CH_4 pure gas selectivity as a function of CO_2 fugacity for the PEBAX®1657/PDMS-PEG blend membranes is shown in Figure 7.10.

As a consequence of the above observations for the pure gas permeabilities, the CO_2/H_2 as well as the CO_2/CH_4 selectivity increase with increasing pressure. At any single CO_2 fugacity the CO_2/H_2 selectivity values are reasonable equal for all different PDMS-PEG additive concentrations. The CO_2/CH_4 selectivity values at equal CO_2 fugacity, however, drop with increasing PDMS-PEG concentration. This is due to the stronger effect of the higher free volume and as such lower diffusivity selectivity for CO_2/CH_4.

7.4.5   Mixed gas permeation characteristics

To study the effect of the presence of one component in the feed mixture on the permeation performance of the other component in the feed mixture, mixed gas separation measurements with the PEBAX®1657/PDMS-PEG blend membranes have been performed. Feed mixtures containing 70/30 vol.% CO_2/H_2 and feed mixtures containing 50/50 vol.% CO_2/CH_4 have been used. The temperature was kept constant at 35℃ and the CO_2 partial pressure was varied from 4 to 25 bar (CO_2/H_2 pressures up to 35 bar and CO_2/CH_4 pressures up to 50 bar). The mixed gas separation performance of these membranes is compared to the pure gas analog (which was discussed in the previous paragraph). Figure 7.11 presents the results.

Chapter 7
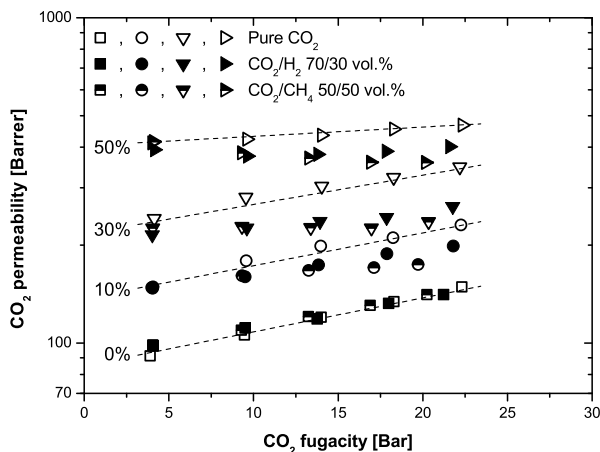
Figure 7.11: CO_2 permeability of (1) pure gas CO_2 (open symbols), (2) 70/30 vol.% CO_2/H_2 mixed gas (filled symbols) and (3) 50/50 vol.% CO_2/CH_4 mixed gas (partially filled symbols) at 35°C as a function of CO_2 fugacity for PEBAX®1657 (squares) and PEBAX®1657/PDMS-PEG blend membranes with 10 wt.% (circles), 30 wt.% (downward triangles) and 50 wt.% (right-sided triangles) PDMS-PEG additive. The dashed lines indicate the trend for the pure gas permeability and are drawn to guide the eye.

For the pristine PEBAX®1657 block copolymer (squares), the mixed gas CO_2 permeability equals the CO_2 permeability measured under pure gas conditions. This indicates that the presence of the second component does not influence the permeability of the plasticizing component. Similar results have been obtained by Freeman *et al.* for crosslinked PEO networks [50, 51]. The membranes with PDMS-PEG as additive show different behavior. At low CO_2 fugacity (∼4 bar) the CO_2 permeability in pure and mixed gas experiments almost coincides, while at higher CO_2 fugacity (> 4 bar) the CO_2 permeability in mixed gas experiments is lower than the pure gas values. A similar trend has been observed by Yeom *et al.* [52] and Ettouney *et al.* [53] who both studied pure and mixed CO_2/N_2 gas separation behavior in PDMS. In particular Yeom *et al.* [52] studied the coupling effect for diffusion as well as sorption. They observed that the decrease in permeability could be entirely attributed to negative sorption coupling effects. We hypothesize that similar negative sorption coupling effects may play a role in our work as well, resulting in a decrease in CO_2 permeability in our PEBAX®1657/PDMS-PEG blend membranes. In addition, the lower CO_2 permeability in CO_2/CH_4 mixed gas experiments compared to CO_2/H_2 mixed gas

experiments could also be (partially) caused by the higher feed pressures used for CO_2/CH_4 separation (maximum 50 bar instead of 35 bar) resulting in a slightly larger reduction in free volume due to compression, thus decreasing gas permeability. When the permeability of the light gases H_2 and CH_4 is considered (results not shown), a strong difference between pure and mixed feed gas conditions is observed in all cases. The plasticizing effect of CO_2 increases H_2 and CH_4 permeability in mixed gas experiments when compared to their pure gas values. This increase is stronger when the CO_2 fugacity and thus the anticipated plasticization effect increases.

Figure 7.12 shows the CO_2/H_2 and CO_2/CH_4 selectivity at 35℃ for the mixed gas experiments as well as the pure gas experiments as a function of the CO_2 fugacity for the PEBAX®1657/PDMS-PEG blend membranes.

As a consequence of the above observations, the CO_2/light gas separation performance under mixed gas conditions is lower than the ideal, pure gas selectivities for all PEBAX®1657/PDMS-PEG blend membranes. The CO_2/H_2 mixed gas selectivity seems to be independent of the CO_2 fugacity and the PDMS-PEG additive concentration at a value of approximately 9 to 10. The CO_2/CH_4 mixed gas selectivity decreases with PDMS-PEG concentration (from ~14 for pristine PEBAX®1657 to ~10 for PEBAX®1657/50PDMS-PEG) and slightly decreases with increasing CO_2 fugacity. Similar dependence of the CO_2/H_2 and CO_2/CH_4 selectivity as a function of feed pressure has been observed by Car *et al.* [23]. The difference between CO_2/H_2 and CO_2/CH_4 is anticipated as in general plasticization has a stronger effect on the CO_2/CH_4 selectivity compared to the CO_2/H_2 selectivity as CH_4 has a larger kinetic diameter than H_2 [50, 51]. Although CO_2/N_2 mixed gas experiments were not performed its behavior is expected to be similar to the behavior observed in CO_2/CH_4 mixed gas measurements and we expect a decrease in CO_2/N_2 mixed gas selectivity with an increase in additive content (analogous to the trend as observed in pure gas experiments). Furthermore, the selectivity will decrease with an increase in CO_2 fugacity. However, this decrease will probably be less significant compared to CO_2/CH_4 as the kinetic diameter of N_2 is smaller than that of CH_4.

In general, mixed gas experiments show that the membrane performance for CO_2/H_2 separation of PEBAX®1657 can be significantly enhanced by blending it with PDMS-PEG as additive. The CO_2 permeability can be increased up to a factor 4 (at 50 wt.% PDMS-PEG) with a constant selectivity over a wide pressure range. In addition, a similar increase in CO_2 permeability can be obtained in CO_2/CH_4 separation at only a modest decrease in selectivity.
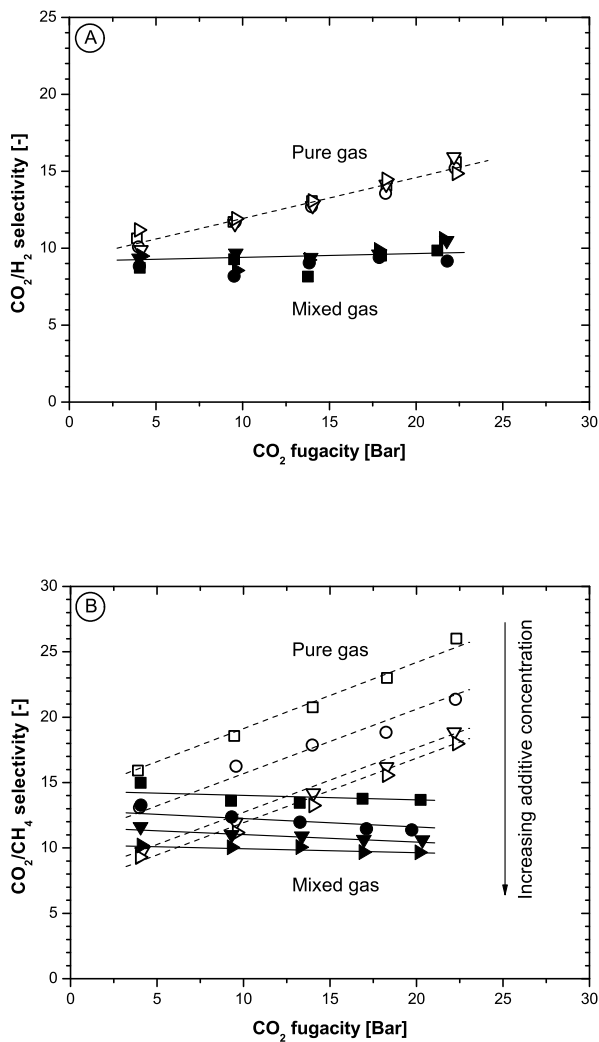
Figure 7.12: Pure gas (open symbols) and mixed gas (closed symbols) selectivity for (a) 70/30 (vol.%) CO_2/H_2 mixed gas and (b) 50/50 (vol.%) CO_2/CH_4 mixed gas at 35°C as a function of CO_2 fugacity for PEBAX$^{®}$1657 (squares) and PEBAX$^{®}$1657/PDMS-PEG blend membranes with 10 wt.% (circles), 30 wt.% (downward triangles) and 50 wt.% (right-sided triangles) PDMS-PEG additive. The lines are drawn to guide the eye.

7.4.6 CO_2/N_2 upper bound relationship

Figure 7.13 presents a CO_2/N_2 permeability/selectivity trade-off curve of the pure gas permeation data obtained in the current work and compares these data with relevant literature data [7, 10–12, 22, 54]. For comparison, the plot also contains the data obtained in our previous work on block copolymers containing PEO, PPO or a mixture of both (●, [13]) and on PEO-*ran*-PPO block copolymers (▲, [55]).

The new generation PEO based block copolymers all outperform the 1st generation of these polymers. Compared to the recent work of Car *et al.* (○), who prepared PEG blend membranes with PEBAX[®] [22] and Polyactive[®] [54], a significant improvement in CO_2 permeability is observed using the PDMS-PEG additive. The maximum CO_2 permeability obtained by blending a polymer with an additive as described in this work (■) is in the same order of magnitude as in our previous work on polyether based block copolymers using monodisperse hard segments (▲, PEO-*ran*-PPO [55]). Although CO_2/N_2 selectivity decreased somewhat upon the increase in CO_2 permeability (and thus additive content) its selectivity remained reasonably high. We expect that
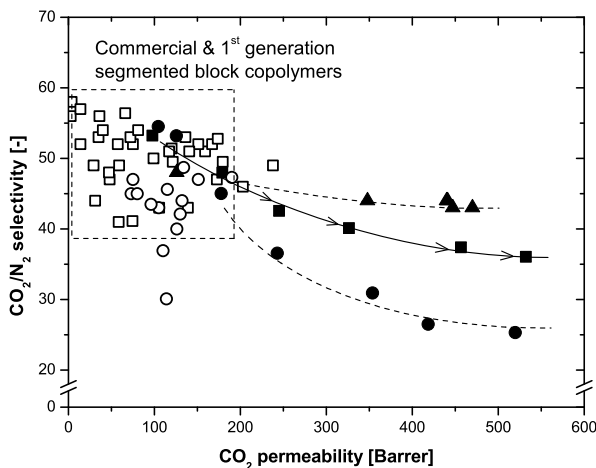
Figure 7.13: Robeson CO_2/N_2 upper bound relationship at 35℃. The data obtained in the current work for blends of PEBAX[®]1657 and PDMS-PEG (■) are compared to the data obtained by Car *et al.* (○) [22, 54]. Furthermore our recent work on polyether based block copolymers using monodisperse hard segments (●,▲) [13, 55] and data on 1st generation segmented block copolymers are incorporated (□) [7, 10–12].

even higher permeabilities combined with good selectivities can be obtained when the concept presented here is applied using even more permeable polymers. As such, blending of the PDMS-PEG additive with the PEO-*ran*-PPO-T6T6T block copolymers we reported recently [55], which have a much higher pristine CO_2 permeability than the modest 100 Barrer of PEBAX®1657, could possibly result in a membrane with a CO_2 permeability well above 500 Barrer while maintaining good CO_2/N_2 selectivity.

7.5 Conclusions

PEBAX®1657/PDMS-PEG blend membranes have been prepared and their pure and mixed gas separation performance have been studied extensively. The results show the strong potential of the concept as a way to significantly increase the gas permeability. The addition of PDMS-PEG as additive to PEBAX®1657 resulted in a factor 5 increase in CO_2 permeability from ∼100 to ∼530 Barrer for a PEBAX®1657 blend membrane containing 50 wt.% PDMS-PEG additive. The CO_2/N_2 and CO_2/CH_4 ideal gas selectivity slightly decreased with additive concentration, but interestingly, the CO_2/H_2 ideal selectivity increased from 9.5 for PEBAX®1657 to 10.6 for PEBAX®1657 with 50 wt.% PDMS-PEG additive (at 35℃ and 4 bar feed pressure). CO_2 sorption experiments revealed that the increase in permeability is dominated by an increase in gas diffusivity, while at the same time the increase in amorphous PEG content in the PEBAX®1657/PDMS-PEG blends leads to a modest increase in CO_2 solubility.

High pressure pure gas permeation experiments show a competition effect between the plasticization phenomena and hydrostatic pressure. In the case of the quadrupolar CO_2, plasticization effects dominate resulting in an overall increase in gas permeability. For the non-polar gases H_2 and CH_4, the hydrostatic pressure dominates the permeation behavior. As a result ideal CO_2/light gas selectivity increased significantly as a function of pressure in pure gas experiments. Similar experiments using gas mixtures as a feed show that the CO_2 permeability is only slightly reduced compared to pure gas conditions. Plasticization effects, due to strong CO_2 sorption, do influence the mixed gas selectivity when compared to pure gas selectivities. The CO_2/H_2 mixed gas selectivity was found to be independent of PDMS-PEG loading as well as pressure and had a high value around 10. CO_2/CH_4 mixed gas selectivity decreased slightly with PDMS-PEG loading and pressure, but always remained above 10.

We expect that even higher permeabilities combined with good selectivities can be obtained when the concept presented here is applied using even more permeable polymers, e.g. blending of the PDMS-PEG additive with the PEO-*ran*-PPO-T6T6T block copolymers we reported recently. These block copolymers have a much higher pristine CO_2 permeability and this could possibly result in a membrane with a CO_2 permeability much higher than 500 Barrer while maintaining good CO_2/N_2 selectivity.

7.6   Acknowledgements

Chapter 7

7.7   References

[1] IPCC; *Special Report on Carbon Dioxide Capture and Storage*; Technical report; Cambridge University Press; Cambridge (England) (2005)

[2] IPCC; *Third Assessment Report: Climate Change 2001*; Technical report; Cambridge University Press; Cambridge (England) (2001)

[3] R. W. BAKER; *Membrane Technology and Applications*; 2nd edition (2000); West Sussex (England): John Wiley & Sons Ltd.; ISBN 978-0470854457

[4] R. W. BAKER; *Future directions of membrane gas separation technology*; Industrial and Engineering Chemistry Research **41** (6) (2001) 1393–1411; DOI: 10.1021/ie0108088

[5] W. J. KOROS AND R. MAHAJAN; *Pushing the limits on possibilities for large scale gas separation: Which strategies?*; Journal of Membrane Science **175** (2) (2000) 181–196; DOI:10.1016/S0376-7388(00)00418-X

[6] V. I. BONDAR, B. D. FREEMAN AND I. PINNAU; *Gas sorption and characterization of poly(ether-b-amide) segmented block copolymers*; Journal of Polymer Science, Part B: Polymer Physics **37** (17) (1999) 2463–2475; DOI: 10.1002/(SICI)1099-0488(19990901)37:17⟨2463::AID-POLB18⟩3.0.CO;2-H

[7] V. I. BONDAR, B. D. FREEMAN AND I. PINNAU; *Gas transport properties of poly(ether-b-amide) segmented block copolymers*; Journal of Polymer Science, Part B: Polymer Physics **38** (15) (2000) 2051–2062; DOI:10.1002/1099-0488(20000801) 38:15⟨2051::AID-POLB100⟩3.0.CO;2-D

[8] H. LIN AND B. D. FREEMAN; *Materials selection guidelines for membranes that remove CO$_2$ from gas mixtures*; Journal of Molecular Structure **739** (1-3) (2005) 57–74; DOI:10.1016/j.molstruc.2004.07.045

[9] K.-I. OKAMOTO, M. FUJII, S. OKAMYO, H. SUZUKI, K. TANAKA AND H. KITA; *Gas permeation properties of poly(ether imide) segmented copolymers*; Macromolecules **28** (20) (1995) 6950–6956; DOI:10.1021/ma00124a035

[10] M. YOSHINO, K. ITO, H. KITA AND K.-I. OKAMOTO; *Effects of hard-segment polymers on CO$_2$/N$_2$ gas-separation properties of poly(ethylene oxide)-segmented copolymers*; Journal of Polymer Science, Part B: Polymer Physics **38** (13) (2000) 1707–1715; DOI:10.1002/1099-0488(20000701)38:13⟨1707::AID-POLB40⟩3.0.CO; 2-W

[11] S. J. METZ, M. H. V. MULDER AND M. WESSLING; *Gas-permeation properties of poly(ethylene oxide) poly(butylene terephthalate) block copolymers*; Macromolecules

Chapter 7

37 (12) (2004) 4590–4597; DOI:10.1021/ma049847w

[12] D. Husken, T. Visser, M. Wessling and R. J. Gaymans; *CO₂ permeation properties of poly(ethylene oxide)-based segmented block copolymers*; Journal of Membrane Science **346** (1) (2010) 194–201; DOI:10.1016/j.memsci.2009.09.034

[13] S. R. Reijerkerk, A. Arun, K. Nijmeijer, R. J. Gaymans and M. Wessling; *Tuning of mass transport in multi-block copolymers for CO₂ capture applications*; Journal of Membrane Science (2009); DOI:10.1016/j.memsci.2009.09.045

[14] G. Holden, H. R. Kricheldorf and R. P. Quirk; *Thermoplastic Elastomers*; 3ʳᵈ edition (2004); Munich (Germany): Hanser Gardner Publications; ISBN 978-1569903643

[15] P. Foy, C. Jungblut and G. E. Deleens; *Mouldable and extrudable polyether-ester-amide block copolymers*; US Patent 4230838 (1980)

[16] P. Foy, C. Jungblut and G. E. Deleens; *Moldable and/or extrudable polyether-ester-amide block copolymers*; US Patent 4331786 (1982)

[17] P. Foy, C. Jungblut and G. E. Deleens; *Mouldable and extrudable polyether-ester-amide block copolymers*; US Patent 4332920 (1982)

[18] I. Blume and I. Pinnau; *Composite membrane, method of preparation and use*; US Patent 4963165 (1982)

[19] J. H. Kim, S. Y. Ha and Y. M. Lee; *Gas permeation of poly(amide-6-b-ethylene oxide) copolymer*; Journal of Membrane Science **190** (2) (2001) 179–193; DOI:10.1016/S0376-7388(01)00444-6

[20] V. Barbi, S. S. Funari, R. Gehrke, N. Scharnagl and N. Stribeck; *SAXS and the gas transport in polyether-block-polyamide copolymer membranes*; Macromolecules **36** (3) (2003) 749–758; DOI:10.1021/ma0213403

[21] L. Liu, A. Chakma and X. Feng; *CO₂/N₂ separation by poly(ether block amide) thin film hollow fiber composite membranes*; Industrial and Engineering Chemistry Research **44** (17) (2005) 6874–6882; DOI:10.1021/ie050306k

[22] A. Car, C. Stropnik, W. Yave and K. V. Peinemann; *PEG modified poly(amide-b-ethylene oxide) membranes for CO₂ separation*; Journal of Membrane Science **307** (1) (2008) 88–95; DOI:10.1016/j.memsci.2007.09.023

[23] A. Car, C. Stropnik, W. Yave and K. V. Peinemann; *Pebax®/polyethylene glycol blend thin film composite membranes for CO₂ separation: Performance with mixed gases*; Separation and Purification Technology **62** (1) (2008) 110–117; DOI:10.1016/j.seppur.2008.01.001

[24] W. Yave, A. Car, K. V. Peinemann, M. Q. Shaikh, K. Rätzke and

Chapter 7

F. Faupel; *Gas permeability and free volume in poly(amide-b-ethylene oxide)/polyethylene glycol blend membranes*; Journal of Membrane Science **339** (1-2) (2009) 177–183; DOI:10.1016/j.memsci.2009.04.049

[25] K. M. Jaipurkar, S. R. Patwardhan and U. K. Kharul; *Gas permeation using poly (ether-b-amide) segmented block copolymer*; Chemical Engineering World **42** (10) (2007) 73–78

[26] J. Li, K. Nagai, T. Nakagawa and S. Wang; *Preparation of polyethyleneglycol (PEG) and cellulose acetate (CA) blend membranes and their gas permeabilities*; Journal of Applied Polymer Science **58** (9) (1995) 1455–1463; DOI:10.1002/app. 1995.070580906

[27] J. Li, S. Wang, K. Nagai, T. Nakagawa and A. W. H. Mau; *Effect of polyethyleneglycol (PEG) on gas permeabilities and permselectivities in its cellulose acetate (CA) blend membranes*; Journal of Membrane Science **138** (2) (1998) 143–152; DOI:10.1016/S0376-7388(97)00212-3

[28] N. P. Patel and R. J. Spontak; *Gas-Transport and Thermal Properties of a Microphase-Ordered Poly(styrene-b-ethylene oxide-b-styrene) Triblock Copolymer and Its Blends with Poly(ethylene glycol)*; Macromolecules **37** (8) (2004) 2829–2838; DOI:10.1021/ma049975k

[29] M. Sadeghi, M. P. Chenar, M. Rahimian, S. Moradi and A. H. S. Dehaghani; *Gas permeation properties of polyvinylchloride/ polyethyleneglycol blend membranes*; Journal of Applied Polymer Science **110** (2) (2008) 1093–1098; DOI:10.1002/app.28740

[30] S. Kulprathipanja; *Separation of polar gases from nonpolar gases*; US Patent 4606740 (1986)

[31] N. N. Li, E. W. Funk, Y. A. Chang, S. S. Kulkarn, A. X. Swamikannu and L. S. White; *Membrane Separation Processes in the Petrochemical Industry: Phase II, Final Report for US Department of Energy*; Technical report (1987)

[32] T. Nakagawa, T. Saito, S. Asakawa and Y. Saito; *Polyacetylene derivatives as membranes for gas separation*; Gas Separation and Purification **2** (1) (1988) 3–8; DOI:10.1016/0950-4214(88)80035-5

[33] T. C. Merkel, V. I. Bondar, K. Nagai, B. D. Freeman and I. Pinnau; *Gas sorption, diffusion, and permeation in poly(dimethylsiloxane)*; Journal of Polymer Science, Part B: Polymer Physics **38** (3) (2000) 415–434; DOI:10.1002/ (SICI)1099-0488(20000201)38:3⟨415::AID-POLB8⟩3.0.CO;2-Z

[34] H. Lin and B. D. Freeman; *Gas solubility, diffusivity and permeability in poly(ethylene oxide)*; Journal of Membrane Science **239** (1) (2004) 105–117;

DOI:10.1016/j.memsci.2003.08.031

[35] C. Yun and Y. Nagase; *Synthesis of PDMS/PEO-grafted aromatic polyamides and the property as the separation membrane*; Polymer Preprints, Japan **55** (1) (2006) 1583

[36] C. Yun, Y. Saito and Y. Nagase; *Synthesis and functionality of PDMS/PEO-grafted aromatic polyamides*; Polymer Preprints, Japan **55** (2) (2006) 2907

[37] H. B. Park, C. K. Kim and Y. M. Lee; *Gas separation properties of polysiloxane/polyether mixed soft segment urethane urea membranes*; Journal of Membrane Science **204** (1-2) (2002) 257–269; DOI:10.1016/S0376-7388(02)00048-0

[38] D. P. Queiroz and M. N. De Pinho; *Structural characteristics and gas permeation properties of polydimethylsiloxane/poly(propylene oxide) urethane/urea bi-soft segment membranes*; Polymer **46** (7) (2005) 2346–2353; DOI:10.1016/j.polymer.2004.12.056

[39] D. Gomes, K. V. Peinemann, S. P. Nunes, W. Kujawski and J. Kozakiewicz; *Gas transport properties of segmented poly(ether siloxane urethane urea) membranes*; Journal of Membrane Science **281** (1-2) (2006) 747–753; DOI:10.1016/j.memsci.2006.05.002

[40] J. G. Wijmans and R. W. Baker; *The solution-diffusion model: A review*; Journal of Membrane Science **107** (1-2) (1995) 1–21; DOI:10.1016/0376-7388(95)00102-I

[41] M. Mulder; *Basic Principles of Membrane Technology*; 2nd edition (1996); Dordrecht (The Netherlands): Kluwer Academic Publishers; ISBN 978-0792342488

[42] Y. Yampolskii, I. Pinnau and B. D. Freeman; *Materials Science of Membranes for Gas and Vapor Separation*; 1st edition (2006); West Sussex (England): John Wiley & Sons Ltd.; ISBN 978-0470853450

[43] A. Bos, I. G. M. Punt, M. Wessling and H. Strathmann; *Suppression of CO_2-plasticization by semiinterpenetrating polymer network formation*; Journal of Polymer Science, Part B: Polymer Physics **36** (9) (1998) 1547–1556; DOI:10.1002/(SICI)1099-0488(19980715)36:9⟨1547::AID-POLB12⟩3.0.CO;2-5

[44] A. Singh, B. D. Freeman and I. Pinnau; *Pure and mixed gas acetone/nitrogen permeation properties of polydimethylsiloxane [PDMS]*; Journal of Polymer Science, Part B: Polymer Physics **36** (2) (1998) 289–301; DOI:10.1002/(SICI)1099-0488(19980130)36:2⟨289::AID-POLB8⟩3.0.CO;2-M

[45] J. Kolařík, L. Fambri, A. Pegoretti and A. Penati; *Prediction of the gas permeability of heterogeneous polymer blends*; Polymer Engineering and Science **40** (1) (2000) 127–131; DOI:10.1002/pen.11145

Chapter 7

[46] D. R. PAUL; *Gas transport in homogeneous multicomponent polymers*; Journal of Membrane Science **18** (C) (1984) 75–86; DOI:10.1016/S0376-7388(00)85026-7

[47] J. H. PETROPOULOS; *Comparative study of approaches applied to the permeability of binary composite polymeric materials*; Journal of Polymer Science. Part A-2, Polymer physics **23** (7) (1985) 1309–1324; DOI:10.1002/pol.1985.180230703

[48] A. SENUMA; *Generalized equation for the permeability of heterogeneous polymer materials*; Macromolecular Chemistry and Physics **202** (9) (2001) 1737–1742; DOI:10.1002/1521-3935(20010601)202:9⟨1737::AID-MACP1737⟩3.0.CO;2-4

[49] S. M. JORDAN AND W. J. KOROS; *Permeability of pure and mixed gases in silicone rubber at elevated pressures*; Journal of Polymer Science, Part B: Polymer Physics **28** (6) (1990) 795–809; DOI:10.1002/polb.1990.090280602

[50] H. LIN, E. VAN WAGNER, B. D. FREEMAN, L. G. TOY AND R. P. GUPTA; *Plasticization-enhanced hydrogen purification using polymeric membranes*; Science **311** (5761) (2006) 639–642; DOI:10.1126/science.1118079

[51] H. LIN, E. VAN WAGNER, R. D. RAHARJO, B. D. FREEMAN AND I. ROMAN; *High-performance polymer membranes for natural-gas sweetening*; Advanced Materials **18** (1) (2006) 39–44; DOI:10.1002/adma.200501409

[52] C. YEOM, S. H. LEE AND J. M. LEE; *Study of transport of pure and mixed CO_2/N_2 gases through polymeric membranes*; Journal of Applied Polymer Science **78** (1) (2000) 179–189; DOI:10.1002/1097-4628(20001003)78:1⟨179::aid-app220⟩3.0.co;2-z

[53] H. M. ETTOUNEY, G. AL-ENEZI, S. E. M. HAMAM AND R. HUGHES; *Characterization of the permeation properties of CO_2-N_2 gas mixtures in silicone rubber membranes*; Gas Separation and Purification **8** (1) (1994) 31–36; DOI: 10.1016/0950-4214(94)85005-4

[54] A. CAR, C. STROPNIK, W. YAVE AND K. V. PEINEMANN; *Tailor-made polymeric membranes based on segmented block copolymers for CO_2 separation*; Advanced Functional Materials **18** (18) (2008) 2815–2823; DOI:10.1002/adfm.200800436

[55] S. R. REIJERKERK, A. C. IJZER, K. NIJMEIJER, A. ARUN, R. J. GAYMANS AND M. WESSLING; *Subambient temperature CO_2 and light gas permeation through segmented block copolymers with tailored soft phase*; ACS Applied Materials & Interfaces (2010); DOI:10.1021/am900754z

Chapter 7

7.8 Supporting Information

7.8.1 Introduction

This supplementary document describes the density and thermal properties of PEBAX®1657, the PDMS-PEG additive and their blends. In particular the thermal behavior of the soft PEG phase is studied as the mass transport properties of the PEBAX®/PDMS-PEG additive blends are only attractive at temperatures were crystallization of the soft PEG phase does not occur as the permeability of semi-crystalline PEG is very low [1].

7.8.2 Experimental

¬ DSC

The thermal properties of the PEBAX®1657/additive blends were characterized with DSC (Perkin Elmer DSC7). The samples were dried in a vacuum oven (30℃) before use. The samples were heated from −80 to 250℃ at a scan rate of 20℃/min. Subsequently, a cooling scan from 250 to −80℃ at a scan rate of 20℃/min followed by a second heating scan under the same conditions as the first heating scan were performed. All measurements were performed using a nitrogen purge gas stream. The thermal properties obtained include the glass transition temperature (T_g) of the polyether phase, and the melting temperature (T_m) and the melting enthalpy (ΔH_m) of the polyether and polyamide phases in the PEBAX®/additive blends. The glass transition temperature is defined as the midpoint of the heat capacity transition of the heating scan. The melting temperatures are defined as the onset of melting while the melting enthalpies are obtained from their respective endothermic peak areas.

¬ Density

The density of the PEBAX®1657/additive blends was determined at room temperature to obtain qualitative information about the polymer free volume. The samples were dried in a vacuum oven (30℃) before use. Density measurements were performed using an AccuPyc 1330 Pycnometer (Micromeritics). The AccuPyc 1330 is a pycnometer of the gas expansion type and measures the amount of displaced gas (helium) at room temperature. Upon filling of the sample chamber and subsequent discharge into a second empty chamber with known volume the pressure is monitored. This allows

Chapter 7

calculation of the sample solid phase volume. The density is subsequently derived using the measured sample weight.

7.8.3 Results & discussion

⌐ **Thermal properties**

The thermal properties of PEBAX®1657, its blend with 10–50 wt.% PDMS-PEG and pure PDMS-PEG were studied by DSC at a temperature range from −80 to 250℃. The thermal properties derived are summarized in Table S7.1 and the corresponding DSC curves are given in Figure S7.1. The DSC curves are limited to a temperature range of −50 to 50℃ (for clarity) as the melting transition of the semi-crystalline PEG soft phase, which is important for the mass transport properties, is located in this region.

Table S7.1: Density and thermal properties as determined by DSC of PEBAX®1657, PEBAX®1657/PDMS-PEG blend membranes and PDMS-PEG.

Sample	PDMS-PEG	Density	PEG			PA	
			T_g	T_m	ΔH_m	T_m	ΔH_m
	[wt.%]	[g/cm³]	[℃]	[℃]	[J/g PEG]	[℃]	[J/g PA]
PEBAX®	0	1.1601	−51.0	15.3	41	205	73
PEBAX®/10PDMS-PEG	11	1.1495	−50.9	18.3	45	204	75
PEBAX®/20PDMS-PEG	21	1.1368	−52.0	17.3	50	206	71
PEBAX®/30PDMS-PEG	30	1.1281	−51.4	17.6	59	203	74
PEBAX®/40PDMS-PEG	40	1.1175	−52.4	15.9	67	203	74
PEBAX®/50PDMS-PEG	50	1.1065	−51.1	15.8	78	203	68
PDMS-PEG	100	1.0396	n.m.	−0.1	88	-	-

On heating from −80 to 250℃ the PEBAX®1657/PDMS-PEG blend membranes pass through an endothermic second order transition (the glass transition temperature, T_g). This transition is followed by an endothermic melting peak of PEG ($T_{m,PEG}$). A second endothermic peak around 200℃ is attributed to the melting transition of the hard segment nylon-6 ($T_{m,PA}$). The melting enthalpies of PEG and PA are determined from the corresponding peak areas.

The glass transition temperature is reasonably constant (around −51℃) with PDMS-PEG additive mass fraction. This indicates that the addition of PDMS-PEG to the PEBAX®1657 matrix has hardly any influence on the chain flexibility of the amorphous PEG soft phase. A glass transition temperature of the PDMS could not be measured (the reported glass transition temperature of pure PDMS is around −123℃
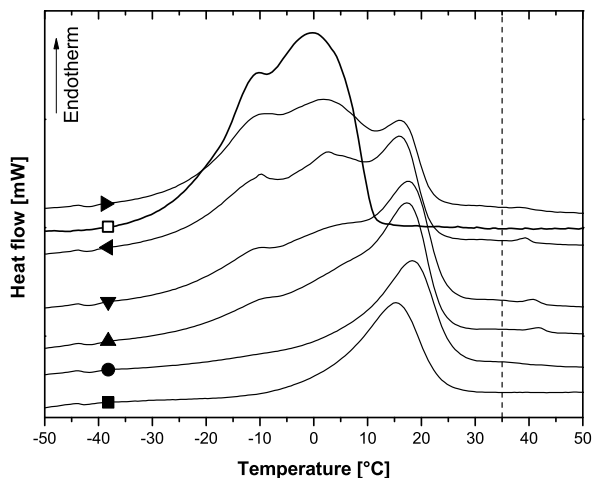
Figure S7.1: Heating scan at a scan rate of 20℃/min (shown only from −50 to 50℃) for (■) PEBAX®1657, PEBAX®1657/PDMS-PEG blends with (●) 10 wt.%, (▲) 20 wt.%, (▼) 30 wt.%, (◄) 40 wt.% and (►) 50 wt.% PDMS-PEG and (□) pure PDMS-PEG. The dashed line indicates the temperature used in the gas permeation experiments as described in the accompanying article.

[2]) as reliable data could not be obtained with the available DSC system at these low temperatures.

The PEBAX®1657 block copolymer has a single melting peak for the PEG segment (around 15℃), while the PEG melting transition of pure PDMS-PEG shows a contribution of two overlapping peaks (around −10℃ and 0℃). Subsequently, the PEBAX®1657/PDMS-PEG blends have different contributions of PEG in their PEG melting peak. For PEBAX®1657 with 10 wt.% PDMS-PEG additive this leads to a broader peak without visible individual contributions, but for higher PDMS-PEG additive fractions two (20 and 30 wt.% additive) and three (40 and 50 wt.% additive) separate contributions are observed (Figure S7.1). The $T_{m,PEG}$ listed in Table S7.1 represents the highest melting transition observed. The soft PEG phase is completely amorphous above room temperature. Therefore, an operating temperature above this temperature is most suitable for gas permeation and a temperature of 35℃ has been used in the accompanying article (indicated by the dashed line in Figure S7.1).

The two overlapping PEG melting peaks of pure PDMS-PEG indicate that PEG crystalline lamellae of different size are formed [3]. Furthermore, these lamellae are

smaller than the PEG lamellae of PEBAX®1657 as the PEG melting temperatures observed for the PDMS-PEG additive are lower than the one observed in PEBAX®1657. This is in accordance with the Gibbs-Thomson relation, which states that thicker lamellae in a crystalline phase show a higher melting temperature than thinner lamellae [3]. This furthermore indicates that the PEG lengths of PDMS-PEG are shorter than the PEG segment length in PEBAX®1657 (1500 g/mol) as the size of PEG crystalline lamellae that can be formed increases with increasing PEG molecular weight [4].

The total mass fraction corrected melting enthalpy of PEG (J/g PEG) increases with increasing PDMS-PEG content in the PEBAX®1657 matrix (Figure S7.2).

At 30, 40 and 50 wt.% PDMS-PEG, this enthalpy is higher than what would have been expected from the proportional addition (additive model) of the enthalpies of both individual components (pure PEBAX®1657 and pure PDMS-PEG). This indicates that the incorporation of high PDMS-PEG concentrations (> 20 wt.%) leads to a higher total crystallization degree of PEG. The absolute contribution of the PEG originating from either the PEBAX®1657 or the PDMS-PEG additive could not been determined, because of the strong overlap of the different peaks.
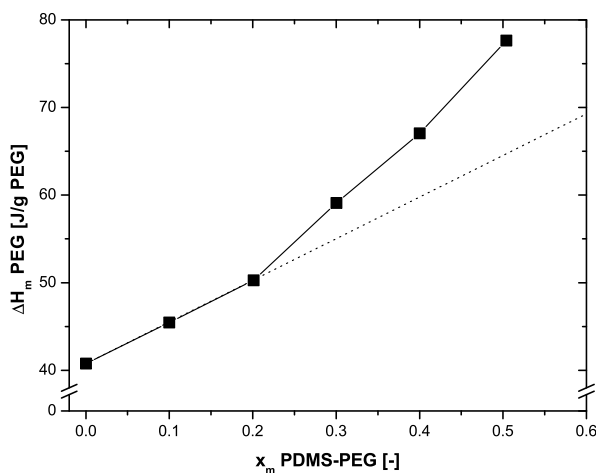
Figure S7.2: Mass fraction corrected melting enthalpy of PEG [J/g] as a function of the PDMS-PEG mass fraction in PEBAX®1657 matrix. The dotted line represents the melting enthalpy that is expected based on the proportional contribution (additive model) of both individual components.

Chapter 7

The melting temperature and mass fraction corrected melting enthalpy (J/g PA) of the hard segment nylon-6 (PA) are reasonably constant with increasing PDMS-PEG mass fraction. This indicates that the PDMS-PEG additive has hardly any influence on the melting and crystallization behavior of the PEBAX®1657 crystalline PA hard segments.

⌐ *Density*

The density of pure PEBAX®1657, its blends with 10–50 wt.% PDMS-PEG and pure PDMS-PEG has been measured and the results are shown in Table S7.1 and Figure S7.3.

The density of PEBAX®1657/PDMS-PEG blend membranes decreases with an increase in the PDMS-PEG additive content due to the addition of the 'low' density PDMS-PEG additive. The measured density of a pristine PEBAX®1657 membrane (1.1601 g/cm^3) and that of pure PDMS-PEG (1.0396 g/cm^3) are used to calculate the density of the PEBAX®1657/PDMS-PEG blend membranes according to the additive model using Equation (S7.1)

$$\rho = \phi_1 \rho_1 + (1 - \phi_1)\rho_2 \tag{S7.1}$$
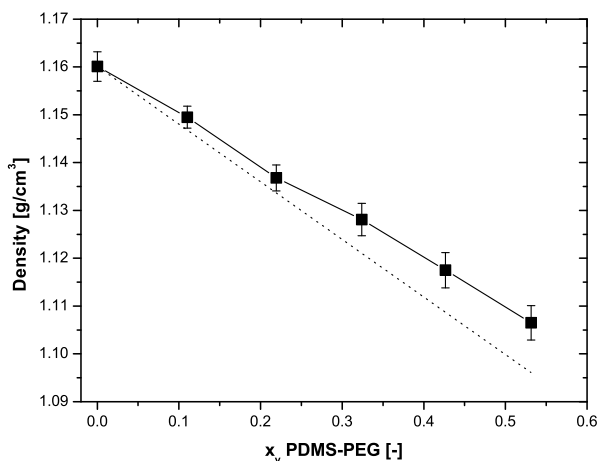
Figure S7.3: Density of PEBAX®1657/PDMS-PEG blend membranes as a function of the volume fraction PDMS-PEG at room temperature. The dotted line represents the densities calculated by the additive model (Equation (S7.1)).

where ϕ_1 [–] and ρ_1 [g/cm^3] represent the volume fraction and density of PDMS-PEG and ρ_2 [g/cm^3] the density of the PEBAX®1657 membrane. The dotted line in Figure S7.3 represents the densities calculated using this additive model. The measured average densities of the blend membranes are slightly higher than the densities calculated by the additive model and this deviation becomes especially visible at PDMS-PEG additive mass fractions higher than 0.2. This indicates that the density of the blend membrane is not a linear function of the composition of the blend and that structural changes (which cannot be predicted by the additive model) most likely occur. It could be envisaged that the addition of the PDMS-PEG to the PEBAX®1657 matrix limits the rotational freedom of the PDMS chain. Furthermore, the higher than expected crystallization degree observed above 20 wt.% additive could also be a factor as the density of crystalline PEO is higher than the density of amorphous PEO [5]. Both effects result in a more densely packed structure (increasing density) explaining the deviation from the additive model.

The density is often used to determine the polymer fractional free volume (FFV), which is related to the gas permeability [6]. However, as the exact elemental composition of the PDMS-PEG additive is unknown, its Van der Waals volume that is necessary to determine the FFV, cannot be calculated. Nevertheless, the specific volume (ν), obtained from density measurements alone, could serve as an indicator for the openness of a polymer [7]. The fractional free volume (or in this case specific volume) is often correlated to the gas diffusivity in the polymer as discussed in the accompanying article.

7.8.4 References

[1] H. LIN AND B. D. FREEMAN; *Gas solubility, diffusivity and permeability in poly(ethylene oxide)*; Journal of Membrane Science **239** (1) (2004) 105–117; DOI: 10.1016/j.memsci.2003.08.031

[2] M. MULDER; *Basic Principles of Membrane Technology*; 2nd edition (1996); Dordrecht (The Netherlands): Kluwer Academic Publishers; ISBN 978-0792342488

[3] L. MANDELKERN; *Crystallization of Polymers: Kinetics and Mechanisms*; 2nd edition (2002); Cambridge (England): Cambridge University Press; ISBN 978-0521816823

[4] D. HUSKEN, J. FEIJEN AND R. J. GAYMANS; *Hydrophilic segmented block copolymers based on poly(ethylene oxide) and monodisperse amide segments*; Journal of Polymer Science, Part A: Polymer Chemistry **45** (19) (2007) 4522–4535; DOI: 10.1002/pola.22186

[5] F. T. SIMON AND J. M. RUTHERFORD JR; *Crystallization and melting behavior of polyethylene oxide copolymers*; Journal of Applied Physics **35** (1) (1964) 82–86; DOI:10.1063/1.1713103

[6] W. M. LEE; *Selection of barrier materials from molecular structure*; Polymer Engineering and Science **20** (1) (1980) 65–69; DOI:10.1002/pen.760200111

[7] Y. YAMPOLSKII, I. PINNAU AND B. D. FREEMAN; *Materials Science of Membranes for Gas and Vapor Separation*; 1st edition (2006); West Sussex (England): John Wiley & Sons Ltd.; ISBN 978-0470853450

Chapter 7

CHAPTER 8

Reflections & outlook

8.1 Introduction

In this last chapter a short reflection on the results obtained in this thesis will be given followed by an outlook. This outlook also describes the current status of membrane technology for post-combustion capture and illustrates how a future, large scale, process could be designed.

8.2 Membrane development for CO_2 capture

The work described in this thesis aimed at the development of polymeric membrane materials for the separation of CO_2 from light gases. In particular, the separation of CO_2 from nitrogen in a post-combustion capture system has been subject of investigation. In general, membranes for post-combustion capture require a high intrinsic permeability due to the low driving force available and the large volume of the flue gas stream [1]. As a consequence, research primarily focused on the development of membrane materials with a high CO_2 permeability rather than a high CO_2/N_2 selectivity.

An interesting class of material for this application are polyether based block copolymers, as they combine a reasonably high CO_2 permeability with a sufficiently high CO_2/N_2 selectivity [2]. Examples of such polymeric membrane materials are the well-known, commercially available, block copolymer families PEBAX® [3, 4] and Polyactive® [5]. These block copolymers served as a starting point for the development of new membrane materials with significantly higher permeabilities. Based on these block copolymer systems, two different strategies have been developed to prepare membranes with improved CO_2 permeability characteristics.

1. The first strategy (polymer design) concerned the synthesis of novel poly(ethylene oxide) based block copolymers analogous to the PEBAX® and Polyactive® families and addressed the poor microdomain morphology found in the commercially available block copolymer systems.

2. The second strategy (polymer blending) focused on the improvement of polyether based block copolymers (like PEBAX®) by the addition of smart polymeric additives.

8.2.1 Strategy 1: Polymer design

The research on polymer design (mainly discussed in **Chapter 2** and **Chapter 3**) focused on the improvement (simplification) of the microdomain morphology of block copolymer systems by tailoring its specific design. This is essential as the microdomain morphology of commercially available block copolymer systems (such as the PEBAX® family) is very complex (Figure 8.1a). The phase separation between the hard and soft segments is poor and the resulting complexity negatively influences the mass transport properties, as mass transport only takes place through the amorphous soft domains of the block copolymer (indicated by the area in the red circle with the letter C). The work described in this thesis showed that the microdomain morphology can to a very large extent be simplified by smart design of the block copolymer system. This simplified morphology resulted in a very pure amorphous soft domain available for gas transport and as a consequence significantly enhanced overall mass transport characteristics (Figure 8.1b).

(a)   (b)
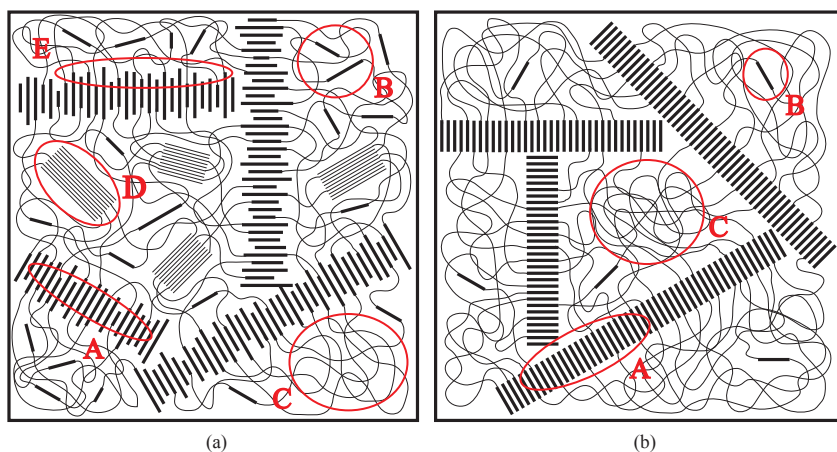
Figure 8.1: Schematic representation of the morphology of (a) commercially available block copolymers (e.g. the PEBAX® family) and (b) block copolymers as developed in this thesis. The indicated areas are representative for (A) crystalline hard segments, (B) non-crystallized rigid hard segments, (C) continuous amorphous soft phase, (D) crystalline soft phase and (E) intermediate region with mixed crystalline hard segments and non-crystalline soft segments.

In general, to have improved mass transport properties, the resulting block copolymer should fulfill the following five criteria: (1) Good phase separation of the hard and soft segments; (2) Complete crystallization of the hard segment; (3) High PEO content; (4) Low glass transition temperature of the soft segment (high chain flexibility); and (5) No soft phase crystallinity or low soft segment melting temperature. Especially the block copolymer system described in **Chapter 3** fulfills all these five criteria to a large extent and shows excellent mass transport characteristics as presented in **Chapter 4**, **Chapter 5** and **Chapter 6**. The pure gas CO_2 permeability of this block copolymer system reached a value up to four times the value of PEBAX®1074, while maintaining a high CO_2/N_2 selectivity (Figure 8.2 later in this chapter, ■). As such, it significantly outperformed the PEBAX®1074 and other 1st generation segmented block copolymers.

8.2.2 Strategy 2: Polymer blending

A second strategy that proved to be successful as a way to improve the CO_2 permeability of commercially available block copolymers, in particular the block copolymer PEBAX®1657, is the addition of smart polymeric additives (**Chapter 7**) to this matrix polymer and obtain so-called 'blend membranes'. Although in this thesis only one specific additive has been tested, the range of potentially interesting additives is much larger. For instance, Car *et al.* [6] and Yave *et al.* [7] have used several other potentially interesting additives and they have been able to improve the CO_2 permeability of PEBAX®1657 multiple-fold compared to its pristine value. Furthermore, they have shown that this concept also works for the Polyactive® block copolymer family [8]. In our case, we used an additive based on poly(dimethyl siloxane) (for high permeability) and poly(ethylene oxide) (for high selectivity). The CO_2 permeability could be increased up to 5 times its original value, while CO_2/N_2 selectivity only slightly decreased (Figure 8.2 later in this chapter, ●). Summarizing, these blend membranes show great promise due to their easy preparation technique.

8.3 Future directions

8.3.1 Polymer design and blending (combination of strategy 1 and 2)

The membrane performance obtained by both strategies is summarized in Figure 8.2. This Robeson plot presents the CO_2/N_2 separation performance of the block copolymers made by polymer design (**Chapter 3** and **Chapter 4**, ■) and polymer blending (**Chapter 7**, ●). In addition it shows data available on commercially available and 1st generation segmented block copolymers.

Although the commercially available PEBAX® and Polyactive® block copolymer families have reasonable CO_2 permeabilities, their permeability characteristics can be significantly improved by smart design of the microdomain morphology (■). Similar high values for the CO_2 permeability can be obtained by polymer blending using a suitable additive (●). Further improvement of the CO_2 permeability of polyether based block copolymer systems could likely be achieved by the combination of both strategies. To illustrate this, the addition of the PDMS-PEG additive (**Chapter 7**, ●)
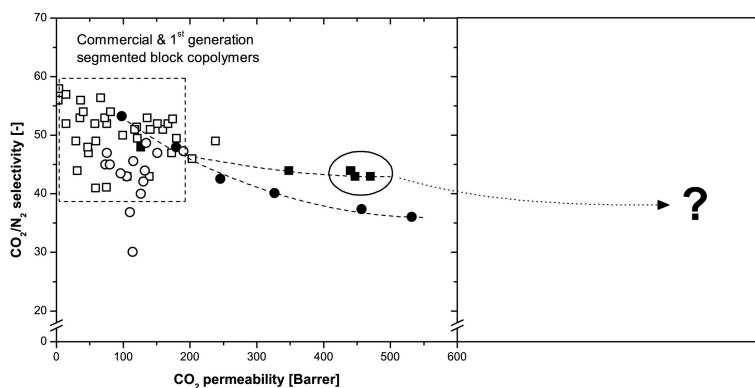
Figure 8.2: Robeson CO_2/N_2 upper bound relationship at 35℃. The data obtained in the thesis using either the polymer design (■) or the polymer blending (●) strategy are compared to the data obtained by Car *et al.* (○) [6, 8]. Furthermore data on 1st generation segmented block copolymers are incorporated (□) [4, 5, 9, 10]. The dotted arrow indicates the expected improvement in membrane separation performance when polymer design and blending (strategy 1 and 2) can be successfully combined.

223

improved a block copolymer with an initial CO_2 separation performance located in the region of the commercial and 1st generation segmented block copolymers (indicated by the boxed area) significantly and it emerged out of this region to permeabilities as high as 570 Barrer (strategy 2). In case a block copolymer with a much higher intrinsic permeability would be chosen as a membrane matrix material instead (for instance the novel PEO based block copolymers developed in **Chapter 3** and indicated by the circled area in Figure 8.2 with initial permeability values of 400 to 500 Barrer), this could result in even higher permeability values. If the additive has a similar effect on the block copolymer with a high intrinsic permeability (which is likely due to their similar nature), its permeability will be enhanced as well and block copolymer membranes with exceptionally high permeabilities might be obtained (as indicated by the arrow in the Robesonplot, Figure 8.2).

8.3.2   Membrane scale-up and the effect of minor components

Although the CO_2 permeability of potentially interesting membrane materials has been significantly improved (and a reasonable CO_2/N_2 selectivity has been maintained) the developed membrane materials are not directly available as a 'drag-and-drop' solution for post-combustion capture, because some remaining challenges still require improvement. Two important membrane aspects that remain a challenge and that need to be addressed before large scale implementation of membrane technology for pre- or post-combustion capture is possible, are (1) membrane scale-up and (2) the effect of minor components present in flue gas on the membrane performance.

⌐ *Membrane scale-up*

All permeation measurements performed in this thesis are done on flat sheet membranes with a thickness of 50–100 μm. This is typical for gas separation research as it allows the rapid screening of the intrinsic permeability characteristics of a membrane material. However, for large scale industrial applications one would require an active separation layer which is as thin as possible to be able to have high fluxes and low membrane areas. Such a thin layer (typically thicknesses of less than 1 μm) has insufficient mechanical stability and needs to be supported. This is done in practice by the preparation of composite membranes, which involves the application of a thin separating layer of the active material on a porous support. This porous support can either be a flat film (to produce spiral wound modules) or a hollow fiber (to produce composite hollow fiber modules) [11].
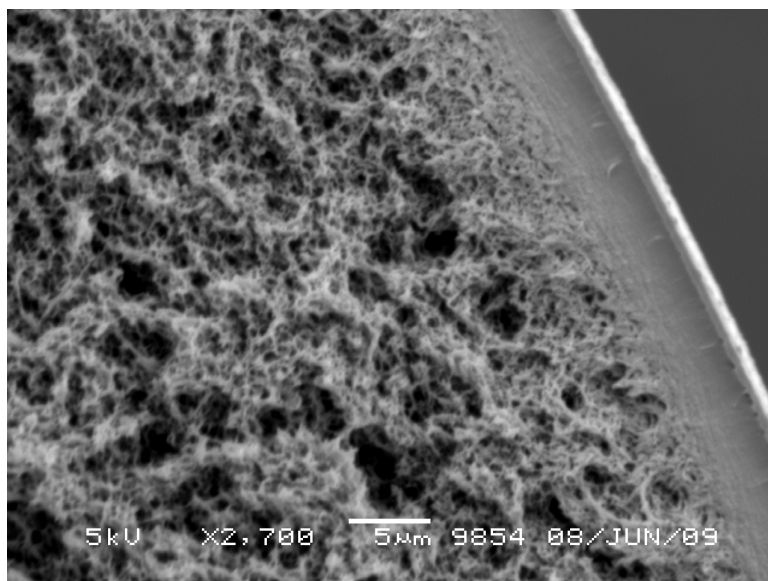
Figure 8.3: SEM image of a poly(phenylene oxide) (PPO) fiber coated with a thin active separation layer of PEBAX$^{\circledR}$ (magnification x2700).

Currently, such composite membranes are prepared within the NanoGLOWA project to be able to bridge the gap to a small pilot scale module to be able to test the membrane performance under realistic conditions. In this case polymeric hollow fibers are used as a support material and the active layer is applied on the hollow fibers by a procedure called 'dip coating'. The application of a thin, defect-free active separation layer is influenced by numerous variables, such as the concentration of the coating solution, its temperature, viscosity, the speed of coating and the number of coating layers. An example of such a composite hollow fiber membrane is shown in Figure 8.3.

It can be envisioned that the development of an optimum composite hollow fiber membrane is not a straightforward task and needs careful examination of the (main) parameters that are of influence to come to a recipe for the large scale production of such hollow fibers.

Chapter 8

225

⌐ *Effect of minor components*

A second and very important challenge is the ability to be able to assess the impact of minor components on the membrane performance. Although the major components of a post-combustion flue gas stream are CO_2, N_2 and water, there are also many other minor components present in flue gas, such as H_2S, SO_2, HCl, HF and fly ash, which can have a significant effect on the final membrane performance [12]. However, unfortunately most researchers only determine the membrane performance using dry, pure gas measurements [13]. Although in this thesis we have been able to assess the influence of water vapor on the membrane performance (**Chapter 6**), the influence of other minor components remains unknown but is assumed to be considerable. It is therefore of vital importance to study the influence of the minor components on the membrane performance [14]. This is however generally not easy to do in a lab environment and can only be assessed in a field test.

8.3.3   Membrane integration into a viable process

The successful development of a suitable membrane (and module) for the separation of CO_2 from flue gas is only one vital step in the road to an overall post-combustion capture system. Besides the membrane and module design, also the process design and economics play an essential role. In particular the energy required for the actual separation of CO_2 is of major importance as this directly reduces the power production in the plant. It is clear that the energy required for the separation and subsequent compression (to prepare the CO_2 for transport and storage) has to be minimized to reduce the impact of CO_2 capture on the power output and thus the price of electricity. A possible process design that takes these factors into consideration will be discussed in the next paragraph.

## 8.4 How could a membrane process for CO_2 capture look like?

Prominent in the field of post-combustion capture is the California (USA) based company Membrane Technology and Research, Inc. (MTR). This company has developed a highly permeable and CO_2-selective membrane, the MTR Polaris™ membrane (which is polar and hydrophilic like the ones described in this thesis), for the separation of CO_2 from post-combustion flue gas streams. Moreover, they performed basic design and economic analysis using their membrane for a post-combustion capture membrane installation in a 600 MW power plant. Due to the similarity between the membrane materials discussed in this thesis and the expected nature of the membrane material developed by MTR, their view on the process is also likely to be applicable to the membrane materials described in this thesis.

The boundary conditions as set by the US Department of Energy (DOE) are as follows [15]:

Capture performance:	$\geq 90\%$ CO_2
Capture costs:	$< \$30$/ton CO_2
Power plant energy losses:	$< 20\%$

In the design of the MTR process, several key issues were addressed, such as compression vs. vacuum operation, single-stage vs. multi-stage and sweep vs. no sweep, finally leading to the process design presented in Figure 8.4 [1].

The driving force in the proposed process is achieved by the application of a vacuum at the permeate side of the first membrane stage, resulting in a permeate pressure of 0.11 bar which is the minimum practical pressure. The feed is slightly compressed with a blower to 1.1 bar. This results in a pressure ratio of 10. Higher feed compression (to generate additional driving force) is economically unfavorable as it consumes significantly more energy primarily due to the large volume of the flue gas stream. Next, the retentate of the first stage (depleted in CO_2) is used as feed for the second stage. To generate additional driving force for the permeation of CO_2, an air sweep is used at the permeate side. Besides the creation of a driving force inside the module, this air sweep further increases the driving force of the whole process as after exiting the counter current module it contains several vol.% of CO_2 and is used to fire the boiler. In this way the flue gas that exits the boiler contains a higher concentration of
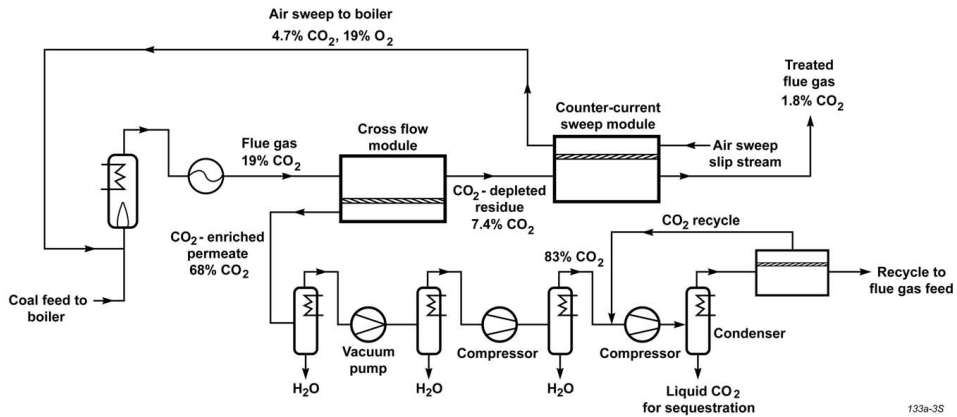
Figure 8.4: MTR's process design to effectively capture 90% of the CO_2 using 12% of the power plant output. The process simultaneously captures > 99% of SO_2 and water [1].

CO_2 (19 vol.% CO_2) as opposed to the combustion in normal air (10–15 vol.% CO_2) facilitating its removal. The flue gas that exits the second module as the retentate now only contains 1.8 vol.% CO_2 and is released to the atmosphere. The permeate of the first module is enriched in CO_2 and in addition contains large quantities of water. After removal of the water and subsequent compression and condensation of the captured CO_2 it is ready for sequestration. Overall this process captures 90% of the CO_2 and uses only 12% of the power plant output, which is well within the requirements set by the US Department of Energy.

8.5   References

[1] T. C. Merkel, H. Lin, Z. He, R. Daniels, S. Thompson, A. Serbanescu and R. W. Baker; *A membrane process to capture CO_2 from power plant flue gas*; in *International Congress on Membranes and Membrane Processes (ICOM)*; Honolulu (HI), United States of America (2008)

[2] H. Lin and B. D. Freeman; *Materials selection guidelines for membranes that remove CO_2 from gas mixtures*; Journal of Molecular Structure **739** (1-3) (2005) 57–74; DOI:10.1016/j.molstruc.2004.07.045

[3] V. I. Bondar, B. D. Freeman and I. Pinnau; *Gas sorption and characterization of poly(ether-b-amide) segmented block copolymers*; Journal of Polymer Science, Part B: Polymer Physics **37** (17) (1999) 2463–2475; DOI: 10.1002/(SICI)1099-0488(19990901)37:17⟨2463::AID-POLB18⟩3.0.CO;2-H

[4] V. I. Bondar, B. D. Freeman and I. Pinnau; *Gas transport properties of poly(ether-b-amide) segmented block copolymers*; Journal of Polymer Science, Part B: Polymer Physics **38** (15) (2000) 2051–2062; DOI:10.1002/1099-0488(20000801) 38:15⟨2051::AID-POLB100⟩3.0.CO;2-D

[5] S. J. Metz, M. H. V. Mulder and M. Wessling; *Gas-permeation properties of poly(ethylene oxide) poly(butylene terephthalate) block copolymers*; Macromolecules **37** (12) (2004) 4590–4597; DOI:10.1021/ma049847w

[6] A. Car, C. Stropnik, W. Yave and K. V. Peinemann; *PEG modified poly(amide-b-ethylene oxide) membranes for CO_2 separation*; Journal of Membrane Science **307** (1) (2008) 88–95; DOI:10.1016/j.memsci.2007.09.023

[7] W. Yave; *Nanostructured membranes for CO_2 capture: "Small concepts for Big challenges"*; in *XXVI EMS Summer School – Membrane Technlogy for CO_2 Separation*; Ratzeburg, Germany (2009)

[8] A. Car, C. Stropnik, W. Yave and K. V. Peinemann; *Tailor-made polymeric membranes based on segmented block copolymers for CO_2 separation*; Advanced Functional Materials **18** (18) (2008) 2815–2823; DOI:10.1002/adfm.200800436

[9] M. Yoshino, K. Ito, H. Kita and K.-I. Okamoto; *Effects of hard-segment polymers on CO_2/N_2 gas-separation properties of poly(ethylene oxide)-segmented copolymers*; Journal of Polymer Science, Part B: Polymer Physics **38** (13) (2000) 1707–1715; DOI:10.1002/1099-0488(20000701)38:13⟨1707::AID-POLB40⟩3.0.CO; 2-W

[10] D. Husken, T. Visser, M. Wessling and R. J. Gaymans; *CO_2 permeation*

Chapter 8

properties of poly(ethylene oxide)-based segmented block copolymers; Journal of Membrane Science **346** (1) (2010) 194–201; DOI:10.1016/j.memsci.2009.09.034

[11] R. W. BAKER; *Membrane Technology and Applications*; 2$^{\text{nd}}$ edition (2000); West Sussex (England): John Wiley & Sons Ltd.; ISBN 978-0470854457

[12] H. SIJBESMA, K. NYMEIJER, R. VAN MARWIJK, R. HEIJBOER, J. POTRECK AND M. WESSLING; *Flue gas dehydration using polymer membranes*; Journal of Membrane Science **313** (1-2) (2008) 263–276; DOI:10.1016/j.memsci.2008.01.024

[13] C. E. POWELL AND G. G. QIAO; *Polymeric CO_2/N_2 gas separation membranes for the capture of carbon dioxide from power plant flue gases*; Journal of Membrane Science **279** (1-2) (2006) 1–49; DOI:10.1016/j.memsci.2005.12.062

[14] C. A. SCHOLES, S. E. KENTISH AND G. W. STEVENS; *Effects of minor components in carbon dioxide capture using polymeric gas separation membranes*; Separation and Purification Reviews **38** (1) (2009) 1–44; DOI:10.1080/15422110802411442

[15] US DEPARTMENT OF ENERGY; *Carbon Sequestration Technology Roadmap and Program Plan 2007* (2007)

Summary

The work described in this thesis is dedicated to the development of polymeric membrane materials for the separation of CO_2 from light gases, and in particular to the separation of CO_2 from nitrogen as required in a post-combustion capture configuration for the separation of CO_2 from flue gases. An attractive group of materials for this separation are multi-block copolymers containing polyether based soft segments, as they combine a reasonably high CO_2 permeability with a sufficiently high CO_2/N_2 selectivity. Examples of such polymeric membrane materials are the well-known, commercially available, block copolymer families PEBAX® and PolyActive®. Their practical use is nonetheless limited as obtained gas permeabilities are too low for an economically viable process. In this thesis two different design strategies to tune and significantly increase the performance of polyether based multi-block copolymer membranes are investigated.

The first strategy (polymer design, **Chapter 2–6**) explores the synthesis of novel poly(ethylene oxide) based block copolymers analogous to the PEBAX® and Poly-Active® families and addresses the poor microdomain morphology found in these commercially available block copolymer systems, which is to a significant extent responsible for their 'low' CO_2 permeability. The second strategy (polymer blending, **Chapter 7**) focuses on the improvement of polyether based block copolymers (like PEBAX®) by the addition of smart polymeric additives.

In **Chapter 2, "Tuning of mass transport properties in multi-block copolymers for CO_2 capture applications"**, the CO_2 gas separation properties of three series of polyether based block copolymers are discussed. The block copolymers consist of either poly(ethylene oxide) (PEO), poly(propylene oxide) (PPO) or a mixture of both as a soft segment. The hard segment is constant throughout the three series and is a monodisperse di-amide (denoted TΦT). The influence of the soft segment properties (type and length) and the operating temperature on the pure gas CO_2 permeability and pure CO_2/light gas selectivity is studied in detail. The prepared block copolymers have an improved microdomain morphology and show improved CO_2 separation behavior compared to similar commercially available materials and this highlights the advantage of the well-defined block copolymer morphology of the newly developed materials. These multi-block copolymers offer a versatile tool to tailor the mass transfer and separation properties of membranes for gas and vapor separation.

In **Chapter 3, "Poly(ethylene oxide) based block copolymers with exceptionally low soft phase melting temperature and crystallinity"**, the synthesis and thermo-mechanical properties of a series of segmented block copolymers based on a novel type of PEO based soft segment are described. The PEO melting temperature and crystallinity, which are important parameters for the application of these block copolymers as gas separation membranes, is significantly lowered compared to the commercially available materials. Furthermore, the use of a monodisperse tetra-amide (T6T6T) hard segment resulted in a very fast and complete crystallization of these segments and thus a very well-defined microdomain morphology is obtained. The combination of these properties gives the developed materials high potential for use in gas separation applications.

In **Chapter 4, "Sub-ambient temperature CO_2 and light gas permeation through segmented block copolymers with tailored soft phase"**, the pure gas separation properties of the block copolymers synthesized in Chapter 3 are examined in detail. Overall high CO_2 permeabilities (up to 470 Barrer at 35℃, which is four times higher than the values obtained for membranes prepared from PEBAX®1074, which is the commonly used polymer) were obtained. Due to the low PEO melting temperature and crystallinity, the membranes demonstrated also excellent permeation characteristics at sub-ambient temperatures. This has been found a major advantage compared to the materials reported earlier as they do not posses these favorable low temperature characteristics. These newly developed materials thus offer a desirable set of properties over a wide temperature range, being highly relevant for practical applications, such as the removal of CO_2 from natural gas to meet pipeline specifications.

In **Chapter 5, "On the effects of plasticization in CO_2/light gas separation using polymeric solubility selective membranes"**, the high pressure CO_2/H_2 and CO_2/CH_4 pure and mixed gas separation performance of the block copolymers described in Chapter 3 and 4 is studied in further detail. Plasticization effects due to strong sorption of CO_2 at elevated pressures and/or reduced temperatures increase the permeability of H_2 and CH_4 in mixed gas experiments compared to their pure gas values, while the permeability of CO_2 was unaffected. Consequently, mixed gas selectivities were systematically lower than pure gas selectivities. The difference between both values was found to be exclusively dependent on and directly related to the concentration of CO_2 in the polymer matrix.

In **Chapter 6, "Highly hydrophilic, rubbery membranes for CO_2 capture and dehydration of flue gas"**, the membrane materials developed in Chapter 3 are investigated for their potential to simultaneously remove CO_2 and water vapor in a post-combustion capture configuration. In particular the influence of the water vapor activity on the gas permeability is studied. The water vapor permeability of all materials increases exponentially with the amount of water vapor present in the feed stream. Simultaneous water vapor/gas permeability measurements revealed that the gas permeability decreased only slightly in the presence of water vapor (as compared to the dry gas permeation described in Chapter 4). Furthermore, no noticeable difference in membrane performance has been observed between the use of pure or mixed gas. Because of the hydrophilic and polar character of the membrane materials, these are very effective in the simultaneous removal of CO_2 and water vapor from flue gases.

In **Chapter 7, "Poly(ethylene glycol) and poly(dimethyl siloxane): Combining their advantages into efficient CO_2 gas separation membranes"**, we explore the second strategy, the concept of polymer blending as a versatile tool to obtain highly permeable, yet sufficiently selective membrane materials for CO_2 separation. The beneficial properties of poly(dimethyl siloxane) (PDMS) (high permeability) and poly(ethylene glycol) (PEG) (high selectivity) are successfully combined in PEBAX® based membranes using a simple blending technique. The thermal-mechanical and gas transport properties for pure as well as mixed gases (CO_2/H_2 and CO_2/CH_4) were extensively studied. The permeability of the blend membranes could be significantly enhanced with increasing weight fraction of the additive (which contained the highly permeable PDMS), while sufficiently high selectivity was maintained. These results show the strong potential of this concept as a route to significantly improve the gas permeability of (currently existing) membranes.

Finally **Chapter 8, "Reflections & outlook"**, looks back on the results obtained in the preceding chapters and elaborates on the two main strategies followed in this thesis. Furthermore, it provides ideas and needs for future research and shortly discusses a possible process design for the separation of CO_2 from a post-combustion flue gas stream as proposed by Membrane Technology & Research Inc. (MTR).

Samenvatting

Het werk beschreven in dit proefschrift is gewijd aan de ontwikkeling van polymeer membraanmaterialen voor de scheiding van CO_2 van andere gassen, en dan met name de scheiding van CO_2 van stikstof, zoals vereist in een 'post-combustion capture' configuratie voor de verwijdering van CO_2 uit rookgassen. Een aantrekkelijke groep van materialen voor deze scheiding is de groep van multi-blokcopolymeren met polyether-gebaseerde zachte segmenten, omdat zij een redelijk hoge CO_2 permeabiliteit combineren met een voldoende hoge CO_2/N_2 selectiviteit. Voorbeelden van dergelijke polymeer membraanmaterialen zijn de bekende, commercieel verkrijgbare, blokcopolymeren PEBAX® en PolyActive®. De praktische toepasbaarheid van deze materialen is echter beperkt, omdat de gaspermeabiliteit te laag is voor een economisch rendabel proces.

In dit proefschrift worden twee verschillende strategieën onderzocht en beschreven om de eigenschappen van deze polyether-gebaseerde multi-blokcopolymeer membranen te beïnvloeden en te sturen en zo de algehele prestaties te verbeteren.

De eerste strategie (het ontwerpen van polymeren, **Hoofdstuk 2–6**) verkent de synthese van nieuwe blokcopolymeren op basis van poly(ethyleenoxide) vergelijkbaar met de eerder genoemde materialen PEBAX® en PolyActive®. Dit onderzoek is met name gericht op het verbeteren van de gebrekkige fasescheiding, zoals aanwezig in de commercieel beschikbare blokcopolymeren, omdat dit in belangrijke mate verantwoordelijk is voor hun lagere CO_2 permeabiliteit. De tweede strategie (het mengen van polymeren, **Hoofdstuk 7**) richt zich op de verbetering van polyether-gebaseerde blokcopolymeren (zoals PEBAX®) door de toevoeging van zorgvuldig geselecteerde slimme polymeer additieven.

In **Hoofdstuk 2, "Tuning of mass transport properties in multi-block copolymers for CO_2 capture applications"**, worden de CO_2-gasscheidingseigenschappen van drie blokcopolymeer series met polyether-gebaseerde zachte segmenten besproken. De blokcopolymeren hebben poly(ethyleenoxide) (PEO), poly(propyleenoxide) (PPO) of een mengsel van beide als zachte segmenten. Het harde segment is gelijk in alle drie de reeksen en is een di-amide met een uniforme lengte (aangeduid als TΦT). De invloed van de eigenschappen van het zachte segment (type en lengte) en de experimentele temperatuur op de puur gas CO_2-permeabiliteit en selectiviteit is in detail bestudeerd. De gesynthetiseerde blokcopolymeren hebben een verbeterde fasescheiding en vertonen

een beter CO_2-scheidingsgedrag ten opzichte van soortgelijke commercieel beschikbare materialen. Dit bevestigt het positieve effect van de goed gedefinieerde fasescheiding van de nieuw ontwikkelde materialen. Deze multi-blokcopolymeren vormen derhalve een veelzijdig instrument om de massaoverdracht en de gasscheidingseigenschappen van membranen voor gas- en dampscheiding naar eigen wens en inzicht te beïnvloeden.

In **Hoofdstuk 3, "Poly(ethylene oxide) based block copolymers with exceptionally low soft phase melting temperature and crystallinity"**, worden de synthese en thermo-mechanische eigenschappen van een reeks van gesegmenteerde blokcopolymeren gebaseerd op een nieuw type poly(ethyleenoxide) (PEO) zacht segment beschreven. De smelttemperatuur en kristalliniteit van PEO, welke belangrijke parameters zijn voor de toepassing van deze blokcopolymeren als gasscheidingsmembraan, zijn aanzienlijk verlaagd ten opzichte van de commercieel beschikbare materialen. Bovendien resulteert het gebruik van een tetra-amide (T6T6T) met een uniforme lengte als hard segment in een zeer snelle en volledige kristallisatie van deze segmenten en wordt derhalve een zeer goed gedefinieerde fasescheiding verkregen. De combinatie van deze eigenschappen geeft de ontwikkelde materialen een groot potentieel voor het gebruik in gasscheidingstoepassingen.

In **Hoofdstuk 4, "Sub-ambient temperature CO_2 and light gas permeation through segmented block copolymers with tailored soft phase"**, worden de puur gas scheidingseigenschappen van de blokcopolymeren, gesynthetiseerd in hoofdstuk 3, in detail onderzocht. De materialen bezitten een hoge CO_2-permeabiliteit (tot 470 Barrer bij 35℃, circa vier keer hoger dan de overeenkomstige waarde van membranen gemaakt van het veelgebruikte, commercieel verkrijgbare polymeer PEBAX®1074). Als gevolg van de lage smelttemperatuur en kristalliniteit van het PEO bezitten deze membranen ook uitstekende transporteigenschappen bij temperaturen lager dan kamertemperatuur. Dit is een groot voordeel ten opzichte van de materialen eerder beschreven in de literatuur. Deze nieuw ontwikkelde materialen hebben aldus een gewenste combinatie van eigenschappen over een breed temperatuursgebied, wat zeer relevant is voor praktische toepassingen zoals de verwijdering van CO_2 uit aardgas om te voldoen aan de uiteindelijke productspecificaties.

In **Hoofdstuk 5, "On the effects of plasticization in CO_2/light gas separation using polymeric solubility selective membranes"**, worden de CO_2/H_2 en CO_2/CH_4 puur- en menggas scheidingseigenschappen van de blokcopolymeren

beschreven in hoofdstuk 3 en 4 nader bestudeerd als functie van de druk en de temperatuur. Verwekingseffecten als gevolg van de sterke sorptie van CO_2 in deze blokcopolymeren bij verhoogde druk en/of verlaagde temperatuur verhogen de doorlaatbaarheid van het membraan voor H_2 en CH_4 in menggas experimenten in vergelijking met puur gas experimenten, terwijl de permeabiliteit van CO_2 niet verandert. Als gevolg hiervan zijn de menggas selectiviteiten systematisch lager dan puur gas selectiviteiten. Het verschil tussen beide waarden blijkt uitsluitend afhankelijk te zijn van en rechtstreeks verband te houden met de concentratie van CO_2 in het polymeer.

In **Hoofdstuk 6, "Highly hydrophilic, rubbery membranes for CO_2 capture and dehydration of flue gas"**, zijn de membraanmaterialen, ontwikkeld in hoofdstuk 3, onderzocht op hun potentieel om tegelijkertijd zowel CO_2 alsmede waterdamp te verwijderen uit rookgassen in een 'post-combustion capture' configuratie. Met name de invloed van de waterdampactiviteit op de gaspermeabiliteit is bestudeerd. De waterdampdoorlaatbaarheid van alle materialen neemt exponentieel toe met de hoeveelheid waterdamp die aanwezig is in het rookgas. Uit metingen waarbij transport van waterdamp en gas gelijktijdig plaatsvindt is gebleken dat de gas permeabiliteit slechts licht daalt in de aanwezigheid van waterdamp (in vergelijking met het droge puur gas permeatiegedrag beschreven in hoofdstuk 4). Er is geen merkbaar verschil in de prestaties van het membraan waargenomen tussen het gebruik van puur gas dan wel menggas. Door het hydrofiele en polaire karakter van het membraanmateriaal zijn deze membranen zeer effectief in het gelijktijdig verwijderen van zowel CO_2 als waterdamp uit rookgassen.

In **Hoofdstuk 7, "Poly(ethylene glycol) and poly(dimethyl siloxane): Combining their advantages into efficient CO_2 gas separation membranes"**, onderzoeken we de tweede strategie: het concept van het mengen van polymeren. Dit concept is een veelzijdig instrument om hoogpermeabele, maar toch voldoende selectieve membraanmaterialen voor CO_2 scheiding te ontwikkelen. De gunstige eigenschappen van poly(dimethyl siloxaan) (PDMS) (hoge permeabiliteit) en poly(ethyleen glycol) (PEG) (hoge selectiviteit) zijn succesvol gecombineerd in PEBAX® gebaseerde membranen met behulp van een eenvoudige mengtechniek. De thermo-mechanische eigenschappen en het gastransport voor pure gassen alsmede menggassen (CO_2/H_2 en CO_2/CH_4) zijn uitgebreid bestudeerd. De gaspermeabiliteit van membranen bereid met deze mengtechniek kan aanmerkelijk worden verbeterd door het toevoegen van het additief, terwijl er een voldoende hoge selectiviteit wordt gehandhaafd. Deze

resultaten tonen de enorme mogelijkheden aan van dit concept als een eenvoudige manier om een aanzienlijke verbetering van de gaspermeabiliteit van (op dit moment bestaande) membranen te bewerkstelligen.

Hoofdstuk 8, "Reflections & Outlook", tenslotte, blikt terug op de behaalde resultaten in de voorgaande hoofdstukken en gaat dieper in op de twee belangrijkste strategieën gevolgd in dit proefschrift. Bovendien biedt het ideeën en beschrijft het aandachtspunten voor toekomstig onderzoek. Als laatste wordt beschreven hoe een mogelijk integraal proces voor de verwijdering van CO_2 uit een 'post-combustion' rookgas, zoals ontworpen door Membrane Technology & Research Inc. (MTR), eruit zou kunnen zien.

Dankwoord

Het is voorbij... Het is zo cliché, maar als je eraan begint lijkt vier jaar promoveren een eeuwigheid te zijn. Nu het moment daar is zijn de jaren werkelijk voorbij gevlogen. Met veel plezier kijk ik terug op mijn tijd hier in Twente, in totaal bijna 10 jaar. Dit moment wil ik graag gebruiken om iedereen die, op welke wijze dan ook, heeft meegeholpen aan de totstandkoming van mijn proefschrift, te bedanken. Want ondanks dat er maar één naam op de omslag staat, is het zeker geen 'one man job'.

Allereerst wil ik de persoon bedanken die mij de mogelijkheid heeft gegeven om aan dit avontuur te beginnen, mijn promotor Matthias Wessling. Matthias, eens zei je tegen mij (ergens in de gangen van het CT-gebouw geloof ik) dat als ik aan een promotie dacht maar eens langs moest komen. Enige maanden later zat ik in je kantoor en had je de ideale plek voor mij. Je grenzeloze enthousiasme deed mij al snel besluiten deze plek te aanvaarden en te promoveren in de membraantechnologie.

Veel dank ben ik daarnaast verschuldigd aan mijn dagelijkse begeleider Kitty Nijmeijer. Ik heb de begeleiding altijd als zeer prettig ervaren en dat komt mede door jouw vriendelijke en altijd positieve karakter. Ondanks je drukke agenda kon ik altijd binnenlopen voor een vraag of een praatje buiten het werk om. Tevens wil ik je ook erg bedanken voor alle geboden vrijheid, het vertrouwen en de mogelijkheid die je mij hebt gegeven om in de laatste maanden mijn proefschrift ten dele bij Emeline te kunnen schrijven. Het is niet makkelijk om zover van elkaar te zijn. Op deze manier konden we meer tijd met elkaar doorbrengen en dit betekent dan ook veel voor mij. Wat ik nooit zal vergeten is je lach, want die is onmiskenbaar en altijd van ver te horen ☺.

Verder wil ik de overige leden van mijn promotiecommissie bedanken voor het accepteren van de uitnodiging om in mijn promotiecommissie plaats te nemen en voor het goedkeuren van mijn proefschrift. Especially I would like to acknowledge Dr. Freeman for flying all over the Atlantic to be present here. In addition I would like to thank you for your kind invitation to come over to Texas to collaborate and study the mixed gas sorption behavior of some of our materials. I believe we were able to enrich the set of data by the collaboration and get a clear view of all parameters involved. In that respect I would also like to thank Dr. Cláudio Ribeiro Jr. for his help with the measurements.

Tevens wil ik enkele (ex-)collega's binnen de groep speciaal bedanken. Greet, nooit hoefde ik mij zorgen te maken over de administratieve zaken rond het promoveren. Alles was altijd prima in orde. Eveneens was het altijd mogelijk binnen te stappen voor een praatje. Onze snoeppot had een grote aantrekkingskracht, maar als hij leeg was vulde je hem met regelmaat bij. Op het lab werd ik snel wegwijs gemaakt in de kunst van gasscheiding en het gebruik van een GC door Tymen Visser en kon ik altijd bouwen op de kennis van Herman Teunis als er met de opstelling iets niet helemaal liep zoals het zou moeten. Knutselen in de verschillende boxen was altijd in uitstekende handen bij John Heeks en nooit was iets te veel gevraagd. Dank hiervoor!

Futhermore, I would like to thank all the NanoGLOWA project members and especially our close collaborators. I also would like to take this opportunity to thank my two colleagues within the project, Jens Potreck and Nicolas Hengl, for the smooth cooperation, the scientific discussions and the enjoyable trips we made to several places in Europe for our project meetings.

On the subject of collaboration I would like to acknowledge in particular Dr. Reinoud Gaymans & Dr. Araichimani Arun. By combining the knowledge of the synthesis of well-defined block copolymer systems with the art of membrane science we have been able to produce a nice set of membranes and scientific output. The road has not always been without obstacles, but in the end I look back on a fruitful collaboration. Arun, I wish you all the best with your own research group back in India and your future work on engineering plastics.

Veel dank ben ik evenzo verschuldigd aan de verschillende studenten die hebben bijgedragen aan dit proefschrift. Allereerst mijn twee masterstudenten Anne Corine IJzer en Michel Knoef. Jullie hebben beiden enorm veel werk verzet in het lab en hadden een enorm enthousiasme voor het onderwerp en de membraantechnologie in het algemeen. Dit maakte het tot een plezier om jullie begeleider te zijn. Jullie inzet heeft zich uitbetaald in een totaal van 3 artikelen en één patent. Van meer kan en mag een AIO denk ik niet dromen. Nogmaals enorm bedankt voor jullie inzet.

Naast masterstudenten hebben ook verschillende bachelorstudenten binnen het Nano-GLOWA project hun afstudeeropdracht gedaan. Ik wil deze mogelijkheid gebruiken om Soubhik Datta, Frank Schrama en Danny Hoogendoorn te bedanken voor hun werk en inzet op drie totaal verschillende onderwerpen binnen het project. Ondanks dat jullie werk niet direct is terug te vinden in dit proefschrift, heeft het ons project vooruit geholpen en is daarom zeker niet van minder waarde. I also had the opportunity to work with two international Erasmus exchange students: Charline Sandevoir & Rut Jordana. Rut, part of your work you will find in chapter 6. Charline, your work did not find its way into the thesis, but it already showed us the advantages of blending. I believe there is still a lot for us to explore. Thank you both for all the work.

There is no work environment without direct colleagues and I especially would like to thank all my colleagues from the membrane technology group. I always felt at home in the group and it feels kind of strange that it will end now soon and that I will be leaving this great group of people. I really enjoyed the open atmosphere and the many activities outside working hours, such as the bata-444-race, the bike tour, the 'Sinterklaas' and Christmas celebrations, dinners, pubquiz and bowling evenings etc. In particular I would like to thank my (former) roommates for the nice time in the office. First in the old 'Langezijds' building Jens, Alisia & Bernke (1330, das prettig!) and later in 'Meander' (ME323) Jens, David, Paul, Izabela, Marlon & Elif.

Naast het werk in de groep heb ik ook een leerzame en waardevolle tijd gehad binnen het bedrijfshulpverleningsteam (BHV-team) van de Horst. Alle oefeningen en soms serieuze uitrukken maakten de BHV tot een hecht team en een goed geoliede machine. Gelukkig heeft zich nooit een ernstig ongeval voorgedaan. Dank mede-redders!

Van een goed begin van de werkweek was ik altijd verzekerd met Antoine, Harmen & Tiemen op de zondagavond in de Geus (en later thuis en in de Beiaard). Heerlijk om de week te beginnen met een speciaalbiertje. Naast een ontspannende zondagavond was het op maandagavond altijd goed toeven met het 'recreatieteam' (Bart, Eddy, Antal, Nienke, Fred, Joram, Kenneth & Roeland). Mannen (en Nienke) bedankt voor deze ontspannende momenten.

Also I would like to thank my two paranymphs that will be next to me on the podium. Géraldine and Nicolas, together you form the French connection for me here in NL. I'm very glad that you two will be on my side the 19th. I wish you both all the best for the future here in the 'low' (and wet and cold and . . .) country. I will be exploring your home country soon and enjoy a baguette. Vive la France!

(P + M) & J, jullie hebben mij al deze jaren in Twente gesteund. Zelf wisten jullie al dat ik aan dit avontuur zou beginnen ver voordat ik het zelf wist. Jullie hebben altijd interesse getoond in mijn studie en werk, ondanks dat het zeker niet altijd duidelijk zal zijn geweest wat er daar in het oosten nu precies gebeurde. Bedankt voor al jullie support en interesse. Wat de toekomst precies gaat brengen weet ik niet, maar zoals de bekende krantenkop zegt: 'Chemie is overal'.

Emeline, spending all this time away from each other was not easy. Those years are now almost over. I know both our PhD journeys could not have been more different. However, we will embark on the next journey together and I'm looking forward to that moment. I know it will be great. I love you!

SANDER

Curriculum Vitae

Sander Reijerkerk was born on the 28th of May 1982 in the city of Deventer, The Netherlands. He received his Dutch pre-university diploma (VWO) in June 2000 from the Geert Groote College, also situated in Deventer. In September 2000 he started his study Chemical Engineering at the University of Twente, Enschede, The Netherlands. In the last two years of his study he focused on material science and in particular on polymer science and engineering. He performed his internship at the McMaster University, Hamilton (Ontario), Canada within the polymer and colloid chemistry research group of prof. Harald Stöver. Here he worked on an industrial financed project (Syngenta, UK) to develop polymeric microcapsules for the controlled release of specific components, such as pesticides. Immediately after he conducted his master assignment within the Synthesis and Technology of Engineering Plastics (STEP) research group headed by Dr. Gaymans, where he worked on the synthesis and characterization of hydrophilic poly(ethylene oxide) based block copolymers. He graduated in May 2006 and obtained his M.Sc. diploma. After his graduation he started in June 2006 as a Ph.D. student in the Membrane Science & Technology group at the University of Twente and worked on the design of membranes (especially block copolymer based membranes) for CO_2 separation, of which the results are described in this thesis.

List of publications

Peer-reviewed articles

S.R. Reijerkerk, A. Arun, R.J. Gaymans, K. Nijmeijer, M. Wessling; *Tuning of mass transport properties in multi-block copolymers for CO_2 capture applications*; Journal of Membrane Science (2009); DOI:10.1016/j.memsci.2009.09.045

A.C. IJzer, A. Arun, **S.R. Reijerkerk**, K. Nijmeijer, M. Wessling, R.J. Gaymans; *Synthesis and properties of hydrophilic segmented block copolymers based on poly(ethylene oxide)-ran-poly(propylene oxide)*; Journal of Applied Polymer Science, accepted for publication

S.R. Reijerkerk, A.C. IJzer, K. Nijmeijer, A. Arun, R.J. Gaymans, M. Wessling; *Sub-ambient temperature CO_2 and light gas permeation through segmented block copolymers with tailored soft phase*; ACS Applied Materials & Interfaces (2010); DOI: 10.1021/am900754z

S.R. Reijerkerk, K. Nijmeijer, C.P. Ribeiro Jr., B.D. Freeman, M. Wessling; *On the effects of plasticization in CO_2/light gas separation using polymeric solubility selective membranes*; Macromolecules, prepared for submission

S.R. Reijerkerk, R. Jordana, K. Nijmeijer, M. Wessling; *Highly hydrophilic, rubbery membranes for CO_2 capture and dehydration of flue gas*; International Journal of Greenhouse Gas Control, submitted for publication

S.R. Reijerkerk, M.H. Knoef, K. Nijmeijer, M. Wessling; *Poly(ethylene glycol) and poly(dimethyl siloxane): Combining their advantages into efficient CO_2 gas separation membranes*; Journal of Membrane Science (2010); DOI:10.1016/j.memsci.2010.02.008

A. Fonseca, **S.R. Reijerkerk**, J. Potreck, K. Nijmeijer, Z. Mekhalif, J. Delhalle; *Very short functionalized carbon nanotubes for membrane applications*; Desalination **250** (3) (2010), pages 1150–1154; DOI:10.1016/j.desal.2009.09.130

Patents

R.J. Gaymans, D. Husken, **S.R. Reijerkerk**; *Block copolymer elastomer*; WO2008064857 (A1), Stichting Dutch Polymer Institute (2008)

M.H. Knoef, **S.R. Reijerkerk**, M. Wessling, D.C. Nijmeijer; *Polymer composition comprising a blend of a multi-block thermoplastic elastomer and a polymer comprising a Group 14 metal*; European patent application 09161009.7 - 1521, University of Twente, Membrane Technology Group (2009)

Presentations

S.R. Reijerkerk, D. Husken, A. Arun, K. Nijmeijer, M. Wessling, R.J. Gaymans; *Tuning of mass transport in macromolecular structures*; Dutch Polymer Days 7 (February 2007), Lunteren, The Netherlands

S.R. Reijerkerk, J. Potreck, K. Nijmeijer, M. Wessling; *Nanostructured membranes for CO_2 capture*; Network Young Membrains 9 (September 2007), Thessaloniki, Greece

S.R. Reijerkerk, A. Arun, A.C. IJzer, K. Nijmeijer, R.J. Gaymans, M. Wessling; *Segmented block copolymers: A molecular toolbox to tailor mass transport properties of polymeric nanocomposites*; International Congress on Membranes and Membrane Processes (ICOM) (July 2008), Honolulu (HI), USA

S.R. Reijerkerk, A. Arun, A.C. IJzer, K. Nijmeijer, R.J. Gaymans, M. Wessling; *Novel PEO-based block copolymers for CO_2 removal with extremely low soft phase melting temperature*; Network Young Membrains 10 (September 2008), Berlin, Germany

S.R. Reijerkerk, M.H. Knoef, K. Nijmeijer, M. Wessling; *PEBAX$^{®}$ blend membranes for CO_2 separation: The influence of blending on CO_2/H_2 separation*; Network Young Membrains 11 (September 2009), Mèze, France

S.R. Reijerkerk, K. Nijmeijer, M. Wessling; *High pressure CO_2 separation using solubility selective membranes: Influence of temperature and pressure on CO_2/CH_4 separation*; EUROMEMBRANE (September 2009), Montpellier, France (granted a travel award by the European Membrane Society)

S.R. Reijerkerk, A.C. IJzer, M.H. Knoef, R.J. Gaymans, K. Nijmeijer, M. Wessling; *Strategies for the development of polymeric membranes for CO_2 capture*; Netherlands Process Technology Symposium 9 (October 2009), Veldhoven, The Netherlands

S.R. Reijerkerk, A.C. IJzer, M.H. Knoef, R.J. Gaymans, K. Nijmeijer, M. Wessling; *Design strategies for polymeric membranes for CO_2 capture*; Dutch Polymer Days 10 (February 2010), Veldhoven, The Netherlands